

**I. TRANSITION METAL LIGANDS FOR  
SUZUKI-MIYAJIURA CROSS-COUPPLING  
REACTIONS AND THE  
COORDINATION OF RADIONUCLIDES**

**II. STUDIES TOWARDS AURORA KINASE  
INHIBITION FOR PET IMAGING**

A thesis presented to The Faculty of Graduate Studies of Lakehead University by

**CLIFFORD AGYEI**

In partial fulfillment of the requirements for the degree of Doctor of Philosophy in  
Chemistry and Material Science.

September 22, 2023

## Abstract

This thesis is wide-ranging covering disparate areas of synthetic organic and metal-organic chemistry, unified by the general use of these projects in medicinal chemistry.

Two organometallic palladium complexes **2.3** and **2.4**, the 2-methyl-4-phenyl-1,3-thiazole and the 4-phenyl-1,3-thiazol-4-ylamine ligand respectively were synthesized and characterized using NMR, mass spectrometry, IR, and X-ray crystallography. These catalysts were tested with various substrates to understand the influence of these catalysts on substrates with electron-withdrawing groups or electron-donating groups in the Suzuki-Miyaura cross-coupling reaction. Several aryl halides and different boronic acid pairs were studied yielding a conversion rate between 27-97 % when 5 mol % of each palladium catalyst was used at 60 °C for 8 hours. The relative rate of electron poor aryl halides was faster than electron rich aryl halides with catalyst **2.4** (amine substituted catalyst) showing preference for electron-withdrawing group (EWG > EDG). The relative rates of the electron rich aryl halides were faster than the electron poor aryl halides when the catalyst with the methyl substituted ligand (catalyst **2.3**) was used and we get the opposite preference for electron-donating group (EDG > EWG). The latter behavior is unique in Suzuki-Miyaura coupling reactions, which makes catalyst **2.3** a useful addition to the family of Suzuki-Miyaura catalytic systems.

Technetium-99m (Tc-99m) is the most widely used radioisotope in medical imaging accounting for over 76,000 scans per day. Currently, all Tc-99m used in Canada is derived from Mo-99/Tc-99 generators where the Mo-99 is isolated from the fission of U-235 produced by a limited number of nuclear reactors that rely on highly enriched uranium (HEU) as feed stock. There is increasing pressure to move away from uranium sources that requires HEU because of its alternate use in weapons. Unfortunately, the alternative sources of Mo-99 often result in a low specific activity product, meaning a significantly higher mass of molybdate is required to deliver the same activity. As a result, a more efficient solid support is required for the generator to deliver the same activity of Tc-99m. This work describes the preparation and testing methods of the new solid supports including “hot” testing with Mo-99. The design requirements that provide selective binding of molybdate over pertechnetate will be discussed. Polymer-based resins were synthesized as an alternative solid support for nuclear medicine scans using modified seeded nanoparticles. Quaternary methyl ammonium ion based resins were synthesized by grafting or immobilization of glycidyltrimethyl ammonium chloride or Girard’s reagent T onto silica gel using 3-(Triethoxysilyl) propylamine and (3-glycidyloxypropyl)trimethoxysilane and as coupling agents respectively. The uptake behavior of the two resins were studied towards molybdate with a column loading efficiencies of 199 and 195 mg of Mo/g of resin respectively. The resins prepared had high loading and selectivity for molybdate and releases pertechnetate.

There has been a growing interest in aurora kinases (AURK) family of proteins as potential targets for cancer therapy. The three mammalian proteins, aurora A, B and C play a central role in cellular mitosis, however aurora C is exclusively expressed in testis. The function of aurora A is in spindle formation and centrosome maturation, and aurora B is required for proper microtubule attachment to kinetochore and plays a central role in cytokinesis as a chromosomal passenger protein. Overexpression of aurora proteins is common in certain tumors and is thought to induce tumorigenesis, thus inhibition studies have begun targeting their homologous ATP-binding pocket. Although, there is growing interest in designing small molecule inhibitors, there has been little research around the potential of targeting this family of kinases for molecular imaging.

Radiotracers such as [<sup>18</sup>F]fluorodeoxyglucose which can be used to monitor metabolism and glucose uptake in highly proliferative tissues and are useful in identifying cancer but are not tumor-specific. This chapter looks at the synthesis of a common intermediate which could be functionalized to create other analogues as well as being radiolabeled for F-18 compounds.

## **Acknowledgements**

I would like to thank almighty God for his guidance and protection throughout these years. I would like to express my sincere gratitude to my supervisors Dr. Michael Campbell and Dr. Craig MacKinnon without whom this research would not have been possible, and for teaching me to be a chemist and allowing me to call the Campbell laboratory and MacKinnon laboratory home for the last five years. They went above and beyond to make my graduate studies experience as enjoyable, educational, and stress-free as possible.

I would like to thank my committee members Dr. Christina Gottardo, Dr. Jinqiang Hou, and Dr. Stephen Foley for their input and guidance in my research and the writing of this thesis. Thank you to Dr. Magajna and Dr. Mawhinney for their support and for the ever-tedious administrative portion of getting this degree.

I would like to thank the Lakehead University Chemistry department technician team for fixing everything I broke and answering all my questions.

I would like to extend many thanks to Dr. Craig M. Robertson, University of Liverpool for running our samples on the X-Ray Crystallography Instrument. I would like to thank staff of Lakehead University instrumentation laboratory; Greg Kepka, Dr. Guosheng Wu and Mike Sorokopud.

Lastly to my lovely wife, Philippa, my daughters; Alexandra, Maame Yaa, Akosua and Pamela Agyei for their support throughout the years. I am truly blessed to be surrounded by people who lift me up and encourage me to be the best version of myself. Your unconditional love and support have made me who I am today. Thank you for being my first line support.

## **Dedication**

This thesis is dedicated to my mom Vida Amma Konadu of blessed memory. You are forever in my heart.

## Table of Contents

Abstract .....	i
Acknowledgements .....	iv
Dedication .....	v
List of Figure.....	xii
List of Tables.....	xv
List of Schemes .....	xvi
List of Synthesized Compounds .....	xix
List of Abbreviations.....	xxx
Chapter 1-Introduction.....	1
1.1 OVERALL THEME OF THE THESIS .....	1
1.1.1 Specific Goals of the Thesis .....	1
1.1.1.1 Tuning the Electronics in Suzuki- Miyaura Cross-Coupling Reactions Using Thiazole-Based Ligands. ....	2
1.1.1.2 The Development of a New High-Capacity Solid Support Resins for Use in Mo/Tc-99m Generators .....	3
1.1.1.3 Studies Towards Aurora Kinase Inhibition for PET imaging .....	3
Chapter 2- Tuning the Electronics in Suzuki-Miyaura Cross- Coupling Reactions Using Thiazole-Based Ligands.....	4
2.0 SUMMARY: .....	4
2.1 INTRODUCTION .....	5
2.2 LITERATURE REVIEW .....	6
2.2.1 General Cross-Coupling Mechanism .....	8

2.2.2 Suzuki Cross-Coupling Reaction Mechanism .....	14
2.3 LIGAND DESIGN .....	16
2.3.1 Effect of the Ligands on the Resulting Properties of the Compound.....	16
2.3.1.1 Electronic Effects.....	16
2.3.1.2 Steric Effects .....	18
2.3.2 Ligand Design in Catalytic Organometallic Chemistry.....	20
2.4 NITROGEN CONTAINING AROMATIC LIGANDS GENERALLY USED IN COORDINATION AND ORGANOMETALLIC CHEMISTRY. ....	23
2.4.1 Using Thiazole in a Ligand System.....	26
2.4.2 Properties and Use of Thiazole .....	27
2.5. POTENTIAL ADVANTAGES OF THIAZOLE LIGANDS .....	28
2.6 RESULTS AND DISCUSSION.....	32
2.6.1 Synthesis of Thiazole Ligands .....	32
2.6.2 Synthesis of Palladium Complex.....	33
2.6.3 Crystal Structure of Compound [(MePhTz)Pd(CH <sub>3</sub> COO)] <sub>2</sub> 2.3.....	34
2.7 RATE STUDIES.....	42
2.7.1 NMR Analysis of the rate studies.....	48
2.8 ANALYSIS .....	51
2.9 OTHER LIGANDS ATTEMPTED.....	55
2.10 EXPERIMENTAL.....	57
2.10.1 General Synthetic and Instrumental Details .....	57
2.10.2 Ligands Preparation .....	58
2.10.3 Synthesis of Palladium(II) Complex (2.3) .....	60



2.10.4 Synthesis of Palladium (II) Complex (2.4) .....	60
2.10.5 Crystal Structure of Compound [(MePhTz)Pd(CH <sub>3</sub> COO)] <sub>2</sub> (2.3) .....	61
2.10.6 Suzuki-Miyaura Coupling. ....	62
2.11 RATE STUDIES.....	76
2.12 CONCLUSION .....	78
<b>Chapter 3-The Development of New High-</b>	
<b>Capacity Solid Support Resins for Use in Mo/Tc-99m Generators.....</b>	<b>79</b>
3.1 INTRODUCTION: .....	79
3.2 LITERATURE REVIEW .....	80
3.3 CURRENT SOLID SUPPORT .....	82
3.4 DESIGN CONSIDERATION .....	83
3.4.1 High Binding to Molybdate and Low Binding to Pertechnetate.....	84
3.4.2 Low Swelling.....	86
3.4.3 Low Cost of Synthesis .....	86
3.4.4 Use in Hospital Nuclear Medicinal Labs.....	86
3.5 SYNTHESIS/METHODS.....	88
3.5.1 Silica Beads .....	88
3.5.2 General Synthesis for Grafting/Immobilization of Beads on Amines .....	89
3.5.3 General Synthesis for Grafting/Immobilization of Silica Beads, with an Amine, and an Epoxide.....	90
3.5.4 Grafting/Immobilization of Silica Gel and (3-Glycidyoxypropyl) trimethoxysilane .....	91

<b>3.5.5 Grafting/immobilization of Silica Gel and (3-Glycidyoxypropyl)</b>	
<b>trimethoxysilane and Girard's Reagents T</b> .....	<b>92</b>
<b>3.6 Cold Studies</b> .....	<b>92</b>
<b>3.6.1 Preparation of Ammonia Molybdate Test Solution</b> .....	<b>92</b>
<b>3.6.2 Uptake Measurement-Cold Studies (Inductively coupled plasma</b>	
<b>atomic emission spectroscopy)</b> .....	<b>93</b>
<b>3.6.2.1 Column loading efficiency.</b> .....	<b>93</b>
<b>3.7 Hot Technetium testing</b> .....	<b>96</b>
<b>3.8 CHARACTERIZATION</b> .....	<b>99</b>
<b>3.8.1 Scanning Electron Microscopy</b> .....	<b>99</b>
<b>3.8.2 Particle size analysis</b> .....	<b>105</b>
<b>3.9 RESULTS AND DISCUSSION</b> .....	<b>107</b>
<b>3.10 HOT MO/Tc ANALYSIS</b> .....	<b>109</b>
<b>3.11 EXPERIMENTAL</b> .....	<b>110</b>
<b>3.11.1 Chemicals</b> .....	<b>110</b>
<b>3.11.2 Preparation of the silica gel.</b> .....	<b>110</b>
<b>3.11.3 Functionalization of surface of silica</b> .....	<b>110</b>
<b>3.11.3.1 Grafting/immobilization of Silica gel and N-[3-(Trimethoxysilyl)propyl]</b>	
<b>ethylenediamine (2)</b> .....	<b>110</b>
<b>3.11.3.2 Grafting/Immobilization of glycidyltrimethylammonium chloride (3)</b>	
<b>with modified silica gel (compound 4)</b> .....	<b>111</b>
<b>3.11.3.3 Grafting/Immobilization of silica gel with (3-Glycidyoxypropyl)</b>	
<b>trimethoxysilane (6)</b> .....	<b>112</b>

3.11.3.4 Grafting/Immobilization of Girard's reagent T with modified silica (compound 8) .....	113
3.11.3.5 Grafting/immobilization of Silica gel and 3-trimethoxysilylpropylamine (10) .....	114
3.11.3.6 Grafting/Immobilization of glycidyltrimethylammonium chloride (GTMACl) with modified silica gel (compound 11) .....	114
3.12 CONCLUSION .....	115
Chapter 4- Studies towards aurora kinase inhibitors for PET imaging .....	117
4.1 INTRODUCTION: .....	117
4.2 LITERATURE REVIEW.....	118
4.2.1 Aurora kinase and cancer.....	118
4.2.2 Binding modes of Aurora kinase to ATP .....	119
4.3 NOVEL AURKA/B/C INHIBITORS .....	120
4.4 ANALOGUES AND <sup>18</sup> F-RADIOLABELLED TRACER COMPOUND.....	125
4.5 MEDICAL USE OF THIAZOLE LIGANDS .....	126
4.6 GOALS OF THE PROJECT .....	128
4.7 RETROSYNTHETIC ANALYSIS.....	131
4.8 RESULTS AND DISCUSSION.....	133
4.8.1 Thiazole-enaminone synthesis (4) .....	133
4.8.3 Synthesis of guanidine.....	134
4.8.3.1 Tert-butyl-4-(p-nitrophenyl)-1-piperazinecarboxylate (7).....	134
4.8.3.2 Tert-butyl-4-(p-aminophenyl)-1-piperazinecarboxylate (8).....	135
4.8.3.3 Tert-butyl-4-(p-guanidinophenyl)-1-piperazinecarboxylate (9) .....	135

4.8.4 Tert-butyl-4-(p-[4-(2,4-dimethyl-1,3-thiazol-5-yl)-2-pyrimidinylamino]phenyl)-1-piperazinecarboxylate (10).....	136
4.8.5 [4-(2,4-dimethyl-1,3-thiazol-5-yl)-2-pyrimidinyl][p-(1-piperazinyl)phenyl]amine (11) .....	137
4.9 GENERAL RESULTS/DISCUSSION .....	138
4.10 EXPERIMENTAL.....	140
4.10.1 General synthetic and instrumental details .....	140
4.10.2 Thiazole synthesis.....	141
4.10.3 Guanidine Synthesis.....	142
4.11 CONCLUSION AND FUTURE WORK.....	148
Chapter 5: Conclusion and Future work .....	149
Chapter 6: References.....	152

## List of Figure

Figure 1.1: Synthesized thiazole-based ligands (catalyst).....	2
Figure 1.2: Some synthesised resins for Mo/Tc-99m generators .....	3
Figure 1.3: Proposed imaging agent for aurora kinase .....	3
Figure: 2.1: Example of back bonding in an organometallic complex with a ligand that donates through its $\pi$ -system. ....	18
Figure 2.2: Tolman cone angle for a monodentate ligands .....	19
Figure 2.3: Example of some palladium-catalyzed reactions .....	20
Figure 2.4: Mechanism of metal-catalyzed aryl fluorination .....	21
Figure 2.5: structure of 2,2'-bipyridine .....	23
Figure 2.6: Structure of 2,2'-bipyridine derivative for anion recognition .....	23
Figure 2.7: Symmetric isomers (2,2', 3,3' and 4,4') of bipyridine .....	24
Figure 2.8: Asymmetric isomers (2,3', 2,4' and 3,4') of bipyridine .....	24
Figure 2.9: Trivalent lanthanide atom of general formula $[L_nX_3]$ .....	25
Figure 2.10: The intermolecular N...H-C interaction between two thiazole rings ....	26
Figure 2.11: The numbering system in thiazole .....	28
Figure 2.12: Metalated and metal-mediated reactions of thiazole.....	28
Figure 2.13: Bond angle of bithiazole compared to bipyridine.....	29
Figure 2.14: Metal complexes possessing different substituted thiazole ligands.....	30
Figure 2.15: 2,2'-bithiazole and 4,4'-bithiazole isomers of bithiazole. ....	31
Figure 2.16: Thiazole protected phosphine iridium complex.....	32
Figure 2.17: Solid state crystal structure of palladium(II) dimer complex of ligand	
2.3. Colour Scheme: (Sulfur atoms are yellow, oxygens are red, nitrogens are	

periwinkle or royal blue, palladium(II) are teal, and carbons are grey. Hydrogen atoms have been omitted for clarity. Figure b shows the Pd-Pd bond distances. .... 35

**Figure 2.18: Measurement of Pd-Pd (A), Pd-N (B), Pd-C (C) bond distances reported in Table 2.1 ..... 36**

**Figure 2.19: List of Boronic acid used in this study as indicated in Table 2.2. .... 39**

**Figure 2.20: <sup>1</sup>H NMR of the mixture of 4-(biphenyloxy)phenylmethane and 4'-(benzyloxy)-4-biphenylamine with chemical shift and integration. .... 49**

**Figure 2.21: <sup>1</sup>H NMR of 4-(biphenyloxy)phenylmethane with chemical shift and integration. .... 50**

**Figure 2.22: <sup>1</sup>H NMR of 4'-(benzyloxy)-4-biphenylamine with chemical shift and integration. .... 51**

**Figure 2.23: Potential application of catalyst 2.3 and 2.4. .... 55**

**Figure 3.1: Determining column loading efficiency of the resin. .... 94**

**Figure 3.2: Hydrogen bond interaction between the pertechnetate and the hydroxyl of the resin (R is alkoxy silane group) ..... 98**

**Figure 3.3: Scanning electron microscopy image of silica beads ..... 100**

**Figure 3.4: scanning electron microscopy image of compound 2 ..... 100**

**Figure 3.5: Scanning electron microscopy image of compound 4..... 101**

**Figure 3.6: Scanning electron microscopy image of compound 6..... 101**

**Figure 3.7: Scanning electron microscopy image of compound 8..... 102**

**Figure 3.8: Scanning electron microscopy image of compound 9..... 102**

**Figure 3.9: Scanning electron microscopy image of compound 11..... 103**

**Figure 3.10: Particle size distribution of silica gel..... 106**

<b>Figure 3.11: Particle size distribution of compounds 4.....</b>	<b>106</b>
<b>Figure 3.12: Particle size distribution of compound 8 .....</b>	<b>106</b>
<b>Figure 3.13: Particle size distribution of compounds 11.....</b>	<b>107</b>
<b>Figure 4.1: The five main area of aurora kinase binding sites<sup>108</sup> .....</b>	<b>120</b>
<b>Figure 4.2: Some selected Aurora kinase A/B/C inhibitors.....</b>	<b>122</b>
<b>Figure 4.3: N-[<sup>18</sup>F]fluoroethylated analogue compounds derived from CYC-116 inhibitor.....</b>	<b>126</b>
<b>Figure 4.4: Thiazole hybrid antimicrobial agent.....</b>	<b>127</b>
<b>Figure 4.5: Thiazole antiviral agent containing oxalamide moiety. ....</b>	<b>128</b>
<b>Figure 4.6: Thiazole-derivative as anti-cancer activities. ....</b>	<b>128</b>
<b>Figure 4.7: Structure of thiazole derivative used for an anticonvulsant activity. ....</b>	<b>128</b>
<b>Figure 4.8: Binding interactions of CYC 116 showing solvent exposed region. ....</b>	<b>129</b>

## List of Tables

<b>Table 2.1: Comparative data of ligands with respect to phenythiazole. ....</b>	<b>37</b>
<b>Table 2.2: Suzuki-Miyaura coupling reaction of different aryl halides and boronic acids using palladium catalyst 2.4.....</b>	<b>39</b>
<b>Table 2.3 Methylene NMR integral ratio of EDG vs EWG and protons of bromobenzene (standard) using catalyst 2.3.....</b>	<b>46</b>
<b>Table 2.4 Methylene NMR integral ratio of EDG vs EWG and protons of bromobenzene (standard) using catalyst 2.4.....</b>	<b>46</b>
<b>Table 3.1: Compound numbers, names and structure used in this chapter where blue circle represent silica gel. ....</b>	<b>87</b>
<b>Table 3.2: ICP-AES results of modified resins showing Mo remaining in solution after treatment with resin and the column loading efficiency of the various modified resins. ....</b>	<b>95</b>
<b>Table 3.3: Activity on resin, activity flow through, total activity and % Tc retained on resins.....</b>	<b>98</b>
<b>Table 3.4: Scanning electron microscopy of the size of modified silica beads and size of resins (nm) .....</b>	<b>104</b>



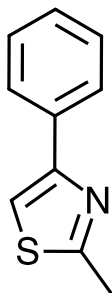
## List of Schemes

Scheme 2.1 Palladium(II) catalyzed reactions of aryl/alkyl halides. <sup>1</sup> .....	6
Scheme 2.2: Aryl-aryl C-C bond activation using aryl halide and aryl ketone.....	7
Scheme 2.3: Aryl-alkyl C-C bond formation for chemoselective alkylation of thiols <sup>7</sup>	7
Scheme 2.4: Carbon-heteroatom bond formation by iron-catalyzed <i>O</i> -arylation .....	8
Scheme 2.5: General mechanism of cross-coupling reactions.....	9
Scheme 2.6: Concerted addition of non-polar substrate to hydrogen or hydrocarbon .....	10
Scheme 2.7: Concerted addition of H <sub>2</sub> with Vaska's complex .....	10
Scheme 2.8: S <sub>N</sub> Ar type nucleophilic substitution oxidative addition.....	11
Scheme 2.9: Ionic-type oxidative addition of hydrochloric acid. <sup>9</sup> .....	11
Scheme 2.10: The transmetalation process .....	12
Scheme 2.11: Transmetalation leading to a complex formation.....	12
Scheme 2.12: Mononuclear and binuclear reductive elimination reactions.....	13
Scheme 2.13: Mechanism of the Suzuki-Miyaura cross-coupling reaction .....	14
Scheme 2.14: Proposed pathways for explaining the role of a base in the transmetalation step in Suzuki-Miyaura reaction.....	15
Scheme 2.15: Synthesis of 2-methyl-4-phenyl-1,3-thiazole.....	33
Scheme 2.16: Synthesis of 4-phenyl-1,3-thiazol-2-ylamine.....	33
Scheme 2.17: Synthesis of the palladium(II) complex 2.3, the dimer structure was determined by X-ray crystallography .....	34
Scheme 2.18: Synthesis of palladium complex, 2.4.....	34

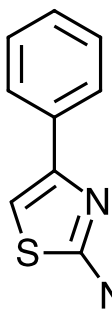
<b>Scheme 2.19: Method for determining the effect of catalyst on electron-donating effect in the Suzuki-Miyaura cross-coupling reaction. ....</b>	<b>45</b>
<b>Scheme 2.20: Method for determining the effect of catalyst on electron-withdrawing effect in the Suzuki-Miyaura cross-coupling reaction. ....</b>	<b>45</b>
<b>Scheme 2.21: Results of the rate studies on electron-withdrawing and or donating group.....</b>	<b>47</b>
<b>Scheme 2.22: Electronic effects in the Suzuki-Miyaura cross-coupling.....</b>	<b>53</b>
<b>Scheme 2.23 Mechanism of oxidative addition of palladium to the aryl halides in Suzuki-Miyaura cross-coupling reaction.<sup>74</sup>.....</b>	<b>53</b>
<b>Scheme 2.24: Mechanism of para and ortho with palladium attack in nucleophilic aromatic substitution. ....</b>	<b>54</b>
<b>Scheme 2.25: Synthesis of 4-Methyl-2-(2-thienyl)-1,3-thiazole .....</b>	<b>56</b>
<b>Scheme 2.26: Synthesis of 2-Methyl-4-(3-pyridyl)-1,3-thiazole .....</b>	<b>56</b>
<b>Scheme 3.1: Protonation states of polyamine-based resin developed by Donia. ....</b>	<b>83</b>
<b>Scheme 3.2: Resin containing ammonium group. ....</b>	<b>84</b>
<b>Scheme 3.3: The decay of molybdate anion to pertechnetate .....</b>	<b>84</b>
<b>Scheme 3.4: Interactions between resin and molybdate and pertechnetate ions .....</b>	<b>85</b>
<b>Scheme 3.5: The reaction of quaternary ammonium ion resin with molybdate. ....</b>	<b>85</b>
<b>Scheme 3.6: Condensation of silanol sites with methoxy group.....</b>	<b>88</b>
<b>Scheme 3.7: Silica Beads preparation .....</b>	<b>89</b>
<b>Scheme 3.8: Synthetic route to resins (silica gel + amine (1 or 9)).....</b>	<b>90</b>
<b>Scheme 3.9: Synthetic route of resins (compounds 4 and 11) .....</b>	<b>91</b>

<b>Scheme 3.10: Synthetic route to resin (Silica gel+ (3-Glycidyloxypropyl) trimethoxysilane (5).....</b>	<b>92</b>
<b>Scheme 3.11: Synthetic route to compound 8.....</b>	<b>92</b>
<b>Scheme 4.1: Functionalized replacement of morpholine with piperazine with fluorine-18 and other alkylated analogues.....</b>	<b>130</b>
<b>Scheme 4.2: The radiolabeling step of the retrosynthesis from enaminone (4) and guanidine (9). .....</b>	<b>131</b>
<b>Scheme 4.3 Formation of the enaminone. ....</b>	<b>132</b>
<b>Scheme 4.4: The guanidine formation.....</b>	<b>133</b>
<b>Scheme 4.5: Formation of enaminone .....</b>	<b>134</b>
<b>Scheme 4.6: Synthesis of <i>tert</i>-butyl-4-(<i>p</i>-nitrophenyl)-1-piperazinecarboxylate. ....</b>	<b>134</b>
<b>Scheme 4.7: Synthesis of <i>tert</i>-butyl-4-(<i>p</i>-aminophenyl)-1-piperazinecarboxylate... </b>	<b>135</b>
<b>Scheme 4.8: Synthesis of <i>tert</i>-butyl-4-(<i>p</i>-guanidinophenyl)-1-piperazinecarboxylate .....</b>	<b>136</b>
<b>Scheme 4.9: Synthesis of <i>tert</i>-butyl-4-(<i>p</i>-guanidinophenyl)-1-piperazinecarboxylate using scandium triflate, a Lewis acid. ....</b>	<b>136</b>
<b>Scheme 4.10: Synthesis of <i>tert</i>-butyl-4-(<i>p</i>-[4-(2,4-dimethyl-1,3-thiazol-5-yl)-2-pyrimidinylamino] phenyl)-1-piperazinecarboxylate .....</b>	<b>137</b>
<b>Scheme 4.11: Deprotection of <i>tert</i>-butyl-4-(<i>p</i>-[4-(2,4-dimethyl-1,3-thiazol-5-yl)-2-pyrimidinylamino] phenyl)-1-piperazinecarboxylate .....</b>	<b>138</b>
<b>Scheme 4.12: Abstraction of the amine by the base. ....</b>	<b>139</b>

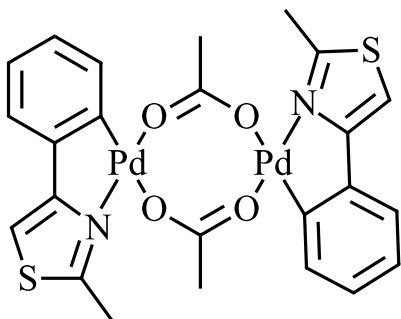
## List of Synthesized Compounds



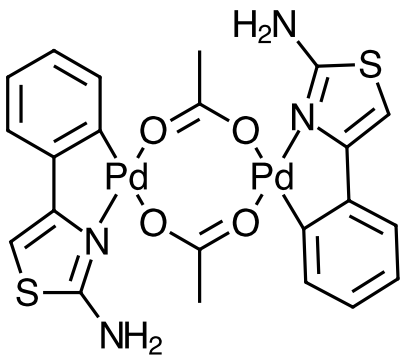
2-Methyl-4-phenyl-1,3-thiazole (2.1) ..... 58



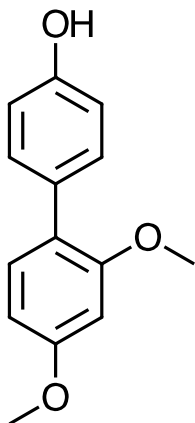
4-Phenyl-1,3-thiazol-2-ylamine (2.2) ..... 59



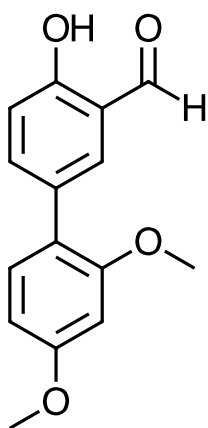
Palladium(II) Complex (2.3) ..... 60



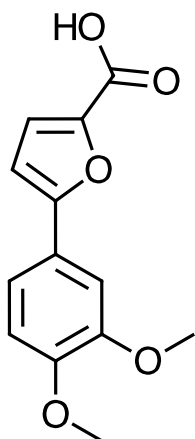
Palladium(II) Complex (2.4) ..... 60



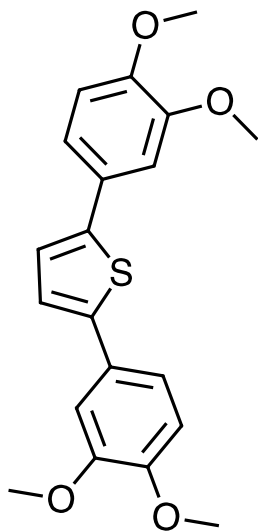
**2',4'-Dimethoxy-4-biphenylol (2.5)..... 62**



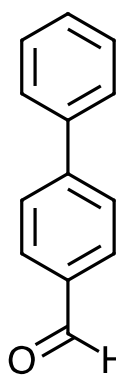
**4-Hydroxy-2',4'-dimethoxy-3-biphenylcarbaldehyde (2.6) ..... 63**



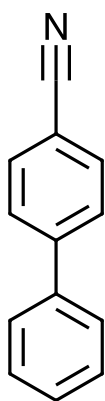
**5-(3,4-Dimethoxyphenyl)-2-furoic acid (2.8) ..... 64**



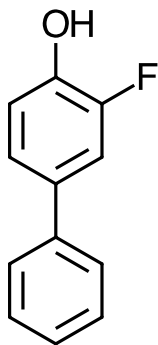
**2,5-Bis(3,4-dimethoxyphenyl)thiophene (2.9)..... 65**



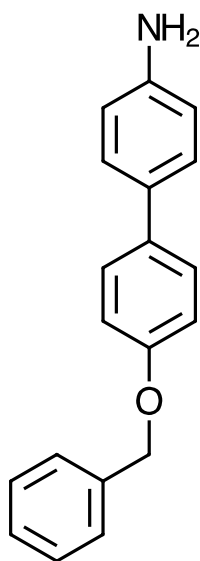
**4-Biphenylcarbaldehyde (2.10)..... 66**



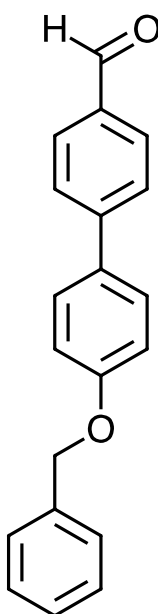
**4-Biphenylcarbonitrile (2.11) ..... 67**



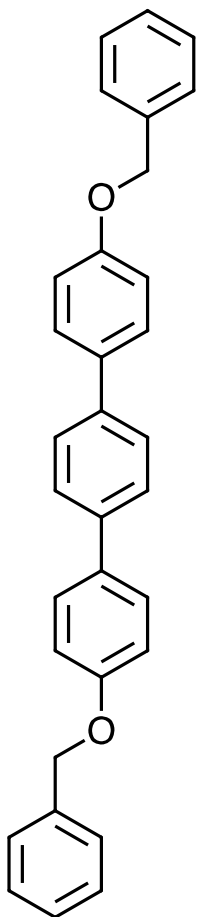
**2-Fluoro-4-biphenylol (2.12)..... 67**



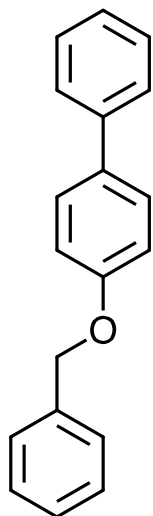
**4'-(Benzyloxy)-4-biphenylamine (2.14)..... 68**



**4'-(Benzyloxy)-4-biphenylcarbaldehyde (2.15)..... 69**

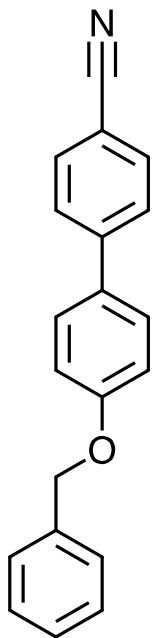


**4,4'-Bis(benzyloxy)-1,1':4'', 1''-terphenyl (2.16) ..... 70**

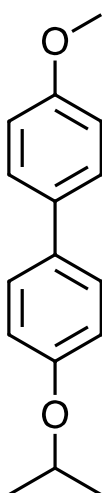


**4-(Biphenyloxy)phenylmethane (2.17) ..... 71**

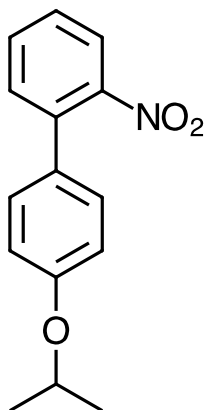


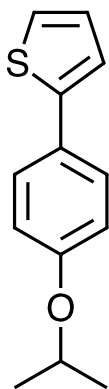


4'-(Benzyloxy)-4-biphenylcarbonitrile (2.18) ..... 72

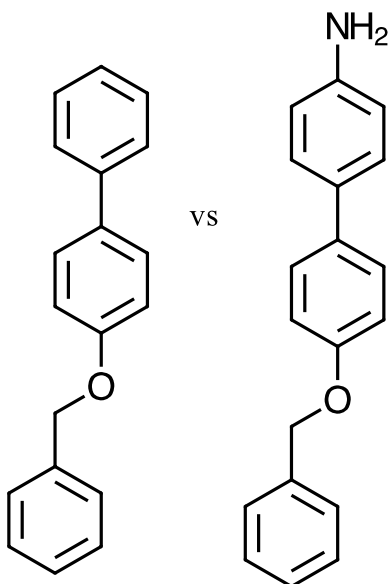


4-Isopropoxy-4'-methoxybiphenyl (2.20) ..... 73



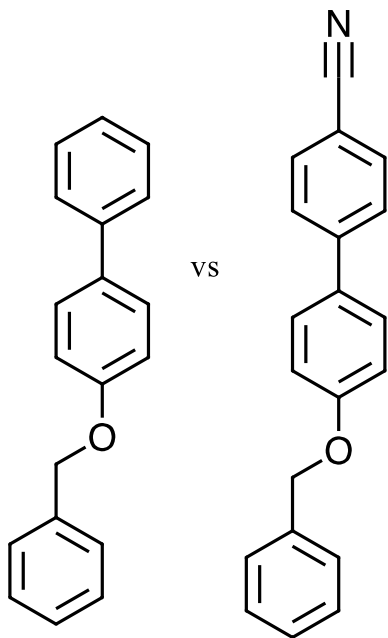


**2-(*p*-Isopropoxyphenyl) thiophene (2.22) ..... 75**



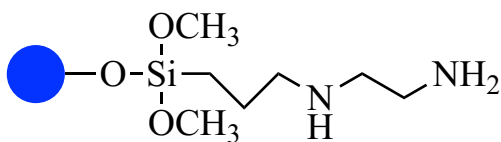
**4-(Benzyloxy)-1,1'-biphenyl vs 4'-(Benzyloxy)-4'-**

**biphenylamine (P2.18 vs P2.9) ..... 76**



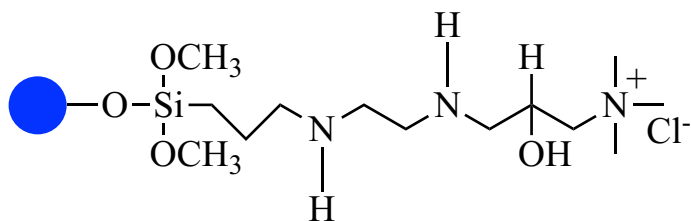
4-(Benzyloxy)-1,1'-biphenyl vs 4'-(Benzyloxy)-4-

biphenylcarbonitrile (P2.18 vs P2.19)..... 77



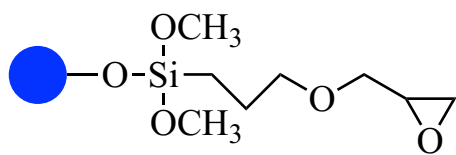
Silica gel and N-[3-(Trimethoxysilyl)propyl]

ethylenediamine (2) ..... 110



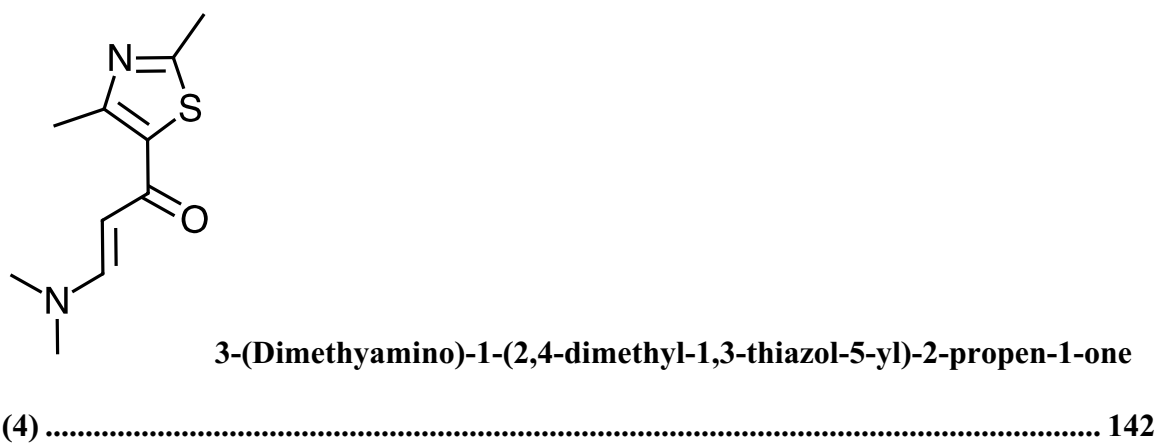
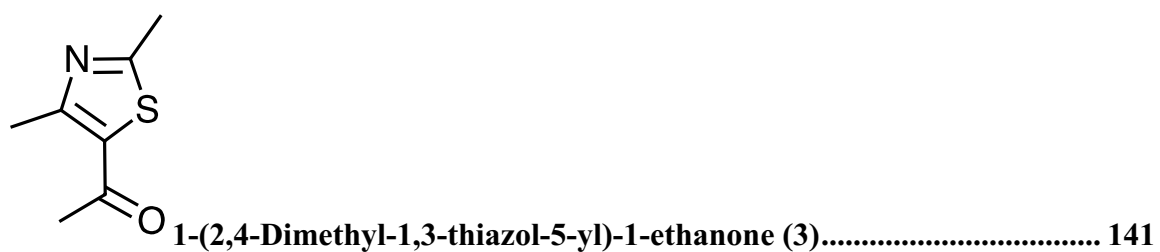
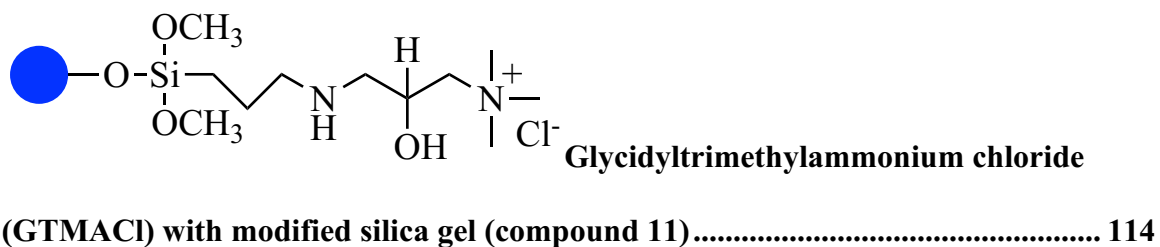
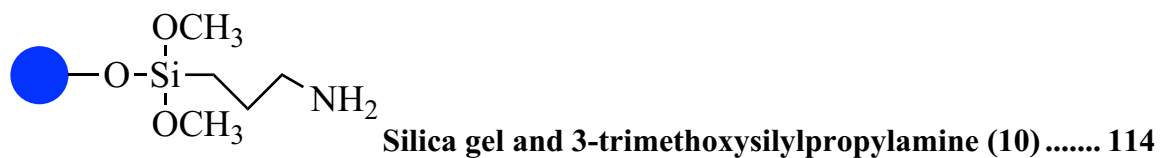
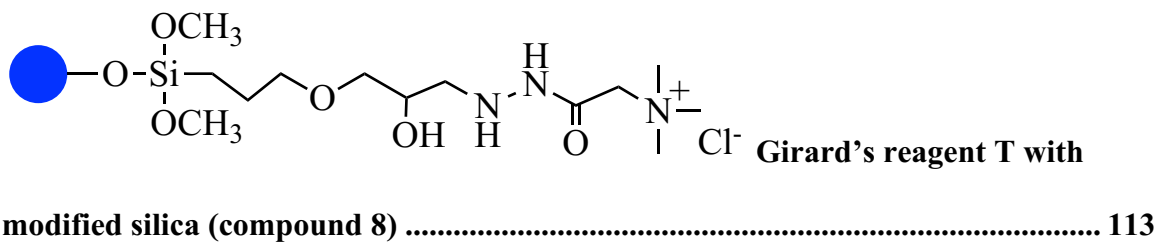
Glycidyltrimethylammonium

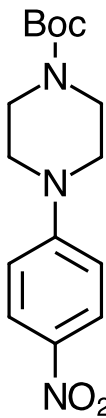
chloride (3) with modified silica gel (compound 4) ..... 111



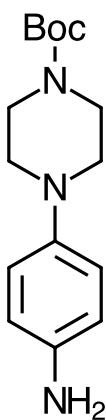
Silica gel with (3-Glycidyloxypropyl)

trimethoxysilane (6)..... 112

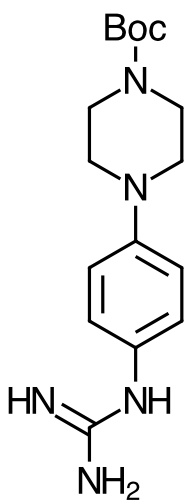




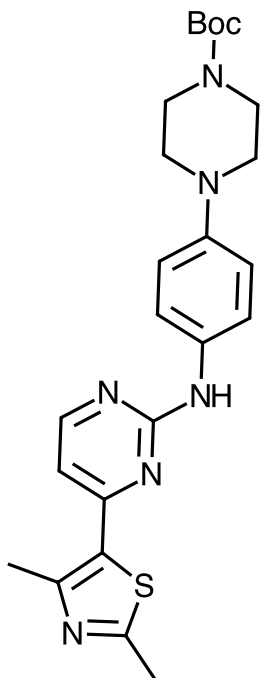
*Tert-butyl-4-(p-nitrophenyl)-1-piperazinecarboxylate (7) ..... 142*



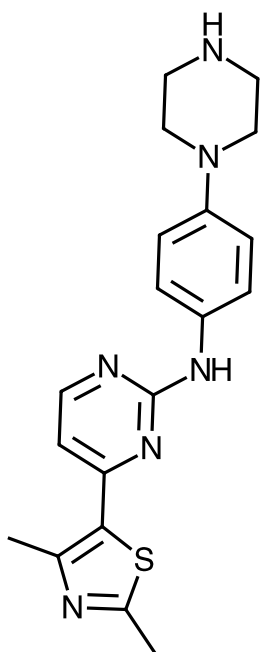
*Tert-butyl-4-(p-aminophenyl)-1-piperazinecarboxylate (8) ..... 143*



*Tert-butyl-4-(p-guanidinophenyl)-1-piperazinecarboxylate (9) ..... 144*



*Tert*-buty-4-(*p*-[4-(2,4-dimethyl-1,3-thiazol-5-yl)-2-pyrimidinylamino] phenyl)-1-piperazinecarboxylate (10) ..... 146



*Tert*-buty-4-(*p*-[4-(2,4-dimethyl-1,3-thiazol-5-yl)-2-pyrimidinylamino] phenyl)-1-piperazinecarboxylate (11) ..... 147

## List of Abbreviations

$^1\text{H}$ NMR	Hydrogen NMR
$^{13}\text{C}$ NMR	Carbon 13 NMR
AML	acute myeloid leukemia
Ar-F	Aryl fluoride
Ar-X	Aryl halide
ArF	Aryl fluoride
ATP	ATP Adenosine triphosphate
AURK	Aurora kinases K
AURKA	Aurora kinases A
AURKB	Aurora kinases B
BINAP	2,2'-Bis(dphenylphosphino)-1,1'binaphthyl)
Boc	<i>Tert</i> -butyloxycarbonyl
Calc.	Calculated
$^{\circ}\text{C}$	Degree celsius
$\text{CDCl}_3$	Chloroform D
CYC-116.	[4-(2-amino-4-methyl-1,3-thiazol-5-yl)-N-[4-(morpholin-4-yl)phenyl] pyrimidin-2-amine]
DFT	Density functional theory
DMF	dimethylformamide
DMF-DMA	<i>N,N</i> -dimethylformamide dimethyl acetal
DMSO	Dimethyl sulfoxide
DNA	Deoxyribonucleic acid

DPEphos	Bis[(2-diphenylphosphino)phenyl] ether
dppe	1,2-Bis(diphenylphosphino)ethane
EDG	Electron-donating group.
Equiv	Equivalence
EWG	Electron-withdrawing group.
FDG	Fluorodeoxyglucose
FET	Fuoroethyltosylate
FT-IR	Fourier transform infra-red spectroscopy.
g	Gram
GBq	Gigabecquerel
GOPTS	3-Glycidoxypropyl)trimethoxysilane
GTMACl	Glycidyltrimethylammonium chloride
GTPases	Guanosine triphosphate
H <sub>2</sub> O	Water
HEU	Highly enriched uranium
HIV	Human immunodeficiency virus
HOMO	Highest-occupied molecular orbital
Hz	Hertz
ICP	Inductively coupled plasma.
ICP-AES	Inductively coupled plasma atomic emission spectroscopy.
J	Coupling Constant
K <sub>222</sub>	Kryptofix-222
KF	Potassium fluoride



LEDs	light-emitting diodes
LUMO	Lowest-unoccupied molecular orbital
MBq	Megabecquerel
MeOH	Methanol
MePhTz	Methyl phenyl thiazole
MeV	Mega electron volts
Mg	Milligram
MgSO <sub>4</sub>	Magnesium sulphate
MHz	Megahertz
mL	Millilitre
mmol	Millimole
Mo	Molybdenum
mp	Melting point
MURR	Missouri University Research reactor
NaTcO <sub>4</sub>	Sodium pertechnetate
NIH3T3	Fibroblast cell line
NMR	Nuclear magnetic resonance
OAc	Acetate
OH	Hydroxide
Pd	Palladium
PET	Positron emission tomography
PIN	Prostatic intraepithelial neoplasia
QMA	Quaternary methyl ammonium

RNA	Ribonucleic acid
SAR	Structure activity relationship
SEM	Scanning electron microscopy
Si-OH	Silanol
SiO <sub>2</sub>	Silicon dioxide
S <sub>N</sub> 2	Substitution nucleophilic bimolecular
S <sub>N</sub> Ar	Nucleophilic aromatic substitution
Spec	Spectrometer
STK-15	Serine/Threonine kinase-15
tBuBrettPhos	[3,6-Dimethoxy-2',4',6'-tris(1-methylethyl)[1,1'-biphenyl]-2-yl]bis(1,1 dimethylethyl)phosphine
Tc	Technetium
<sup>99m</sup> Tc	Technetium 99m
TcO <sub>4</sub> <sup>-</sup>	Pertechnetate anion
TEOS	Tetraethyl orthosilicate
THMD	2,2,6,6-tetramethyl-3,5-heptanedione
TFA	Trifluoroacetic acid
TLC	Thin layer chromatography
TMS	Tetramethylsilane
TMSPED	Trimethoxysilylpropyl ethylenediamine

# **Chapter 1-Introduction**

## **1.1 Overall Theme of the Thesis**

Three projects have been completed over the course of this thesis. It covers three different but related topics. The first project looks at the design and synthesis of novel transition metal ligands and the effect they have on cross-coupling reactions, specifically Suzuki-Miyaura cross-coupling. The second looks into the preparation and testing of solid support resins that allow high loading and selectivity in  $^{99}\text{Mo}/^{99\text{m}}\text{Tc}$  radioisotope generators. The final topic looks at the synthesis of a common intermediate which could be functionalized to create other analogues as well as being radiolabeled for F-18 compounds in the study of aurora kinase inhibitors.

### **1.1.1 Specific Goals of the Thesis**

Practical uses for metal-organic species cover a vast range of applications, united by some design elements common to both industrial and biological uses (and everything in between). Specifically, modifying the organic ligand's steric size and electronics in order to tune the reactivity at the metal is central to original research in this area. This thesis will first explore thiazole-containing organics for synthesis (as ligands in a Suzuki catalyst) (Figure 1.1); this coupling reaction is common in industrial polymer, materials, pharmaceutical and medicinal chemistry. A second project in this thesis, is exclusively in the medical domain and involves designing an inorganic support resin used as a radioisotope generator to allow for use of low specific activity Mo/Tc-99m generators as seen in Figure 1.2. The third project is also in the medical domain and incorporates thiazole

chemistry, this time in the synthesis of aurora kinase inhibitors for cancer research (Figure 1.3).

In order to appreciate the choices of targets, it is necessary to review the general nature of organometallic compounds and their ligands, specifically their use in medicinal chemistry. Some background on the history and current uses of the thiazole ring will also be covered, along with a justification for its further study in this thesis.

### 1.1.1.1 Tuning the Electronics in Suzuki- Miyaura Cross-Coupling Reactions Using Thiazole-Based Ligands.

The goal of this project is to synthesize thiazole-based ligands and see how the changes made will affect the Suzuki cross-coupling reaction. Two ligands were synthesized, one containing a methyl and the other an amine. The amine (NH<sub>2</sub>) puts more electron density on the thiazole ring and consequently adds electron density to the palladium. The reactivity was tuned to see how the changes made affects the selectivity of the Suzuki cross-coupling reactions.

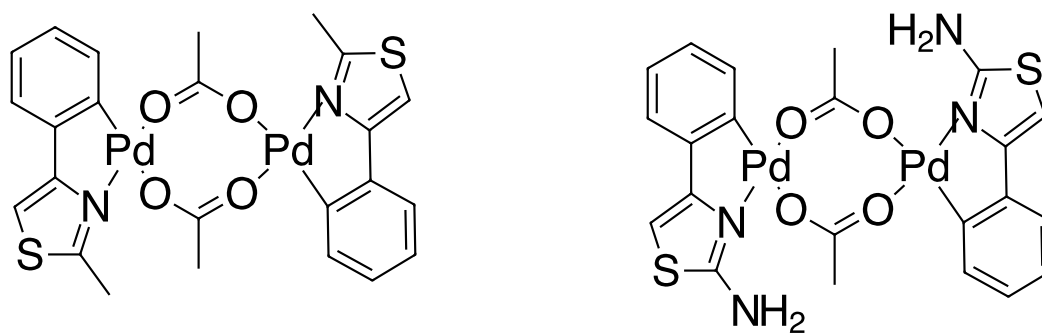


**Figure 1.1: Synthesized thiazole-based ligands (catalyst)**

### 1.1.1.2 The Development of a New High-Capacity Solid Support Resins for Use in Mo/Tc-99m Generators

The principal goal of this project is to develop new high-capacity solid support resins for use in Mo/Tc-99m generators. These resins will permit higher loading capacity allowing for the use of low specific activity (the activity per quantity of atoms of a particular radionuclide) Mo-99 when prepared from non-uranium-based processes. The resin prepared had high loading and selectivity for molybdate and releases pertechnetate.

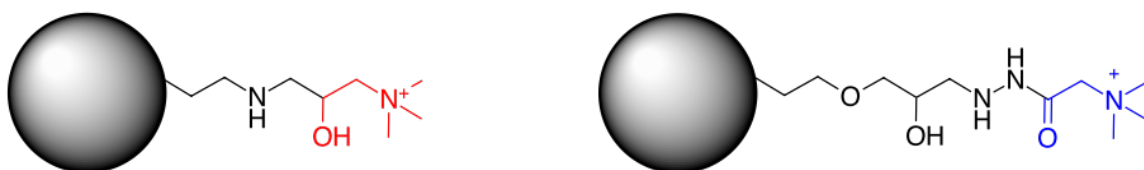


Figure 1.2: Some synthesised resins for Mo/Tc-99m generators

### 1.1.1.3 Studies Towards Aurora Kinase Inhibition for PET imaging

The goal of this project is to develop imaging agents that are selective for aurora kinase to develop a synthetic strategy that allows for easy diversification and structure activity relationship (SAR) analysis.

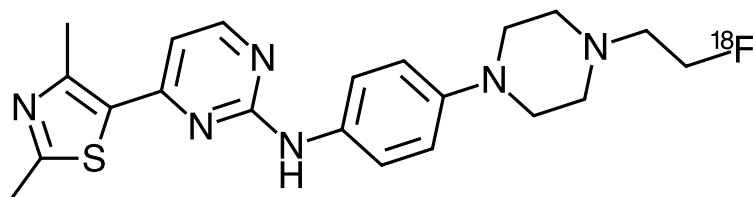
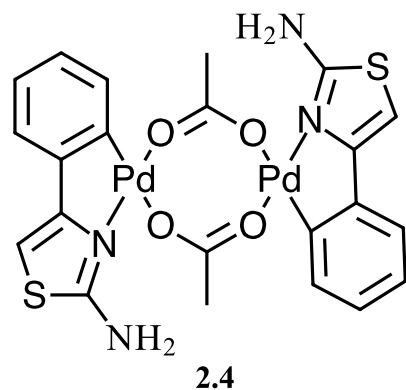
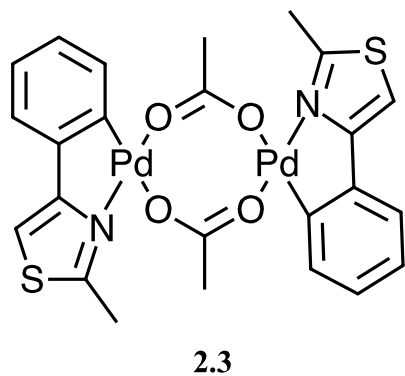


Figure 1.3: Proposed imaging agent for aurora kinase

## Chapter 2- Tuning the Electronics in Suzuki-Miyaura Cross-Coupling Reactions Using Thiazole-Based Ligands.

### 2.0 Summary:

Two organometallic palladium complexes **2.3** and **2.4**, bearing either the 2-methyl-4-phenyl-1,3-thiazole or the 4-phenyl-1,3-thiazol-4-ylamine ligand respectively were synthesized and characterized using NMR, mass spectrometry, IR, and X-ray crystallography. These catalysts were evaluated for their activity in the Suzuki-Miyaura coupling reaction. Specifically, various substituents on the haloaryl substrate, from electron-withdrawing to electron-donating, were investigated to see their influence on the efficacy of the coupling reaction (in overall yield and relative reaction rate). Several aryl halides and different boronic acid pairs were studied yielding a conversion between 27-97 % (isolated yield) using 5 mol % of each palladium catalyst used at 60 °C after 8 hours. The relative rates of electron-rich aryl halides were faster than for electron-poor aryl halides (EDG > EWG) for catalyst **2.3** (methyl-substituted thiazole ligand). On the other hand, the rates for electron-poor aryl halides were faster (EWG > EDG) for catalyst **2.4** (amine-substituted thiazole ligand) was used. The former behavior is unique in Suzuki-Miyaura coupling reactions (as there is a shift towards the electron-donating group), which makes catalyst **2.3** a useful addition to the family of Suzuki-Miyaura catalytic systems.



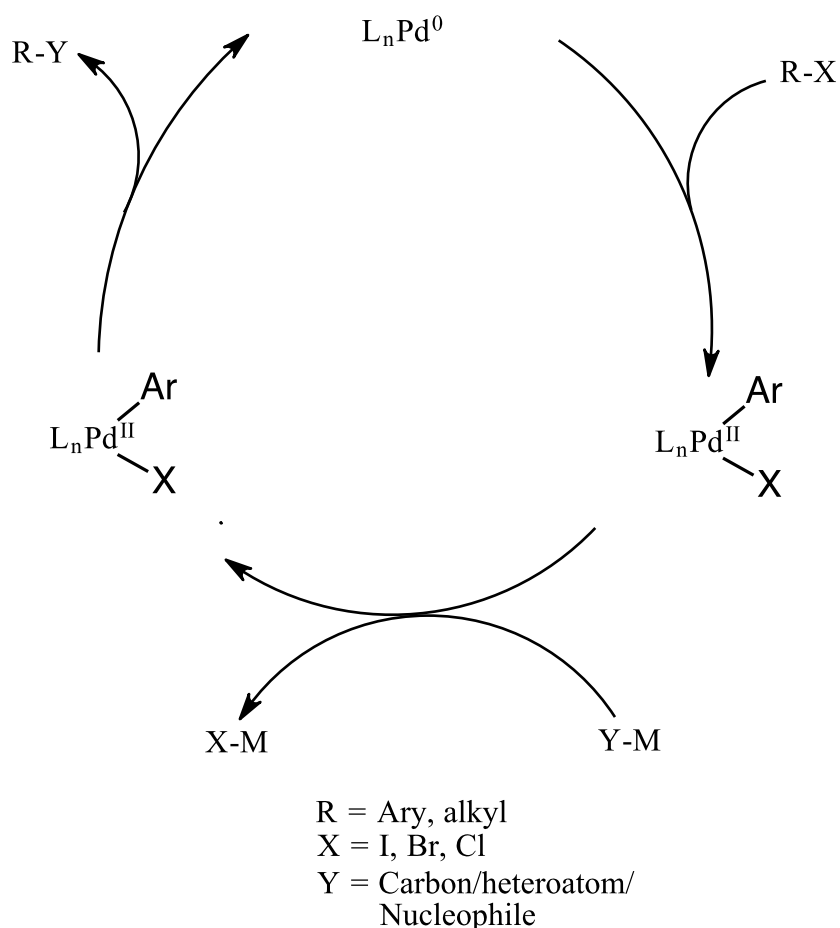
## 2.1 Introduction

Coordination compounds are complexes that contain a central metal atom or ions surrounded by ions or electron-rich molecules, which are called ligands. Organometallic compounds have a metal(s)-carbon bond between the metal and at least one ligand.

This chapter of the thesis investigates thiazole-based ligands as an alternative to pyridine-based ligands (pyridine is often used as a nitrogen donor). A couple of these thiazole-containing ligands were synthesized and attached to palladium. The resulting organometallic compounds were found to catalyze Suzuki-Miyaura cross-coupling reactions. Two thiazole-based ligands were synthesized, the difference being that one has a methyl (**2.3**) and the other has an amino substituent (**2.4**). The amino substituent puts more electron density on the thiazole ring and consequently adds electron density onto the palladium metal. It is envisaged that the changes made on the ligand will affect the selectivity of the Suzuki-Miyaura cross-coupling reactions.

## 2.2 Literature Review

Palladium-catalyzed coupling reactions such as Stille, Kumada, Negishi, Buchwald-Hartwig amination and Suzuki-Miyaura are of great importance to synthetic chemists. A common characteristic of these catalytic reactions is the formation of an alkyl or an aryl palladium(II) intermediate which is functionalized to form a carbon-carbon or carbon-heteroatom bond as shown in Scheme 2.1 below.

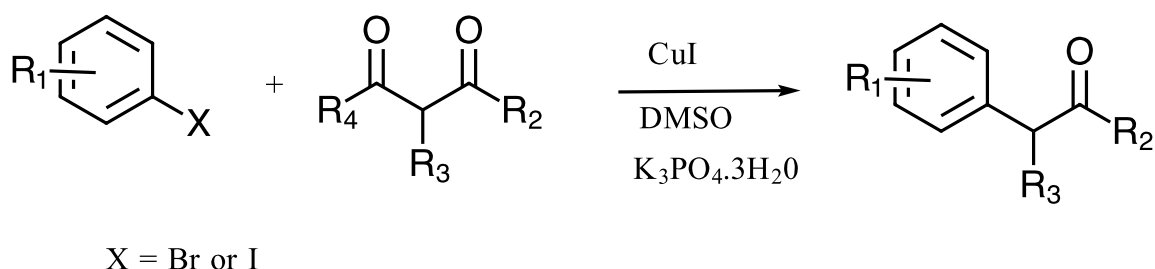


**Scheme 2.1 Palladium(II) catalyzed reactions of aryl/alkyl halides.<sup>1</sup>**

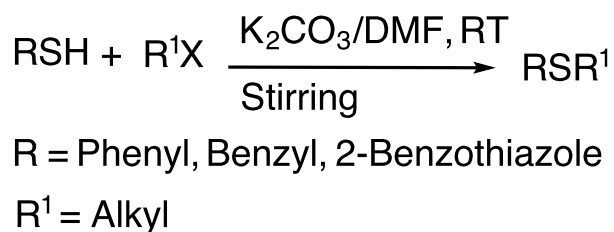
The Suzuki-Miyaura cross-coupling reaction dates to 1979 when Suzuki reported the coupling of organohalides with vinylboranes or (arylhalides and arylboronic acids). It



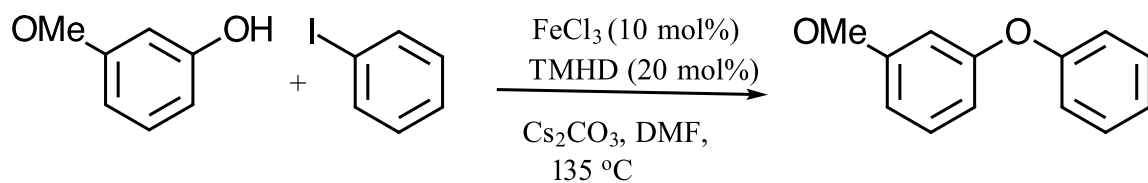
is a versatile and powerful transition metal-catalyzed reaction leading to a new carbon-carbon, i.e. (C<sub>aryl</sub>-C<sub>aryl</sub>), (C<sub>aryl</sub>-C<sub>alkyl</sub>), or carbon-heteroatom bond as shown in Schemes 2.2 to 2.4 below.<sup>2,3,4,5,6</sup> Suzuki cross-coupling reactions have certain advantages relative to other cross-coupling reactions by overcoming problems inherent in the other methods, for example, the toxicity of the organotin reagents in the Stille system, or the air-sensitivity of the Grignard and Negishi couplings. The boronic acids used in Suzuki systems are stable in the presence of base and the reactions can even take place in water as the solvent. This makes them more stable to air and water than Grignard or Negishi reagents, and they do not use the toxic organotin compounds that are required for the Stille reaction.



**Scheme 2.2: Aryl-aryl C-C bond activation using aryl halide and aryl ketone.**



**Scheme 2.3: Aryl-alkyl C-C bond formation for chemoselective alkylation of thiols<sup>7</sup>**

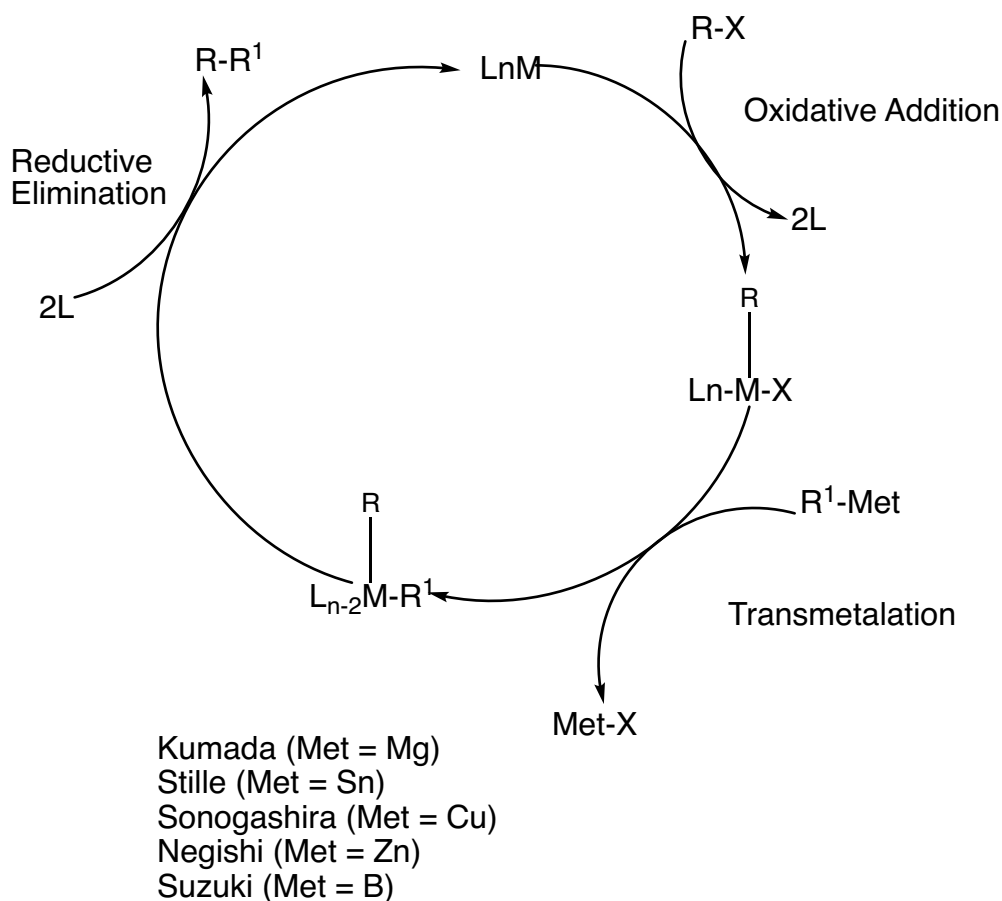


**Scheme 2.4: Carbon-heteroatom bond formation by iron-catalyzed *O*-arylation**

### 2.2.1 General Cross-Coupling Mechanism

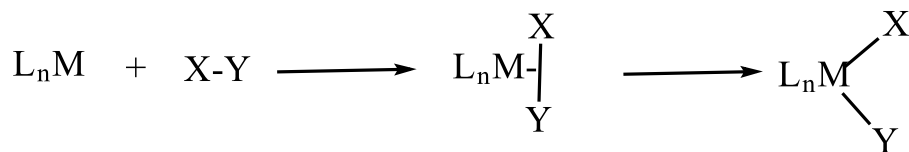
There are several common mechanistic features of these families of cross-coupling reactions which can be broken down into three key steps as shown in Scheme 2.5. Oxidative addition of the aryl halide (Ar-X) to the catalyst is the first step followed by transmetalation and then reductive elimination to generate the biaryl (R-R<sup>1</sup>) product and regenerate the catalyst. For coordinatively saturated (18-electron) complexes, prior to the oxidation addition step the catalyst dissociates one of its ligands. For example, an 18e-, *d*<sup>10</sup> Pd(0) would dissociate one of its initial ligands to form a 16e- (still *d*<sup>10</sup> Pd(0)) complex that has a vacant coordination space at the metal.

In the first step, the aryl halide (Ar-X) is added to the metal centre to generate new M-Ar and M-X bonds, which necessarily increases the formal oxidation state of the metal by +2. Oxidative addition may proceed by many different pathways depending on the substrate and the metal involved. (Schemes 2.6 to 2.9).

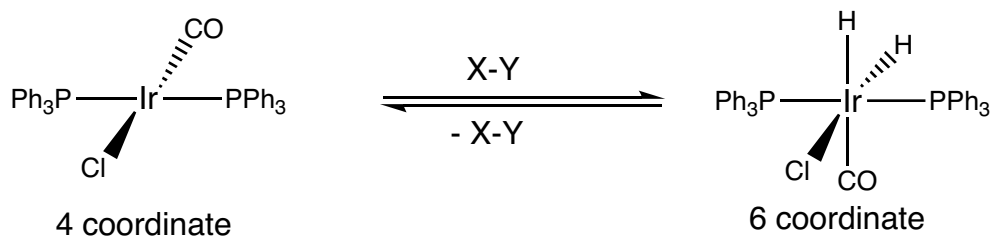


**Scheme 2.5: General mechanism of cross-coupling reactions**

The concerted pathway oxidative addition occurs when a ligand approaches the metal centre side-on resulting in activation (cleavage) of a sigma bond on the incoming ligand. The cleaved bond may be polar, as shown in Scheme 2.6, or non-polar as in the case of H<sub>2</sub> adding to Vaska's compound shown in Scheme 2.7. In this example, Iridium changes its oxidation state from +1 to +3 and its electron count increases from 16e to 18e.<sup>8</sup> The mechanism is a combination of donation of the electrons from the ligand's s-bond to the metal in concert with back-donation from the metal to the ligand's antibonding sigma\* orbital, resulting in a three-centred intermediate and ultimately two new M-R bonds and cleavage of the original ligand sigma bond.



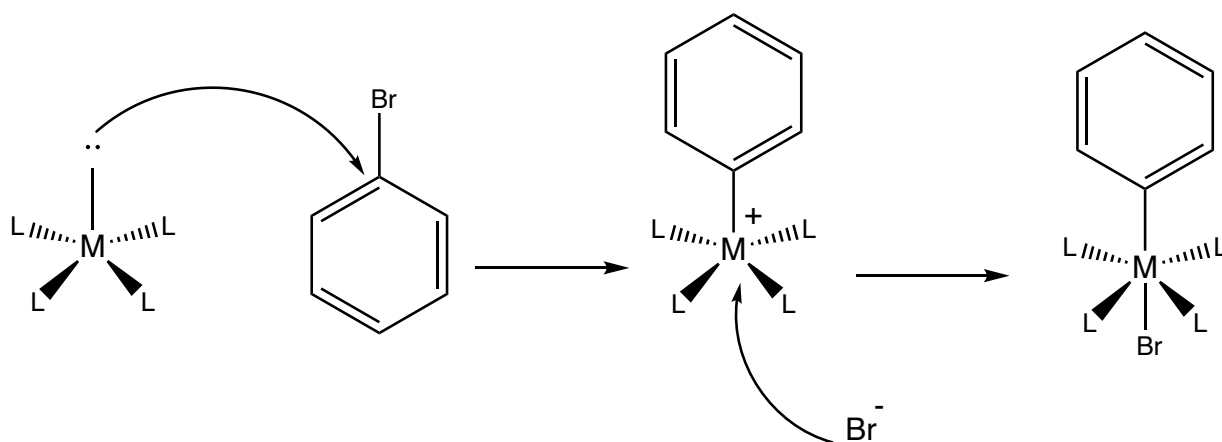
**Scheme 2.6: Concerted addition of non-polar substrate to hydrogen or hydrocarbon**



X-Y = H<sub>2</sub> as in Vaska's complex

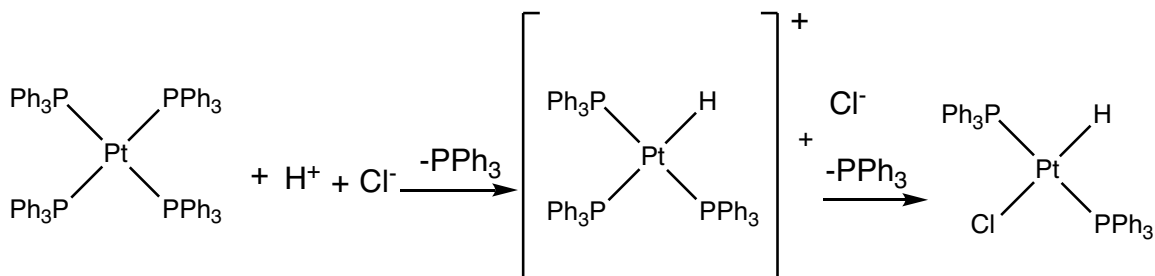
**Scheme 2.7: Concerted addition of H<sub>2</sub> with Vaska's complex**

In the nucleophilic aromatic substitution (S<sub>N</sub>Ar-type) mechanism, the oxidative addition occurs through nucleophilic attack by the metal on the less electronegative atom in the substrate which leads to the cleavage of the arylhalide bond to form an [M-R]<sup>+</sup> intermediate which results in the coordination of the anion to the cationic metal center. An example is seen in the square planar complex with bromobenzene as shown in Scheme 2.8. This mechanism often results in a *trans* addition of the Ar-X, rather than the *cis* addition seen in the concerted mechanism.



**Scheme 2.8:  $S_NAr$  type nucleophilic substitution oxidative addition.**

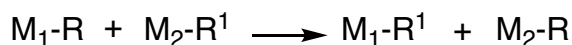
The ionic oxidative addition is like the  $S_NAr$  type of addition. In this version, the substrate must first dissociate into a cation and an anion. The two fragments then add stepwise to the metal center. An example is shown in Scheme 2.9. This also results in a *trans* addition (square planar).



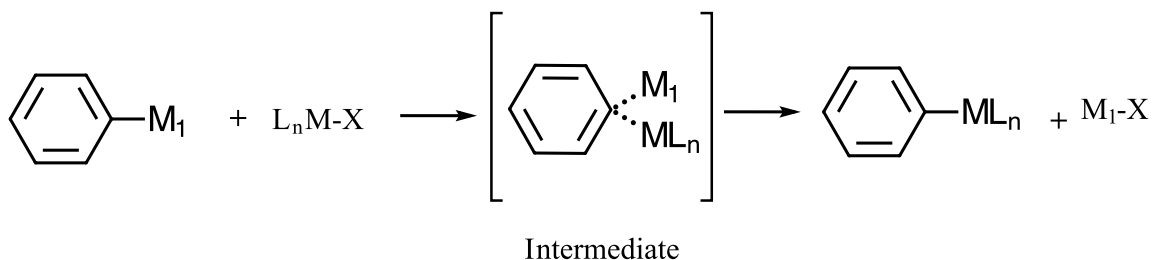
**Scheme 2.9: Ionic-type oxidative addition of hydrochloric acid.<sup>9</sup>**

Non-concerted mechanisms can also proceed by homolytic cleavage of the A-B bond, which would follow the same sort of pathway as the  $S_NAr$  or ionic mechanisms, except with radical intermediates instead of ionic ones.

Transmetalation occurs when there is a transfer of ligands from one metal to another. This often occurs by the transfer of an organic group from a main group ( $M_1-R$ ) metal to a transition metal ( $M_2-R^1$ ) where R and  $R^1$  can be aryl, alkyl, alkynyl, allyl or a halogen group as in Scheme 2.10. A typical example is seen in Scheme 2.11. Again, the process can involve a concerted transition state or proceed through ionic or radical intermediates.



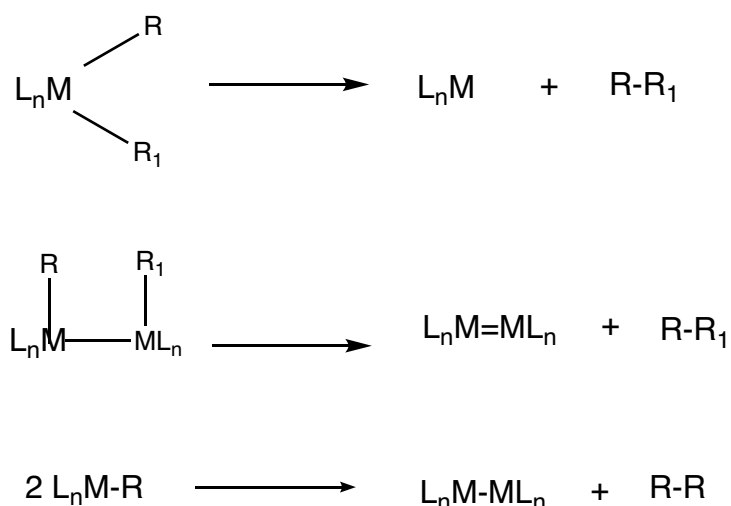
**Scheme 2.10: The transmetalation process**



**Scheme 2.11: Transmetalation leading to a complex formation.**

Reductive elimination is the reverse of oxidative addition. Reductive elimination occurs when the oxidation state of the metal decreases as the bond forms between the two ligands, resulting in the creation of the desired product. Reductive elimination can be mononuclear or binuclear. Examples are seen in  $d^6$  and  $d^8$  metals as in Pd(IV), Rh(III) and Pd(II) and Ni(II). Mononuclear elimination requires that the two organic groups be *cis* to one another. In the binuclear reductive elimination, the d-electron counts of each metal

increases by one and the oxidation state decreases by one.<sup>10</sup> The two kinds of reductive elimination are seen in Scheme 2.12.



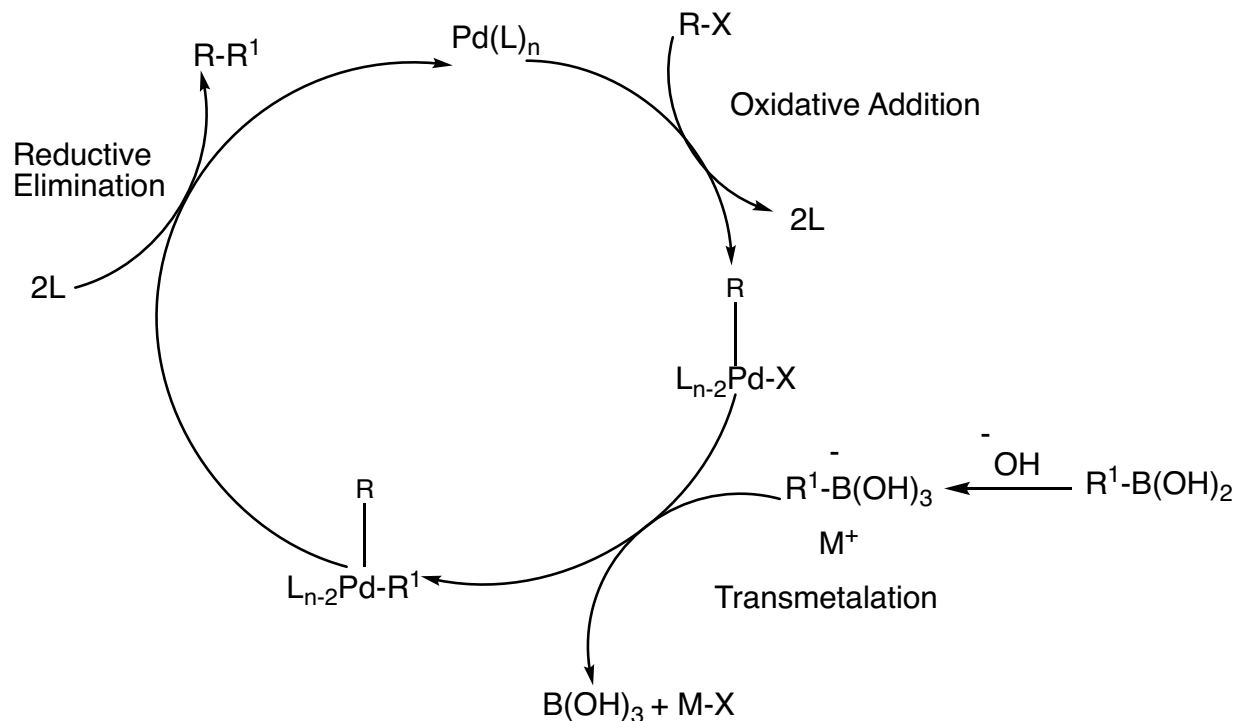
**Scheme 2.12: Mononuclear and binuclear reductive elimination reactions.**

This kind of monometallic catalytic cycle requires metals with two accessible oxidation states that differ by 2, since the oxidative addition oxidizes a metal by 2 and the reductive elimination reduces it by two. Fortunately, this requirement is met by many transition metals such as palladium(0/II/IV), rhodium(I/III), and nickel(0/II/IV).

Palladium-catalyzed reactions work particularly well and are often used in the Suzuki, Stille, etc. systems. These reactions are generally tolerant of a variety of functional groups and occur under mild conditions. The downside is that a transmetalation is required, which requires the synthesis of an organometallic reagent such as organoboron or organotin. This step may be challenging or costly. Nonetheless, the advantages of these catalytic systems often outweigh the inconvenience of the presynthetic step.

## 2.2.2 Suzuki Cross-Coupling Reaction Mechanism

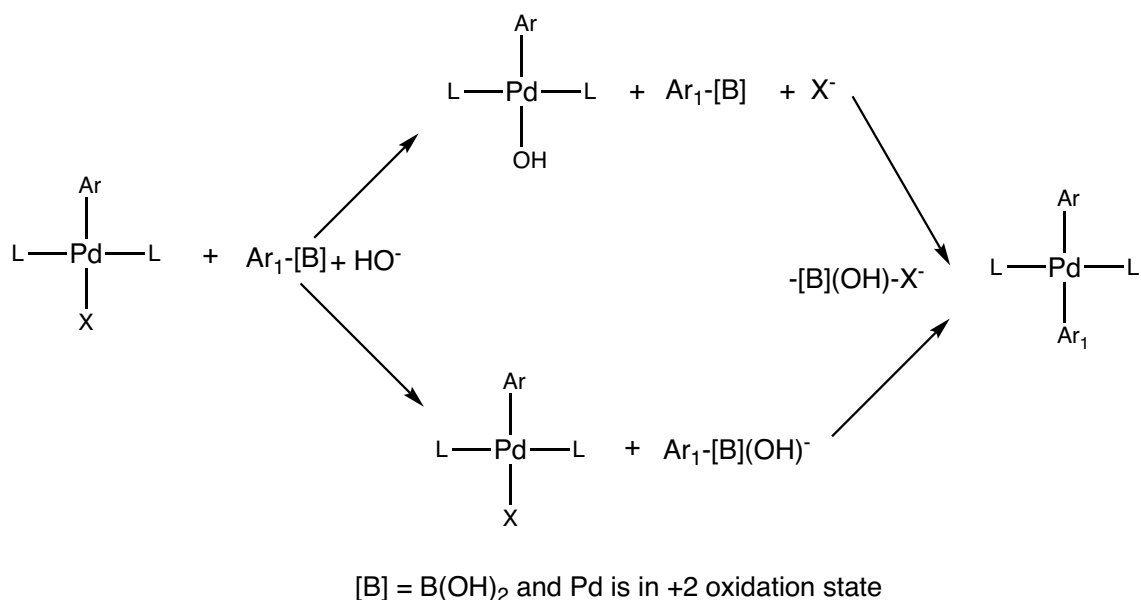
The Suzuki cross-coupling reaction is a palladium catalyzed reaction between an organo-boronic acid and an aryl halide. It is arguably the most useful method for the building of carbon-carbon bonds used in recent times in synthetic organic chemistry because of its low toxicity and its insensitivity to functional groups.<sup>11</sup> The mechanism of the Suzuki cross-coupling reaction is similar to other metal-catalyzed cross-couplings with an additional synthetic step of activating the boronic acid with a base to give the corresponding borate which aids in the polarization of the carbon boron bond (C-B bond) aiding in the transmetalation with palladium as depicted in Scheme 2.13.<sup>2,12</sup>



**Scheme 2.13: Mechanism of the Suzuki-Miyaura cross-coupling reaction**



The base is also necessary as part of the catalytic cycle mechanism. Several pathways have been proposed to account for the part played by the base in this reaction, but there is some debate as to the exact nature of its role. Two examples are given here to illustrate the potential mechanism. The first pathway is exchange of a halogen after the oxidative addition step with a nucleophile which can be the strong base used in the reaction ( $\text{OH}^-$ ). The  $\text{OH}^-$  can displace the halogen which acts as the leaving group from the metal which in turn form the intermediate shown in Scheme 2.14.<sup>13</sup> The intermediate will then react with the boronic acid through transmetalation to form  $\text{Ar-Pd-Ar}_1$  compound. In the other pathway, the base reacts with the boronic acid to form the resulting borate,  $\text{Ar-[B](OH)}^-$ , which exchanges the aryl group with the halogen group in the palladium(II) complex in the transmetalation step. The second pathway is currently considered to be more likely because of how fast the ligand exchange occurs in this pathway.<sup>14</sup>



**Scheme 2.14: Proposed pathways for explaining the role of a base in the transmetalation step in Suzuki-Miyaura reaction.**

## **2.3 Ligand Design**

### **2.3.1 Effect of the Ligands on the Resulting Properties of the Compound**

There are a limited number of metals, and the only real change possible with the same metal is its oxidation state. On the other hand, there is an infinite variability in the ligands. Indeed, the ligands chosen for the organic and medicinal compounds are not randomly chosen off the shelf, but rather they have been developed to maximize the desired properties of the metal-organic species. Therefore, ligand design is an essential part in the study of new organometallic and coordination compounds. It will lead in the discovery of new and improved metal-catalyzed reactions used in the synthesis of a broad spectrum of molecules. This section of the thesis gives an overview of the important concepts in ligand design.

#### **2.3.1.1 Electronic Effects**

The nature of the electronic linkage (bond) between the ligand and the metal depends on the relative energies of the orbitals on the ligand and the metal. In coordination chemistry, this is most easily visualized as a Lewis acid-base adduct between the empty orbitals on the positively charged metal cation (the Lewis acid) and the lone pair on the non-metal donor ligand (the Lewis base). Therefore, most coordination compounds contain donor atom(s) from groups 15 (N, P), 16 (O, S), or 17 (any of the halogens). Because of the energy difference between the metal cation and the electronegative non-metal donor atom, the lowest-unoccupied molecular orbital (LUMO) is approximated as being “entirely” based on the metal, while the highest-occupied molecular orbital (HOMO) is effectively a linear combination of the lone pairs on the ligands.

Organometallic bonding, on the other hand, forms bonds that are more closely related to shared covalent bonds, even if the two electrons forming the bond initially came from the ligand. Therefore, metal-alkyl bonds are polar covalent, akin to, for example, the bond between a carbon and a halogen like Cl, Br, or I. Because of the octet rule, metal-alkyls are strictly a  $\delta$ -bonded system. Donor atoms with multiple lone pairs can donate twice to the metal centre, assuming the metal has the correct orientation (of empty orbitals) to receive both pairs; these are called  $\pi$ -donor ligands and effectively form, *e.g.* a M=O double bond.<sup>15</sup>

Another way to form an M=C double bond arises in “ $\pi$ -acid” ligands, which themselves have a  $\pi$ -system and a lone pair. These ligands can donate electrons from their lone pair or  $\pi$ -system and in turn accept electrons from the metal into their empty  $\pi^*$  antibonding levels (Figure 2.1); examples include carbon monoxide, cyclopentadienyl, alkenes and alkynes, and vinyl ligands. The same type of back-and-forth synergistic bonding can also occur when the donor atom on the ligand is a heavy element that has access to low-lying *d*-orbitals, and also with phosphines that can accept electrons from the metal into low-lying  $\delta^*$  P-R bonds (*e.g.*, PF<sub>3</sub>).<sup>16</sup>

As a general rule, the more electron donation from the ligand, the more electron-rich the metal centre is, which makes it more amenable to oxidation. The opposite is also true - the more electron-withdrawing the ligand, the less electron density is on the metal, making it susceptible to reduction (and less amenable to oxidation).

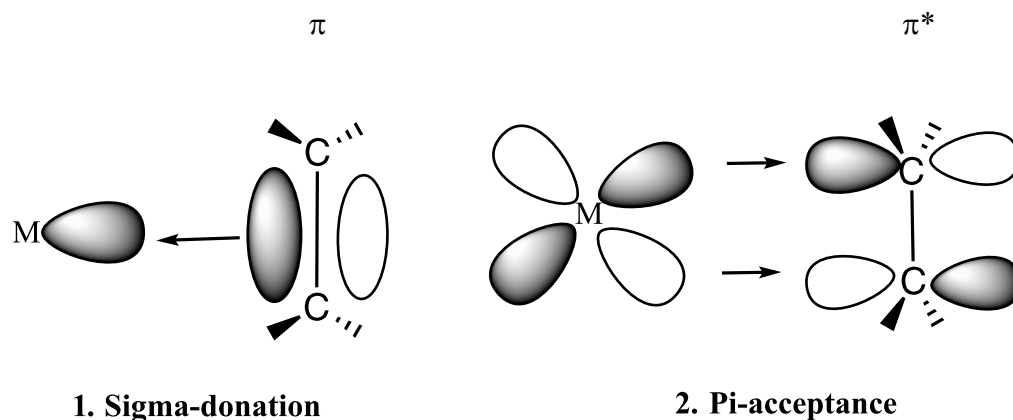


**Figure: 2.1: Example of back bonding in an organometallic complex with a ligand that donates through its  $\pi$ -system.**

### 2.3.1.2 Steric Effects

In addition to the electronic effects of the ligand on the metal, the physical size of the ligand can play a role. Steric properties describe the space a ligand occupies around the metal centre. This can affect the stability and reactivity of the metal-ligand complex by controlling access of external reactants to the metal center. One common way to change the sterics is to modify substituent groups at the ligands. For example, on an aryl group bound to a metal, *ortho*-substitution will have a greater effect on sterics than the same substituent at the *meta*- or *para*-position. Changing the substituents on an aryl, or indeed any group, will increase the overall steric coverage of the metal the closer it is physically to the metal centre.<sup>17,18</sup>

In bidentate ligands, the angle between the metal and the two donor atoms on the ligand is referred to as the bite angle. In general, the most stable complexes are obtained

when a five- or six-membered ring can form *e.g.*, when the bridge between two phosphorus donor atoms consist of two or three carbon atoms as in dppe and DPEphos.

Reported DFT calculations show that the steric bulk affects the reaction energies of addition reactions which generate six-coordinate complexes by tens of  $\text{kcal mol}^{-1}$ . The ligand steric bulk is calculated to have a reduced effect (a few  $\text{kcal mol}^{-1}$ ) on  $\text{S}_{\text{N}}2$  addition barriers, which only require access to one side of the square plane of the ligand.<sup>19, 20</sup>

One way to estimate the steric effects (or “bulk”) of a ligand in a metal complex is the Tolman cone angle illustrated in Figure 2.2. It is the angle formed with the metal at the vertex and the outermost edge of van der Waals spheres of the ligand atoms at the perimeter of the cone (usually the ligand hydrogen atoms) or substituents over all rotational orientations. This concept is often applied to phosphines. Phosphine ligands that are sterically hindered are used to create empty coordination sites ( $16e$  complex) which help to fine tune the catalytic activity in complexes. The larger cone angle usually results in faster dissociation of the phosphine ligands largely because of steric hindrance.<sup>21-23</sup>

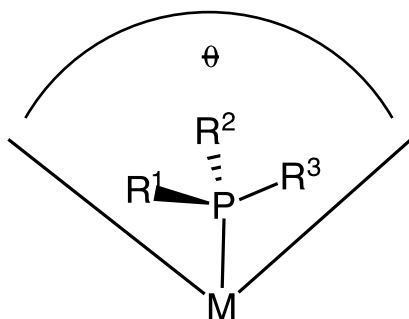


**Figure 2.2: Tolman cone angle for a monodentate ligands**

In combination, the sterics and electronics of the ligand help in controlling all aspects of reactivity of the metal centre, including *kinetic vs.* thermodynamic stabilities and the redox reactions at the metal ion.

### 2.3.2 Ligand Design in Catalytic Organometallic Chemistry

A good ligand should allow a catalyst to have high turn-over frequencies, high turn-over numbers and more importantly a good yield of a single product. Organometallic compounds are a major platform for the design of effective catalysts.<sup>24</sup> Examples include palladium-catalyzed coupling reactions such as the Suzuki reaction<sup>25</sup>, Stille reaction<sup>26</sup>, Buchwald's palladium-catalyzed amination reactions<sup>27</sup>, Heck coupling reaction<sup>28</sup>(Figure 2.3), trifluoromethylation of aryl halides or triflates using custom-made dialkylbiphenyl phosphine ligands, fluorination<sup>29</sup>, olefin metathesis, transfer hydrogenation (which can be achieved with organic molecule acting as a hydrogen donor) etc.

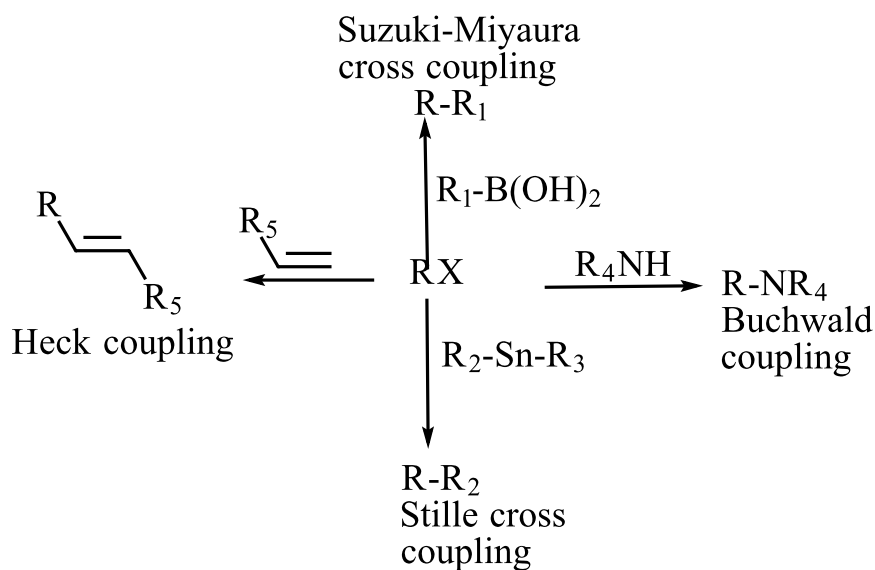


**Figure 2.3: Example of some palladium-catalyzed reactions**

Catalysts need not be complex, especially for industrial processes. Stam *et. al.*, reported of the syntheses and structural aspects of rigid arylpalladium(II) and Platinum(II) complexes by the x-ray crystal structure of *o, o*-bis[(dimethylamino)methyl]phenyl

platinum/palladium(II) bromide.<sup>36</sup> This complex was design in such a way that the halogen serves as a leaving group which can be exchanged with another substrate.<sup>30</sup>

One example of potential interest to the medical imaging community is the formation of aryl-fluoride bonds using palladium complexes of the form [LPdAr(F)] (Figure 2.4) where Ar is an aryl group, L is a biaryl monophosphine ligand, and palladium is in +2 oxidation state. These complexes can give Ar-F bonds through reductive elimination. On this basis, aryl bromides and triflates have been converted to fluorinated arenes using simple fluoride salts (cesium fluoride) which will allow the introduction of fluorine atoms into advanced and highly functionalized intermediates (Figure 2.4). [(tBuBrettPhos)Pd (Ar)F] where the Ar is 3,5-dimethylphenyl has been used for aryl amination reactions to produce aryl fluorides in good yield (where Y is a carbon, nucleophile or a heteroatom).<sup>31</sup>

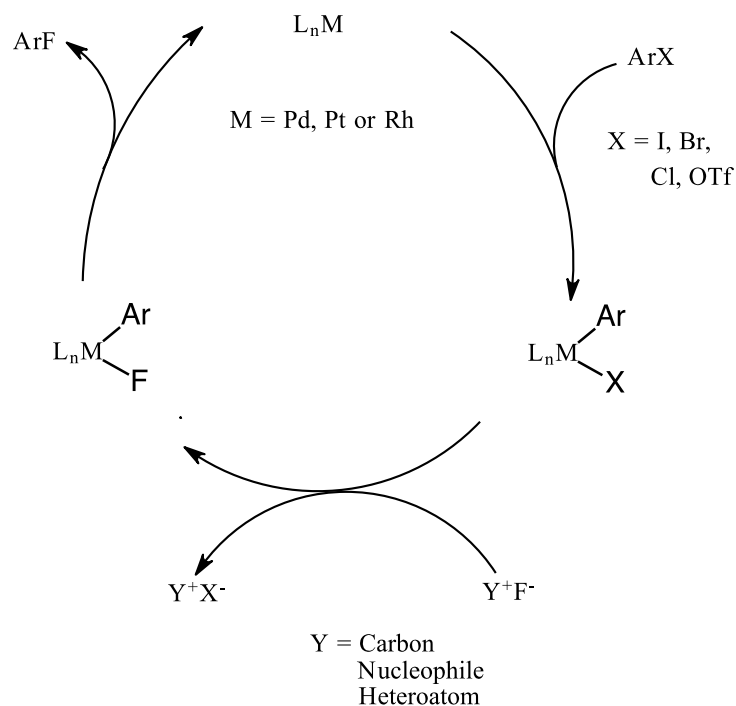


**Figure 2.4: Mechanism of metal-catalyzed aryl fluorination**

The design features of palladium-catalyzed reactions are based on the fact that palladium organometallic compounds potentially have access to three oxidation states that vary by 2 electrons each, namely the 0, 2+, and 4+ states. The 2+ oxidation state is the most stable, and complexes having this oxidation state are often stable even in ambient conditions (stable to oxygen, water, etc.). Palladium can be reduced to zero, which helps in breaking the carbon-palladium bond and is often the first step in palladium catalyzed chemistry.<sup>32</sup> Typical examples of this type of catalyzed reaction include carbon-carbon cross-coupling reaction as seen in Suzuki reactions (which is the focus of this chapter)

Although an organometallic complex must by definition contain at least one carbon-donor ligand, ligands that donate through atoms other than carbon are also present in most organometallic species and in fact are often more important functionally than the carbon-based ones. Group 15 and 16 elements such as nitrogen, phosphorus, oxygen, and sulphur have been used extensively in reactions with transition metals, which have been investigated due to their catalytic activities.<sup>33,34</sup> The nitrogen donors in oligopyridines, especially bipyridine and terpyridine, have received special attention due to their ease of syntheses and their predictable behavior in coordination chemistry.<sup>35</sup> The bidentate bipyridine ligand, commonly known as "bipy" is only one of a series of polydentate pyridine ligands, many of which can act as chelates while some act as bridging ligands.<sup>36</sup> They have been used as metal chelating ligands due to their redox stability and ease of functionality. They have stable redox properties, and the neutral forms bind readily to many metal cations.<sup>37,38</sup> This ligand has been described as the most widely used ligand of the last two decades; its role in the development and understanding of the thermodynamics and kinetics of complexation of metals cannot be overemphasized. An example is seen in the



attachment of 2 equivalents of 4-chloro carbonyl-2,2'-bipyridine on a diamine derivative of calix-4-arene for anion recognition (Figure 2.6).<sup>39,40</sup>

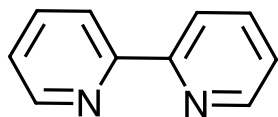


**Figure 2.5: structure of 2,2'-bipyridine**

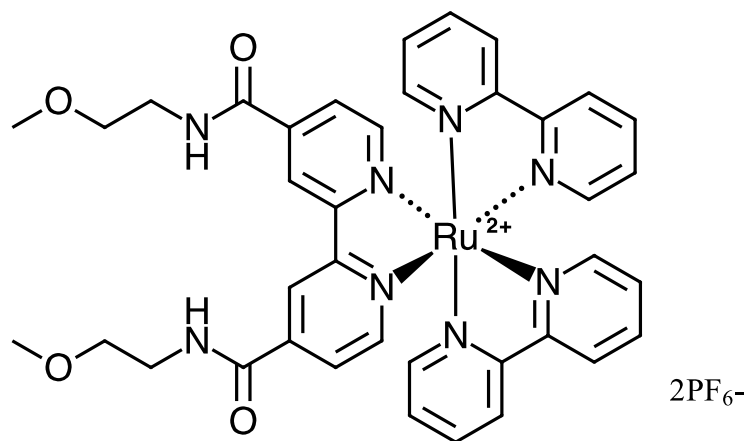


**Figure 2.6: Structure of 2,2'-bipyridine derivative for anion recognition**

## **2.4 Nitrogen Containing Aromatic Ligands Generally Used in Coordination and Organometallic Chemistry.**

Aromatic nitrogen heterocycles represent an important class of ligands in coordination chemistry. Monodentate ligands, such as pyridine, and chelating ligands, such as the aforementioned 2,2'-bipyridine (bipy) and 2,2':5',2''-terpyridine (terpy) readily form stable complexes with most transition metal ions and have been extensively used in both analytical and preparative coordination chemistry. Six-membered aromatic nitrogen

heterocycles (azines) have relatively low energy  $\pi^*$  orbitals that act as good acceptors of metal  $d$ -orbital electron density in metal-ligand back-bonding. In contrast, the  $\pi$ -excessive five-membered aromatic nitrogen heterocycles (azoles) are good  $\pi$ -donors and can also exist as anionic ligands by deprotonation of acidic N-H group in the free ligand.

There are different isomers of bipyridine which include symmetric isomers (2,2', 3,3' and the 4,4') and asymmetric isomers (*e.g.*, the 2,3', 2,4' and 3,4' isomers). 2,2'-Bipyridine and its relatives (phenanthroline, etc.), form a 5-membered C-N-M-N-C metallocycle with donation from the two nitrogen lone pairs forming bonds with the metal centre (Figure 2.7). Other isomers (Figure 2.7 and 2.8) may bridge multiple metal centres or deprotonate at the C-H alpha to the bridge position to form an organometallic C-N-M-C-C metallocycle. Examples where the bipyridine is monodentate or where it bridges two metal centres are also known. An additional coordination mode is one in which the 2,2'-bipyridine is deprotonated at C3 and the ligand functions as a C-donor or a cyclometallating C, N-donor.<sup>41</sup>

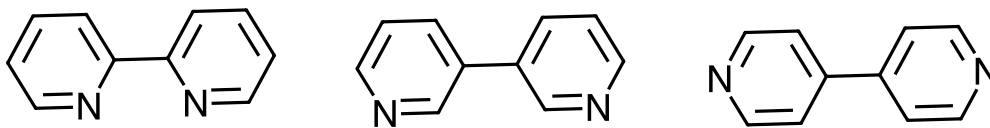


**Figure 2.7: Symmetric isomers (2,2', 3,3' and 4,4') of bipyridine**

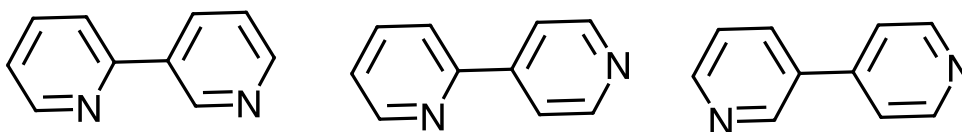


**Figure 2.8: Asymmetric isomers (2,3', 2,4' and 3,4') of bipyridine**

Some materials using oligopyridyl ligands are themselves functional materials for use in devices, such as in light-emitting diodes (LEDs). For example, neutral  $[\text{Eu}(\text{dibenzoylmethanide})_3]$  units have been used for chelating to bidentate 1,10-phenanthroline binding sites that were incorporated within photoluminescent conducting polymers which offers remarkable advantages for cascade reactions with tridentate *N*-heterocyclic ligands when incorporated into a trivalent lanthanide atom of general formula  $[\text{L}_n\text{X}_3]$  (Figure 2.9).<sup>42,43</sup>

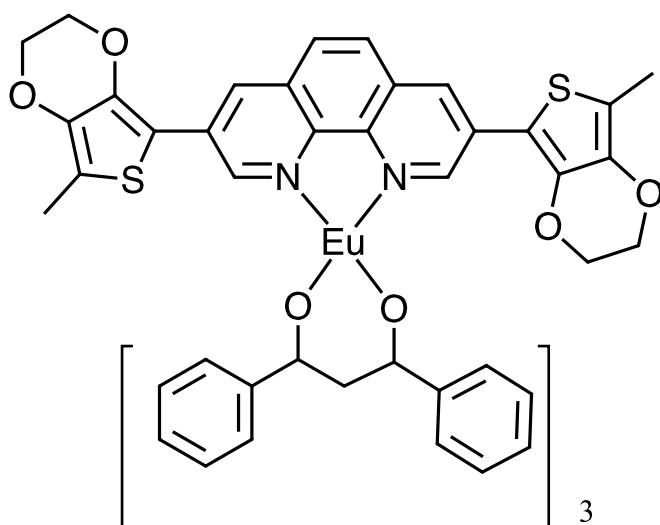


**Figure 2.9: Trivalent lanthanide atom of general formula  $[\text{L}_n\text{X}_3]$**

Linear heterocyclic aromatic compounds having various acceptor and donor spacers prepared from carbon-carbon and nitrogen bond cross-coupling have been prepared in which the nitrogen coordination sites come from imidazole, phenanthroline or pyridine. This bond formation effectively helps to extend heterocyclic aromatic systems. In addition to this, sulphur-containing ligands such as thiophene and oligothiophene compounds, produced by C-C bond cross-coupling reactions, have been extensively used in molecular

electronics because of their excellent electronic and optical properties.<sup>26,44-48</sup> The common characteristics of these class of ligands is that they have different electron-withdrawing units which bears the metal binding group (bipyridine/pyridine, imidazole, pyrazole, phenanthroline) and an electron-donating (thiophene, etc.)

#### 2.4.1 Using Thiazole in a Ligand System.

Another aromatic ring system with a nitrogen Lewis basic lone pair is the thiazole ring. It incorporates one sulfur and one nitrogen; it is a five-membered aromatic ring (because the S atom itself donates 2 electrons to the  $4n+2$  aromatic count). There are two possible isomers, where the sulfur and nitrogen are in the 1,2- and 1,3-positions. Of these, the 1,3-isomer is better known. The three carbon positions (2, 4, and 5) can undergo electrophilic aromatic substitution; unlike benzene, however, the 2- and 4-positions can undergo nucleophilic substitutions as well.<sup>49,50</sup>

In a detailed study related to the solid-state semiconducting properties of thiazoles, Usta *et al.*<sup>26</sup> reported that thiazoles have lower LUMO energies (0.2-0.3 eV) as compared to thiophenes, they have a very large dipole moment (1.61 D for thiazole and 0.52 D for thiophene), and they have non-bonded intermolecular interactions, between "N" and position -5 C-H which helps in the planarity of the compound. (Shown in Figure 2.10).

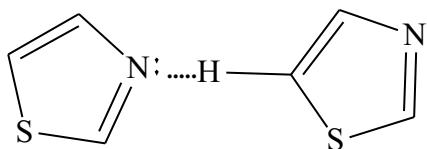


**Figure 2.10: The intermolecular N...H-C interaction between two thiazole rings**

Like pyridine, thiazole is an aromatic ring with a two-electron imine donor, so it has the potential to replace pyridine in any of the latter's ligand systems. The presence of the sulfur and the fact that it is a five-membered ring means that it will have different donor properties and bond angles. When incorporated into a polydentate ligand, these properties will result in a difference in donor strength of the ligand and a larger bite angle. The lone pair orbitals on the N of the thiazole ring can overlap with the vacant metal orbitals to produce metal-nitrogen  $\sigma$ -bonding interaction. The presence of heteroatoms in thiazole prevents the electron density to be distributed evenly over the ring and results in weaker resonance stabilization.

#### 2.4.2 Properties and Use of Thiazole

The 1,3-thiazole ring (hereafter, the 1,3-isomer will be assumed) possesses a pyridine-like N-atom and a thiophene-like S-atom. Thiazole is a five-membered ring heterocyclic compound but properties such as basicity, odour, solubility, reactivity, isosterism and resistance to electrophilic attack resembles the six-membered heteroatomic ring such as pyridine and pyrimidine and thiazole differs from the other five-membered ring such as thiophene, pyrrole, furan and selenophene. Some thiazole derivatives are stable and resist electrophilic attack unless some tunings of the properties are done on them, whereas some derivatives show the reverse.<sup>51</sup>

The  $\pi$ -system consists of four  $2p_z$  orbitals (one on each carbon and the nitrogen) and one  $3p_z$  orbital on the sulfur. The sulfur donates two electrons to the  $\pi$ -system, making this a  $\pi$ -excessive heteroaromatic system—*i.e.*, there are six  $\pi$ -electrons on only five atomic

centres. However, the excess electron density is concentrated mainly on the heteroatoms. The  $\pi$ -electron density on positions 4 and 5 would predict higher reactivity with electrophiles, but the 2-position seems to be the most reactive in some cases (nucleophilic attack) (Figure 2.11).<sup>52</sup>

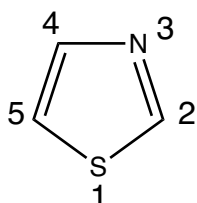


**Figure 2.11: The numbering system in thiazole**

The 2-position is also notable as it gives rise to the most stable metallated species (Figure 2.12). The 2-metallated thiazoles can be utilized for the (electrophilic) introduction of other functionalities, such as through, alkylation, halogenation, carboxylation, cyano and carbonylation.

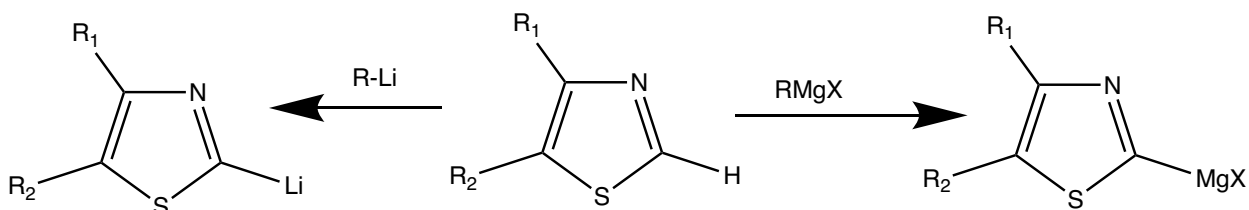


**Figure 2.12: Metalated and metal-mediated reactions of thiazole**

## 2.5. Potential Advantages of Thiazole Ligands

Thiazoles are more electron-donating than pyridine and have some synthetic advantages (greater variety of synthetic routes and milder synthetic conditions) as well as having different bond angles compared to pyridine (Figure 2.11). In bithiazole, the internal

ring angles make the coplanar *syn* conformation of the dimer more stable than that of bipyridine.<sup>53</sup> The thiazole ring contains a potential second donor atom (the sulfur) in addition to the aromatic imine donor common to both thiazole and pyridine, although the sulfur is a much weaker donor than the nitrogen. The combination of these factors (electronic and geometric) will result in a difference in donor strength of the ligand and a different bite angle (Figure 2.13). The bite angle would suggest that a larger metal centre would be required to span the chelating nitrogens and/or the M-N bond lengths would have to increase to maintain the same N-M-N angle.

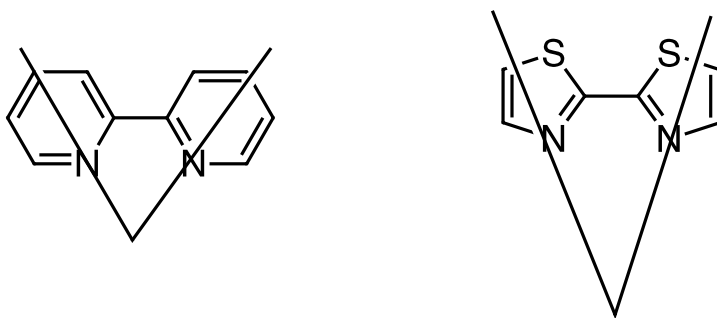


**Figure 2.13: Bond angle of bithiazole compared to bipyridine.**

For cases where a smaller physical size is required, thiazole may be a better choice than benzene, pyridine, or thiophene for drug design. This means thiazole has an advantage when incorporating a metal or an enzyme in the binding process as compared to the compounds such as benzene, pyridine or thiophene when they are used as ligands because of its smaller size. The donor ability and the lone pair (there are nominally 3 lone pairs, and as a practical matter, two are potentially available for binding to a metal - one on S and one on N) on the thiazole helps in contributing to binding to a metal.

Electronically, thiazoles are planar and aromatic, and they are characterized by having a larger  $\pi$ -electron delocalization when compared to pyridine, oxazole, or

imidazole. The  $\pi$ -electron density on positions 4 and 5 would predict higher reactivity with electrophiles, but the 2-position seems to be the most reactive in some cases (nucleophilic attack).<sup>52,77</sup>

This section will present the potential catalytic advantages of thiazole-containing scaffold ligands for metal catalysis. Below are examples of how thiazoles have been used in the literature in organometallic complexes, both as functional materials of interest in their own right or in catalytic systems.

The versatility of thiazoles is evident in how they can be modified by the introduction of a variety of substituents such as amines, carboxylic acids, phosphines etc. at position 2. Some mono- and dinuclear Pd(II) complexes with 2-amino-substituted thiazole ligands (shown in Figure 2.14, “N-N” could be phenanthroline or bipy) are promising antitumor candidates, studied for cellular uptake of palladium.

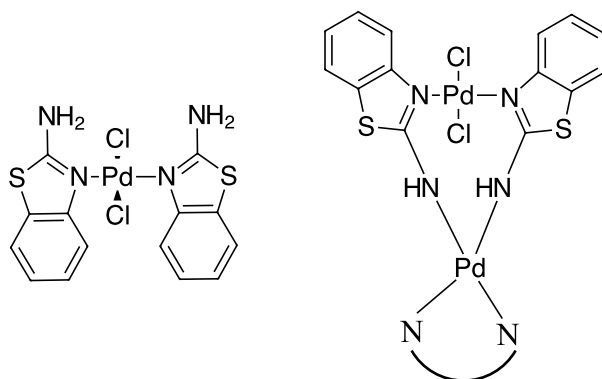


**Figure 2.14: Metal complexes possessing different substituted thiazole ligands.**

The bithiazole moiety, the thiazole equivalent of bipy can also be used to bind to metal cations. Two derivatives of bithiazole, 2,2'-bithiazole and 4,4'-bithiazole shown in Figure 2.15 share with bipy the same chelating geometry, *i.e.*, interacting with the metal through their two nitrogen atoms to form a stable 5-membered metalloheterocycles. The



difference in the N-M-N bite angle between bithiazoles and bipyridine may cause the former to have greater selectivity for specific metals e.g., large, or heavy metals such as lead or mercury. In cases where the bite angle is not an issue for making metal complexes, bipyridine and bithiazole ligands may be geometrically interchangeable (the electronics will still be different due to the presence of the electron-rich sulfur). Bithiazoles have chelating abilities, and they form stable complexes with several metal ions, which form chromophores (absorb in the visible region) and can be used in photocatalysis.<sup>54</sup>

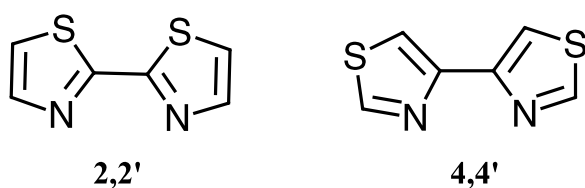


**Figure 2.15: 2,2'-bithiazole and 4,4'-bithiazole isomers of bithiazole.**

A final illustrative example of a useful family of complexes with thiazole ligands is a set of iridium phosphine thiazole complexes. A family of ligands with different-sized rings attached to position four or five of the thiazole ring have been used for the asymmetric hydrogenation of aryl alkenes and aryl alkene esters. It has been demonstrated that the ring size influences the stereochemical outcome of the desired product. When the iridium complex bearing a six membered ring is attached to the 4-5 position of the thiazole, the best results is achieved compared to when they are bonded to five or seven membered rings (Figure 2.16).<sup>55</sup>

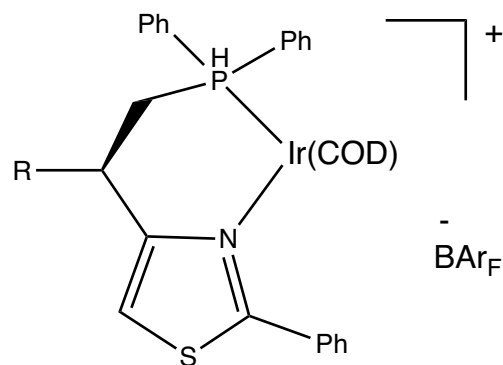


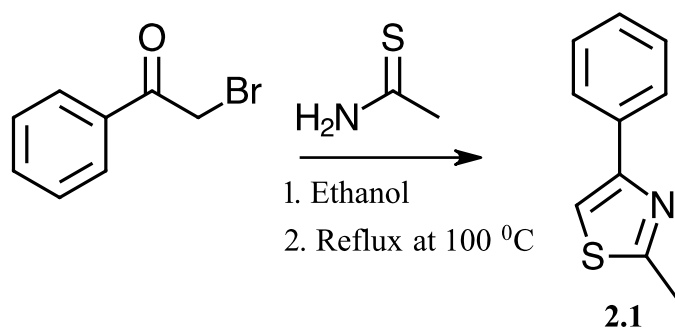
**Figure 2.16: Thiazole protected phosphine iridium complex.**

## 2.6 Results and Discussion

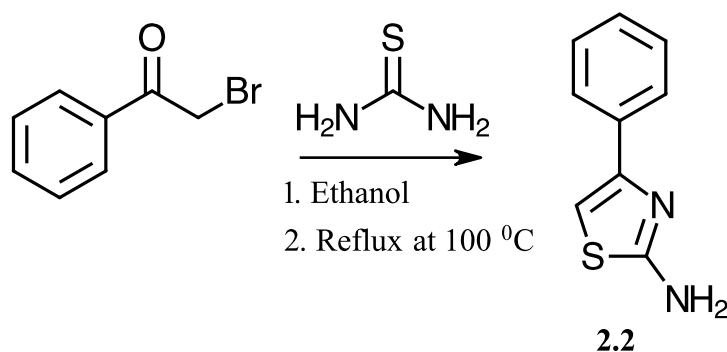
### 2.6.1 Synthesis of Thiazole Ligands

One method to synthesize the thiazole ring is through the Hantzsch condensation, wherein a 1-halo-2-ketone is reacted with a thioamide. 2-Bromoacetophenone was chosen as the halo-ketone because it is commercially available and inexpensive, and its lower volatility compared to 2-chloroacetophenone reduces the notorious lachrymatory effect of the 2-halo-ketone unit (2-chloroacetophenone was a commercially available anti-riot and chemical warfare tear gas agent only replaced because the material had long-term storage issues that reduced its effectiveness).<sup>56-58</sup> The 2-bromoacetophenone was reacted with thioacetamide or thiourea to form the title ligands 2-methyl-4-phenyl-1,3-thiazole (**2.1**) with an 84 % yield and 4-phenyl-1,3-thiazol-4-ylamine (**2.2**) with a 82 % yield as shown in Scheme 2.15 and 2.16 respectively. The range of possible R-groups that can be synthesized and tested, however this was not an exhaustive list; other R-groups tried in this thesis are discussed in section 2.9. They are not discussed further here because they did not act as ligands for palladium(II), which is the goal of this section. The difference between

**2.1** and **2.2** is the R-group at the 2-position on the ring, namely methyl (weakly donating) and amino (strongly donating) respectively. The scope of flexibility of the R-group on the bromoketone has not been fully explored but other groups have been used, including pyridine.



**Scheme 2.15: Synthesis of 2-methyl-4-phenyl-1,3-thiazole**

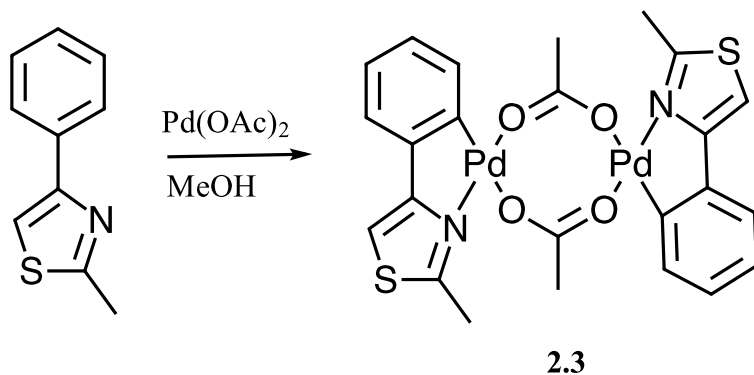


**Scheme 2.16: Synthesis of 4-phenyl-1,3-thiazol-2-ylamine**

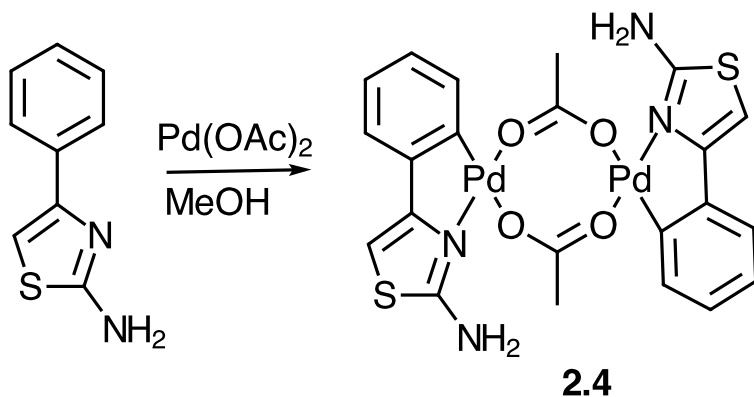
### 2.6.2 Synthesis of Palladium Complex

To prepare the palladium complexes and to confirm our hypothesis that thiazole ligands can be used as an important anchor for the metalation in heterocyclic aromatic rings, compound **2.1** or **2.2** was treated with stoichiometric amount of palladium acetate in methanol to yield the thiazole palladacycles **2.3** in 80 % yield and **2.4** in 96.4 % yield as

shown below (Schemes 2.17 and 2.18). The pyridine ligand did not form isolable organometallic products with palladium(II).



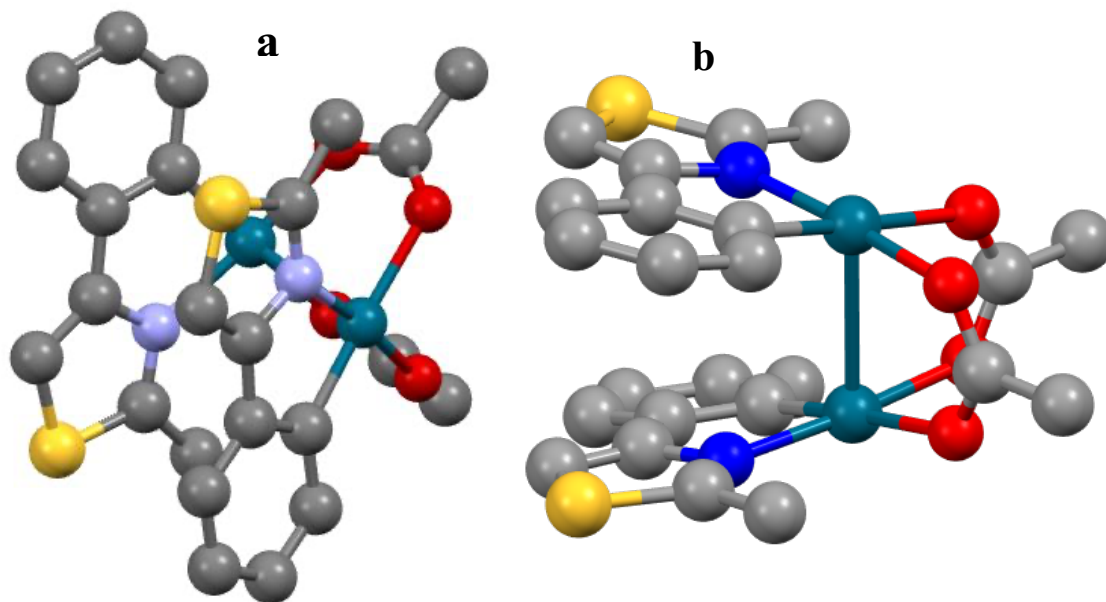
**Scheme 2.17: Synthesis of the palladium(II) complex 2.3, the dimer structure was determined by X-ray crystallography.**



**Scheme 2.18: Synthesis of palladium complex, 2.4**

### 2.6.3 Crystal Structure of Compound [(MePhTz)Pd(CH<sub>3</sub>COO)]<sub>2</sub> 2.3

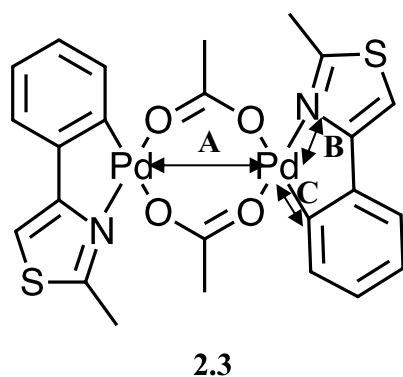
Single crystals of compound 2.3 were obtained by slow evaporation of a mixture of hexane and dichloromethane.



**Figure 2.17: Solid state crystal structure of palladium(II) dimer complex of ligand 2.3. Colour Scheme: (Sulfur atoms are yellow, oxygens are red, nitrogens are periwinkle or royal blue, palladium(II) are teal, and carbons are grey. Hydrogen atoms have been omitted for clarity. Figure b shows the Pd-Pd bond distances.**

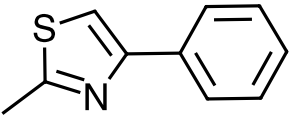
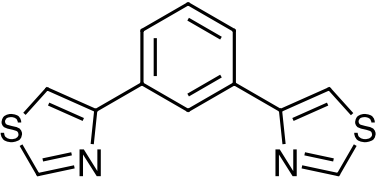
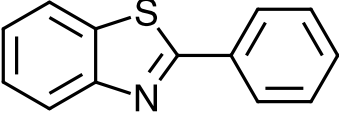
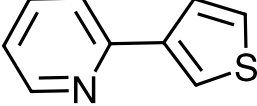
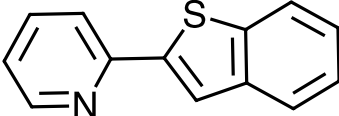
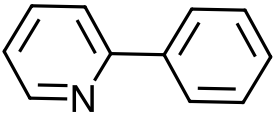
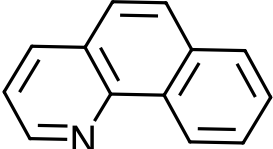
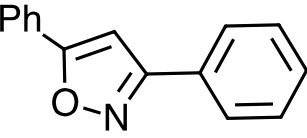
The palladium atoms in compound **2.3** are coordinated in a square-based pyramidal orientation. Ligand **2.1** is bidentate attaching through the thiazole nitrogen and the *ortho* carbon (which has lost its H). The compound crystallizes as a dimer, held together by two acetate anions each bridging the two Pd(II) centres in a  $\kappa^2O, O'$  fashion. Because the acetate ions are bridging, the atoms of the palladium are in close proximity which results in a short Pd-Pd intermolecular distance of 2.866 Å, a roughly average distance compared to comparable Pd(II) dimers with this bridging acetate moiety, which range from 2.822<sup>59</sup> to 3.044 Å<sup>60</sup> This distance is considerably longer than double the ionic radii of two Pd(II) ions<sup>61</sup> (1.280 Å for four-coordinate, 1.720 Å for six-coordinate), but considerably shorter than the sum of the Van der Waals radii of two Pd atoms (3.260 Å).<sup>62</sup>

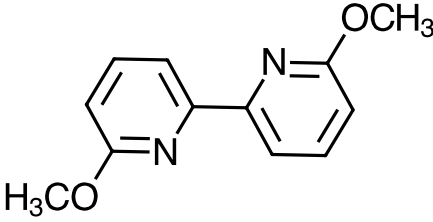
Previously studied examples of these acetate-supported dimers have ligands containing aromatic rings, usually with two or more rings that are (at least roughly) coplanar. This sets up the perfect situation for  $\pi$ -stacking between these ligand rings. Interestingly, for the two extreme cases given above, *i.e.*, the shortest and longest Pd(II)-Pd(II) distances, are not  $\pi$ -stacked. More representative examples with ligands closer to our phenylthiazole are shown in the Table 2.1, along with some comparative metrical data and some bond distances as seen in Figure 2.18.



**Figure 2.18: Measurement of Pd-Pd (A), Pd-N (B), Pd-C (C) bond distances reported in Table 2.1**

**Table 2.1: Comparative data of ligands with respect to phenythiazole.**

Ligand	A Pd(II) - Pd(II)	B Pd(II) -N	C Pd(II) -C	D ligand angle <sup>a</sup>	Ref.	Notes
	2.866	2.038, 2.040	1.962, 1.965	15.55	this work	
	---	2.030, 2.014, 2.049, 2.066	1.892, 1.881	---	<sup>11</sup>	monomer (unbridged acetate)
	2.858	2.030, 2.045	1.965, 1.969	5.2	<sup>63</sup>	
	2.857	2.023 (both)	1.941, 1.951	14.36	<sup>64</sup>	
	2.852	2.017, 2.022	1.967, 1.969	2.46	<sup>64</sup>	
	2.866, 2.896, 2.870	1.993 to 2.009	1.958 to 1.976	1.18, 9.08, 9.96	<sup>65</sup>	CF <sub>3</sub> CO <sub>2</sub> <sup>-</sup> , 3 molecules in assymmetric unit
	2.842, 2.882	1.999, 2.001	1.999, 2.001	4.20, 9.07	<sup>66</sup>	C/N disorder in bound ligands
	2.837, 2.842	1.977, 1.990, 1.991, 2.001	1.981, 1.982, 1.995, 2.004	7.45, 11.64	<sup>67</sup>	2 molecules in asymmetri c unit

	A	B	C	D		
Ligand	Pd(II) - Pd(II)	Pd(II) -N	Pd(II) -C	ligand angle <sup>a</sup>	Ref.	Notes
	2.847	2.070, 2.078	1.960, 1.948	10.59	<sup>68</sup>	

<sup>a</sup>a measure of the coplanarity of the rings, 0° is coplanar; this was measured using the Mercury software, taking the average plane of each ring, and calculating the angle between the planes.

#### 2.6.4 Catalytic Coupling Using Suzuki-Miyaura Coupling Reaction.

To probe the catalytic prowess or activity of the synthesized catalyst, several boronic acid-aryl halide pairs were reacted under Suzuki-Miyaura cross-coupling conditions. Selected combinations of the five boronic acids shown in Figure 2.19 were coupled with a variety of aryl halides. The results are summarized in Table 2.2. Products **2.5** to **2.19** were synthesized via the coupling of aryl boronic acids such as 2.24-2.28 (Figure 2.19) with aryl halides in the presence of a palladium catalyst **2.4**; the results are shown in Table 2.4. Cesium carbonate, Cs<sub>2</sub>CO<sub>3</sub> was used as the base.<sup>2,3,12,14,69,70</sup>



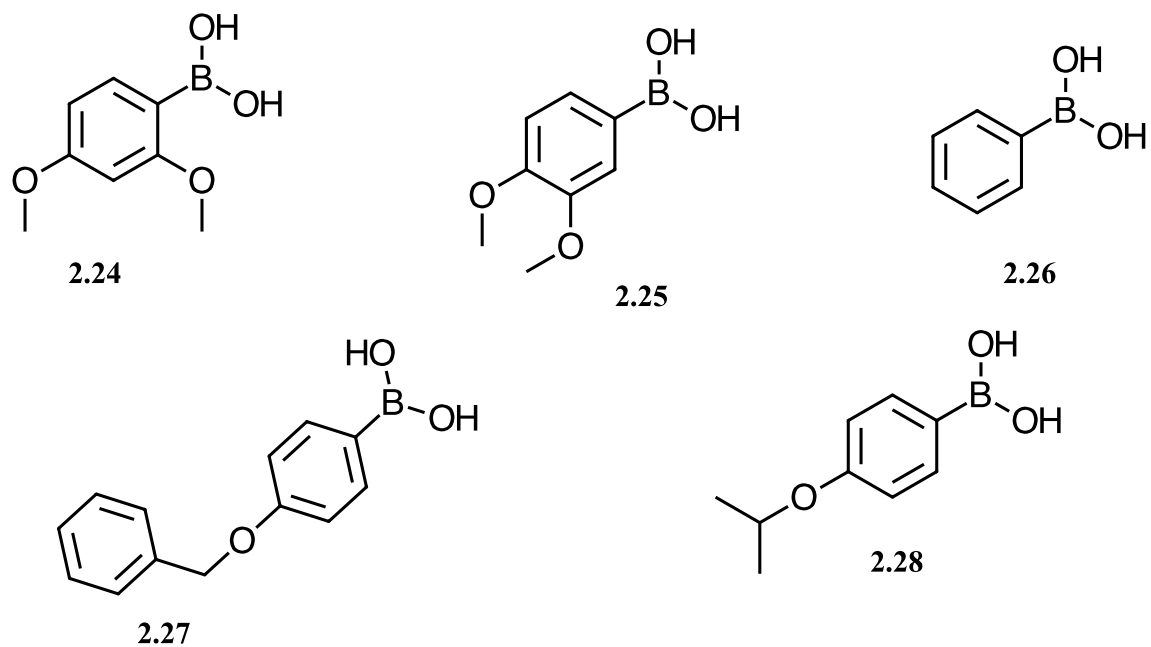
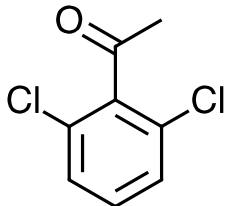
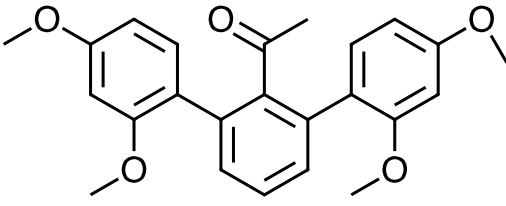
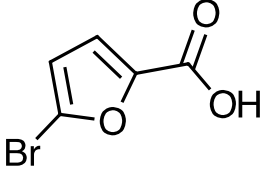
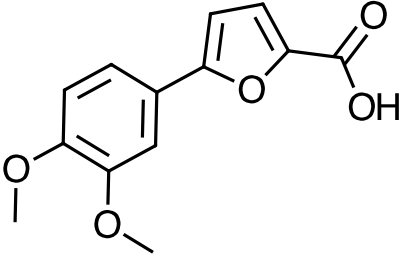
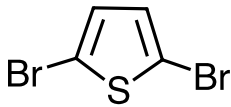
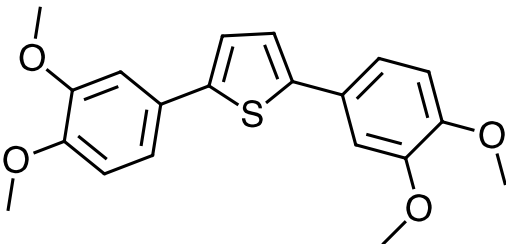
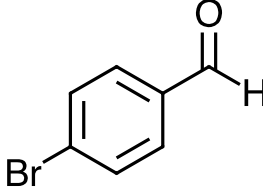
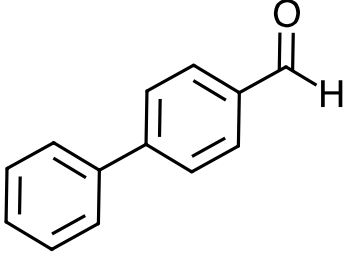
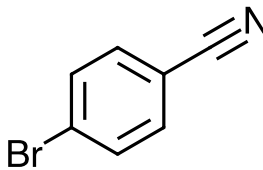
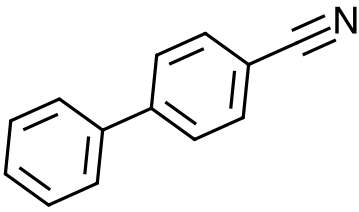
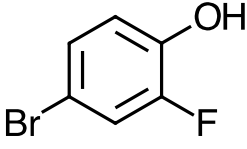
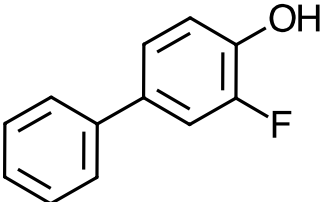
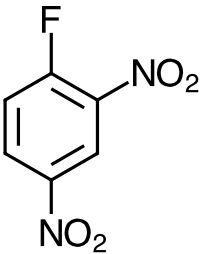
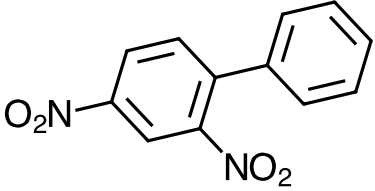
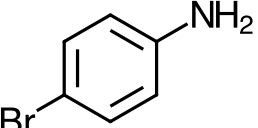
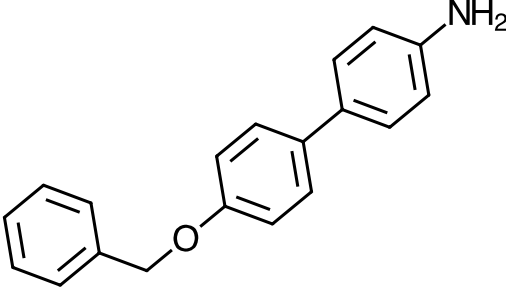
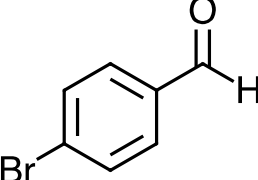
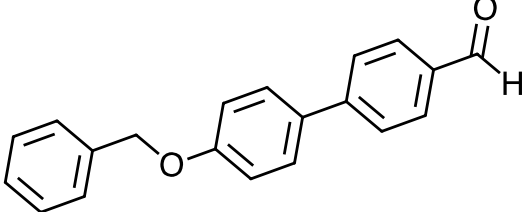
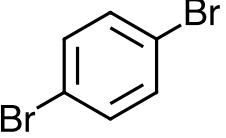
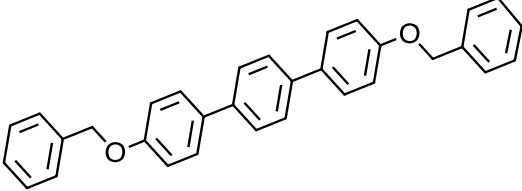
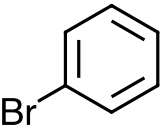
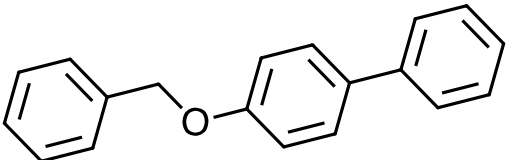
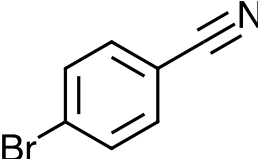
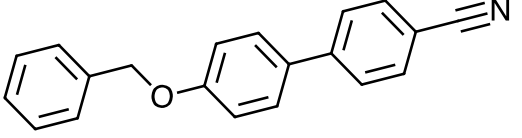
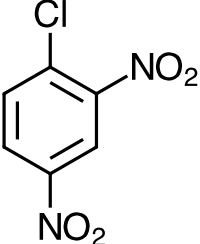
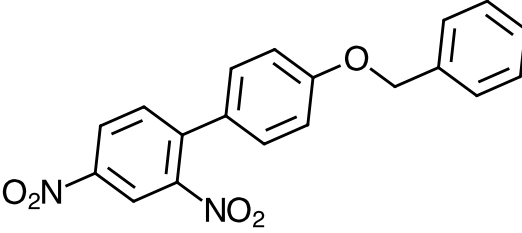


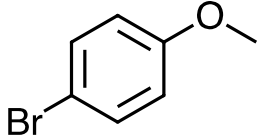
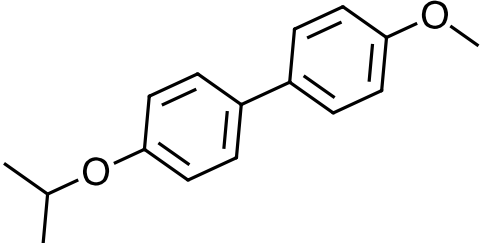
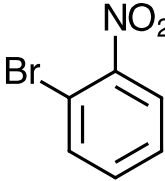
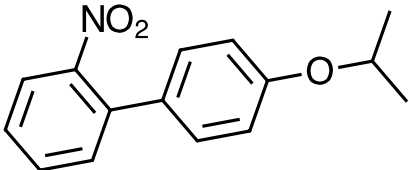
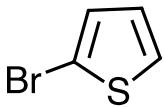
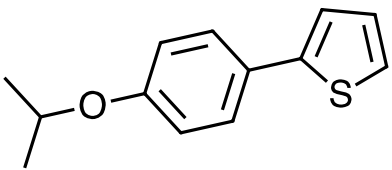
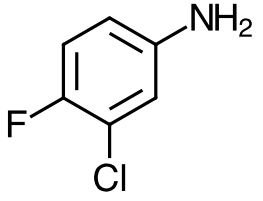
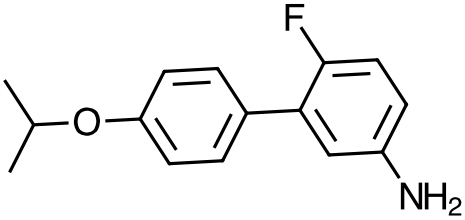
Figure 2.19: List of Boronic acid used in this study as indicated in Table 2.2.

Table 2.2: Suzuki-Miyaura coupling reaction of different aryl halides and boronic acids using palladium catalyst 2.4.

Entry	Aryl halide	Aryl-B(OH) <sub>2</sub>	Expected Product	Yield (%)
2.5		2.24		84
2.6		2.24		70

Entry	Aryl halide	Aryl-B(OH) <sub>2</sub>	Expected Product	Yield (%)
2.7		2.24		No reaction
2.8		2.25		75
2.9		2.25		73
2.10		2.26		88
2.11		2.26		94
2.12		2.26		98

Entry	Aryl halide	Aryl-B(OH) <sub>2</sub>	Expected Product	Yield (%)
2.13		2.26		No reaction
2.14		2.27		94
2.15		2.27		86
2.16		2.27		27
2.17		2.27		98
2.18		2.27		76
2.19		2.27		No reaction

Entry	Aryl halide	Aryl-B(OH) <sub>2</sub>	Expected Product	Yield (%)
2.20		2.28		97
2.21		2.28		70
2.22		2.28		70
2.23		2.28		No reaction

**Reaction condition:** Arylboronic acid 0.5 mmol, Aryl halide 0.5 mmol, Cs<sub>2</sub>CO<sub>3</sub> 1 mmol, palladium catalyst (2.4) 5 mol% in 1:1 mixture of DMF and water at 60 °C for 8 hrs. \*\* Reaction with chlorides and fluorides did not yield any results. List of boronic acid as used are in Figure 2.35.

## 2.7 Rate Studies

Suzuki catalyst systems tend to work faster for electron-poor aryl systems. The goal of this rate study is to determine if the change in the R-group on the phenylthiazole ligand (2.3 or 2.4 each containing a different thiazole ligand were prepared by reaction of the ligand with palladium acetate) will affect this relative rate. Therefore, competition reactions were performed on aryl halides with either an EDG or an EWG.

For the purpose of this investigation, 4-bromoaniline (**2.9**) is serving as the electron rich aryl halide and 4-bromobenzonitrile (**2.19**) is acting as the electron poor. Each of these was reacted with (4-benzyloxybenzeneboronic acid (**2.27**)). The relative coupling rates were determined by comparison to the coupling rate of the unsubstituted 4-bromobenzene (**2.17**).

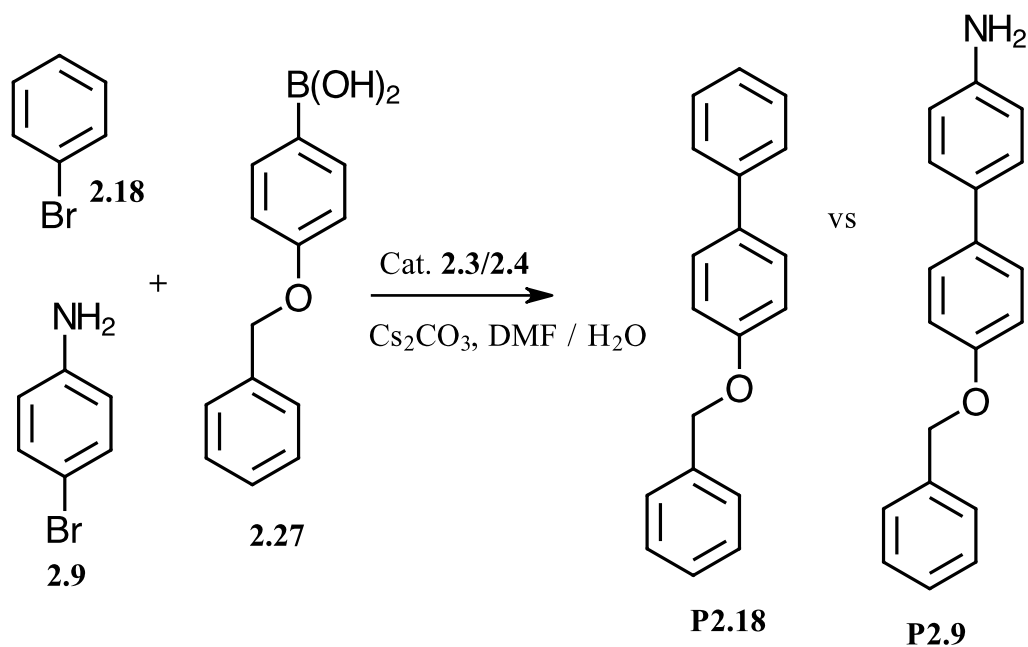
Compound **2.27**, 4-benzyloxybenzeneboronic acid was chosen because of its distinctive and well separated methylene peak in the NMR of the resulting products which allows for identification and quantification of the coupled products.

The reactions were set up with equimolar amounts of the aryl bromide (one of which was always **2.17**) and a limited amount of boronic acid **2.27**. Therefore, the two bromides had to compete for the limited boronic acid, leading to a preference in product distribution based on the speed with which each bromide reacted. The relative rates were determined by looking at the product distribution (**P2.18** and **P2.9**, Scheme 2.19 and **P2.18** and **P2.19**, Scheme 2.20). The relative rates were determined from the relative integration of these two (2) methylene peaks in the proton NMR. The results are given in Table 2.3 (for catalyst **2.3**) and Table **2.4** (for catalyst **2.4**), which give the relative ratio of the coupled product with electron-donating or withdrawing groups compared to the standard (bromobenzene).

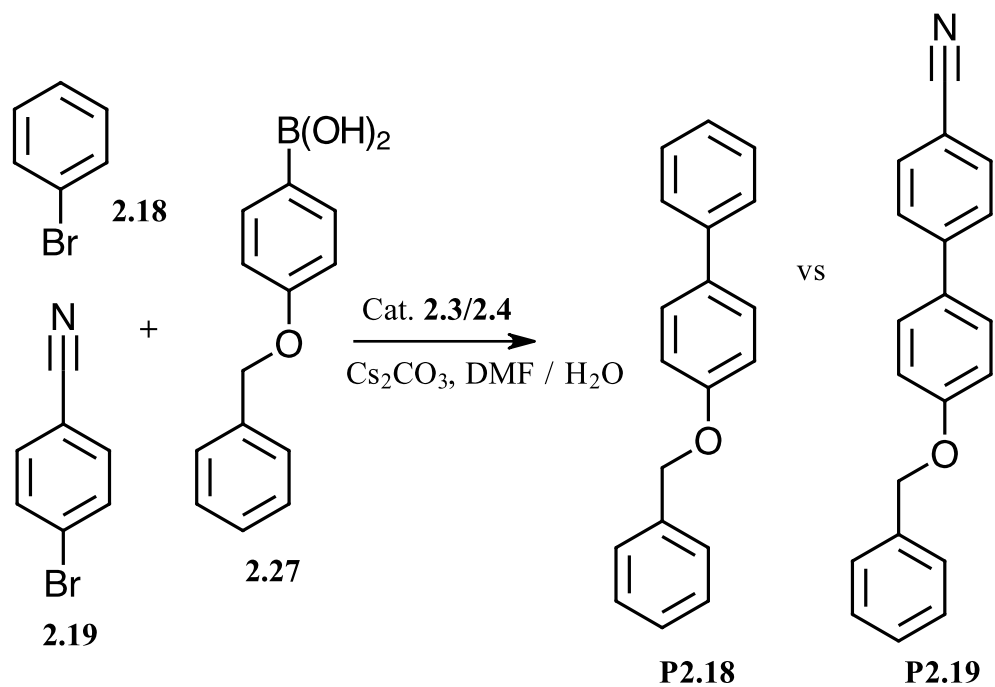
The observed NMR data show that typical selectivity was observed for catalyst **2.4** *i.e.*, the substrate where the EWG reacts faster than the substrate with the EDG attachment (EWG>EDG). Conversely, the relative rate for the electron-rich aryl halide was faster when catalyst **2.3** was used, *i.e.*, there was a shift in selectivity favouring the aryl halide with the electron-donating group which is unusual which makes catalyst 2.3 a suitable catalyst for increasing the amount of electron rich product with electron-donating groups.

It was also observed that electron-withdrawing groups in this kind of cross-coupling reaction occurs faster than the corresponding compounds with electron-donating group as can be seen in Table 2.3 when catalyst **2.4** was used. The difference between the two catalysts **2.3** and **2.4** is the electron-donating strength of a single substituent on the catalyst ligand. Catalyst **2.4** has the more electron-donating strength ( $\text{NH}_2$ ) (which consequently adds more electron density on the palladium. This result is unsurprising if the rate-determining step is the initial oxidative addition of the aryl halide (assuming the steric footprint of the two groups are similar, which should be the case here). The more electron-donating the ligand, the more electron-rich the metal, and the more easily oxidation can take place at the metal.

Complementary to this is catalyst **2.3**, which has a weaker electron-donating group on its ligand ( $\text{CH}_3$ ) and subsequently has lower electron density on the metal. In this case, it appears the reaction occurs more slowly overall (both the EWG and the EDG-containing substrates are slower than bromobenzene), but the preference flips to the EDG-bearing substituent, which is 1.2 times faster than the substrate containing the electron-withdrawing group. This result seems to support the fact that the oxidative addition is rate-determining when using the electron-rich catalyst **2.4**. In the case of the less electron-rich catalyst **2.3**, the oxidative addition is slower as seen by the apparent decrease in the overall rate. Further, the switch may in fact cause another step in the catalytic cycle to dominate the kinetics, leading to the change in preference on the substrate from EWG to EDG.



**Scheme 2.19: Method for determining the effect of catalyst on electron-donating effect in the Suzuki-Miyaura cross-coupling reaction.**



**Scheme 2.20: Method for determining the effect of catalyst on electron-withdrawing effect in the Suzuki-Miyaura cross-coupling reaction.**

**Table 2.3 Methylene NMR integral ratio of EDG vs EWG and protons of bromobenzene (standard) using catalyst 2.3.**

<b>Catalyst 2.3</b>	<b>Integration ratio</b>
EDG (NH <sub>2</sub> ): Standard	0.4:1
EWG (CN): Standard	0.33:1

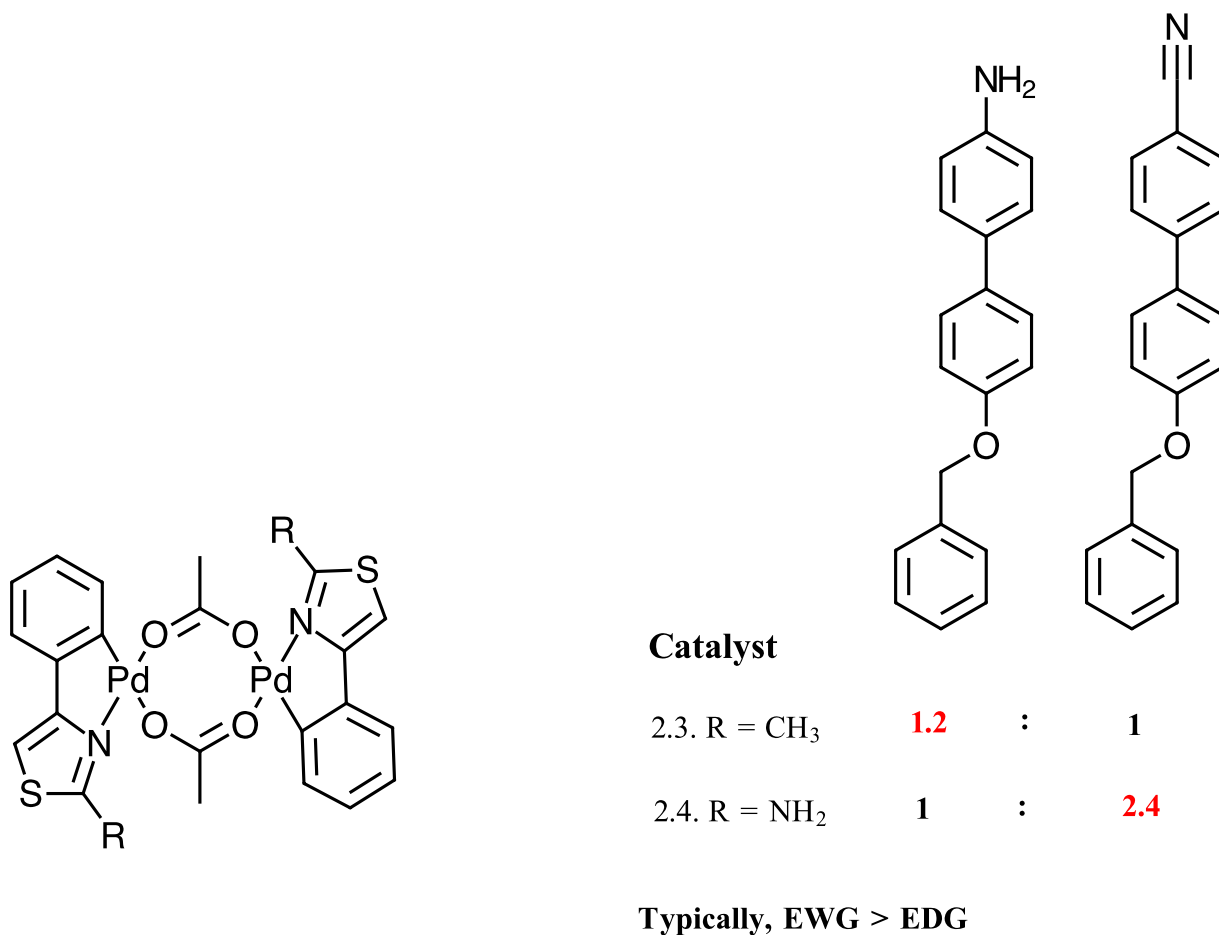
**Table 2.4 Methylene NMR integral ratio of EDG vs EWG and protons of bromobenzene (standard) using catalyst 2.4.**

<b>Catalyst 2.4</b>	<b>Integration Ratio</b>
EDG (NH <sub>2</sub> ): Standard	0.9: 1
EWG (CN): Standard	2.12: 1

The reactivity of the two catalysts **2.3** and **2.4** show that palladium catalysts using these thiazole systems are tunable to prefer either an EDG or an EWG-substituted substrate. From the data presented in Tables 2.3 and 2.4 (a comparison of EWG or EDG with the standard)(bromobenzene)), if the bromobenzene reaction is assumed to be roughly constant for all reaction mixtures, catalyst **2.4** is the faster catalyst overall. If there is only one potential coupling site in the substrate, be it EDG or EWG, catalyst **2.4** would be preferred (6.42 faster in creating electron-withdrawing and 2.25 in electron-donating products).



Suzuki cross-coupling-reaction of haloaromatic containing electron-withdrawing groups (EWG) occurs at faster rates compared to their corresponding reactions of haloaromatics with electron-donating groups. By having a methyl group as a substituent of the catalyst, the normal reactivity, where EWG occurring faster than electron-donating group (EDG) was flipped to get preference for electron-donating group as seen in Scheme 2.21.



**Scheme 2.21: Results of the rate studies on electron-withdrawing and or donating group.**

### 2.7.1 NMR Analysis of the rate studies

Figure 2.20 is the  $^1\text{H}$  NMR of the mixture of 4-(biphenyloxy)phenylmethane (**2.17**) and 4'-(benzyloxy)-4-biphenylamine (**2.14**) with its chemical shift and integrations. The peak at 5.11 ppm is 4-(biphenyloxy)phenylmethane whereas the peak at 5.07 ppm is 4'-(benzyloxy)-4-biphenylamine. This was confirmed by synthesizing each of these two compounds individually. Figures 2.21 and 2.22 shows the individual synthesized compounds which shows the chemical shift and its integrations, an indication of the two products formed. The relative rates were found by looking at the product distribution of the two products formed (**2.14** and **2.17**) by looking at the NMR of the reaction mixture. The relative amounts were found by looking at the relative integration of the two methylene peaks in the  $^1\text{H}$  NMR.

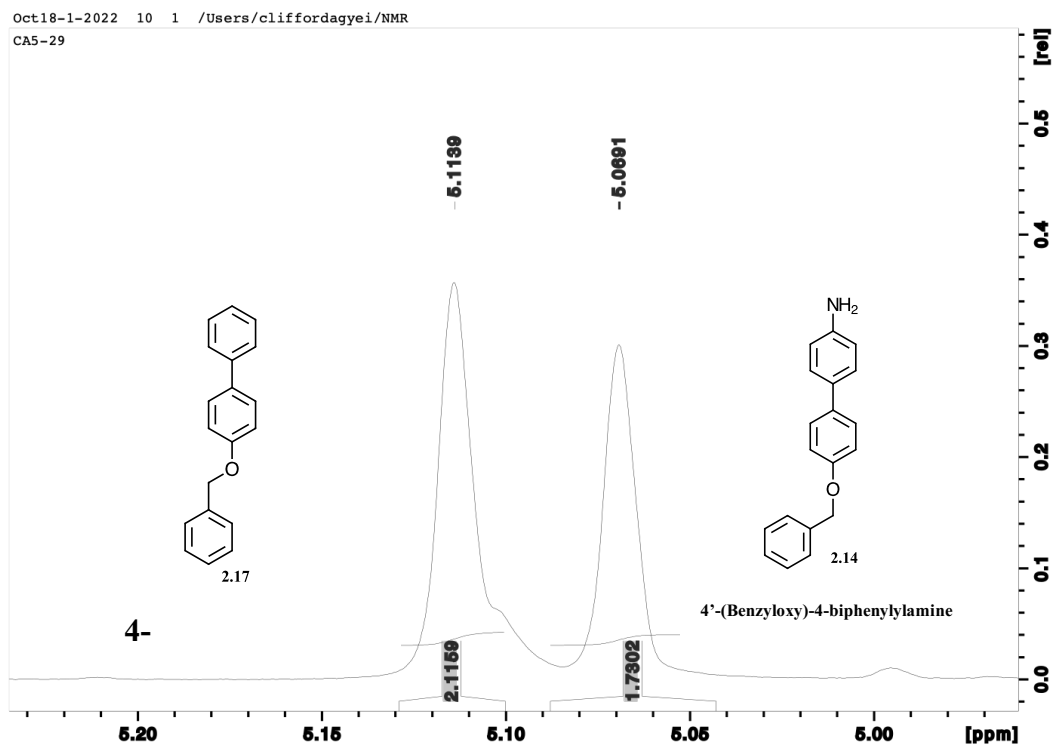


**Figure 2.20:  $^1\text{H}$  NMR of the mixture of 4-(biphenyloxy)phenylmethane and 4'-(benzyloxy)-4-biphenylamine with chemical shift and integration.**

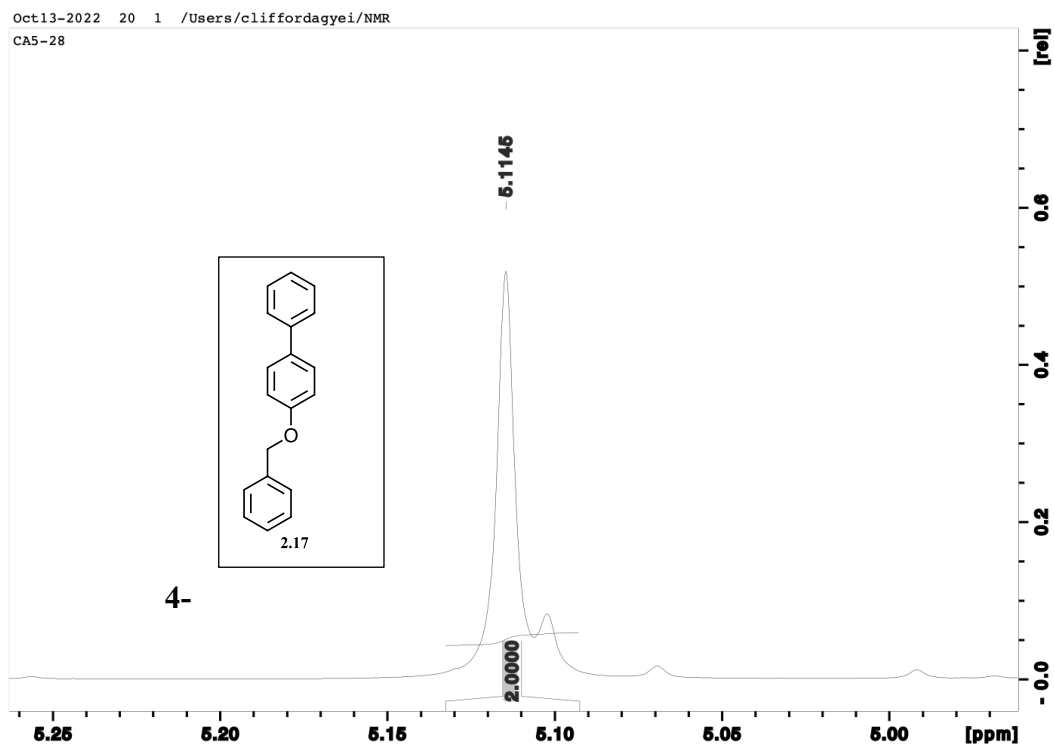


**Figure 2.21:  $^1\text{H}$  NMR of 4-(biphenyloxy)phenylmethane with chemical shift and integration.**

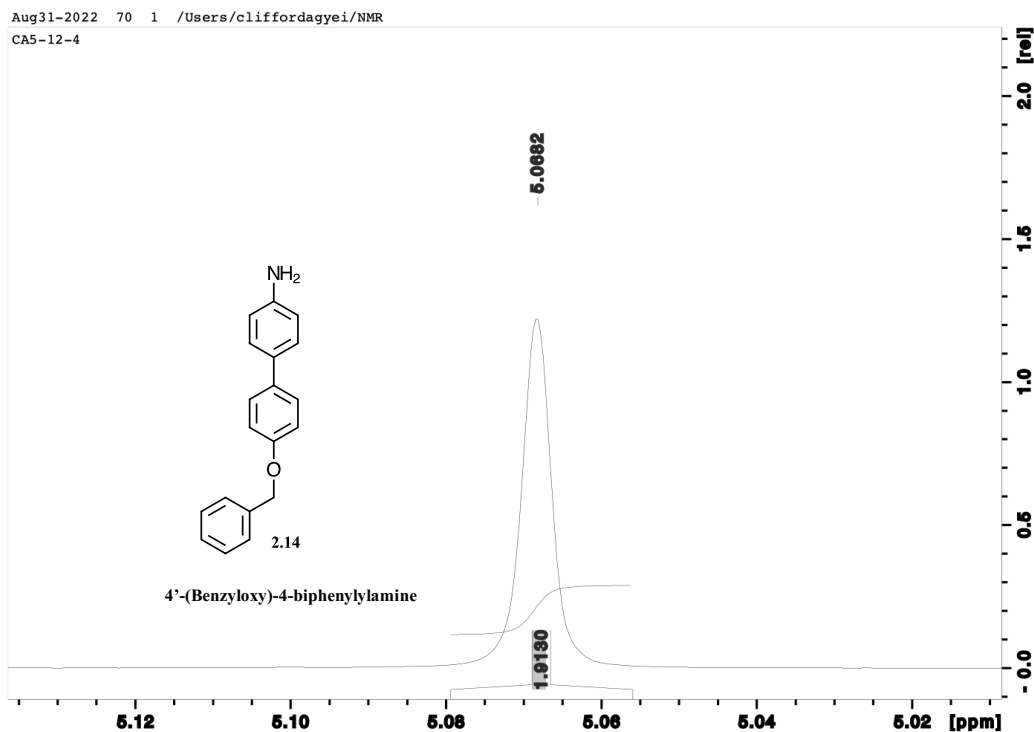


**Figure 2.22:**  $^1\text{H}$  NMR of 4'-(benzyloxy)-4-biphenylamine with chemical shift and integration.

## 2.8 Analysis

When considering the catalyst in this Suzuki-Miyaura cross-coupling reaction, there are three potential differences between catalysts **2.3** (containing a methyl substituent) and **2.4** (amino substituent). The first is the steric<sup>17,18</sup> difference between the two groups; this difference is likely to be negligible due to the free rotation about the C-R bond (the cone angles will be very similar).

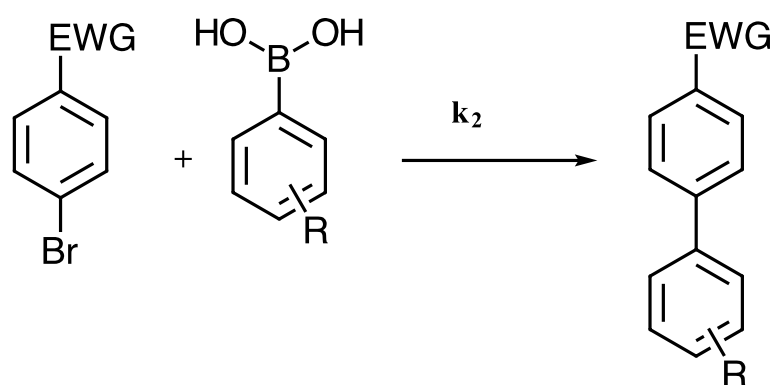
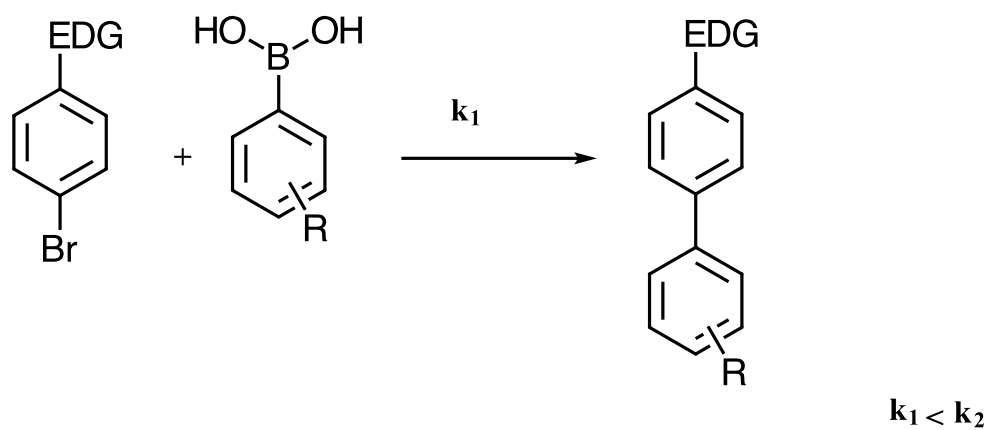
The second is the potential for the amino group in **2.4** to act as a ligand or to otherwise directly participate in the catalytic cycle through coordination chemistry. There is no

definitive evidence in this system to make a decision about any amino-bound intermediates, but we do note that there are many examples of amino-substituted bithiazole ligands where the thiazole nitrogen binds to the metal cation, but the amino nitrogen does not.<sup>71</sup>

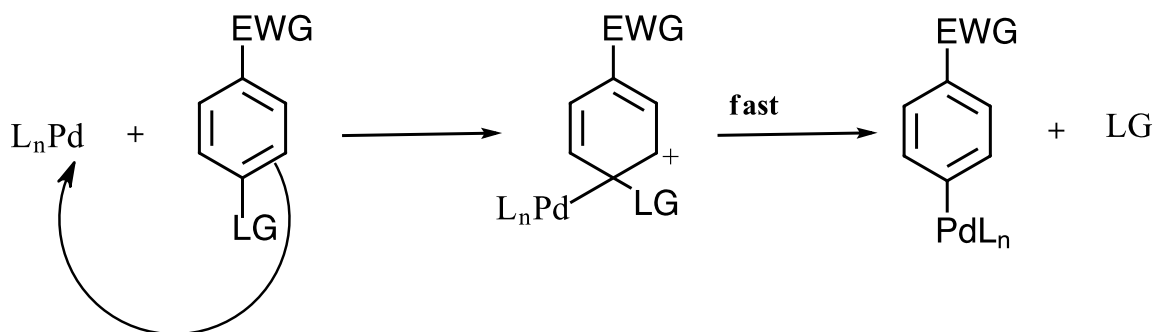
That leaves the third consideration, which is the electronic effect on the metal<sup>16</sup>. This is the most likely consideration, given that the reaction rate seems to be higher for all substrates when there is an electron-donating group on the ligand.

From the Suzuki-Miyaura cross-coupling reactions performed, it was observed that reactions involving bromoaromatics with electron-donating groups occur slower than reactions with electron-withdrawing groups as seen in Scheme 2.22.<sup>72</sup> The rate determining step in this kind of reaction involving the oxidative addition step occurs in a fashion which can be compared to nucleophilic aromatic substitution where the reaction happens through a negatively charged intermediate.<sup>73</sup> When there is an electron-withdrawing group on the aromatic halide ring in the coupling reaction, the reaction happens faster since the intermediate negatively charged carbanion is stabilized by the electron-withdrawing group.

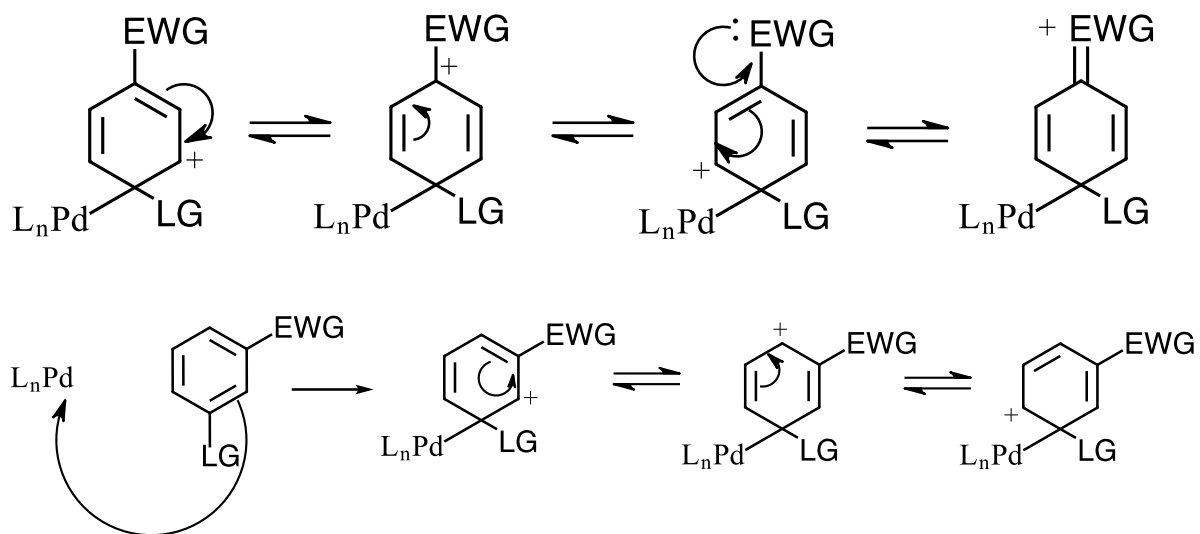
The oxidative addition first step is enhanced by electron-withdrawing groups in the *ortho*- and *para*- positions due to stabilization of the intermediate. When the electron-withdrawing group is *ortho*- or *para*- to the leaving group the reaction occurs faster due to resonance than when the electron-withdrawing group is placed at the *meta*- position as seen in Scheme 2.23. The anion in the *ortho*- or *para*-intermediate is delocalized to the more electronegative atom attached to the electron-withdrawing substituent, whereas in the *meta*-intermediate, does not withdraw electrons in the  $\pi$ -system (no resonance advantage) but rather in the  $\sigma$  bond (inductive effect) as seen in Scheme 2.24.



**Scheme 2.22: Electronic effects in the Suzuki-Miyaura cross-coupling**



**Scheme 2.23 Mechanism of oxidative addition of palladium to the aryl halides in Suzuki-Miyaura cross-coupling reaction.**<sup>74</sup>



**Scheme 2.24: Mechanism of para and ortho with palladium attack in nucleophilic aromatic substitution.**

One potential application of the developed catalyst in this chapter could be in a system where both electron deficient and electron rich aryl bromides are present. The developed catalysts will be a simple way of favouring one coupled product or the other. To get preference for the electron rich bromide, catalyst **2.3** would be selected vs. catalyst **2.4** to get coupling at the electron deficient bromide, as illustrated in Figure 2.23.



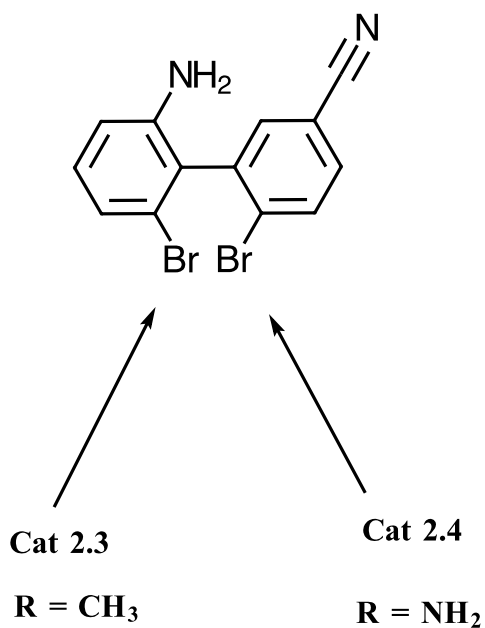
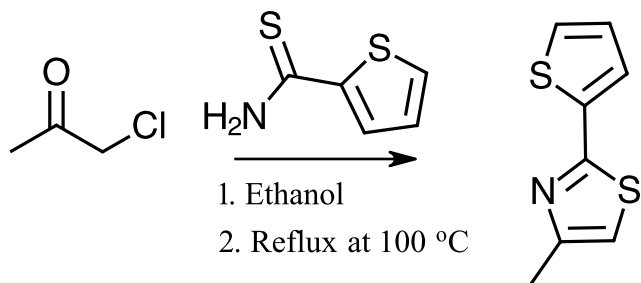


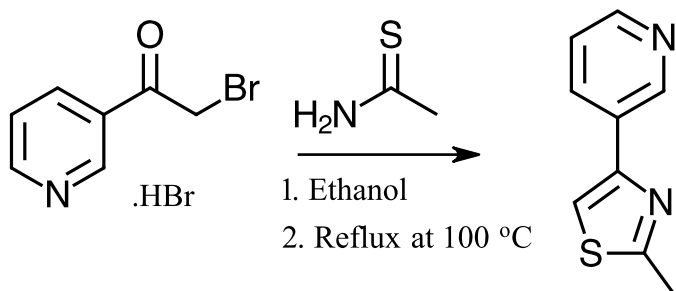
**Figure 2.23: Potential application of catalyst 2.3 and 2.4.**

## 2.9 Other Ligands Attempted.

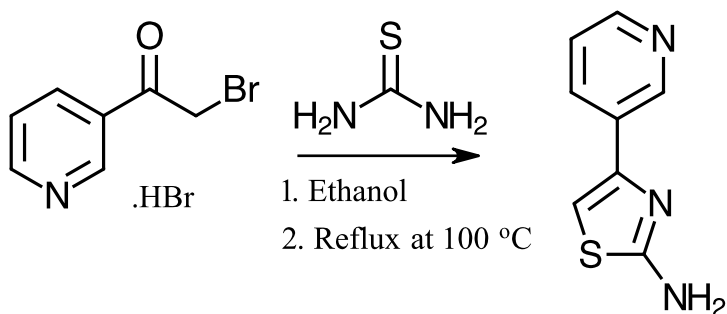
In order to further investigate the range of thiazole ligands which will allow for tuning of the catalytic properties, the following ligands were prepared using the Hantzsch thiazole synthesis. The synthesis of these ligands was successful, but after reaction with Pd(II) a pure single-component palladium(II) product could not be obtained. Three candidates that were synthesized were 2-(2-thienyl)-4-methylthiazole, 2-methyl-4-(3-pyridyl)thiazole, and 2-amino-4-(3-pyridyl)thiazole, shown in Schemes 2.25 to 2.27, respectively.



**Scheme 2.25: Synthesis of 4-Methyl-2-(2-thienyl)-1,3-thiazole**



**Scheme 2.26: Synthesis of 2-Methyl-4-(3-pyridyl)-1,3-thiazole**



**Scheme 2.27: Synthesis of 4-(3-Pyridyl)-1,3-thiazol-2-ylamine**

## 2.10 Experimental

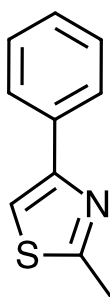
### 2.10.1 General Synthetic and Instrumental Details

Unless otherwise indicated, all reactions were conducted under an inert atmosphere of dry nitrogen. Nuclear magnetic resonance spectra were obtained using a Bruker Avance NEO 500 MHz NMR spectrometer at the Lakehead University Instrument Laboratory using Topspin software. All spectra were recorded at room temperature and chemical shifts were internally referenced to tetramethylsilane (TMS) and are reported in parts per million (ppm). NMR spectral data is reported in the following order: chemical shift (ppm), multiplicity, coupling constant (Hz) and number of protons. The solvent signals were used as references and the chemical shifts converted to the TMS scale ( $\text{CDCl}_3$ :  $\delta_{\text{C}} = 77.00$  ppm and  $\delta_{\text{H}} = 7.26$  ppm;  $\text{d}^6$ -DMSO:  $\delta_{\text{C}} = 39.53$  and  $\delta_{\text{H}} = 2.50$ ;  $\text{d}^4$ -MeOH:  $\delta_{\text{C}} = 49.03$  ppm and  $\delta_{\text{H}} = 3.31$  ppm). The splitting patterns were designated using the following abbreviations: s (singlet), d (doublet), t (triplet), q (quartet), quint. (quintuplet), m (multiplet), br (broad). Mass spectra were obtained on an Advion-Expression Compact Mass Spectrometer. Infrared spectra were collected on a Nicolet 380 FT-IR with a resolution of  $1 \text{ cm}^{-1}$ . Glassware used for all reactions was oven dried, evacuated, and purged with  $\text{N}_2$  (g) several times and allowed to cool to room temperature. 2,4-dimethoxyphenylboronic acid, 3,4-dimethoxyphenylboronic acid, phenylboronic acid, 4-benzyloxybenzeneboronic acid, 4-isopropoxyphenylboronic acid and arylhalides such as 4-iodophenol (**2.5**), 5-bromosalicylaldehyde (**2.6**), 2,6-dichloroacetophenone (**2.7**), 5-bromo-2-furoic acid (**2.8**), 2,5-dibromothiophene (**2.9**), 4-bromobenzaldehyde (**2.10**), 4-bromobenzonitrile (**2.11**), 4-bromo-2-fluorophenol (**2.12**), 1-fluoro-2,4-dinitrobenzene (**2.13**), 4 bromoaniline (**2.14**), bromobenzaldehyde (**2.15**), 1,4 dibromobenzene (**2.16**),

bromobenzene (**2.17**), 4-bromobenzonitrile (**2.18**), 1-chloro-2,4-dinitrobenzene (**2.19**), 4-bromoanisole (**2.20**), 5-bromo-2-furoic acid (**2.21**), 2-bromothiophene (**2.22**), 3-chloro-4-fluoroaniline (**2.23**) were obtained commercially from Sigma Aldrich, ChemImpex or Fisher Scientific and used as received. Thin layer chromatography (TLC) was performed using Silicycle UltraPure silica gel 200  $\mu\text{m}$ . Hexane and ethyl acetate were used as mobile phases in flash chromatography unless otherwise stated.

### 2.10.2 Ligands Preparation

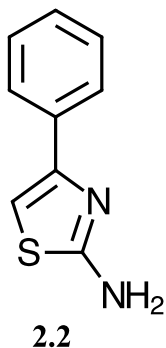
#### Preparation of 2-methyl-4-phenyl-1,3-thiazole (**2.1**)



**2.1**

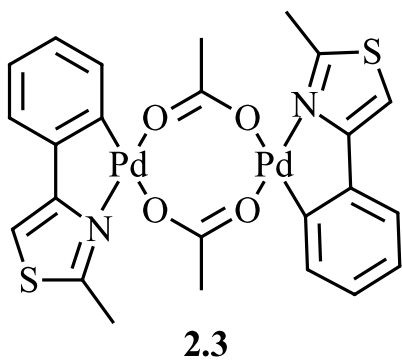
2-Bromoacetophenone (3.0 g, 15.0 mmol) was weighed into 75 mL of dry ethanol in a 500 mL round bottom flask equipped with a stir bar and a reflux condenser. Thioacetamide (1.14g, 15.0 mmol) was added. The resulting mixture was refluxed under nitrogen gas for 3 hours and was allowed to cool. After the 3-hour period, the solution was poured into 100 mL of distilled water and was neutralized to a pH of 9 using saturated sodium carbonate. The organic product was extracted with ether and dried with  $\text{MgSO}_4$ . The solvent was removed *via* rotary evaporation. The residue was purified by chromatography on silica gel (4:1 hexane: ethyl acetate) to afford a light-yellow solid (2.22 g, 83.77 % yield).; mp 64-67 °C; IR (neat) 3106, 1684, 1495;  $^1\text{H}$  NMR (500 MHz,  $\text{CDCl}_3$ )  $\delta$  7.87 (d,  $J = 7.1$  Hz, 2H), 7.41 (dd,  $J = 7.4$  Hz, 2H), 7.32 (d,  $J = 7.4$  Hz 1H), 7.29 (s, 1H), 2.77 (s, 3H);  $^{13}\text{C}$  NMR (125 MHz,  $\text{CDCl}_3$ )  $\delta$  165.8, 155.17, 134.56, 128.70, 127.96, 126.32, 112.23, 19.33. Mass spec. calc. for  $\text{C}_{10}\text{H}_9\text{NS}$ : 175.05; found: 175.9 (100 %,  $\text{M}^+\text{H}$ ).

## Preparation of 4-phenyl-1,3-thiazol-2-ylamine (2.2)



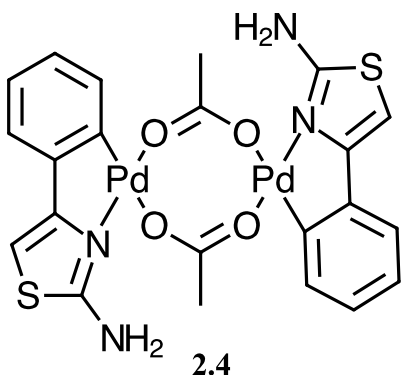
2-bromoacetophenone (1.0 g, 5.02 mmol) was weighed into 75 mL of dry ethanol in a 500 mL round bottom flask equipped with a stir bar and a reflux condenser. Thiourea (0.38 g, 5.02 mmol) was added. The resulting mixture was refluxed under nitrogen gas for 3 hours and was allowed to cool. After the 3-hour period, the solution was poured into 100 mL of distilled water and was neutralized to a pH of 9 using saturated sodium carbonate. The organic product was extracted with ether and dried with  $\text{MgSO}_4$ . The solvent was removed *via* rotary evaporation. The residue was purified by chromatography on silica gel (4:1 hexane: ethyl acetate) to afford a light-yellow solid (0.72 g, 82.3 %); mp 146-149 °C; IR (neat) 3433, 1597, 1532, 1442;  $^1\text{H}$  NMR (500 MHz,  $\text{CDCl}_3$ )  $\delta$  7.78 (d,  $J = 7.85$  Hz, 2H), 7.38 (d,  $J = 7.85$  Hz, 1H), 7.29 (dd,  $J = 7.35$  Hz, 2H), 6.73 (s, 1H), 5.03 (s, 2H);  $^{13}\text{C}$  NMR (125 MHz,  $\text{CDCl}_3$ )  $\delta$  167.07, 151.38, 134.66, 128.59, 127.96, 126.00, 102.93. Mass spec. calc. for  $\text{C}_9\text{H}_9\text{N}_2\text{S}$ : 176.04; found: 178.3 (100 %,  $\text{M}+\text{H}$ ).

### 2.10.3 Synthesis of Palladium(II) Complex (2.3)



To 2-methyl-4-phenyl-1,3-thiazole (**2.1**) (0.26 g, 1.47 mmol, 1.4 equiv) in MeOH (32 mL) in a 200 mL round bottom flask open to air at 23 °C and equipped with a magnetic stir bar was added palladium acetate (Pd(OAc)<sub>2</sub>) (0.23g, 1.47 mmol, 1 equiv.) and stirred at room temperature for 23 hours. The reaction mixture was then filtered, and the precipitate was washed with diethyl ether (20 mL), collected and dried. The product was obtained as a brown solid (0.795 g, 79.5 % yield).; mp 156-158 °C; <sup>1</sup>H NMR (500 MHz, CDCl<sub>3</sub>) δ 7.31-7.94 (m, 10H), 2.72 (s, 6H), 1.91 (s, 6H); Lack of solubility prevented definitive NMR characterization and assignment. Uncoordinated ligand peaks are similar to the coordinated peaks. IR (neat) 3089, 1706, 1612, 1491; Mass spec. calc. for C<sub>24</sub>H<sub>22</sub>N<sub>2</sub>O<sub>4</sub>Pd<sub>2</sub>S<sub>2</sub>: 677.91; found: 680.9 (100 %, M+H).

### 2.10.4 Synthesis of Palladium(II) Complex (2.4)



To 4-phenyl-1,3-thiazol-2-ylamine (**2.2**) (0.26 g, 1.5 mmol, 1.4 equiv.) in MeOH (32 mL) in a 200 mL round bottom flask open to air at 23 °C and equipped with a magnetic stir bar was added palladium acetate, (Pd(OAc)<sub>2</sub>) (0.24 g, 1.5 mmol, 1 equiv.) and stirred at

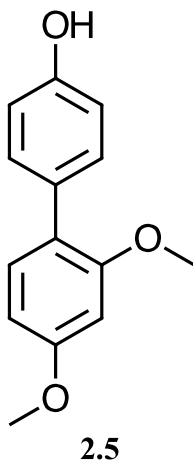
room temperature for 23 hours. The reaction mixture was then filtered, and the precipitate was washed with diethyl ether (20 mL), collected and dried. The product was obtained as a brown solid (0.795 g, 96.4 % yield).; mp 204-207 °C; IR (neat) 3426, 1700, 1653, 1559, 1442; <sup>1</sup>H NMR (500 MHz, CDCl<sub>3</sub>) δ 7.79 (d, J = 7.35 Hz, 2H), 7.40 (d, J = 7.14, 2H), 7.39 (dd, J = 12.95, 7.14 Hz, 2H), 7.25 (dd, J = 10.95, 6.55 Hz, 2H), 7.06 (s, 2H), 7.01 (s, 4H), 1.84 (s, 6H); <sup>13</sup>C NMR (125 MHz, CDCl<sub>3</sub>) δ 172.88, 168.64, 150.32, 146.12, 135.39, 128.92, 128.91, 127.63, 125.99, 101.94, 22.15. Mass spec. calc. for C<sub>22</sub>H<sub>20</sub>N<sub>4</sub>O<sub>4</sub>Pd<sub>2</sub>S<sub>2</sub>: 678.91; found: 680.2 (100 %, M-H).

#### **2.10.5 Crystal Structure of Compound [(MePhTz)Pd(CH<sub>3</sub>COO)]<sub>2</sub> (2.3)**

Single crystals of compound 2.3 were obtained by slow evaporation of a mixture of hexane and dichloromethane and submitted for X-ray diffraction analysis. An appropriate crystal was selected and mounted on a MiTeGen tip using parabar oil on a Bruker D8 Venture diffractometer. The crystals were kept at 200.0 K during data collection. Using Olex2,<sup>75</sup> the structure was solved with the XT structure solution program<sup>76</sup> using intrinsic phasing and refined with the XL refinement package<sup>77</sup> using least squares minimization.

## 2.10.6 Suzuki-Miyaura Coupling.

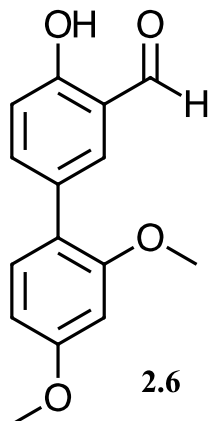
### 2',4'-Dimethoxy-4-biphenylol (2.5)



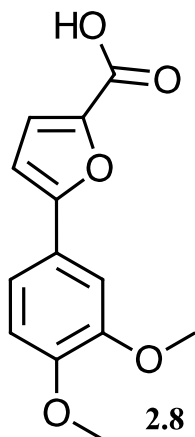
4-Iodophenol (0.11 g, 0.5 mmol), 2,4-dimethoxyphenylboronic acid (91 mg, 0.5 mmol), cesium carbonate,  $\text{Cs}_2\text{CO}_3$  (0.33 g, 1 mmol) and palladium(II) complex, 2.4 (20 mg, 5 mol %) were added to a round bottom flask equipped with a magnetic stir bar. The reaction was stirred at 60 °C for 8 hours in DMF and water (1:1) (6 mL). After this period, the solution was cooled to room temperature, and diluted with dichloromethane (30 mL). 15 mL of water was added to the mixture, and the product extracted into dichloromethane. The organic layer was dried over  $\text{MgSO}_4$  and concentrated under vacuum. The residue was purified by chromatography on silica gel (4:1 hexane: ethyl acetate) to afford a light-yellow solid (80 mg, 84.2 % yield).; mp 52-54 °C; IR (neat) 3744, 3588, 1601, 1266, 1209;  $^1\text{H}$  NMR (500 MHz,  $\text{CDCl}_3$ )  $\delta$  9.86 (s, 1H), 7.36 (d,  $J = 8.65$  Hz, 1H), 7.21 (d,  $J = 16.25$  Hz, 2H), 6.92 (d,  $J = 7.4$  Hz, 1H), 6.83 (d,  $J = 9.5$  Hz, 2H), 6.52 (d,  $J = 8.20$  Hz, 1H), 3.84 (s, 3H), 3.79 (s, 3H);  $^{13}\text{C}$  NMR (125 MHz,  $\text{CDCl}_3$ )  $\delta$  160.83, 159.94, 157.35, 130.42, 129.98, 129.67, 123.21, 115.3, 106.25, 98.97, 55.32, 55.27. Mass spec. calc. for  $\text{C}_{14}\text{H}_{14}\text{O}_3$ : 230.09; found: 231.0 (100 %, M+H).



#### 4-Hydroxy-2',4'-dimethoxy-3-biphenylcarbaldehyde (2.6)



5-Bromosalicylaldehyde (100 mg, 0.5 mmol), 2,4-dimethoxyphenylboronic acid (91 mg, 0.5 mmol), cesium carbonate, Cs<sub>2</sub>CO<sub>3</sub> (0.33 g, 1 mmol) and palladium(II) complex, **2.4** (20 mg, 5 mol %) were added to a round bottom flask equipped with a magnetic stir bar. The reaction was stirred at 60 °C for 8 hours in DMF and water (1:1) (6 mL). After this period, the solution was cooled to room temperature, and diluted with dichloromethane (30 mL). 15 mL of water was added to the mixture, and the product eluted with dichloromethane. The organic layer was dried over MgSO<sub>4</sub> and concentrated under vacuum. The residue was purified by chromatography on silica gel (4:1 hexane: ethyl acetate) to afford a bright yellow solid (90 mg, 70 % yield).; mp 59-61 °C; IR (neat) 1654, 1609, 1277, 1236; <sup>1</sup>H NMR (500 MHz, CDCl<sub>3</sub>) δ 11.01 (s, 1H), 9.99 (s, 1H), 7.73 (dd, J = 8.45, 2.1 Hz, 1H), 7.72 (d, J = 1.95 Hz, 1H), 7.21 (d, J = 8.75 Hz, 1H), 7.13 (d, J = 8.4 Hz, 1H), 7.10 (d, J = 2.45 Hz, 1H), 6.68 (dd, J = 8.45, 1.8 Hz, 1H), 3.84 (s, 3H), 3.75 (s, 3H); <sup>13</sup>C NMR (125 MHz, CDCl<sub>3</sub>) δ 196.47, 163.40, 161.04, 160.06, 135.21, 131.95, 131.57, 131.34, 120.78, 118.48, 104.14, 100.10, 98.92, 55.67, 55.34. Mass spec. calc. for C<sub>15</sub>H<sub>14</sub>O<sub>4</sub>: 258.089; found: 258.6 (100 %, M+H).

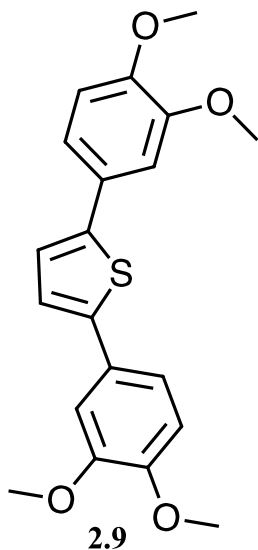


### 5-(3,4-Dimethoxyphenyl)-2-furoic acid (**2.8**)

5-Bromo-2-furoic acid (95 mg, 0.5 mmol), 3,4-dimethoxyphenylboronic acid (90 mg, 0.5 mmol), cesium carbonate,  $\text{Cs}_2\text{CO}_3$  (0.33 g, 1 mmol) and palladium(II) complex, **2.4** (20 mg, 5 mol %) were added to a round bottom flask equipped with a magnetic stir bar. The reaction was stirred at 60 °C for 8 hours in DMF and water (1:1) (6 mL). After this period,

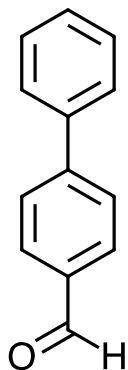
the solution was cooled to room temperature, and diluted with dichloromethane (30 mL). 15 mL of water was added to the mixture, and the product eluted with dichloromethane. The organic layer was dried over  $\text{MgSO}_4$  and concentrated under vacuum. The residue was purified by chromatography on silica gel (1:1 hexane: ethyl acetate) to afford a dark yellow solid (90 mg, 75 % yield).; mp 307-309 °C; IR (neat) 3393, 2925, 1725, 1607, 1249, 1182;  $^1\text{H}$  NMR (500 MHz,  $\text{CDCl}_3$ )  $\delta$  8.19 (s, 1H), 7.78 (dd,  $J = 7.4, 1.3$  Hz, 1H), 7.39 (d,  $J = 10$  Hz, 1H), 7.11 (d,  $J = 2.15$  Hz, 1H), 7.09 (d,  $J = 8.8$  Hz, 1H), 6.90 (d,  $J = 7.95$  Hz, 1H), 3.92 (s, 3H), 3.89 (s, 3H);  $^{13}\text{C}$  NMR (125 MHz,  $\text{CDCl}_3$ )  $\delta$  171.13, 149.26, 149.14, 148.46, 134.37, 122.7, 120.94, 119.22, 111.61, 111.42, 110.51, 55.85, 55.76. Mass spec. calc. for  $\text{C}_{13}\text{H}_{12}\text{O}_5$ : 248.068; found: 247.40 (100 %, M-H).

### 2,5-Bis(3,4-dimethoxyphenyl)thiophene (2.9)



2,5-Dibromothiophene (121 mg, 0.5 mmol), 3,4-dimethoxyphenylboronic acid 182 mg, 1.0 mmol), cesium carbonate, Cs<sub>2</sub>CO<sub>3</sub> (0.66 g, 1 mmol) and palladium(II) complex, **2.4** (40 mg, 5 mol %) were added to a round bottom flask equipped with a magnetic stir bar. The reaction was stirred at 60 °C for 8 hours in DMF and water (1:1) (12 mL). After this period, the solution was cooled to room temperature, and diluted with dichloromethane (30 mL). 30 mL of water was added to the mixture, and the product eluted with dichloromethane. The organic layer was dried over MgSO<sub>4</sub> and concentrated under vacuum. The residue was purified by chromatography on silica gel (4:1 hexane: ethyl acetate) to afford a bright yellow solid (130 mg, 73 % yield). ; mp 68-70 °C; IR (neat) 1601, 1254, 1176; <sup>1</sup>H NMR (500 MHz, CDCl<sub>3</sub>) δ 7.18 (d, J = 10.37 Hz, 2H), 7.11 (d, J = 2.07 Hz, 2H), 7.09 (d, J = 10.34 2H), 6.93 (d, J = 8.27 Hz, 2H), 3.95 (s, 6H), 3.92 (s, 6H); <sup>13</sup>C NMR (125 MHz, CDCl<sub>3</sub>) δ 149.17, 148.73, 142.86, 134.24, 127.57, 123.10, 111.46, 110.38, 56.03. Mass spec. calc. for C<sub>20</sub>H<sub>20</sub>O<sub>4</sub>S: 356.108; found: 357.1 (100 %, M+H).

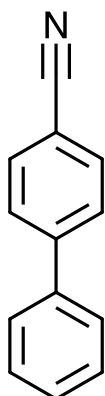
#### 4-Biphenylcarbaldehyde (2.10)



**2.10**

4-Bromobenzaldehyde (93 mg, 0.5 mmol), phenylboronic acid (61 mg, 0.5 mmol), cesium carbonate,  $\text{Cs}_2\text{CO}_3$  (0.33 g, 1 mmol) and palladium(II) complex, **2.4** (20 mg, 5 mol %) were added to a round bottom flask equipped with a magnetic stir bar. The reaction was stirred at 60 °C for 8 hours in DMF and water (1:1) (6 mL). After this period, the solution was cooled to room temperature, and diluted with dichloromethane (30 mL). 15 mL of water was added to the mixture, and the product eluted into dichloromethane. The organic layer was dried over  $\text{MgSO}_4$  and concentrated under vacuum. The residue was purified by chromatography on silica gel (4:1 hexane: ethyl acetate) to afford a brown solid (80 mg, 88 % yield).; mp 102-104 °C; IR (neat) 1654, 1599;  $^1\text{H}$  NMR (500 MHz,  $\text{CDCl}_3$ )  $\delta$  10.04 (s, 1H), 7.94 (d,  $J = 8.4$  Hz, 2H), 7.73 (d,  $J = 8.25$  Hz, 2H), 7.62 (d,  $J = 7.05$  Hz, 2H), 7.47 (t,  $J = 14.85$  Hz, 2H), 7.41 (d,  $J = 7.4$  Hz, 1H);  $^{13}\text{C}$  NMR (125 MHz,  $\text{CDCl}_3$ )  $\delta$  191.96, 139.68, 135.15, 132.43, 130.30, 129.02, 128.48, 127.67, 127.36. Mass spec. calc. for  $\text{C}_{13}\text{H}_{10}\text{O}$ : 182.073; found: 183.0 (100 %, M+H).

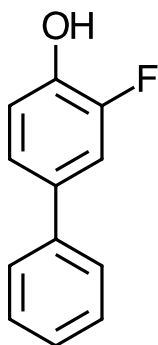
#### 4-Biphenylcarbonitrile (2.11)



2.11

4-Bromobenzonitrile (91 mg, 0.5 mmol), 4-phenylboronic acid (61 mg, 0.5 mmol), cesium carbonate,  $\text{Cs}_2\text{CO}_3$  (0.33 g, 1 mmol) and palladium(II) complex, **2.4** (20 mg, 5 mol %) were added to a round bottom flask equipped with a magnetic stir bar. The reaction was stirred at 60 °C for 8 hours in DMF and water (1:1) (6 mL). After this period, the solution was cooled to room temperature, and diluted with dichloromethane (30 mL). 15 mL of water was added to the mixture, and the product extracted into dichloromethane. The organic layer was dried over  $\text{MgSO}_4$  and concentrated under vacuum. The residue was purified by chromatography on silica gel (4:1 hexane: ethyl acetate) to afford a light-yellow colour (85 mg, 94.4 % yield).; mp 86-88 °C; IR (neat) 3076, 2227, 1606;  $^1\text{H}$  NMR (500 MHz,  $\text{CDCl}_3$ )  $\delta$  7.73 (d,  $J = 8.5$  Hz, 2H), 7.68 (d,  $J = 8.5$  Hz, 2H), 7.59 (d,  $J = 7.20$  Hz, 2H), 7.49 (td,  $J = 7.15, 7.75$  Hz, 2H), 7.43 (dd,  $J = 7.25, 7.35$  Hz, 1H);  $^{13}\text{C}$  NMR (125 MHz,  $\text{CDCl}_3$ )  $\delta$  145.66, 139.15, 132.58, 129.09, 128.64, 127.71, 127.21, 118.93, 110.88. Mass spec. calc. for  $\text{C}_{13}\text{H}_9\text{N}$ : 179.074; found: 180.0 (100 %, M+H).

#### 2-Fluoro-4-biphenylol (2.12)

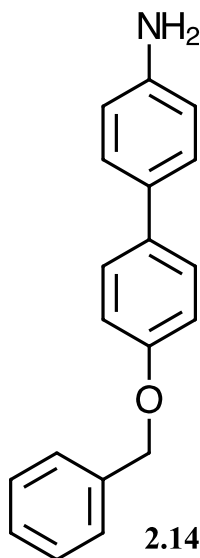


2.12

4-Bromo-2-fluorophenol (96 mg, 0.5 mmol), 4-phenylboronic acid (61 mg, 0.5 mmol), cesium carbonate,  $\text{Cs}_2\text{CO}_3$  (0.33 g, 1 mmol) and palladium(II) complex, **2.4** (20 mg, 5 mol %) were added to a round bottom flask equipped with a magnetic stir bar. The reaction was stirred at 60 °C for 8 hours in DMF and water (1:1) (6 mL). After this period, the solution was cooled to room temperature, and diluted with dichloromethane (30 mL). 15 mL of

water was added to the mixture, and the product eluted with dichloromethane. The organic layer was dried over MgSO<sub>4</sub> and concentrated under vacuum. The residue was purified by chromatography on silica gel (4:1 hexane: ethyl acetate) to afford a beige solid (92 mg, 98 % yield).; mp 98-100 °C; IR (neat) 3649, 1600, 1373, 1117; <sup>1</sup>H NMR (500 MHz, DMSO) δ 9.89 (s, 1H), 7.61 (d, J = 7.2 Hz, 1H), 7.47 (dd, J = 10.6, 2.2 Hz, 2H), 7.41 (dd, J = 7.95, 2.2 Hz, 1H), 7.33 (d, J = 1.85 Hz, 1H), 7.25 (dd, J = 6.45, 1.9 Hz, 1H), 6.98 (d, J = 9.1 Hz, 1H); <sup>13</sup>C NMR (125 MHz, CDCl<sub>3</sub>) δ 152.69, 150.8, 144.40, 139.45, 129.33, 127.33, 126.58, 122.56, 118.51, 114.12. Mass spec. calc. for C<sub>12</sub>H<sub>9</sub>FO: 188.064; found: 188.0 (100 %, M-H).

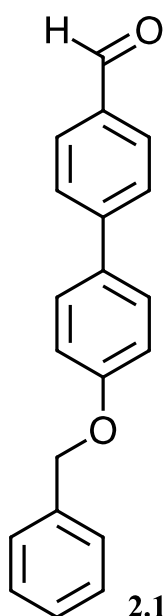
#### 4'-(Benzyloxy)-4-biphenylamine (2.14)



4-Bromoaniline (86 mg, 0.5 mmol), 4-Benzyloxybenzeneboronic acid (114 mg, 0.5 mmol), cesium carbonate, Cs<sub>2</sub>CO<sub>3</sub> (0.33 g, 1 mmol) and palladium(II) complex, **2.4** (20 mg, 5 mol %) were added to a round bottom flask equipped with a magnetic stir bar. The reaction was stirred at 60 °C for 8 hours in DMF and water (1:1) (6 mL). After this period, the solution was cooled to room temperature, and diluted with dichloromethane (30 mL). 15 mL of water was added to the mixture, and the product eluted into dichloromethane. The organic layer was dried

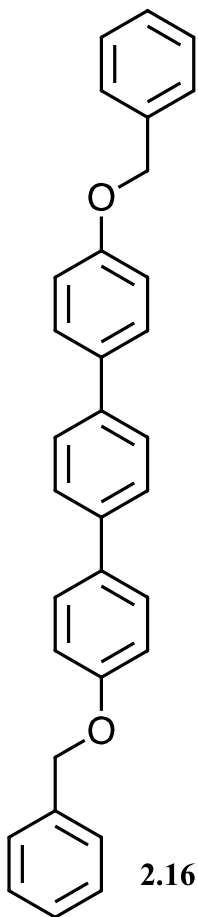
over MgSO<sub>4</sub> and concentrated under vacuum. The residue was purified by chromatography on silica gel (4:1 hexane: ethyl acetate) to afford a crystalline white colour (130 mg, 94.4 % yield).; mp 38-40 °C; IR (neat) 3465, 1685, 1606, 1300, 1249; <sup>1</sup>H NMR (500 MHz,

CDCl<sub>3</sub>) δ 7.28-7.48 (m, J = 8.65, 7.2, 8.45 Hz, 9H), 7.00 (d, J = 8.7 Hz, 2H), 6.739 (d, J = 8.4 Hz, 2H), 5.09 (s, 2H), 5.06 (s, 2H); <sup>13</sup>C NMR (125 MHz, CDCl<sub>3</sub>) δ 157.64, 155.17, 145.31, 137.11, 134.13, 131.33, 128.61, 127.96, 127.79, 127.63, 127.51, 127.43, 70.10. Mass spec. calc. for C<sub>19</sub>H<sub>17</sub>NO: 275.131; found: 276.10 (100 %, M+H).



#### 4'-(Benzyloxy)-4-biphenylcarbaldehyde (2.15)

4-Bromobenzaldehyde (93 mg, 0.5 mmol), 4-benzyloxybenzeneboronic acid (114 mg, 0.5 mmol), cesium carbonate, Cs<sub>2</sub>CO<sub>3</sub> (0.33 g, 1 mmol) and palladium(II) complex, **2.4** (20 mg, 5 mol %) were added to a round bottom flask equipped with a magnetic stir bar. The reaction was stirred at 60 °C for 8 hours in DMF and water (1:1) (6 mL). After this period, the solution was cooled to room temperature, and diluted with dichloromethane (30 mL). 15 mL of water was added to the mixture, and the product extracted with dichloromethane. The organic layer was dried over MgSO<sub>4</sub> and concentrated under vacuum. The residue was purified by chromatography on silica gel (9.5:0.5 dichloromethane: methanol) to afford a bright yellow solid (120 mg, 86 % yield).; mp 112-114 °C; IR (neat) 1700, 1599, 1241, 1117; <sup>1</sup>H NMR (500 MHz, CDCl<sub>3</sub>) δ 10.00 (s, 1H), 7.89 (d, J = 8.25 Hz, 2H), 7.68 (d, J = 8.25 Hz, 2H), 7.57 (d, J = 8.7 Hz, 2H), 7.42 (d, J = 9.5, 5.1, 2H), 7.38 (dd, J = 4.1, 3.55 Hz, 2H), 7.06 (d, J = 8.75 Hz, 2H), 6.96 (dd, J = 7.85, 7.05 Hz, 1H), 5.10 (s, 2H); <sup>13</sup>C NMR (125 MHz, CDCl<sub>3</sub>) δ 159.27, 146.49, 137.84, 136.66, 134.67, 132.26, 130.32, 129.48, 128.57, 128.10, 127.47, 127.04, 114.8, 70.07. Mass spec. calc. for C<sub>20</sub>H<sub>16</sub>O<sub>2</sub>: 288.115; found: 289.10 (100 %, M+H).

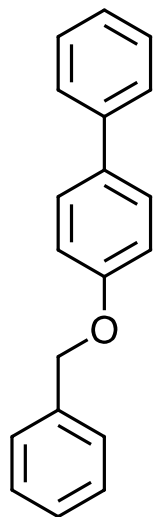


**4,4'-Bis(benzyloxy)-1,1':4'', 1''-terphenyl (2.16)**

1,4-Dibromobenzene (118 mg, 0.5 mmol), 4-benzyloxybenzeneboronic acid (228 mg, 1.0 mmol), cesium carbonate, Cs<sub>2</sub>CO<sub>3</sub> (0.66 g, 1 mmol) and palladium(II) complex, **2.4** (40 mg, 5 mol %) were added to a round bottom flask equipped with a magnetic stir bar. The reaction was stirred at 60 °C for 8 hours in DMF and water (1:1) (12 mL). After this period, the solution was cooled to room temperature, and diluted with dichloromethane (30 mL). 30 mL of water was added to the mixture, and the product extracted with dichloromethane. The organic layer was dried over MgSO<sub>4</sub> and concentrated under vacuum. The residue was purified by chromatography on silica gel (4:1 hexane: ethyl acetate) to afford a light-brown solid (60 mg, 27 % yield).; mp 80-82 °C; IR (neat) 1599, 1249, 1172; <sup>1</sup>H NMR (500 MHz, CDCl<sub>3</sub>) δ 7.03-7.67 (m, J = 8.75, 7.26, 1.34, 18H), 6.96 (d, J = 7.43 Hz, 4H), 5.06 (s, 4H); <sup>13</sup>C NMR (125 MHz, CDCl<sub>3</sub>) δ 158.76, 137.05, 129.47, 128.71, 128.57, 128.13, 127.92, 127.47, 126.6, 114.82, 70.06. Mass spec. calc. for C<sub>32</sub>H<sub>26</sub>O<sub>2</sub>: 442.193; found: 445.2 (100 %, M+1), 441.2 (100 %, M-H).



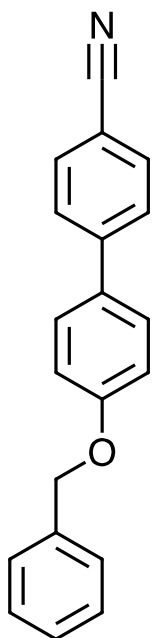
#### 4-(Biphenyloxy)phenylmethane (**2.17**)



**2.17**

4-Bromobenzene (79 mg, 0.5 mmol, 0.052 mL), 4-benzyloxybenzeneboronic acid (114 mg, 0.5 mmol), cesium carbonate, Cs<sub>2</sub>CO<sub>3</sub> (0.33 g, 1 mmol) and palladium(II) complex, **2.4** (20 mg, 5 mol %) or **2.3** (16 mg, 5 mol %) were added to a round bottom flask equipped with a magnetic stir bar. The reaction was stirred at 60 °C for 8 hours in DMF and water (1:1) (6 mL). After this period, the solution was cooled to room temperature, and diluted with dichloromethane (30 mL). 15 mL of water was added to the mixture, and the product extracted with dichloromethane. The organic layer was dried over MgSO<sub>4</sub> and concentrated under vacuum. The residue was purified by chromatography on silica gel (4:1 hexane: ethyl acetate) to afford a yellowish-brown solid for catalyst **2.3** (160 mg, 98 % yield) and a yellow solid for catalyst **2.4** (166 mg, 98.1 % yield).; mp 89-92 °C; IR (neat) 1608, 1270, 1243; <sup>1</sup>H NMR (500 MHz, CDCl<sub>3</sub>) δ 7.28-7.55 (m, J = 12H), 7.05 (d, J = 8.74 Hz, 2H), 5.11 (s, 2H); <sup>13</sup>C NMR (125 MHz, CDCl<sub>3</sub>) δ 158.36, 140.79, 136.99, 134.04, 128.72, 128.62, 128.18, 128.00, 127.49, 126.75, 126.69, 115.14, 70.10. Mass spec. calc. for C<sub>19</sub>H<sub>16</sub>O: 260.120; found: 260.9 for **2.3** and 260.7 for **2.4** (100 %, M+H).

#### 4'-(Benzyloxy)-4-biphenylcarbonitrile (2.18)

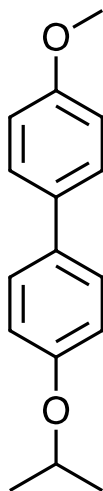


**2.18**

4-Bromobenzonitrile (91 mg, 0.5 mmol), 4-benzyloxybenzeneboronic acid (114 mg, 0.5 mmol), cesium carbonate, Cs<sub>2</sub>CO<sub>3</sub> (0.33 g, 1 mmol) and palladium(II) complex, **2.4** (20 mg, 5 mol %) were added to a round bottom flask equipped with a magnetic stir bar. The reaction was stirred at 60 °C for 8 hours in DMF and water (1:1) (6 mL). After this period, the solution was cooled to room temperature, and diluted with dichloromethane (30 mL). 15 mL of water was added to the mixture, and the product eluted with dichloromethane. The organic layer was dried over MgSO<sub>4</sub> and concentrated under vacuum. The residue was purified by chromatography on silica gel

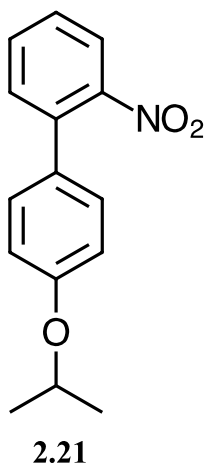
(4:1 hexane: ethyl acetate) to afford a creamy solid (108 mg, 76 % yield).; mp 132-135 °C; IR (neat) 2224, 1623, 1314, 1289, 1267; <sup>1</sup>H NMR (500 MHz, CDCl<sub>3</sub>) δ 7.69 (d, J = 8.50 Hz, 2H), 7.63 (d, J = 8.56 Hz, 2H), 7.54 (dd, J = 8.8, 2.09, 2H), 7.45 (d, J = 7.07 Hz, 2H), 7.41 (dd, J = 7.15, 1.94 Hz, 2H), 7.35 (dd, J = 7.16, 6.3 Hz, 1H), 7.07 (d, J = 8.8 Hz, 2H), 5.12 (s, 2H); <sup>13</sup>C NMR (125 MHz, CDCl<sub>3</sub>) δ 159.39, 145.19, 136.63, 132.58, 131.78, 128.67, 128.39, 128.13, 127.46, 127.13, 119.08, 115.48, 110.18, 70.13. Mass spec. calc. for C<sub>20</sub>H<sub>15</sub>NO: 285.115; found: 286.1 (100 %, M+H).

#### 4-Isopropoxy-4'-methoxybiphenyl (2.20)



4-Bromoanisole (94 mg, 0.063 mL, 0.5 mmol), 4-isopropoxyphenylboronic acid (90 mg, 0.5 mmol), cesium carbonate,  $\text{Cs}_2\text{CO}_3$  (0.33 g, 1 mmol) and palladium(II) complex, **2.4** (20 mg, 5 mol %) were added to a round bottom flask equipped with a magnetic stir bar. The reaction was stirred at 60 °C for 8 hours in DMF and water (1:1) (6 mL). After this period, the solution was cooled to room temperature, and diluted with dichloromethane (30 mL). 15 mL of water was added to the mixture, and the product extracted into dichloromethane. The

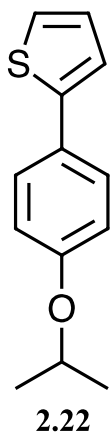
**2.20** organic layer was dried over  $\text{MgSO}_4$  and concentrated under vacuum. The residue was purified by chromatography on silica gel (4:1 hexane: ethyl acetate) to afford an off-white colour (118 mg, 97 % yield).; mp 123-125 °C; IR (neat) 2951, 2839, 1607, 1276, 1251;  $^1\text{H}$  NMR (500 MHz,  $\text{CDCl}_3$ )  $\delta$  7.44-7.49 (m,  $J = 8.1$  Hz, 2H), 7.24-7.31 (m,  $J = 1.3$  Hz, 2H), 6.88-8.97 (m,  $J = 2.65$  Hz, 4H), 4.56 (sept,  $J = 6.85$  Hz, 1H), 3.83 (s, 3H), 1.33 (d,  $J = 6.1$  Hz, 6H);  $^{13}\text{C}$  NMR (125 MHz,  $\text{CDCl}_3$ )  $\delta$  158.7, 157.01, 127.7-127.73, 114.13-114.17, 116.61, 69.96, 55.34, 22.11. Mass spec. calc. for  $\text{C}_{16}\text{H}_{18}\text{O}_2$ : 242.131; found: 243.1 (100 %, M+H).



#### 4'-Isopropoxy-2-nitrobiphenyl (2.21)

1-Bromo-2-nitrobenzene (101 mg, 0.5 mmol), 4-isopropoxyphenylboronic acid (90 mg, 0.5 mmol), cesium carbonate, Cs<sub>2</sub>CO<sub>3</sub> (0.33 g, 1 mmol) and palladium(II) complex, 2.4 (20 mg, 5 mol %) were added to a round bottom flask equipped with a magnetic stir bar. The reaction was stirred at 60 °C for 8 hours in DMF and water (1:1) (6 mL). After this period, the solution was cooled to room temperature, and diluted with dichloromethane (30 mL). 15 mL of water was added to the mixture, and the product eluted with dichloromethane. The organic layer was dried over MgSO<sub>4</sub> and concentrated under vacuum. The residue was purified by chromatography on silica gel (4:1 hexane: ethyl acetate) to afford a dark yellow solid (90 mg, 70.3 % yield).; mp 275-277 °C; IR (neat) 1611, 1526, 1476, 1356, 1244; <sup>1</sup>H NMR (500 MHz, CDCl<sub>3</sub>) δ 7.79 (dd, J = 7.12, 1.4 Hz, 1H), 7.59 (td, J = 6.3, 1.23 Hz, 1H), 7.45 (td, J = 3.2, 1.37 Hz, 1H), 7.42 (dd, J = 1.91, 1.58 Hz, 1H), 7.23 (d, J = 8.74 Hz, 2H), 6.92 (d, J = 8.71 Hz, 2H), 4.59 (sept, J = 6.05 Hz, 1H), 1.33 (d, J = 6 Hz, 3H), 1.30 (d, J = 6 Hz, 3H); <sup>13</sup>C NMR (125 MHz, CDCl<sub>3</sub>) δ 158.07, 135.91, 132.03, 129.12, 128.93, 127.62, 123.98, 115.84, 69.90, 22.06. Mass spec. calc. for C<sub>15</sub>H<sub>15</sub>NO<sub>3</sub>: 257.105; found: 258.10 (100 %, M+H).

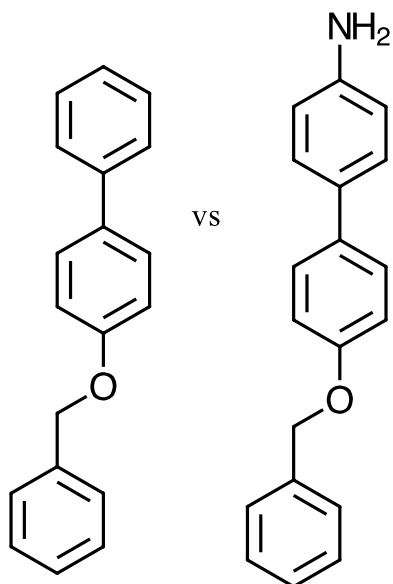
## 2-(*p*-Isopropoxyphenyl) thiophene (2.22)



2-Bromothiophene (82 mg, 0.5 mmol), 4-isopropoxyphenylboronic acid (90 mg, 0.5 mmol), cesium carbonate, Cs<sub>2</sub>CO<sub>3</sub> (0.33 g, 1 mmol) and palladium(II) complex, **2.4** (20 mg, 5 mol %) were added to a round bottom flask equipped with a magnetic stir bar. The reaction was stirred at 60 °C for 8 hours in DMF and water (1:1) (6 mL). After this period, the solution was cooled to room temperature, and diluted with dichloromethane (30 mL). 15 mL of water was added to the mixture, and the product extracted with dichloromethane. The organic layer was dried over MgSO<sub>4</sub> and concentrated under vacuum. The residue was purified by chromatography on silica gel (4:1 hexane: ethyl acetate) to afford a light-brown solid (70 mg, 70 % yield).; mp 68-70 °C; IR (neat) 1602, 1458, 1244, 1181; <sup>1</sup>H NMR (500 MHz, CDCl<sub>3</sub>) δ 7.45 (d, J = 8.75 Hz, 2H), 7.19-7.21 (m, 1H), 7.00-7.05(m, 1H), 6.93 (d, J = 8.75 Hz, 2H), 6.89 (d, J = 8.76, Hz, 1H), 4.57 (sept, J = 6.08 Hz, 1H), 1.36 (s, 3H), 1.34 (s, 3H); <sup>13</sup>C NMR (125 MHz, CDCl<sub>3</sub>) δ 157.50, 144.44, 133.32, 127.78, 127.70, 123.74, 116.07, 69.94, 22.12, 22.10. Mass spec. calc. for C<sub>13</sub>H<sub>14</sub>OS: 218.077; found: 218.8 (100 %, M+H).

## 2.11 Rate Studies

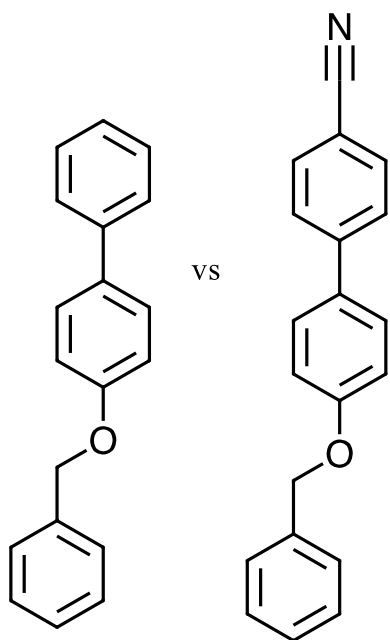
### 4-(Benzyloxy)-1,1'-biphenyl vs 4'-(Benzyloxy)-4-biphenylamine (P2.18 vs P2.9)



4-Bromobenzene (79 mg, 0.5 mmol, 0.052 mL), 4-Bromoaniline (86 mg, 0.5 mmol) and 4-benzyloxybenzeneboronic acid (57 mg, 0.5 mmol), cesium carbonate,  $\text{Cs}_2\text{CO}_3$  (0.33 g, 1 mmol) and palladium(II) complex, **2.3** (16 mg, 5 mol %) or **2.4** (20 mg, 5 mol %) were added to a round bottom flask equipped with a magnetic stir bar. The reaction was stirred at 60 °C for 8 hours in DMF and water (1:1) (6 mL). After this period, the solution was cooled to room

temperature, and diluted with dichloromethane (30 mL). 15 mL of water was added to the mixture, and the product eluted with dichloromethane. The organic layer was dried over  $\text{MgSO}_4$  and concentrated under vacuum. The residue was purified by chromatography on silica gel (4:1 hexane: ethyl acetate) to afford a creamy coloured solid.

**4-(Benzyloxy)-1,1'-biphenyl vs 4'-(Benzyloxy)-4-biphenylcarbonitrile (P2.18 vs P2.19)**



4-Bromobenzene (79 mg, 0.5 mmol, 0.052 mL), 4-Bromobenzonitrile (91 mg, 0.5 mmol) and 4-benzyloxybenzeneboronic acid (57 mg, 0.5 mmol), cesium carbonate, Cs<sub>2</sub>CO<sub>3</sub> (0.33 g, 1 mmol) and palladium(II) complex, **2.3** (16 mg, 5 mol %) or **2.4** (20 mg, 5 mol %) were added to a round bottom flask equipped with a magnetic stir bar. The reaction was stirred at 60 °C for 8 hours in DMF and water (1:1) (6 mL). After this period, the solution was cooled to room temperature,

and diluted with dichloromethane (30 mL). 15 mL of water was added to the mixture, and the product eluted with dichloromethane. The organic layer was dried over MgSO<sub>4</sub> and concentrated under vacuum. The residue was purified by chromatography on silica gel (4:1 hexane: ethyl acetate) to afford a creamy coloured solid.

## 2.12 Conclusion

Thiazole ligated palladacycles **2.3** and **2.4** have been synthesized and characterized. The structure of compound **2.3** was characterized by X-ray crystallography. These novel thiazole-based ligands have been synthesized and used to prepare catalysts which were shown to catalyze Suzuki cross-coupling reactions. These catalysts work very well with aryl bromides and aryl iodides, but they do not catalyzed aryl chlorides and the electronics have been tuned to favour electron-donating group versus electron-withdrawing groups. The reactivity of the prepared catalysts was tested using Suzuki-Miyaura cross-coupling reactions on various aryl halides with different boronic acids at 60 °C after 8 hours under mild conditions with a yield ranging from 27-98 %.

In the rate studies, the relative rate of electron poor aryl halides was faster than electron rich aryl halides with catalyst **2.4** (amine substituted catalyst). The relative rates of the electron rich aryl halides were faster than the electron poor aryl halides when the catalyst with the methyl substituted catalyst (catalyst **2.3**) was used and preference was gotten for electron-donating group (EDG > EWG) which is unusual and makes catalyst **2.3** a suitable catalyst to improve yield of coupling for aryl-halides containing an electron-donating group.

In the future the *o*- vs *m*- vs *p*-substitution with the same substituent will be performed to see how well the different position affects the reactivity in the Suzuki coupling reactions.



# **Chapter 3-The Development of New High-Capacity Solid Support Resins for Use in Mo/Tc-99m Generators.**

## **3.1 Introduction:**

Tc-99m is the most widely used radioisotope in nuclear medical imaging accounting for over 76,000 scans per day.<sup>78</sup> Currently, all the Tc-99m used in Canada is derived from Mo-99/Tc-99 generators, where the Mo-99 is isolated from the fission of U-235 produced by a limited number of nuclear reactors. These reactors rely primarily on highly enriched uranium (HEU) as feed stock. There is increasing pressure to move away from uranium sources that requires HEU because of its alternate use in weapons. Unfortunately, the alternative sources of Mo-99 often result in a low specific activity product, meaning a significantly higher mass of molybdate is required to deliver the same activity of Tc-99m.<sup>78</sup> One way to increase the activity to the same level as the nuclear reactors is to develop a more efficient solid support (for the separation of <sup>99m</sup>Tc radionuclide in a <sup>99</sup>Mo/<sup>99m</sup>Tc generator). This work describes the preparation and testing of methods of new solid supports including “hot” testing with Mo-99. The design requirements that provide selective binding of molybdate over pertechnetate will be discussed. Polymer-based resins were synthesized as an alternative solid support for nuclear medicine scans using modified seeded nanoparticles. Quaternary methyl ammonium ion-based resins were synthesized by grafting or immobilization of glycidyltrimethyl ammonium chloride or Girard’s reagent T onto silica gel using 3-(Triethoxysilyl) propylamine and (3-glycidyloxypropyl) trimethoxysilane and as coupling agents respectively. The uptake

behavior of the two resins were studied with respect to molybdate with a column loading efficiencies of 199 and 195 mg of Mo/g of resin respectively.

### 3.2 Literature Review

Since 2007 there have been a number of interruptions and pressures on the supply of Tc-99m due to unscheduled shutdowns of the nuclear reactors that produce medical isotopes.<sup>78,79</sup> To help mitigate this, a number of alternative approaches have been investigated, such as direct production on a cyclotron via the  $^{100}\text{Mo}(p,2n)^{99\text{m}}\text{Tc}$  reaction.<sup>1, 79-83</sup> The cyclotron approach has the advantage of not requiring HEU but does require day-of-use production and distribution. Due to Canada's large geographic footprint and compounded by weather challenges during the winter months, the distribution is likely to be restricted to urban centres near appropriately equipped cyclotron facilities. An additional challenge is the unwanted co-production of Tc-99g and Tc-95 as well as the very high isotopic purity requirements of the Mo-100 targets.<sup>78, 79-83</sup>

An additional route to the production of Mo-99 for use in generators is via the transmutation of Mo-100. In this process, an electron linear accelerator is used to create high energy x-rays that cause the ejection of a neutron from Mo-100 to produce Mo-99 via the  $^{100}\text{Mo}(\gamma,n)^{99}\text{Mo}$  reaction.<sup>83</sup> While avoiding the use of U-235 this procedure, like the cyclotron route, it requires enriched Mo-100. This costly starting material makes the recovery and recycling of molybdenum from the targets as well as from the generators essential. An additional hurdle to this route is the low specific activity of the product as there is not a time efficient method to separate the Mo-99 from the bulk Mo-100 target.

A lower cost path to Mo-99 is through thermal neutron activation of Mo-98 isotope, which has a high natural abundance. It can be converted to Mo-99 *via* the  $^{nat}\text{Mo}(n,\gamma)^{99}\text{Mo}$  or the more abundant Mo-98 *via* the  $^{98}\text{Mo}(n,\gamma)^{99}\text{Mo}$  reaction. The potential advantage of the  $^{nat}\text{Mo}(n,\gamma)^{99}\text{Mo}$  route is the avoidance of costly isotopically-enriched starting materials as well as not requiring the use of fissile material such as U-235. The obvious downside of this approach is there is no easy or practical method of separating Mo-99 from the other molybdenum isotopes leading to very low specific activity. The use of Mo-98 enriched targets provides a higher specific activity by a factor of approximately 4; however, the cost of enriching the targets makes this approach less desirable.<sup>82</sup>

The low specific activity of the Mo-99 from  $^{nat}\text{Mo}(n,\gamma)^{99}\text{Mo}$  production, as well as the linear accelerator method, necessitates higher loading of molybdenum on the solid support of the generator to get similar activities from the generator. The specific activity resulting from  $^{nat}\text{Mo}(n,\gamma)^{99}\text{Mo}$  is typically in the range of 37 – 370 GBq/g (1 – 10 Ci/g) versus upwards of 185000 GBq/g (5000 Ci/g) if produced by fission of U-235.<sup>1</sup> This means that a typical 370 GBq generator would contain ~2 mg of Mo-99 from fission of U-235 vs. multi-gram quantities of molybdenum required via neutron activation.

To manage this increased loading requirement there are a few options. One option is to increase the volume of alumina absorbent proportionally to manage the additional mass of molybdenum. While this could potentially be done, it creates practical problems. The increased size of the column would require a larger lead or tungsten shield making the generators larger and heavier to use and transport. An additional problem with this route is that the mass of Mo loaded on the column increases but the mass of Tc-99m being eluted

does not. With very large columns and small mass of the eluent the elution profile is likely to be very broad and dilute.

A second option is to identify an alternative solid support of a similar volume/mass to that in current generators, but with a higher loading capacity. While technically more challenging, this would allow for the current generator configuration to be used, with the only change being the solid support. Perhaps most importantly, there would be no change in operating procedures for the end user in the nuclear medicine departments at hospitals. This would allow for generators using Mo-99 from  $^{nat}\text{Mo}(n,\gamma)^{99}\text{Mo}$  or the fission of U-235 to be used interchangeably. The development of improved loading capacity resins would be of benefit to both Mo-99 produced by linear accelerator and by neutron capture.

The work presented in this chapter describes the preparation and testing methods of new solid supports including “hot” testing with Mo-99. The design requirements that provide selective binding of molybdate over pertechnetate will be discussed. Polymer-based resins were synthesized as an alternative solid support for nuclear medicine scans as well as modified seeded nanoparticles.

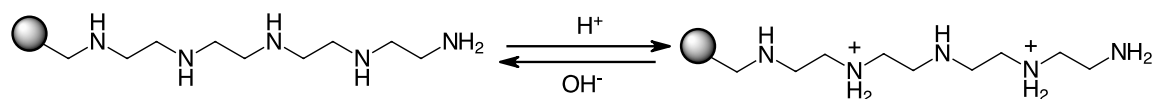
### **3.3 Current Solid support**

There are several solid supports used in the production of  $^{99m}\text{Tc}$  for medical imaging. Examples are activated alumina, zirconium-based material etc. To be able to maintain the supply of  $^{99m}\text{Tc}$  for medical imaging, few grams of acidic alumina ( $\text{Al}_2\text{O}_3$ ) have been used as a sorbent matrix.  $^{99}\text{Mo}$  is extracted from the fission mixture in an alkaline solution as molybdate ion ( $^{99m}\text{MoO}_4^{2-}$ ) and the solution is acidified to maintain a good sorption conditions. After this period, the molybdate is loaded on the pre-acidified column.

The  $^{99m}\text{Tc}$  can be eluted in the form of  $^{99m}\text{TcO}_4^-$  using normal saline which flows through the alumina column.<sup>84,85</sup>

Metal oxide nanoparticles have been used to evaluate the sorption ability of low specific activity  $^{99}\text{Mo}$  in the generation of  $^{99m}\text{Tc}$  for medical imaging. Commercially available metal oxide nanoparticles were investigated under different environmental conditions which include the initial concentration of the molybdate ions, pH and temperature.<sup>86</sup>

Work done by Donia also shows that polyamine-based resins were effective at immobilizing significant quantities of molybdate under acidic conditions.<sup>87</sup> They found the optimal loading pH to be approximately 2. This was explained by the degree of protonation in the polymeric amine resin at pH 2. At higher pH, the equilibrium would be shifted towards the free base, reducing the net positive charge on the resin, and lowering the loading capacity of the solid support. At lower pH, the degree of protonation increases.



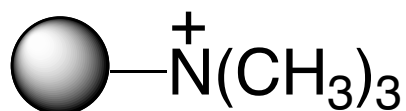
**Scheme 3.1: Protonation states of polyamine-based resin developed by Donia.**

### 3.4 Design Consideration

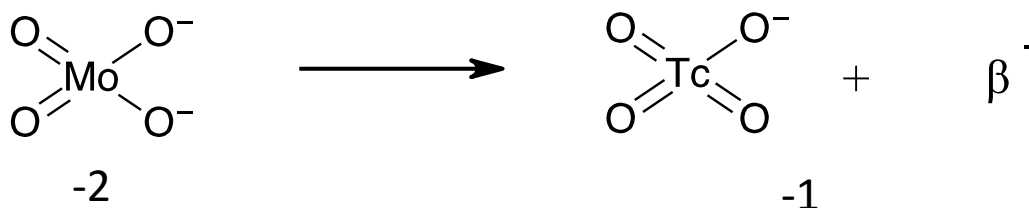
The new resin should have some specific properties to be able to bind molybdate over the pertechnetate. The following properties should be considered.

### 3.4.1 High Binding to Molybdate and Low Binding to Pertechnetate

To get selective binding to the resin, the charge difference between molybdate and pertechnetate could be advantageous to this work. The resin will require a cationic charge to bind the metal-containing anion. The  $^{99}\text{Mo}$  used in generators is in the form of molybdate anion with a **-2** charge. This then decays to  $^{99\text{m}}\text{Tc}$  pertechnetate with a **-1** charge. To accomplish this selectivity, resins which contain ammonium groups were designed as in Scheme 3.2 and Scheme 3.3 below. The resin should be able to work with low specific activity  $^{99}\text{Mo}$  and should have high binding affinity to molybdate and have low binding to pertechnetate.



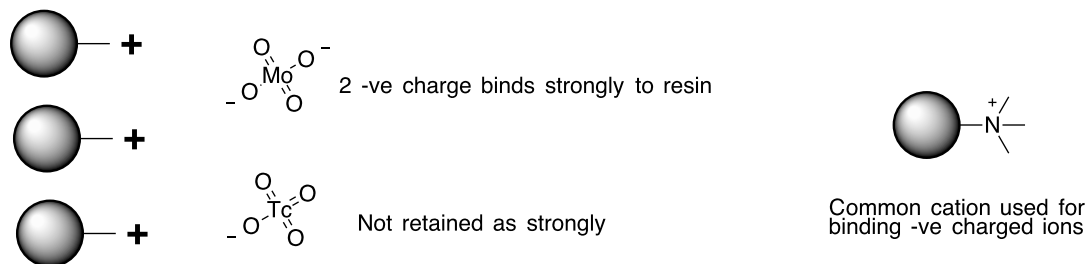
**Scheme 3.2: Resin containing ammonium group.**



**Scheme 3.3: The decay of molybdate anion to pertechnetate**

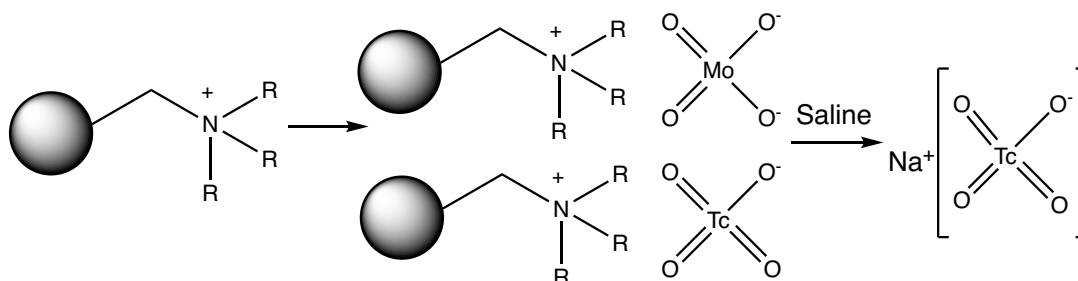
When looking at developing an alternative solid support, silica-based resins offer the most flexibility because they have a larger particle size, which helps prevent clogging. Binding selectivity will be driven by the different charges that exist on the molybdate (-2) vs. the pertechnetate (-1). In order to bind the ions, the resin must have, or be capable of

bearing, a positive charge at the pH at which the column will be eluted. A potential cation for this purpose is the quaternary methyl ammonium (QMA) ion. QMA based resins are commonly used in ion separation and for the immobilization of radionuclides such as F-18 fluoride.



**Scheme 3.4: Interactions between resin and molybdate and pertechnetate ions**

The use of a quaternary ammonium resin is compatible with the use of neutral saline. It is an ion exchange process. The  $\text{Cl}^-$  from the saline exchanges with the  $\text{TcO}_4^-$  on the resin, which gives  $\text{NaTcO}_4$  in solution and in a ready-to-use state (Scheme 3.5).



**Scheme 3.5: The reaction of quaternary ammonium ion resin with molybdate.**

### **3.4.2 Low Swelling**

The resin requires that it should not swell when solvated (smaller column). When the resin swells, it will take up more room in the column lowering the possible molybdenum loading in the same size footprint. Some polymer-based resins showed high molybdate loading but suffered from high swelling.

### **3.4.3 Low Cost of Synthesis**

Generators are typically considered disposable items, it is important when synthesizing resin that it can be done as economically as possible, the resin should not cost more than the product it is distributing.

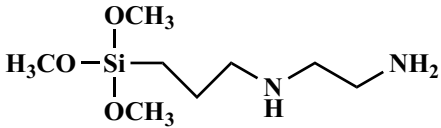
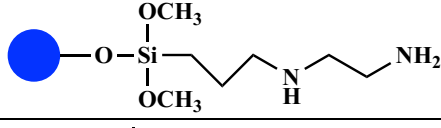
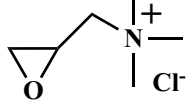
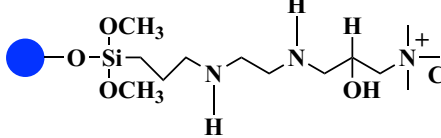
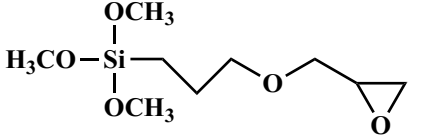
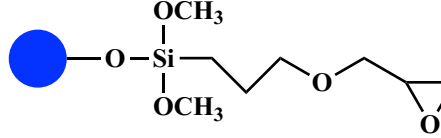
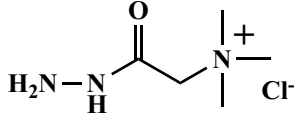
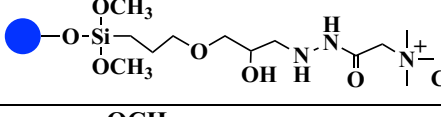
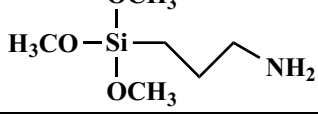
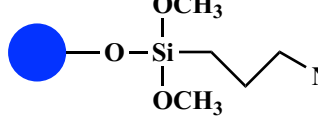
### **3.4.4 Use in Hospital Nuclear Medicinal Labs**

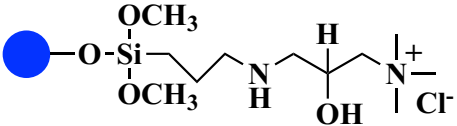
The desired resins must have the same workflow and footprint as current generators used in nuclear medicinal departments at hospitals (lower barrier to adoption) with no change in procedure. This means elution with neutral saline without the use of additives in the mobile phase. The pH of the resin should be neutral since injection of an acid or a base into a patient is not desired or require neutralization after eluting the pertechnetate. US Pharmacopeia<sup>88</sup> requires that in [<sup>99m</sup>Tc] TcO<sub>4</sub><sup>-</sup> generators, more than 95 % of [<sup>99m</sup>Tc] activity must be present as pertechnetate anion. The radiochemical purity should be greater than 90 % and the pH should be between 4.5 to 7.5.

Table 3.1 shows the compound numbers, names and structure used in this chapter where blue circle represent silica gel.



**Table 3.1: Compound numbers, names and structure used in this chapter where blue circle represent silica gel.**

Compound numbers	Compound names	Structure
1	<i>N</i> -[3-(trimethoxysilylpropyl)ethylenediamine	
2	Silica gel- <i>N</i> -[3-(trimethoxysilylpropyl)ethylenediamine	
3	Glycidyltrimethylammonium chloride	
4	Silica gel + <i>N</i> -[3-(trimethoxysilylpropyl)ethylenediamine + Glycidyltrimethylammonium chloride	
5	(3-Glycidyloxypropyl)trimethoxysilane	
6	Silica-(3-Glycidyloxypropyl)trimethoxysilane	
7	Girard's reagent T	
8	Silica + (3-Glycidyloxypropyl)trimethoxysilane + Girard's reagent T	
9	3-(Triethoxysilyl)propylamine	
10	Silica-3-trimethoxysilylpropylamine	

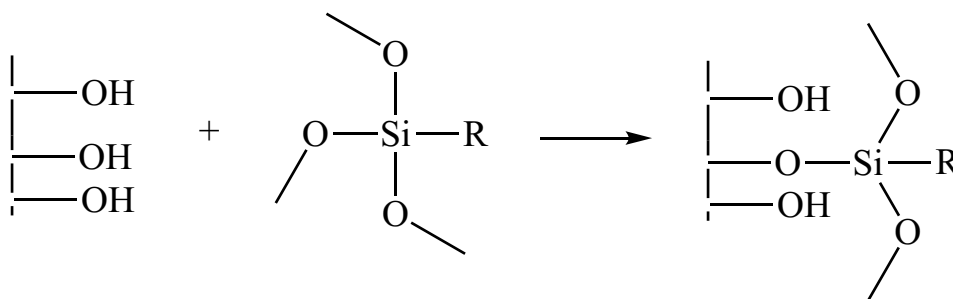
Compound numbers	Compound names	Structure
11	Silica + 3-(Triethoxysilyl)propylamine + Glycidyltrimethylammonium chloride	

## 3.5 Synthesis/Methods

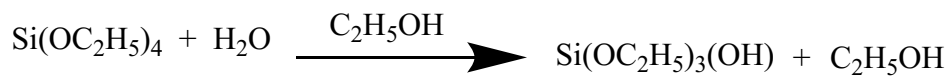
### 3.5.1 Silica Beads

There are different approaches in making a resin, namely the sol gel preparation, modification of commercially available resin, and lastly the silica gel process.

Silica beads can be prepared using sol-gel methods from molecular precursors by creating the resins from scratch. In one instance, they were prepared from tetraethyl orthosilicate (TEOS) in water and alcohol (ethanol) with ammonium hydroxide solution as a catalyst.<sup>89</sup> Condensation between the TEOS and free Si-OH groups (Scheme 3.6) creates a bridging oxygen and initiates the formation of the silicate nanoparticles. There is an increase in particle size with an increase in water concentration (H<sub>2</sub>O/TEOS) and ammonia concentration.<sup>90,91</sup> The presence of concentrated ammonia promotes hydrolysis as well as the promotion of the rate of condensation which will in effect results in higher particle size of the resin.<sup>90,91</sup>



**Scheme 3.6: Condensation of silanol sites with methoxy group**



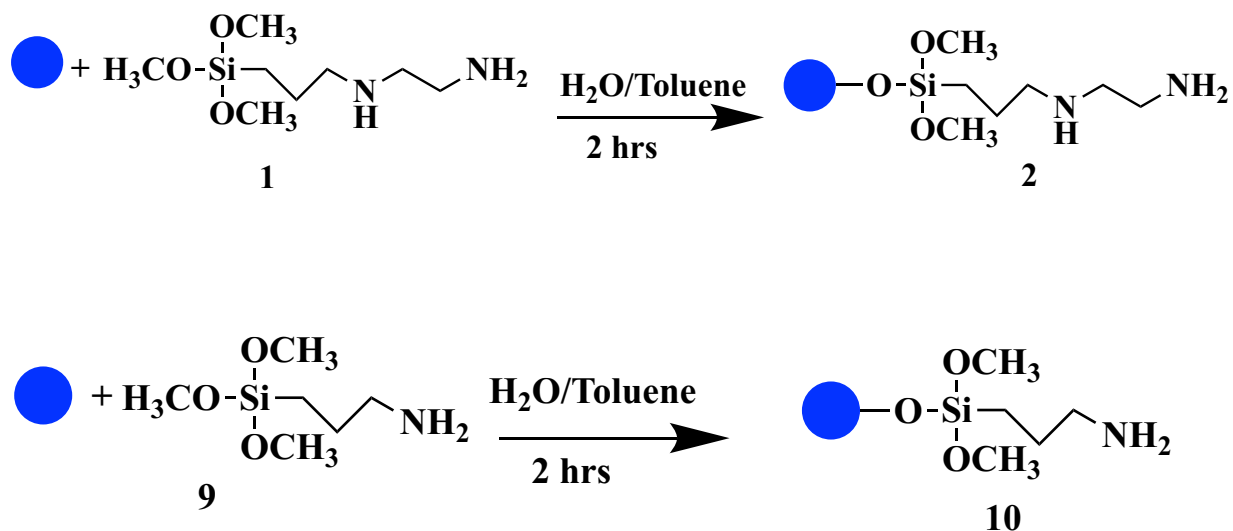
**Scheme 3.7: Silica Beads preparation**

Commercially available amine resins can be used as well for grafting compounds such as epoxides onto them. Examples include SiliaMetS diamine or SiliaBond amine which can be further functionalized. Some commonly used amine resin examples are methylenebisacrylamide (MBA) which is used as a crosslinker for grafting tetraethylenepentamine (TEP) in the polymerization of glycidyl methacrylate (GMA) to give the resin (GMA/MBA/TEP).<sup>87</sup>

Attempts to generate suitably substituted silica beads using a sol-gel method from molecular materials and other commercially available amines failed. The silica nanoparticles thus created were too small and did not bind to the amine precursor. They were also so small that they led to clogging when loaded onto the column. Because of this, cheap commercial silica gel, which has a larger particle size, was used in the subsequent reactions.

**3.5.2 General Synthesis for Grafting/Immobilization of Beads on Amines**

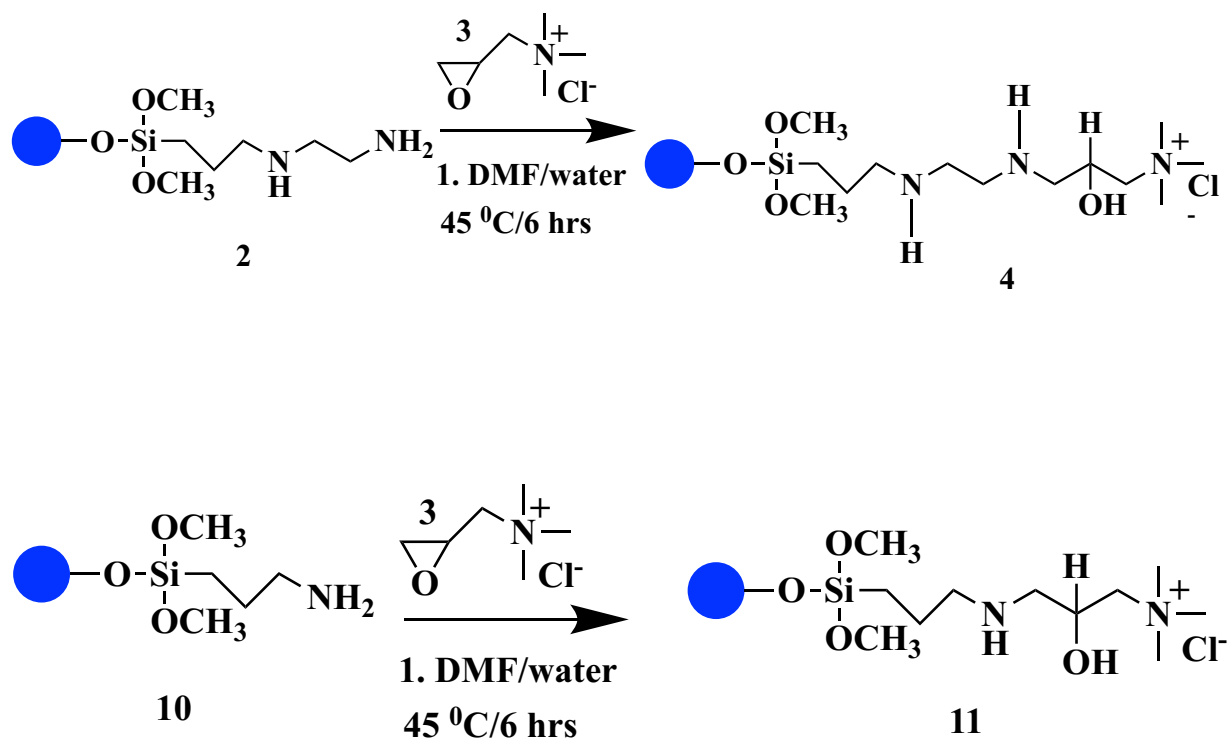
To get functionalization on the surface of silica gel, an amine-containing compound, N-[3-(trimethoxysilyl) propyl]ethylenediamine (**1**) or 3-(Triethoxysilyl)propylamine (**9**), was grafted on the surface of the prepared silica. The presence of the alkoxy silane group in (**1** and **9**), helped in the condensation reaction to yield a chemical bond, resulting in the silica-bound materials **2** and **10**, respectively (Scheme 3.8). These amine containing resins are now ready for further functionalization.



**Scheme 3.8: Synthetic route to resins (silica gel + amine (1 or 9))**

### 3.5.3 General Synthesis for Grafting/Immobilization of Silica Beads, with an Amine, and an Epoxide

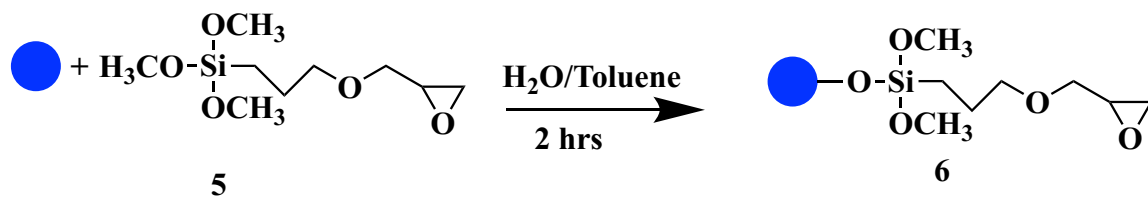
To get positively-charge resins, which will help bind the molybdate (-2 charge) to the resin, a quaternary methyl ammonium ion, (glycidyltrimethylammonium chloride) (**3**) was introduced to the modified resins (**2 and 10**). They were reacted with epoxide **3** to yield compounds **4** and **11** respectively. The products were filtered and washed with ethanol and water to remove excess epoxide and left to dry in the oven at 110 °C to obtain a colourless solid (Scheme 3.9).



**Scheme 3.9: Synthetic route of resins (compounds 4 and 11)**

### 3.5.4 Grafting/Immobilization of Silica Gel and (3-Glycidyoxypropyl) trimethoxysilane

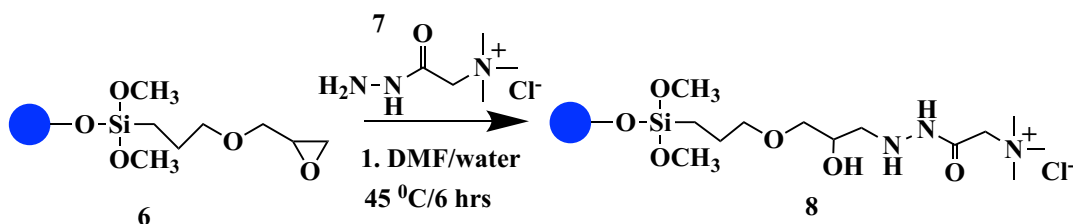
To extend the scope of studies of the resin and get functionalization on the surface of the commercial silica gel, (3-glycidyoxypropyl) trimethoxysilane (**5**) was grafted on the surface of the prepared silica gel. The alkoxy silane group in **5**, undergoes condensation reaction with silica gel to give compound **6** as shown in Scheme 3.10.



**Scheme 3.10: Synthetic route to resin (Silica gel+ (3-Glycidyloxypropyl) trimethoxysilane (5))**

### 3.5.5 Grafting/immobilization of Silica Gel and (3-Glycidyloxypropyl) trimethoxysilane and Girard's Reagents T

Epoxides easily react with amine end group functionality which bonds to silica gel.<sup>92</sup> The silica-(3-glycidyloxypropyl) trimethoxysilane bound resin (6) was further treated with Girard's reagent T (7) in DMF solution which helps in opening the epoxide ring to generate the positive charge on the resin to obtain compound 8 as shown Scheme 3.11.



**Scheme 3.11: Synthetic route to compound 8**

## 3.6 Cold Studies

### 3.6.1 Preparation of Ammonia Molybdate Test Solution

A standard ammonium molybdate solution was prepared by mixing 1.84 g of ammonia molybdate tetrahydrate in 100 mL of deionized water. The mixture was stirred

for 1 hour at room temperature until all the solid has been dissolved to give a molybdenum concentration of 10 mg/mL.

### **3.6.2 Uptake Measurement-Cold Studies (Inductively coupled plasma atomic emission spectroscopy)**

#### **3.6.2.1 Column loading efficiency.**

To determine the loading capacity of the resin, 150 mg was treated with a stock solution of molybdate (4 mL, 10 mg/mL, 40 mg of Mo) for 1 hour. The solution was filtered and 100  $\mu$ L of the filtrate was diluted to 100 mL with deionised water and tested by inductively coupled plasma (ICP) to determine molybdenum concentration.

The resin's loading efficiency was calculated by subtracting the amount of molybdenum held by each of the resins (mg/mL) from the amount of free ammonia molybdate tetrahydrate (stock) which has a concentration of 10 mg/mL (Figure 3.1). This is multiplied by 4 mL of the ammonia molybdate tetrahydrate that was added to each resin in the syringe and then divided by the amount of resin taken into each syringe (0.15 g). The loading efficiency is calculated by the equation:

$$[(L_1 - L_2) * 4 \text{ mL}] / 0.15 \text{ g (Mg of Mo/g of resin)}$$

Where  $L_1$  is the concentration of the stock solution (10 mg/mL) and  $L_2$  is the concentration remaining in solution after interaction with the resin and  $L_1 - L_2$  is the amount of molybdenum bound by each of the resins (mg/mL). This is illustrated schematically by Figure 3.1 below.

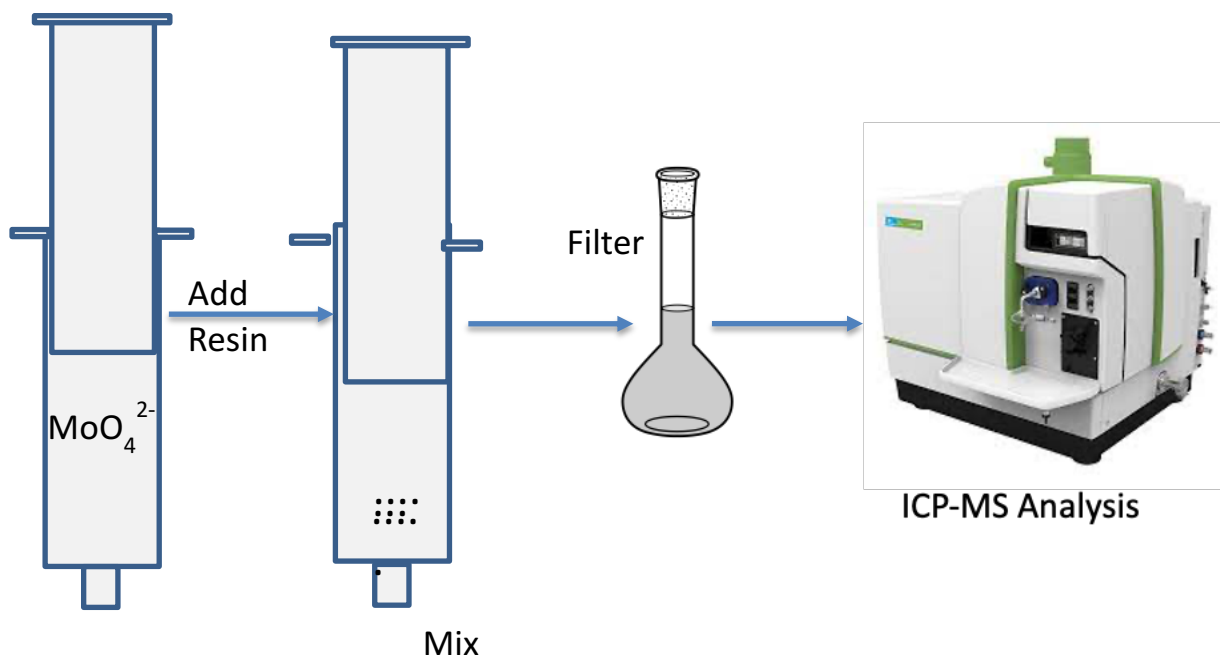


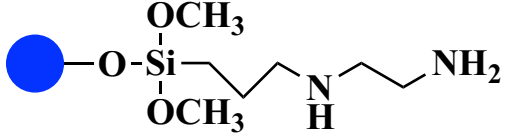
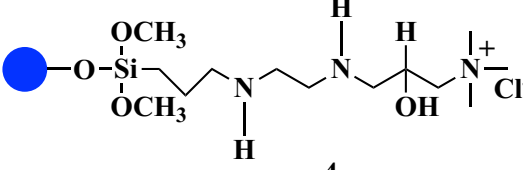
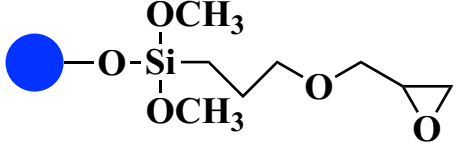
**Figure 3.1: Determining column loading efficiency of the resin.**

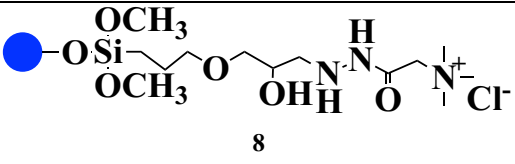
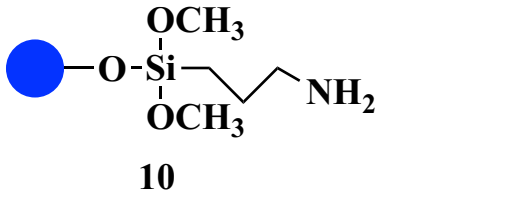
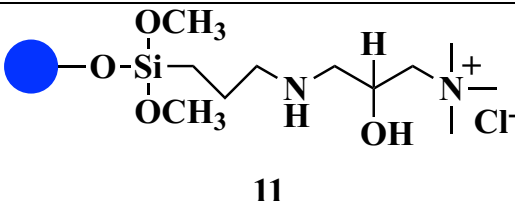
It was found that amine functionalization of the resin (as synthesized by the routes shown in Schemes 3.9 and 3.11) improved the binding of molybdate. Epoxide functionalization improves the resin performance still further, as evident in the column's loading efficiency. From Table 3.2 there is a binding increase from 140 mg (compound 2) to 173 mg (compound 4) of Mo per gram of resin upon the addition of compound 1 and 3 and a binding increase from 11 (compound 10) to 192 mg (compound 11) of Mo per gram of resin upon the addition of compound 9 and compound 3 to the resin respectively. A similar trend is seen in Table 3.2 as the addition of compound 5 to the resin and further addition of the Girard's reagent T (7), an increase of 3 mg (compound 6) to 199 mg (compound 8) of Mo per gram of resin upon the addition of GOPTS (5) and Girard's reagent T (7) respectively. This increase in the loading efficiency is because of the positive charges created on the resin. The addition of positive charges helps improve binding of the



resin to the molybdate but as can be seen in Table 3.2, resins with an epoxide (compounds 4 and 11, with 173 and 192 mg of bound Mo respectively) were less effective (degree of binding) than when the epoxide was subsequently functionalized (compound 8 with 199 mg of bound Mo).

**Table 3.2: ICP-AES results of modified resins showing Mo remaining in solution after treatment with resin and the column loading efficiency of the various modified resins.**

Modified Beads	[Mo] left after treatment with resin- mg/mL (Toluene)	Column loading efficiency- Mg of Mo/g of resin (Toluene)	[Mo] left after treatment with resin- mg/mL- (H <sub>2</sub> O)	Column loading efficiency- Mg of Mo/g of resin- (H <sub>2</sub> O)
 <p style="text-align: center;">2</p>	4.77	140	5.02	132
 <p style="text-align: center;">4</p>	3.53	173	3.61	170
 <p style="text-align: center;">6</p>	9.87	3	9.98	1

Modified Beads	[Mo] left after treatment with resin- mg/mL (Toluene)	Column loading efficiency- Mg of Mo/g of resin (Toluene)	[Mo] left after treatment with resin- mg/mL- (H <sub>2</sub> O)	Column loading efficiency- Mg of Mo/g of resin- (H <sub>2</sub> O)
 <p style="text-align: center;">8</p>	2.52	199	2.53	199
 <p style="text-align: center;">10</p>	9.58	11	9.63	10
 <p style="text-align: center;">11</p>	2.79	192	2.84	191

### 3.7 Hot Technetium testing

Each of the resins (4, 8 and 11) (Table 3.3) was split into two portions. One part of the resin was preconditioned by flowing water through the resin and the other part conditioned with molybdate to potentially saturate any binding sites. This gave a more realistic representation of what the column will look like when used as a generator.

Also, in all the resins, it is evident that the activity on the resin when treated with molybdate, a little bit less of Tc was attached to the resin which is an indication that Mo is

occupying some of the binding sites. However, in compound 4 it didn't make much of a difference in terms of the % Tc recovered compared to the compound 8 and 11.

To show that the resins prepared bind to molybdate ( $\text{MoO}_4^{2-}$ ) and release pertechnetate ( $\text{TcO}_4^-$ ), one has to get selectivity for the resins that bond strongly to molybdate but not pertechnetate. To determine if this selectivity existed in the resin, the resin was first exposed to a flow of radioactive (hot) technetium. The activity of the resin after the flow gave the data shown in Table 3.3.

Upon treatment of the resins with technetium (Tc), it was realized that resin 4's percentage recovery was 0.2 % of the Tc when treated with either water or molybdate solution ( $\text{MoO}_4^{2-}$ ). The percentage recovery of resins 8 and 11 was higher compared to resin 4 when they were treated with either water or molybdate solution (Table 3.3). There is a slightly better recovery of pertechnetate when the two resins (8 and 11) were treated with molybdate solution which indicated an interaction between the  $\text{MoO}_4^{2-}$  and  $\text{TcO}_4^-$ . These results are consistent with column loading efficiencies done in the cold studies.

The reasons for these changes in the column loading efficiencies is potentially due to the relative position of the hydroxyl group (OH) and the positive charges on the resins prepared. In compounds 4 and 11, the OH group is close to the positive charges which is in effect closer to the technetium (Tc) of interest and thereby can form hydrogen bonding interactions with the  $\text{TcO}_4^-$  which will stabilize the pertechnetate binding to the resins as seen in Figure 3.2.

**Table 3.3: Activity on resin, activity flow through, total activity and % Tc retained on resins.**

Sample ID	Activity on Resin (MBq)	Activity Flow Through (MBq)	Total Activity (MBq)	% T Recovered
4 (H <sub>2</sub> O)	90.10	0.16	90.26	0.2
4 (Mo)	88.30	0.17	88.47	0.2
8 (H <sub>2</sub> O)	1.01	81.8	82.81	98.8
8 (Mo)	0.82	92.3	93.12	99.1
11 (H <sub>2</sub> O)	3.31	81.6	84.91	96.1
11 (Mo)	1.06	76.2	77.26	98.6

**Reaction conditions:** Resins sample were either conditioned with distilled water or Mo solution before testing.

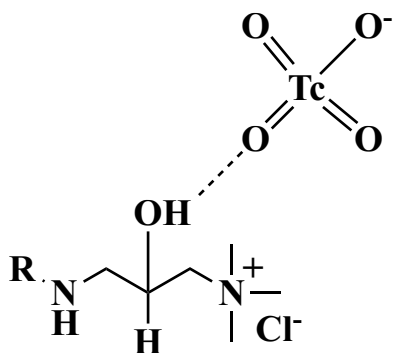


**Figure 3.2: Hydrogen bond interaction between the pertechnetate and the hydroxyl of the resin (R is alkoxy silane group)**

On other hand, in compound **8**, the OH group is farther from the positive charges and cannot form a hydrogen bonding interactions ( $\text{OH}\cdots\text{O}$ ) which helps release the  $\text{TcO}_4^-$ . Therefore, having a longer chain between the OH and the positive charges might help improve binding of the molybdate ion and selectively releases the pertechnetate.

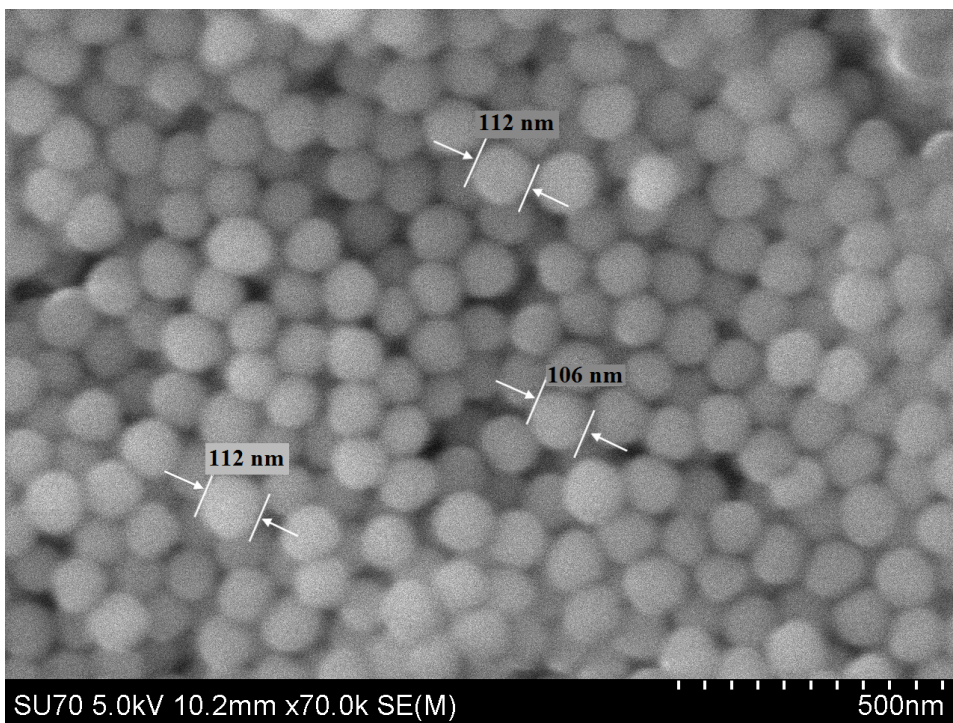
## **3.8 Characterization**

The resins were analyzed by scanning electron microscopy (SEM) for size information and inductively coupled plasma atomic emission spectroscopy (ICP-AES) to determine the amount of molybdenum left after treatment with the modified silica. Bulk size average and distribution was analyzed with a Malvern Mastersizer 2000 particle-size analyzer.

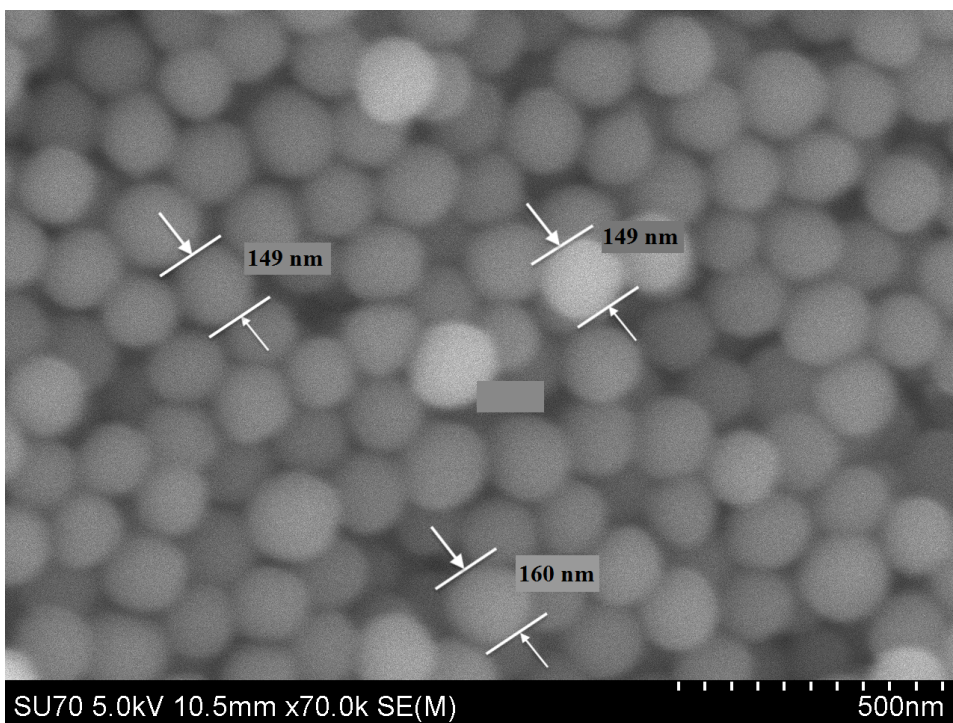
### **3.8.1 Scanning Electron Microscopy**

The bead sizes were measured directly from the scanning electron microscopy (SEM) image. All the images in Figures 3.3 to 3.9 are at the same scale (500 nm is shown by the white hashes on the lower right). Three representative size measurements are shown in each figure.

Figure 3.3 below is the scanning electron microscopy image of the unsubstituted silica beads. Several beads were measured, with the average size found to be 110 nm.

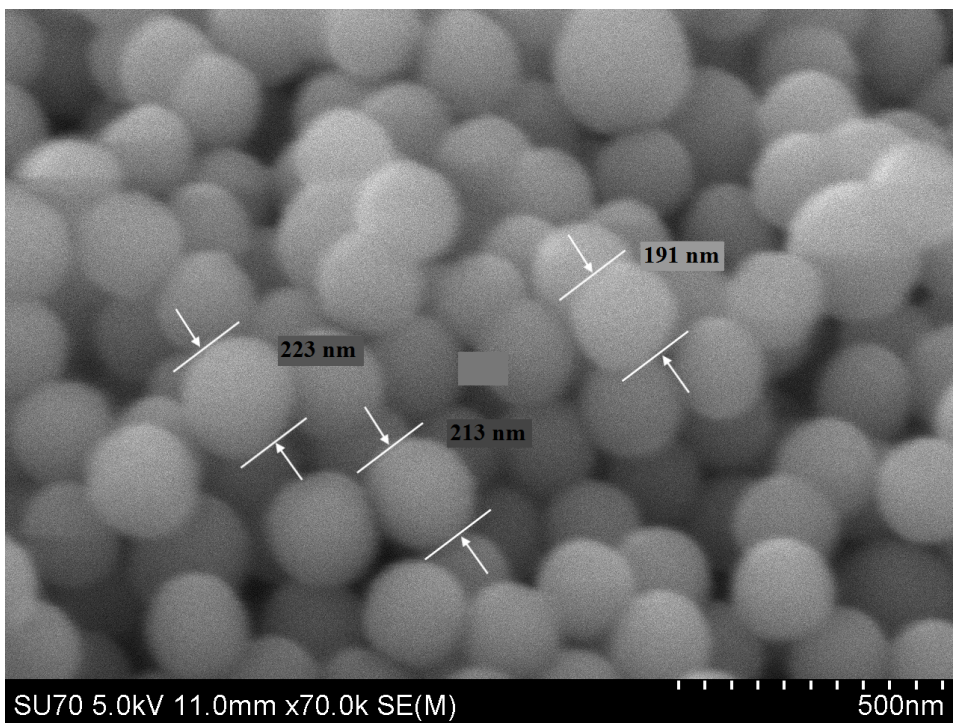


**Figure 3.3: Scanning electron microscopy image of silica beads**

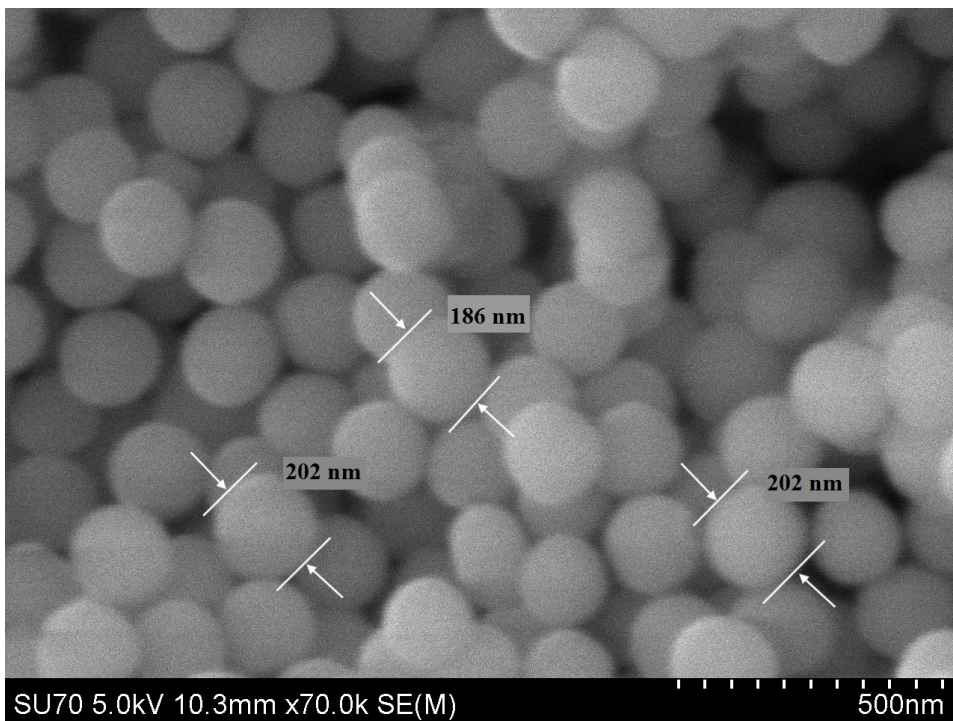


**Figure 3.4: scanning electron microscopy image of compound 2**

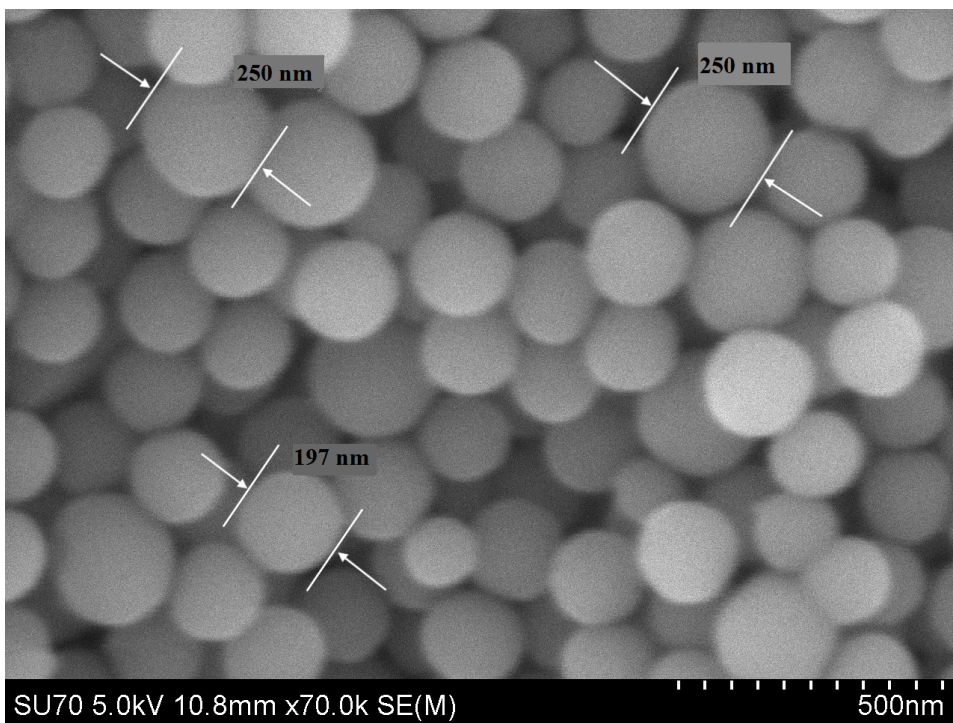




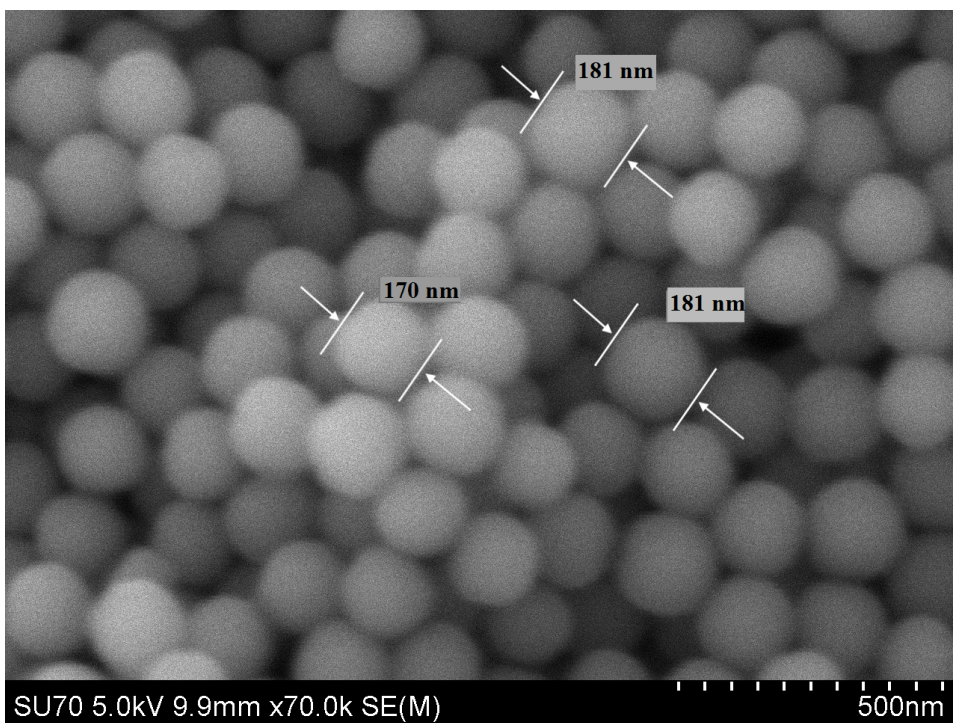
**Figure 3.5: Scanning electron microscopy image of compound 4**



**Figure 3.6: Scanning electron microscopy image of compound 6**

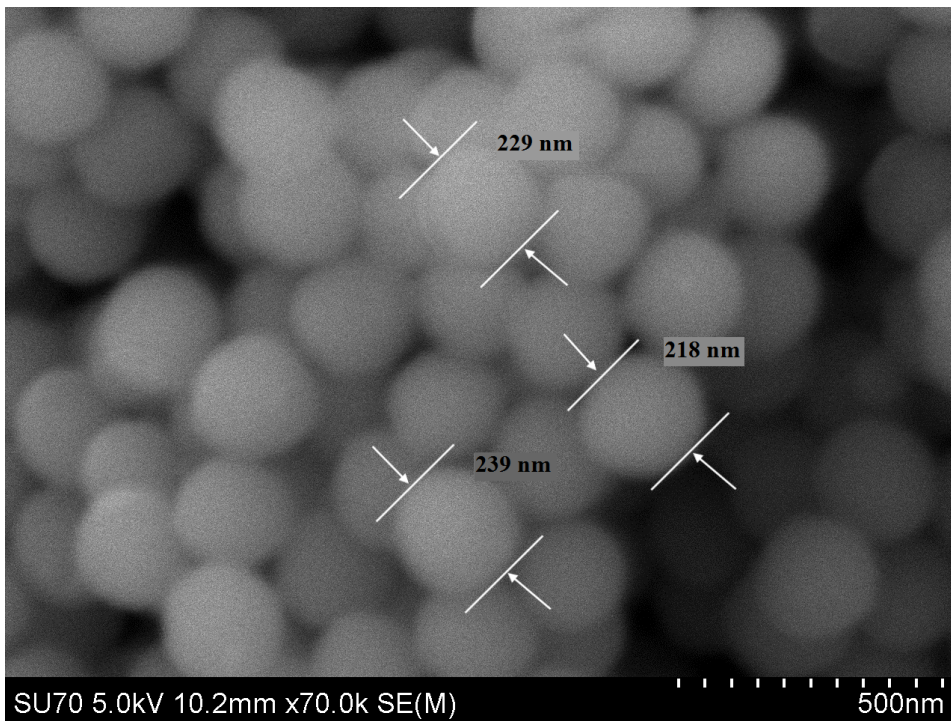


**Figure 3.7: Scanning electron microscopy image of compound 8**



**Figure 3.8: Scanning electron microscopy image of compound 9**

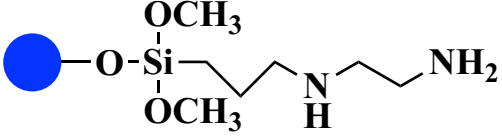
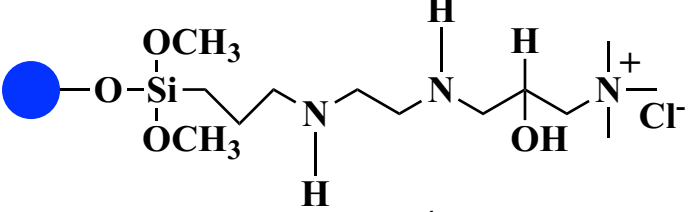
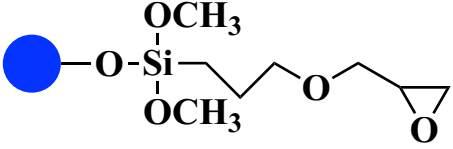
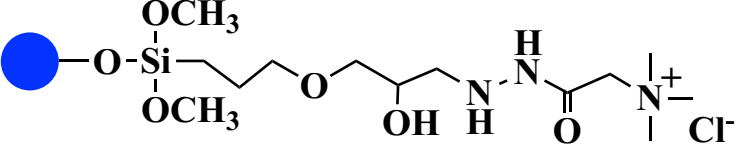
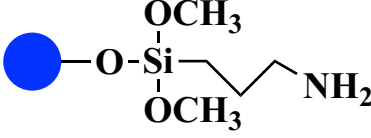


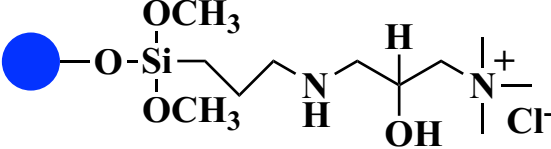


**Figure 3.9: Scanning electron microscopy image of compound 11**

A general trend that is commonly seen in this modified resin is the fact that there is an increase in size of the resins upon each modification as seen in Figures 3.3-3.9 and Table 3.4. This is as a result of the introduction of positively charged quaternary methyl ammonium ions on the resins.

**Table 3.4: Scanning electron microscopy of the size of modified silica beads and size of resins (nm)**

Modified resins	Size of resins (nm)
 <p style="text-align: center;">2</p>	150.00
 <p style="text-align: center;">4</p>	208.33
 <p style="text-align: center;">6</p>	194.44
 <p style="text-align: center;">8</p>	234.26
 <p style="text-align: center;">10</p>	188.00

Modified resins	Size of resins (nm)
 <p style="text-align: center;">11</p>	231.50

### 3.8.2 Particle size analysis

Below in **Figures 3.10-3.13** are the particle size distributions of silica gel and the three modified compounds **4**, **8**, and **11**. A similar trend as seen in the scanning electron microscopy is observed in the particle size analysis as measured on the Malvern Mastersizer 2000 particle size analyser. The average size of silica gel was found to be 64.522  $\mu\text{m}$  whereas the modified gels **4**, **8**, and **11** were found to have average sizes of 13.485  $\mu\text{m}$ ., 30.664  $\mu\text{m}$ ., and 23.949  $\mu\text{m}$ . respectively. Although the size of the modified silica gel was smaller than the unmodified silica gel, this could be attributed to break down from mechanical stirring of the modified particles. Several hours of stirring results in the decrease in size of the modified particles.

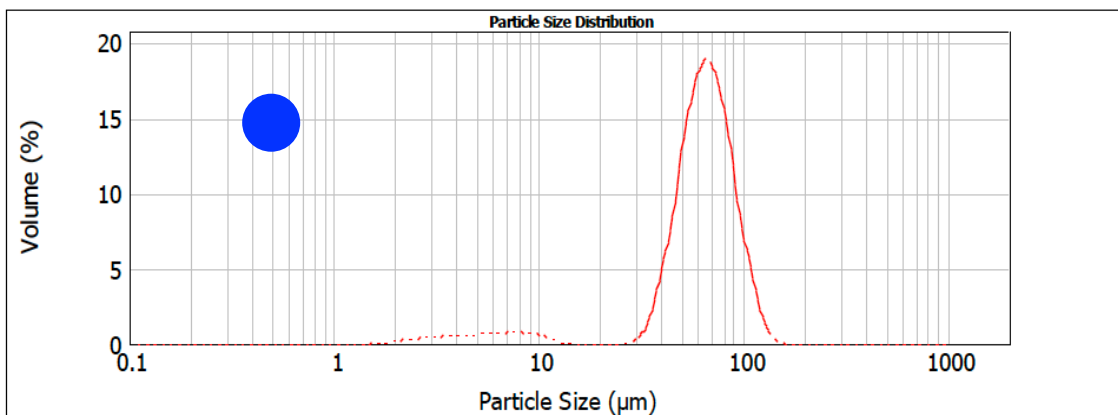


Figure 3.10: Particle size distribution of silica gel

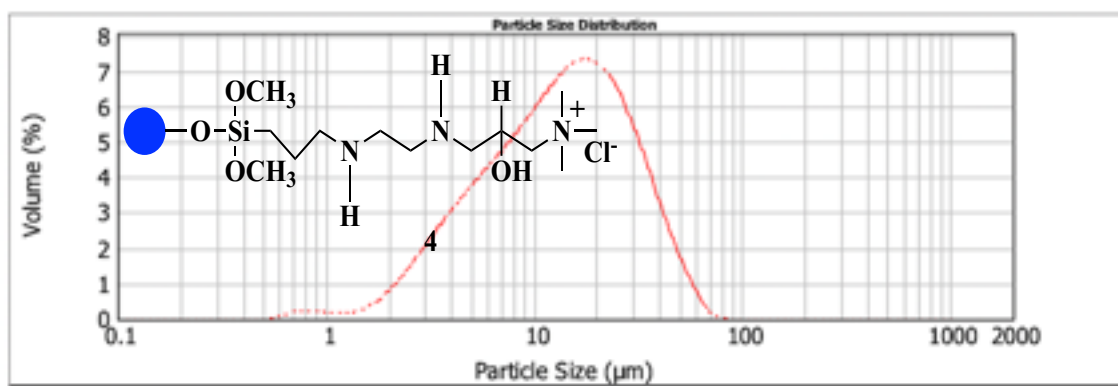


Figure 3.11: Particle size distribution of compounds 4

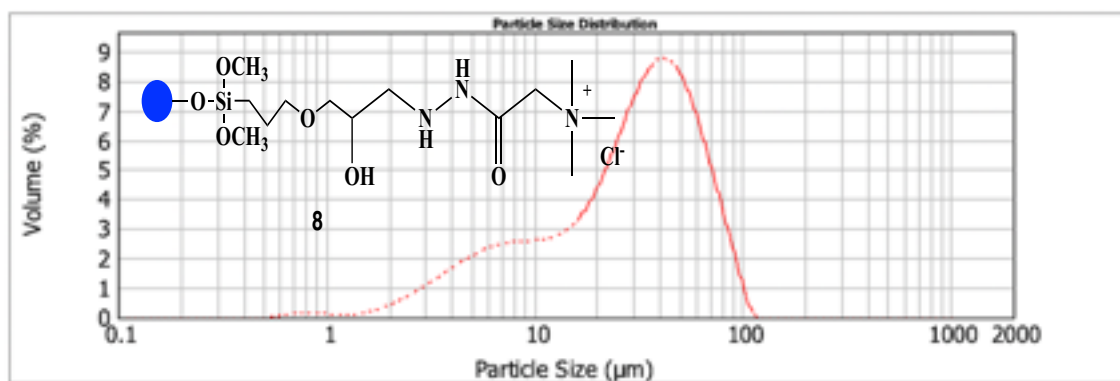
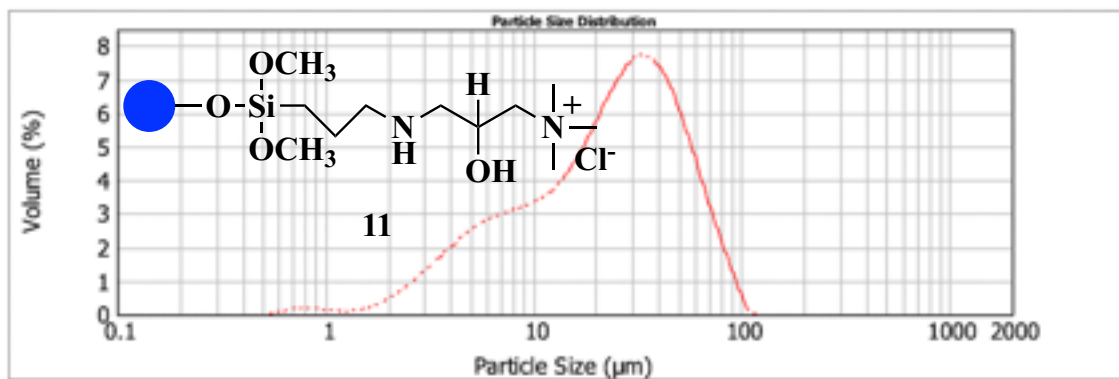


Figure 3.12: Particle size distribution of compound 8



**Figure 3.13: Particle size distribution of compounds 11**

### 3.9 Results and Discussion

The syntheses of the various resins are presented in Schemes 3.7-3.10. Grafting of the N-[3-(trimethoxysilyl) propyl] ethylenediamine (**1**), (3-glycidyloxypropyl)trimethoxysilane (**5**) and 3-trimethoxysilylpropylamine (**10**) occurred at the silanol sites on the surface of the nanoparticles. Toluene was chosen as the solvent in this work to prevent wetting of the resin. Several previous reports suggest that water lowers the contact angle for the amine to bind to the silanol site (hydroxyl group), which leads to a lower condensation product yield; an organic solvent gives a wide contact angle, facilitating the reaction.<sup>92,93</sup> An organic solvent such as toluene, makes the contact angle becomes wide, facilitating the reaction and increasing the affinity for the amine group to react with the silanol. Although according to Delamar *et al.*,<sup>93</sup> since the use of water lowers the condensation product, water (since water is a green solvent, environmentally friendly) was tried in this step and almost the same results were obtained (identical column loading

efficiency) compared to when organic solvent such as toluene was used as seen in Table 3.2.

Epoxide groups (compounds **3**, **5** and **6**) can react easily with the amino group on the end of the modified silica species **2**, **7** and **10**.<sup>94, 95-97</sup> This is seen in Schemes 3.7-3.10 as the coupling agent reacts with the epoxides to form the chemical bond.

Table 3.2 gives a summary of the ICP-AES results (cold Mo studies) of modified resins showing molybdate remaining in a solution after treatment with resin, which is a measure of the column loading efficiency. The initial solution was 10 mg/mL in molybdate. Compounds **2** and **10**, made from the addition of amines **1** and **9** to the unsubstituted resin, give residual molybdate concentrations of 4.77 and 9.58 mg/mL respectively, or 47.7 and 95.8% Mo remaining in solution (and therefore 52.3 and 4.2% uptake). The presence of the alkoxy silane in these amines helps in the condensation reaction with the silanol sites. Upon further addition of the Girard's reagent T (**3**) to compounds **2** and **10** to give compounds **4** and **11**, respectively, there is an improvement in molybdate uptake. The concentration remaining in solution after exposure decreases to 3.53 (**4**) from 4.77 (**2**) mg/mL, indicating an uptake increase from 52.3 to 64.7%. The increase is even more marked for compound **11**, with a decrease in residual concentration from 9.58 to 2.79 mg/mL, corresponding to an uptake increase from 4.2 to 72.1%. Grafting the epoxide to the ethylenediamine increases the number of positive charges on the resin which improves binding of Mo to the resin.

A similar situation occurs with resins **6** and **8**. The initial resin **6** (created by attachment of epoxide **5** to the untreated nanoparticles) showed minimal uptake, with a residual molybdate concentration of 9.87 mg/mL. However, upon treatment with Girard's

reagent T (**7**), the resulting resin **8** had a residual molybdate concentration of 2.52 mg/mL, and improvement from 1.3 to 74.8% uptake. This is attributed to the increase in the number of positive charges on the resin because of the grafting of the Girard's reagent onto the original coating and likely due to the presence of the carbonyl group and position of the hydroxyl group on this resin.

The general trend shows that the opening epoxide rings, which forms additional OH sites, aids in the binding of molybdate to these compounds as seen in Schemes 3.8-3.11 above.

### **3.10 Hot Mo/Tc Analysis**

Radioactive molybdate was bound to the modified resins at the Thunder Bay Regional Health Research Institute (TBRHRI) cyclotron facility using activated [Mo-99] molybdenum pellets. The generator was eluted with normal saline and tested for activity to see how the prepared resins were selective towards molybdenum and able to release pertechnetate in solution. The modified resin **4** showed a lower affinity to molybdenum or technetium strongly binds to the resin with only about 0.02 % of the expected technetium being released. This resin (**4**) shows poor elution of pertechnetate which could be caused by low molybdate affinity, or the technetium binds strongly to the resin. The modified resin, **11** showed a better affinity towards molybdenum with 98.6 % of technetium released and the resin does not bind to the Tc. The modified resin, **8** had the best technetium recovery of about 99.2 % released. In resin (**8**), because of the location of the hydroxyl group as

depicted in the cold studies in **section 3.5**, it is known that resin (**8**) shows very good binding to molybdate, and it is seen here that Mo has been bound to the resin.

The reason for the poor recovery of Tc in resin (**4**) could either be because there is not enough Mo-99 getting onto the resin or the technetium binds to the resin strongly. To confirm the reasons for the lower elution of Tc, a study at the nuclear medicine department of the Thunder Bay regional health research institute was conducted with radioactive Tc and it was found that this resin (**4**) binds strongly to the Tc. On the other hand, good recovery is seen from resin **8**, which (as seen in section 3.4) has a strong affinity for molybdate. In this resin **8**, the hydroxyl group is far away from the charged centre, leading to good recovery of the less highly charged pertechnetate as seen in Table 3.3.

## **3.11 Experimental**

### **3.11.1 Chemicals**

All chemicals were purchased from Sigma Aldrich and were used as received.

### **3.11.2 Preparation of the silica gel.**

Silica gel was dried in an oven at 110 °C for 72 hours.

### **3.11.3 Functionalization of surface of silica**

#### **3.11.3.1 Grafting/immobilization of Silica gel and N-[3-(trimethoxysilyl)propyl] ethylenediamine (2)**

##### **Condition 1**

A mixture of *N*-[3-(trimethoxysilyl) propyl] ethylenediamine (**1**) (1 mL) and toluene (100 mL) (1 %, v/v) was added into a round bottom flask containing silica gel (**3**)



g) and stirred at room temperature for 2 hours. After this period, the crude product was collected by vacuum filtration. The product was washed three times with toluene and heated to 110 °C under vacuum for 16 hours to remove absorbed organics. After this period, the product was dried in the oven for 24 hours at 110 °C to yield compound **2**.

### **Condition 2**

A mixture of *N*-[3-(trimethoxysilyl) propyl] ethylenediamine (**1**) (1 mL) and distilled water (100 mL) (1 %, v/v) was added into a round bottom flask containing silica gel (3 g) and stirred at room temperature for 2 hours. After this period, the crude product was collected by vacuum filtration. The product was washed three times with water and heated to 110 °C under vacuum for 16 hours to remove absorbed organics. After this period, the product was dried in the oven for 24 hours at 110 °C to yield compound **2**.

### **3.11.3.2 Grafting/Immobilization of glycidyltrimethylammonium chloride (3) with modified silica gel (compound 4)**

#### **Condition 1**

A mixture of glycidyltrimethylammonium chloride (**3**) (2 mL) and *N,N*-dimethylformamide (100 mL) (2 %, v/v) was added to a round bottom flask containing 2 g of modified silica gel (Silica gel and **1**). This reaction was stirred at 45 °C for 6 hours. The mixture was collected by vacuum filtration and washed three times with *N,N*-dimethylformamide to remove unreacted glycidyltrimethylammonium chloride molecules (**3**). The product was dried in the oven for 24 hours at 110 °C to yield compound **4**.

## **Condition 2**

A mixture of glycidyltrimethylammonium chloride (**3**) (2 mL) and distilled water (100 mL) (2 %, v/v) was added to a round bottom flask containing 2 g of modified silica gel (Silica gel and TMSPED). This reaction was stirred at 45 °C for 6 hours. The mixture was collected by vacuum filtration and washed three times with N, N-dimethylformamide to remove unreacted glycidyltrimethylammonium chloride molecules (**3**). The product was dried in the oven for 24 hours at 110 °C to yield compound **4**.

### **3.11.3.3 Grafting/Immobilization of silica gel with (3-Glycidyoxypropyl) trimethoxysilane (**6**).**

#### **Condition 1**

A mixture of (3-glycidyoxypropyl)trimethoxysilane (**5**) (1 mL) and toluene (100 mL) (1 %, v/v) was added into a round bottom flask containing silica gel (5 g) and stirred at room temperature for 2 hours. After this period, the crude product was collected by vacuum filtration. The product was washed three times with toluene and heated to 110 °C under vacuum for 16 hours to remove absorbed organics. After this period, the product was dried in the oven for 24 hours at 110 °C to yield compound **6**.

#### **Condition 2**

A mixture of (3-glycidyoxypropyl)trimethoxysilane (**5**) (1 mL) and distilled water (100 mL) (1 %, v/v) was added into a round bottom flask containing silica gel (5 g) and stirred at room temperature for 2 hours. After this period, the crude product was collected by vacuum filtration. The product was washed three times with water and heated to 110 °C

under vacuum for 16 hours to remove absorbed organics. After this period, the product was dried in the oven for 24 hours at 110 °C to yield compound **6**.

#### **3.11.3.4 Grafting/Immobilization of Girard's reagent T with modified silica (compound 8)**

##### **Condition 1**

A mixture of Girard's reagent T (**7**) (5.67g, 2 equiv.) and *N,N*-dimethylformamide (100 mL) (2 %, v/v) was added to a round bottom flask containing 4 g of modified silica gel (Silica + **5**). This reaction was stirred at 45 °C for 6 hours. The crude product was collected by vacuum filtration and washed three times with *N,N*-dimethylformamide. The product was dried in the oven for 24 hours at 110 °C to yield compound **8**.

##### **Condition 2**

A mixture of Girard's reagent T (**7**) (5.67g, 2 equiv.) and distilled water (100 mL) (2 %, v/v) was added to a round bottom flask containing 4 g of modified silica gel (Silica + **5**). This reaction was stirred at 45 °C for 6 hours. The crude product was collected by vacuum filtration and washed three times with distilled water. The product was dried in the oven for 24 hours at 110 °C to yield compound **8**.

### **3.11.3.5 Grafting/immobilization of Silica gel and 3-trimethoxysilylpropylamine (10)**

#### **Condition 1**

A mixture of 3-trimethoxysilylpropylamine (**9**) (1 mL) and toluene (100 mL) (1 %, v/v) or distilled water (100 mL) was added into a round bottom flask containing silica gel (3 g) and stirred at room temperature for 2 hours. After this period, the crude product was collected by vacuum filtration. The product was washed three times with toluene and heated to 110 °C under vacuum for 16 hours to remove absorbed organics. After this period, the product was dried in the oven for 24 hours at 110 °C to yield compound **10**.

#### **Condition 2**

A mixture of 3-trimethoxysilylpropylamine (**9**) (1 mL) and distilled water (100 mL) (1 %, v/v) was added into a round bottom flask containing silica gel (3 g) and stirred at room temperature for 2 hours. After this period, the crude product was collected by vacuum filtration. The product was washed three times with water and heated to 110 °C under vacuum for 16 hours to remove absorbed organics. After this period, the product was dried in the oven for 24 hours at 110 °C to yield compound **10**.

### **3.11.3.6 Grafting/Immobilization of glycidyltrimethylammonium chloride (GTMACl) with modified silica gel (compound 11)**

#### **Condition 1**

A mixture of glycidyltrimethylammonium chloride (**3**) (2 mL) and *N,N*-dimethylformamide (100 mL) (2 %, v/v) or 100 mL of water was added to a round bottom

flask containing 2 g of modified silica gel (Silica gel and **9**). This reaction was stirred at 45 °C for 6 hours. The crude product was collected by vacuum filtration and washed three times with *N,N*-dimethylformamide. The product was dried in the oven for 24 hours at 110 °C. to yield compound **11**.

### **Condition 2**

A mixture of glycidyltrimethylammonium chloride (**3**) (2 mL) and distilled water (100 mL) (2 %, v/v) was added to a round bottom flask containing 2 g of modified silica gel (Silica gel and **9**). This reaction was stirred at 45 °C for 6 hours. The crude product was collected by vacuum filtration and washed three times with distilled water. The product was dried in the oven for 24 hours at 110 °C to yield compound **11**.

### 3.12 Conclusion

Resins derived from silica gel were prepared by grafting an amine such as *N*-[3-(trimethoxysilyl) propyl] ethylenediamine (**1**) or 3-trimethoxysilylpropylamine (**9**) onto silica gel (which was subsequently further coupled with glycidyltrimethylammonium chloride (**3**)) or silica gel was modified with (3-glycidyloxypropyl)trimethoxysilane (**5**) and further coupled with Girard's reagent T (**7**). It was observed that the column loading efficiency also increased upon the addition of the amine and there was a further increment with the addition of the positively charged epoxide. Grafting of the epoxide to the amines also increased the size because the number of positive charges on the resin increases, which also improved binding onto the resin. The prepared resin had high loading and selectivity for molybdate and releasing pertechnetate. The prepared resin will allow for the current generator configuration to be used without change in operating procedures for the end user in the nuclear medicine departments at hospitals. Resins were modified to allow for better recovery of Tc without sacrificing molybdate loading.

## **Chapter 4- Studies towards aurora kinase inhibitors for PET**

### **imaging**

#### **4.1 Introduction:**

There has been a growing interest in the aurora kinases (AURK) family of proteins as targets for cancer therapy.<sup>98</sup> The three mammalian proteins, aurora A, B and C (AURKA/B/C) play a central role in cellular mitosis with aurora C exclusively expressed in testis. The function of aurora A is in spindle formation and centrosome maturation, and aurora B is required for proper microtubule attachment to kinetochore and plays a central role in cytokinesis as a chromosomal passenger protein.<sup>99</sup> Overexpression of aurora proteins is common in certain tumors and is thought to induce tumorigenesis,<sup>100</sup> thus inhibition studies have begun targeting their homologous ATP-binding pocket. Although, there is growing interest in designing small molecule inhibitors, there has been little research around the potential of targeting this family of kinases for molecular imaging.<sup>101</sup>

Radiotracers such as [<sup>18</sup>F]fluorodeoxyglucose which can be used to monitor metabolism and glucose uptake in highly proliferative tissues and are useful in identifying cancer but are not tumor-specific. This chapter looks at the synthesis of a common intermediate which could be functionalized to create other analogues as well as being radiolabeled for F-18 compounds.

## 4.2 Literature review

### 4.2.1 Aurora kinase and cancer

Aurora kinases find their importance in mitosis, so their divergent expression leads to cell modification underlying cancer. Overexpression of aurora kinase leads to instability in the genes which can cause cancer in the organism. The occurrence of extra or missing chromosomes leads to unbalanced chromosome numbers that is not the exact multiple of the haploid number and the content of the DNA which arise from mitotic defects. These defects include centrosome duplication, separation of the centrosome, cytokinesis, and error in the chromosomal biorientation; hence the genes of aurora can be an oncogene. Messenger RNA has been found to be overexpressed in breast tumor cells and plays a critical role in breast tumor cell transformation as seen in the aurora A gene.<sup>102,103</sup> The NIH3T3, embryonic mouse cell line can be transformed by aurora A to induce tumors in the mice.<sup>104</sup>

Overexpression of aurora B also induces tumor cells formation as the kinase is involved in several functions during mitosis and so aurora B can be described as a gene which can transform a cell into a tumor cell. Overexpression of aurora B has been seen in oral cancer, colon cancer, thyroid cancer, and breast cancer.<sup>105</sup>

Aurora kinase C occurs in cells that go through meiosis, cell division of germ cells in sexually reproducing organisms that produces gametes. There have been few studies on the functions of aurora kinase C due to the high sequence homology between aurora B and C which prevents the use of standard approaches to understand the functions at normal cellular levels.<sup>106</sup>



STK-15 (an example of aurora kinase A) is a protein found in centrosomes which is believed to be linked with genetic instability and used in proliferation of prostate cancer. This protein is overexpressed in high grade prostatic intraepithelial neoplasia (PIN) lesions which suggest that aurora A overexpression would precede the progression from benign prostrate cell to malignancy through high grade PIN lesions.<sup>107</sup> This overexpression can potentially be used as a diagnostic marker, which has inspired our research to modify a chemotherapy drug for this purpose to see how they can be used as diagnostic reagent for prostate cancer.

#### **4.2.2 Binding modes of Aurora kinase to ATP**

The kinase binding site has five main binding regions or sites: the hinge region, sugar region, buried region, phosphate region, and the solvent-exposed region.<sup>108</sup> The ATP binding site is a narrow hydrophobic pocket which is located between two lobes which are linked by the hinge region. This region usually has a hydrogen donor surrounded by two hydrogen acceptors derived from the backbone of the protein.<sup>109</sup> The hinge region is the most important area because it forms hydrogen bonds to the adenine moiety of the ATP, and they are the target for most kinase inhibitors because it forms the catalytically active part.<sup>110</sup> The buried region is a very small hydrophobic region next to the main chain of the kinase and cannot accommodate large groups. However, one can introduce large groups by adding diverse structure to the part of the inhibitor that sits in the sugar region and the phosphate binding regions to mimic ATP binding. Therefore, the R group (on the ligand) should be small such as a methyl, amine, or a hydrogen. The ATP tail is placed in the

phosphate binding region (the actual source of power of the ATP which the cell taps for its energy).

The solvent-exposed region of the aurora kinase is where the ligand is exposed to the solvent. The solvent-exposed region<sup>111</sup> is where greater modifications of existing small molecular drug molecules can be done without a loss of activity (Figure 4.1).

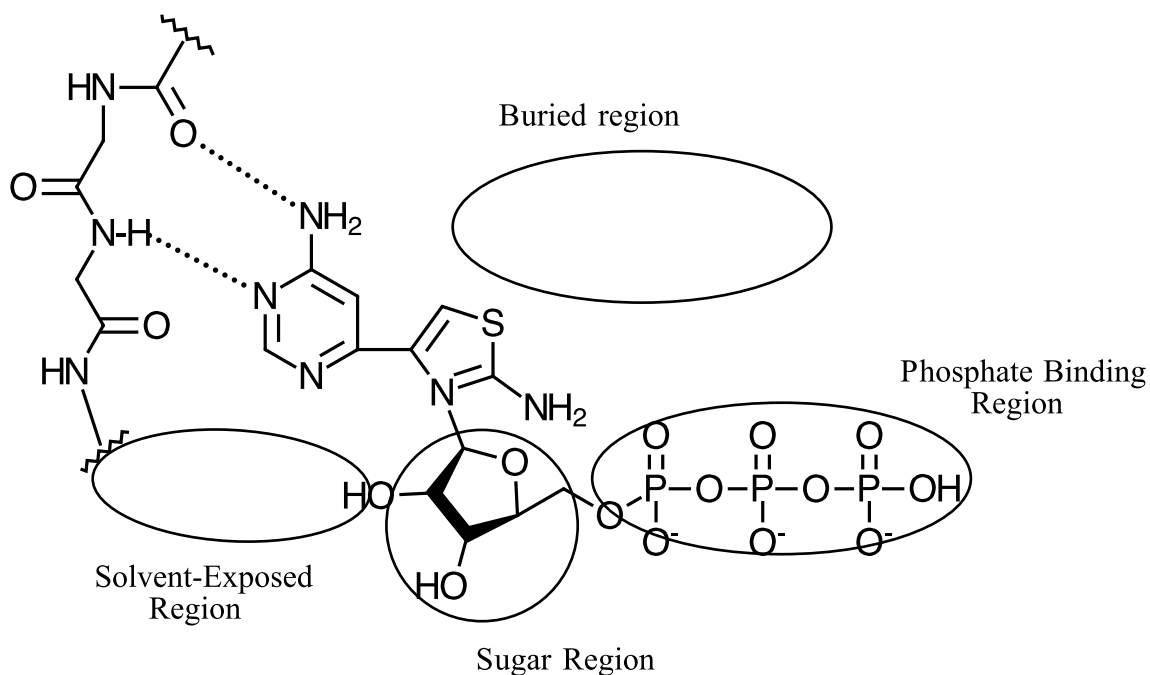
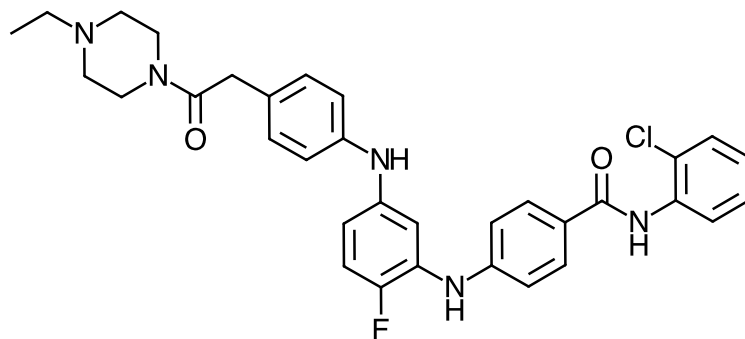


**Figure 4.1: The five main area of aurora kinase binding sites<sup>108</sup>**

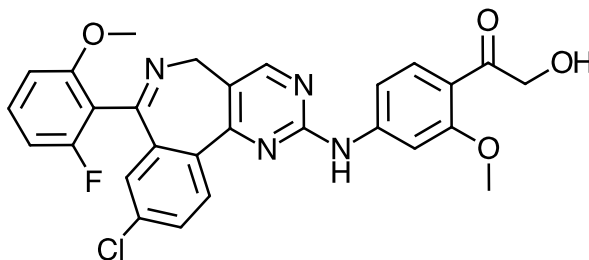
### 4.3 Novel AURKA/B/C inhibitors

The overexpression of AURKA/B/C is associated with genetic instability as well as aneuploidy in tumors<sup>112</sup> and this suggests that a wide range of cancers that results from their overexpression could respond therapeutically to inhibitors of this family of proteins. Inhibitors of AURKA and AURKB induce apoptosis through distinct mechanisms which

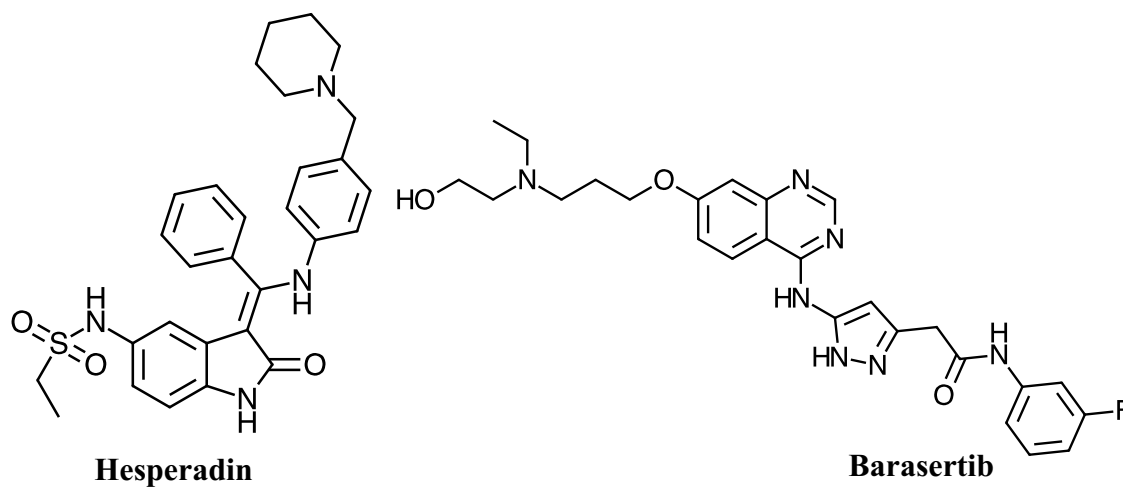
involve defects in mitotic spindle assembly and interferences with normal chromosome alignment, respectively.<sup>113,114</sup> Specifically, AURKA-inhibited cells undergo G1 arrest and exit mitosis leading to cell apoptosis, and AURKB-inhibited cells cause polyploidy due to malfunctioning of the mitotic spindle checkpoint, leading to failure of cytokinesis and cell death.<sup>114</sup> Examples of novel AURK inhibitors include TC-S7010, alisertib (selective AURKA inhibitor), hesperadin, barasertib (selective AURKB inhibitor), and CYC-116 (potent inhibitor of AURKA/B/C). The chemical structure for these compounds is shown in Figure 4.2. The compounds shown in Figure 4.2 all contain an amine (NH) functional group. This common functionality means they all attach to the same binding site.



**TC-S7010**

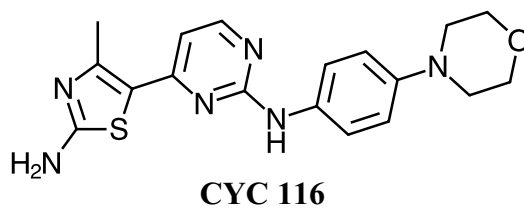


**Alisertib**



**Hesperadin**

**Barasertib**



**CYC 116**

**Figure 4.2: Some selected Aurora kinase A/B/C inhibitors.**

TC-S7010 is a novel, potent, and selective inhibitor of aurora A with an IC<sub>50</sub> of 3.4 nM and has been used to demonstrate a pro-apoptotic effect through the unfolded protein response pathway in HCT116 colon cancer cells. Treatment with TC-S7010 resulted in the accumulation of cells in the sub-G<sub>0</sub>/G<sub>1</sub> phase of the cycle of the cell and a percentage increase of annexin V binding cells to help identify population of cells undergoing apoptosis. Also, TC-S7010 increases the production of reactive oxygen species and stimulation of unfolded protein response mediated pathways.<sup>115</sup>

Alisertib has been evaluated in phase I and II clinical trials in patients with advanced solid tumors; the overall response rate for all treated patients was 27 % when alisertib was administered orally at 50 mg twice daily for 7 days in 21-day cycles.<sup>116</sup> It has shown good safety profiles as well when it is combined with cytotoxic chemotherapeutic drugs in patients with refractory peripheral T-cell lymphoma, and the co-crystal structure of alisertib complexed with AURKA has been elucidated. Although it has shown success in phase I and II trials, alisertib has not gained approval for clinical use; its predecessor MLN8054 showed severe off-target side effects. Its binding mechanism inhibits the autophosphorylation at Thr288 in the ATP-binding pocket, inactivating the catalytic subunit of AURKA with an IC<sub>50</sub> value of 1.2 nM. This inhibition has resulted in cell cycle arrest and apoptosis.<sup>117</sup>

Hesperadin is a human aurora B inhibitor, which prevents phosphorylation of the substrate with an IC<sub>50</sub> value of 40 nM. It inhibits the growth of *trypanosoma brucei* by blocking nuclear division and cytokinesis. Upon treatment of MCF7 (breast cancer cells) and PC3 (prostate adenocarcinoma cell) with hesperadin, the cell's multiplication is inhibited due to multiple mitotic defects caused by the reduction of aurora B activity and

removal of checkpoints proteins (CENP-E and hBUBR1) from kinetochores of mitotic chromosomes in mammalian cells. They allow mammalian cells to enter anaphase with attached chromosomes where aurora B is required to correct syntelic attachment which maintains spindle checkpoint signaling by generating unattached kinetochores.<sup>118</sup>

Barasertib is a prodrug which binds to the phosphate region, rapidly converting to barasertib-hQPA *in vivo*. It selectively inhibits AURKB with an inhibition constant  $K_i$  value  $<0.001 \mu\text{M}$ .<sup>119</sup> Clinical studies have shown success of barasertib against solid malignant tumors as well as refractory acute myeloid leukemia (AML), where one patient achieved a complete response.<sup>120,121</sup> The safety of barasertib has been assessed during combinatorial therapy in elderly patients with newly diagnosed AML and was deemed unfit for intensive induction chemotherapy.<sup>120</sup> Like alisertib, barasertib also inhibits phosphorylation of Thr288 in AURKB, inactivating the catalytic subunit which has resulted in G2/M arrest during the cell cycle, causing apoptosis.<sup>120</sup> Co-crystal structures for barasertib and AURKB have been elucidated, with a similar binding mode to alisertib.

CYC-116 is a pan-AURK inhibitor with promising anticancer properties and significant specificity and potency. The structure of CYC-116 as seen in Figure 4.2 contains an amine group attached to a thiazole ring, which is bound to a central pyrimidine, a second amine group, a benzene, and finally a morpholine ring. It shows an  $\text{IC}_{50}$  value of 44 nM, 19 nM, and 65 nM for AURKA/B/C, respectively.<sup>122</sup> The drug (CYC-116) can be economically mass-produced and is commercially available, however, its binding mode has not been fully elucidated or reported in crystal structure complexed with aurora kinase. This presents an opportunity for further investigation into the binding mechanisms between

CYC-116 and the family of Aurora kinase to determine the specific interactions that could point towards specificity among the three Aurora kinase proteins.

#### **4.4 Analogues and $^{18}\text{F}$ -radiolabelled tracer compound**

Positron emission tomography (PET) is a functional imaging technique involving the injection of positron-emitting compounds (radiotracers) followed by detection of radiation and reconstruction of radiotracer localization in the body. It is an especially useful method for earlier (compared to traditional imaging methods), more accurate diagnoses of tumors based on metabolic differences from surrounding organs and tissues.<sup>123</sup> Radiolabeled pharmaceuticals or biomolecules can allow imaging and quantification of specific biological functions and/or track biomarker distribution in the body. The most used radionuclide is fluorine-18 due to its high positron decay ratio (97 %) and relatively low positron energy, limiting positron diffusion range to 1-2.4 mm in tissues before it interacts with an electron. Upon interaction, positrons and electrons annihilate to give two high-energy photons travelling in approximately opposite ( $180^\circ$ ) directions.<sup>124</sup> The half-life of fluorine-18 is ~110 minutes which allows sufficient time for radiotracer synthesis while limiting radiation exposure from residual radiotracer in the body, and since fluorine-18 is a bioisostere of hydrogen it is readily integrated into pharmaceutical analogues.<sup>125</sup>

PET imaging with [ $^{18}\text{F}$ ]2-deoxy-2-fluoro-D-glucose ([ $^{18}\text{F}$ ]FDG) is a common method and radiotracer for clinical oncology studies. [ $^{18}\text{F}$ ]FDG PET is useful for predicting disease aggressiveness and identifying distant metastases due to its ability to

contrast the metabolism of healthy cells versus rapidly-dividing tumor cells.<sup>126,127</sup> In the last decade it has become an important imaging tool in routine clinical oncology due to the valuable information it provides on increased glucose uptake and glycolysis of cancer cells; this kind of functional information such as this helps depict metabolic abnormalities before morphological alterations occur.<sup>126</sup> For example, [<sup>18</sup>F]FDG PET plays an important role in the detection of recurrent colorectal cancer, with an average sensitivity, specificity, and accuracy for detection 89 %, 92 %, and 90 %, respectively.<sup>126</sup>

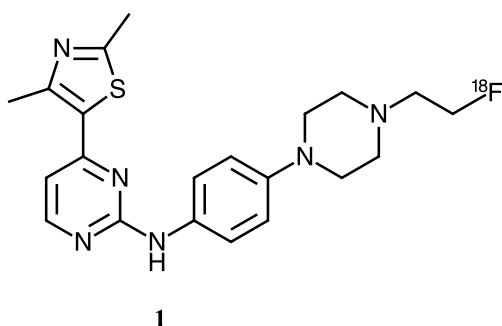


**Figure 4.3: N-[<sup>18</sup>F]fluoroethylated analogue compounds derived from CYC-116 inhibitor.**

## 4.5 Medical use of thiazole ligands

Thiazole ligands have varying coordination abilities towards many transition metal ions. There has been growing interest in investigating thiazoles and their synthesis and applications particularly in the bioactive and biomimicking in their coordination.<sup>128</sup> Thiazoles have several properties which makes them suitable candidate in medicinal chemistry especially in drug design and synthesis. Thiazole is an important scaffold in many vitamins and many important compounds used in medicinal chemistry.<sup>50</sup> Thiazole-



containing compounds have a myriad of applications. Some thiazoles are antifungal, antimalarial, antibacterial, anticancer, antiviral, antioxidants or anti-inflammatory while others are used to treat ulcers, hypertension, Alzheimer's disease, cardiovascular diseases,<sup>129</sup> anti-HIV (ritonavir), or antihypertension.<sup>130-133</sup>

Thiazoles have been used as linkers in a single molecular skeleton to test its microbial activity as shown in Figure 4.4 below.<sup>134</sup> A thiazole derivative has been screened against HIV as seen in Figure 4.5 below.<sup>135</sup> Another thiazole derivative has been found to provide potent antitumor activities in cancer cell lines (Figure 4.6).<sup>136</sup> Thiazole-incorporated azole showed good activity in epilepsy models (Figure 4.7).<sup>137</sup>

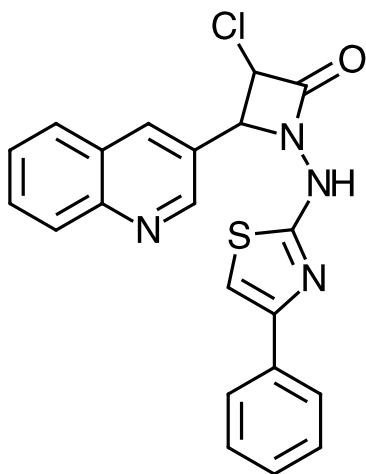


**Figure 4.4: Thiazole hybrid antimicrobial agent.**

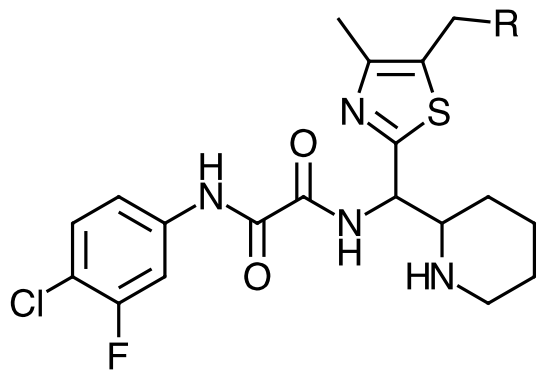


**Figure 4.5: Thiazole antiviral agent containing oxalamide moiety.**

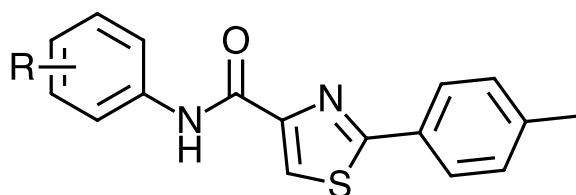


**Figure 4.6: Thiazole-derivative as anti-cancer activities.**

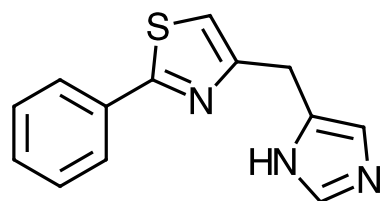


**Figure 4.7: Structure of thiazole derivative used for an anticonvulsant activity.**

## 4.6 Goals of the project

The goal of this project is to develop imaging agents that are selective for aurora kinase and develop a synthetic strategy that allows for easy diversification and structure activity relationship (SAR) analysis. When designing a new radiotracer, it is important to know where the radionuclide can be attached without disrupting the binding interaction

that gives selectivity. In many cases, including the aurora kinases, this requires the positioning of the radiolabel on a solvent exposed region of the molecule. We chose to model our tracer on the known AURK inhibitor CYC-116 seen in Figure 4.8.

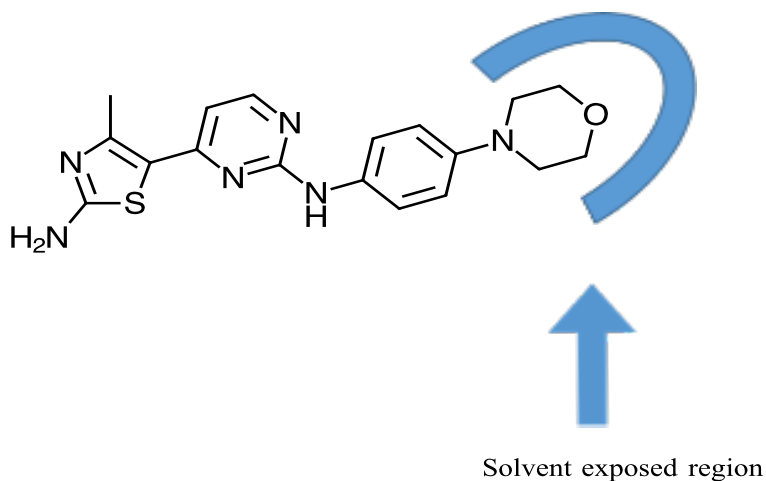
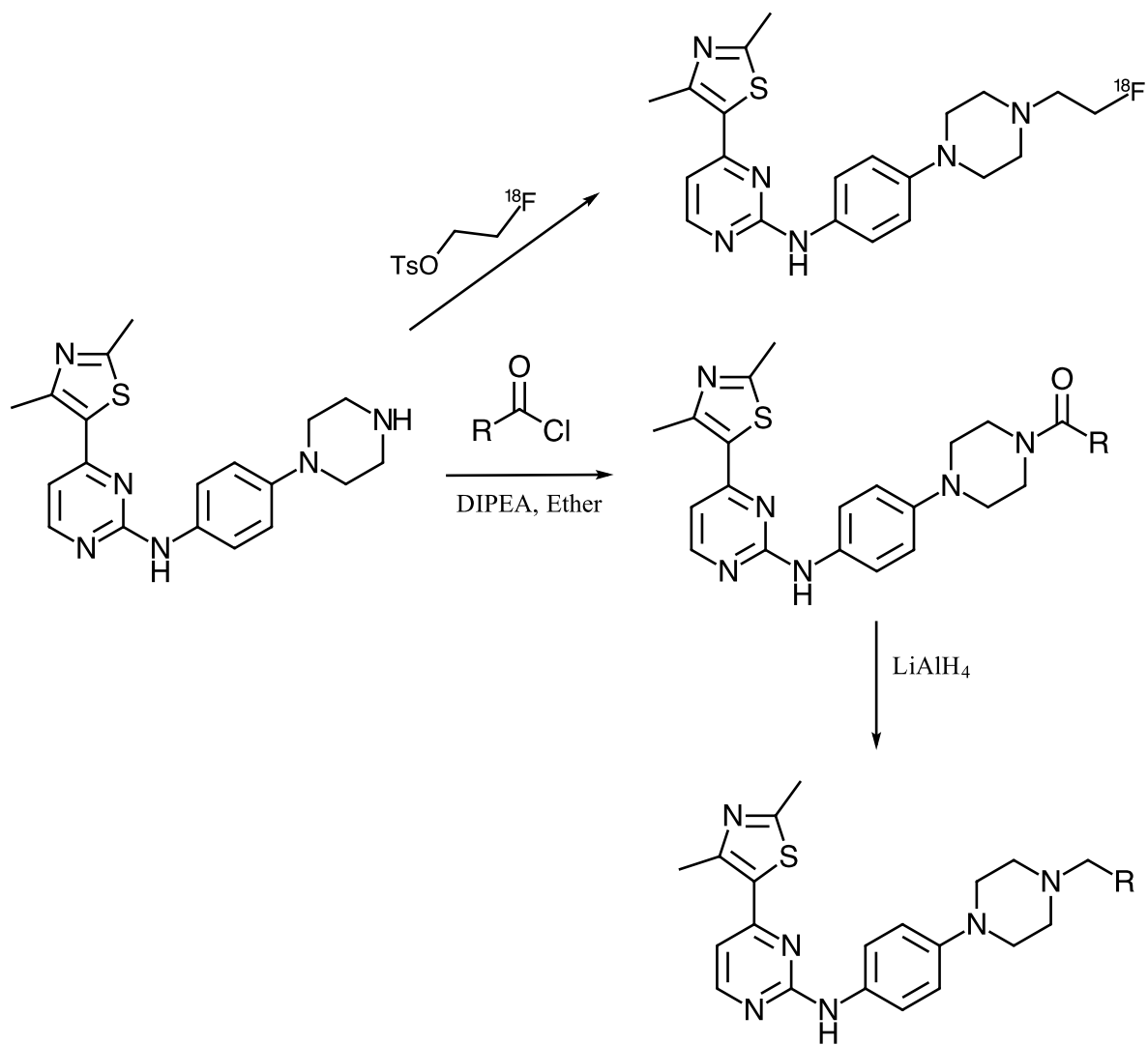


**Figure 4.8: Binding interactions of CYC 116 showing solvent exposed region.**

The proposed route to the new family is to react bromoaniline with cyanamide to get *p*-(2-aminohydrazino) bromobenzene followed by a Buchwald type coupling with a secondary amine (Boc-piperazine). Deprotection of the Boc group will give an intermediate that can be further modified in the solvent-exposed region.<sup>138</sup>

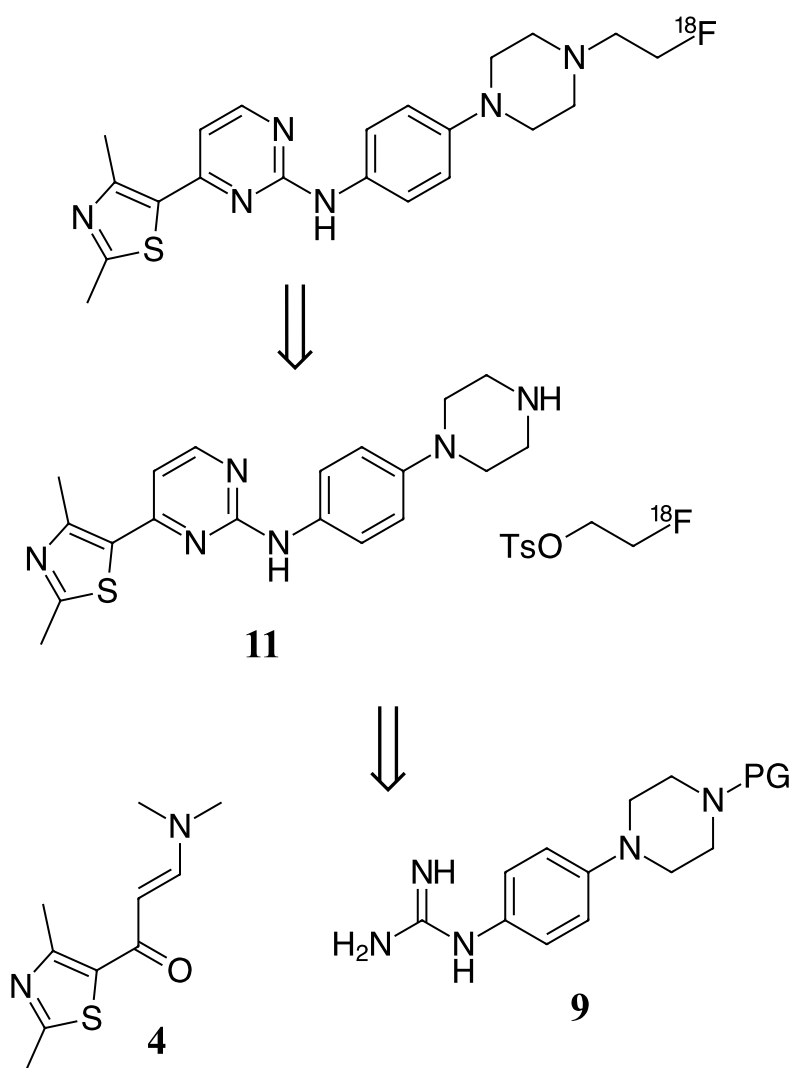
The hope was to take advantage of the known binding interactions of CYC-116 to provide selectivity. Extensive SAR work has indicated the morpholine region is solvent exposed so should be possible to make changes without impacting binding.<sup>139,140</sup> The proposed research replaces the morpholine with a piperazine which can be functionalized with a suitable fluorine-18 labeling group. This will also allow for the creation of acylated analogues of CYC-116 (Scheme 4.2), where R = Aryl, ethyl, propyl etc. (Scheme 4.1).



**Scheme 4.1: Functionalized replacement of morpholine with piperazine with fluorine-18 and other alkylated analogues.**

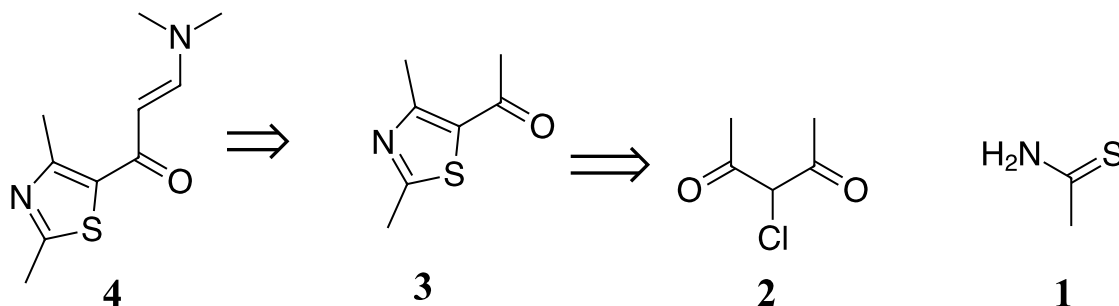
## 4.7 Retrosynthetic analysis

The radiolabeling step will be carried out using the prosthetic group [ $^{18}\text{F}$ ] 2-fluoroethyltosylate (FET). FET is prepared from the reaction of the bistosylate with [ $^{18}\text{F}$ ]KF, base and  $\text{K}_{222}$



**Scheme 4.2: The radiolabeling step of the retrosynthesis from enaminone (4) and guanidine (9).**

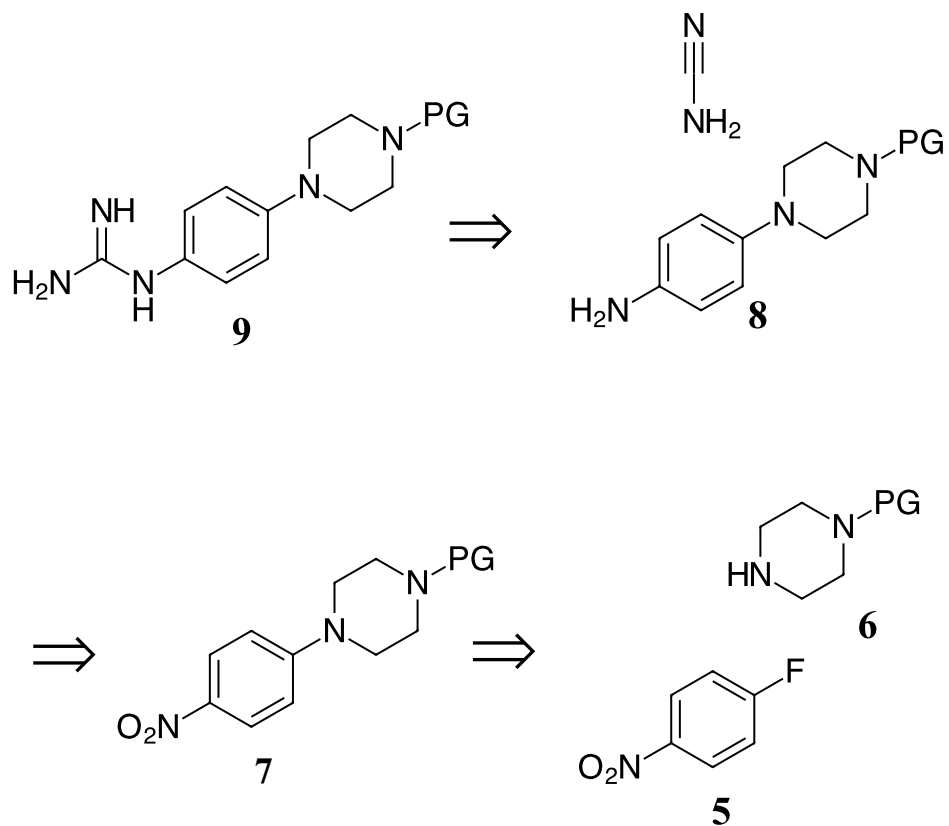
The synthesis of the key intermediate compound **11** will allow for easy radiolabeling as well as the synthesis of other analogues. The piperazine of the key intermediate is protected with suitable protecting group and dissected through the pyrimidine ring. This gives a thiazole and a guanidine as starting materials.



**Scheme 4.3 Formation of the enaminone.**

The thiazole (**3**) is derived from the condensation of thioacetamide with the 3-chloro-2,4-pentanedione.

Synthesis of the guanidine building blocks comes from the nucleophilic aromatic substitution of 4-fluoronitrobenzene.



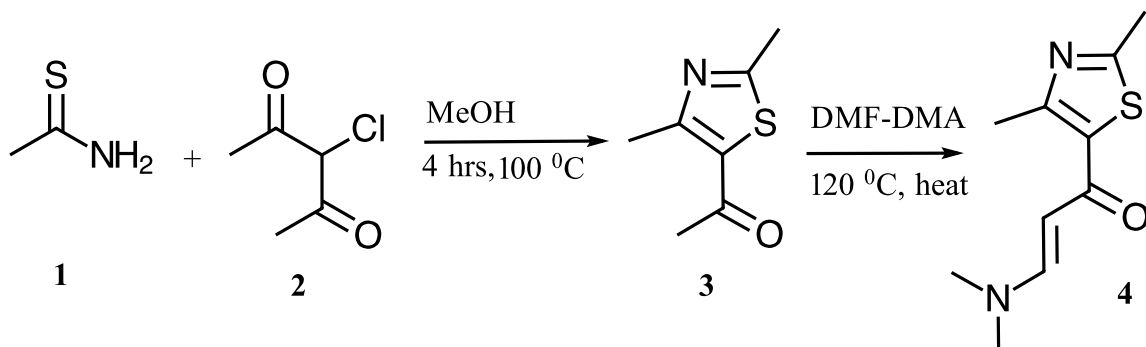
**Scheme 4.4: The guanidine formation**

## 4.8 Results and Discussion

### 4.8.1 Thiazole-enaminone synthesis (4)

To get the starting thiazole, 1-(2,4-dimethyl-1,3-thiazol-5-yl)-1-ethanone (4) was synthesized from the condensation of thioacetamide (1) and 3-chloro-2,4-pentanedione (2) to obtain 1-(2,4-dimethyl-1,3-thiazol-5-yl)-1-ethanone (3) with 98 % yield. 3-(Dimethylamino)-1-(2,4-dimethyl-1,3-thiazol-5-yl)-2-propen-1-one (4) (79 % yield) was synthesized by heating 1-(2,4-dimethyl-1,3-thiazol-5-yl)-1-ethanone (3) in *N,N*-dimethylformamide dimethyl acetal to get the resulting enaminone (4) as shown in

Scheme 4.5 below:

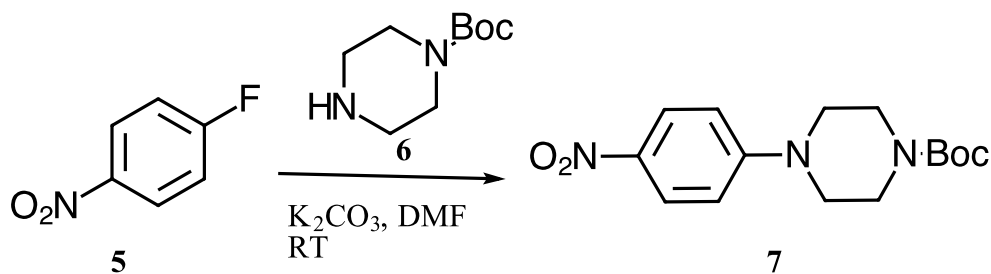


**Scheme 4.5: Formation of enaminone**

### 4.8.3 Synthesis of guanidine

#### 4.8.3.1 *Tert*-butyl-4-(*p*-nitrophenyl)-1-piperazinecarboxylate (7)

Synthesis of the guanidine building blocks starts from the nucleophilic aromatic substitution of 1-fluoro-4-nitrobenzene (5) with 1-Boc-piperazine (6) as a nucleophile in the presence of a base and dimethylformamide (DMF) at room temperature to give *tert*-butyl-4-(*p*-nitrophenyl)-1-piperazinecarboxylate (7) with a yield of 69 % (Scheme 4.6)

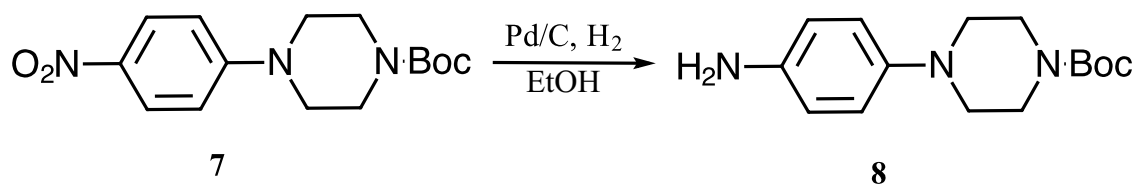


**Scheme 4.6: Synthesis of *tert*-butyl-4-(*p*-nitrophenyl)-1-piperazinecarboxylate.**



#### 4.8.3.2 *Tert*-butyl-4-(*p*-aminophenyl)-1-piperazinecarboxylate (**8**)

The nitro group (**7**) in Scheme 4.6 was reduced to an amine group. This was done by catalytic hydrogenation over palladium on carbon to obtain *tert*-butyl-4-(*p*-aminophenyl)-1-piperazinecarboxylate (**8**), a primary amine with a yield of 89 % (Scheme 4.7). This reaction is conducted at a neutral pH and does not affect the acid sensitive Boc group.

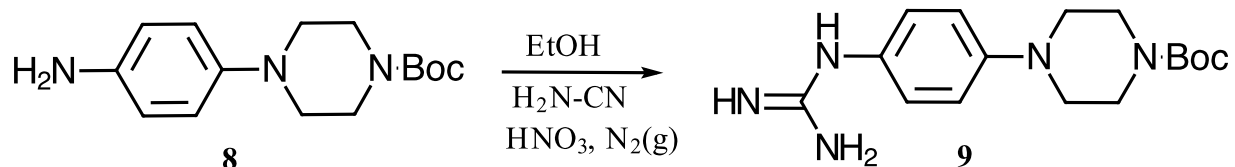


**Scheme 4.7:** Synthesis of *tert*-butyl-4-(*p*-aminophenyl)-1-piperazinecarboxylate

#### 4.8.3.3 *Tert*-butyl-4-(*p*-guanidinophenyl)-1-piperazinecarboxylate (**9**)

##### Condition 1:

*Tert*-butyl-4-(*p*-aminophenyl)-1-piperazinecarboxylate (**8**), a primary amine, is dissolved in ethanol and treated with cyanamide bubbling the gas through the solution to obtain the corresponding guanidine target, *tert*-butyl-4-(*p*-guanidinophenyl)-1-piperazinecarboxylate (**9**) with a yield of only 5 %. This was done in the presence of nitric acid. It should be noted that the ethanol was cooled down to 0 °C before the addition of the cyanamide and the acid. Because the reaction was cooled before the addition of the acid, the Boc protecting group remained intact (Scheme 4.8).

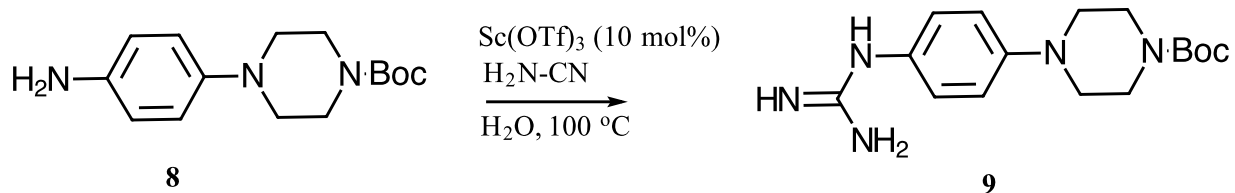


**Scheme 4.8:** Synthesis of *tert*-butyl-4-(*p*-guanidinophenyl)-1-piperazinecarboxylate

#### 4.8.3.4 *Tert*-butyl-4-(*p*-guanidinophenyl)-1-piperazinecarboxylate (9)

##### Condition 2:

Compound (8), a primary amine was treated with cyanamide in the presence of a catalytic amount of scandium (III) triflate. This method does not require the harsh conditions of nitric acid seen in condition 1. The reaction proceeds well in water to give *tert*-butyl-4-(*p*-guanidinophenyl)-1-piperazinecarboxylate (9) with a yield of 70 % (Scheme 4.9).

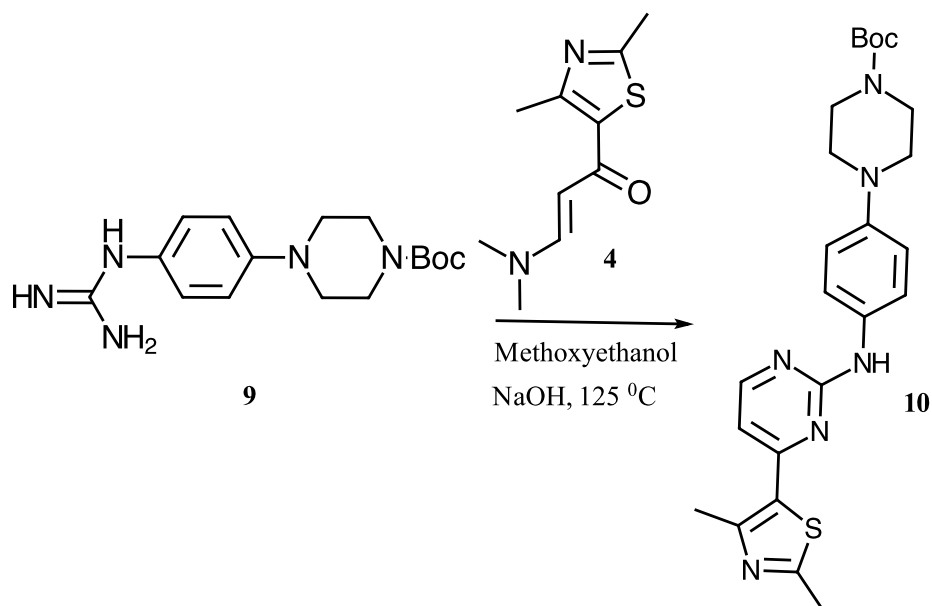


**Scheme 4.9:** Synthesis of *tert*-butyl-4-(*p*-guanidinophenyl)-1-piperazinecarboxylate using scandium triflate, a Lewis acid.

#### 4.8.4 *Tert*-butyl-4-(*p*-[4-(2,4-dimethyl-1,3-thiazol-5-yl)-2-pyrimidinylamino] phenyl)-1-piperazinecarboxylate (10)

The pyrimidine ring was synthesized by the condensation reaction between compound (9) (Scheme 4.6) and compound (4) to give pyrimidine, *tert*-butyl-4-(*p*-[4-(2,4-

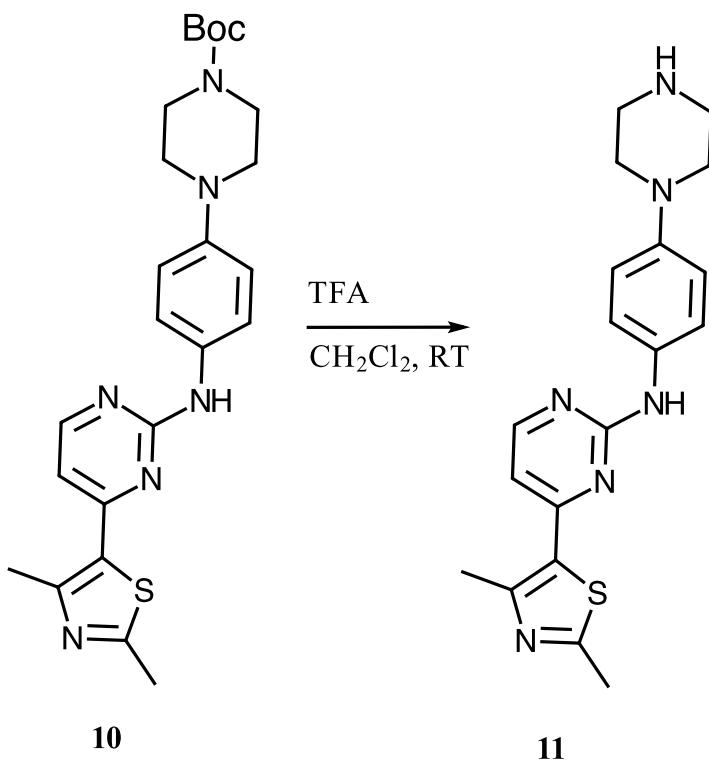
dimethyl-1,3-thiazol-5-yl)-2-pyrimidinylamino] phenyl)-1-piperazinecarboxylate (**10**) with a yield of 39 % (Scheme 4.10).



**Scheme 4.10: Synthesis of tert-butyl-4-(*p*-[4-(2,4-dimethyl-1,3-thiazol-5-yl)-2-pyrimidinylamino] phenyl)-1-piperazinecarboxylate**

#### 4.8.5 [4-(2,4-dimethyl-1,3-thiazol-5-yl)-2-pyrimidinyl][*p*-(1-piperazinyl)phenyl]amine (**11**)

Deprotection of **10** was accomplished by simple carbamate hydrolysis with trifluoroacetic acid (TFA) in dichloromethane to give [4-(2,4-dimethyl-1,3-thiazol-5-yl)-2-pyrimidinyl][*p*-(1-piperazinyl)phenyl]amine (**11**) with a yield of 97 % (Scheme 4.1).

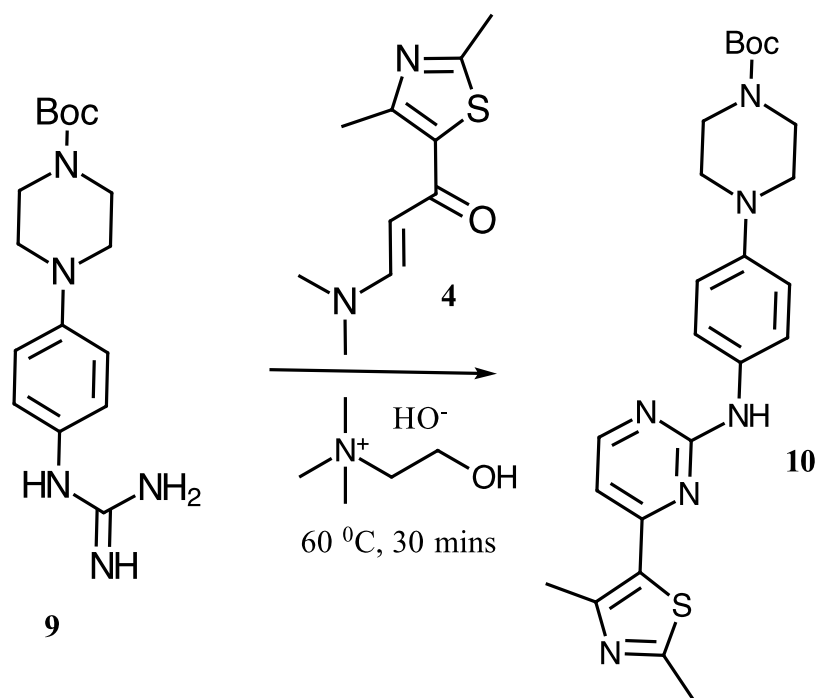


**Scheme 4.11: Deprotection of tert-butyl-4-(*p*-[4-(2,4-dimethyl-1,3-thiazol-5-yl)-2-pyrimidinylamino] phenyl)-1-piperazinecarboxylate**

## 4.9 General Results/Discussion

In the quest to develop an imaging agent that is selective for aurora kinase and develop a synthetic strategy that will allow for easy diversification and structure activity relationship elucidation, a key intermediate analogue of a known aurora kinase inhibitor, CYC 116, which is selective for aurora kinase was prepared. The guanidine synthesis proved to be tedious as the methods<sup>140</sup> used resulted in only 5 % yield of the resulting guanidine seen in condition 1 (Scheme 4.8). This was attributed to the fact that the harsh conditions using nitric acid and heat likely protonated the amine, which would weaken the

nucleophilicity, hence the use of a Lewis acid can improve the efficiency of this protocol.<sup>141</sup> Upon reacting compound (**8**), using these conditions, the yield of compound **9** (Scheme 4.7) was increased to 70%, thus solving problem of converting the amino group to the guanidine. The other low-yield step is the combination of **4** and **9** to give **10** with a yield of 39%. It was hypothesized that the use of sodium hydroxide (in the 2-methoxyethanol solvent) is strong enough to abstract the acidic amine (NH unit), which prevents the reaction from going to completion. To affirm the fact that the base (sodium hydroxide) abstracts the acidic NH, choline hydroxide (Scheme 4.12) was used in the presence of compound (**4**) and compound (**9**) at 60 °C for 30 minutes as described by Chaskar *et. al.*<sup>142</sup> and this also proved futile, an affirmation of the fact that the hydroxide group affecting the reaction by abstracting the acidic amine (NH) thereby preventing the reaction from going to completion.



**Scheme 4.12: Abstraction of the amine by the base.**

## 4.10 Experimental

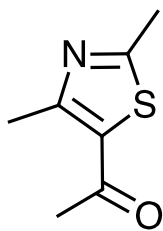
### 4.10.1 General synthetic and instrumental details

Unless otherwise indicated, all reactions were conducted under an inert nitrogen atmosphere. Nuclear magnetic resonance spectra were obtained using a Bruker Avance NEO 500 MHz NMR spectrometer at the Lakehead University Instrument Laboratory using Topspin software. All spectra were recorded at room temperature and chemical shifts were internally referenced to tetramethylsilane (TMS) and are reported in parts per million (ppm). NMR spectral data is reported in the following order: chemical shift (ppm), multiplicity, coupling constant (Hz) and number of protons. The solvent signals were used as references and the chemical shifts converted to the TMS scale ( $\text{CDCl}_3$ :  $\delta_{\text{C}} = 77.00$  ppm and  $\delta_{\text{H}} = 7.26$  ppm;  $\text{d}^6$ -DMSO:  $\delta_{\text{C}} = 39.53$  and  $\delta_{\text{H}} = 2.50$ ;  $\text{d}^4$ -MeOH:  $\delta_{\text{C}} = 49.03$  ppm and  $\delta_{\text{H}} = 3.31$  ppm. The splitting patterns were designated using the following abbreviations: s (singlet), d (doublet), t (triplet), q (quartet), quint. (quintuplet), m (multiplet), br (broad). Mass spectra were obtained on the Advion-Expression Compact Mass Spectrometer; nitrogen atoms tend to protonate in the instrument, leading to +1 mass unit for each N atom in the molecule. Infrared spectra were collected on a Nicolet 380 FT-IR with a resolution of  $1 \text{ cm}^{-1}$ . Glassware used for all reactions were oven dried, evacuated, and purged with  $\text{N}_2$  (g) several times and allowed to cool to room temperature. Thioacetamide (**1**), 3-chloro-2,4-pentanedione (**2**), DMF-DMA, bromoaniline, cyanamide, 2-methoxyethanol, 1-Boc-piperazine, 1-fluoro-4-nitrobenzene (**5**), palladium on carbon (Pd/C) were obtained commercially from Sigma Aldrich, ChemImpex or Fisher Scientific and used as received. Thin layer chromatography (TLC) was performed using Silicycle UltraPure silica gel  $200 \mu\text{m}$ . Hexane and ethyl acetate were used as mobile phase in flash chromatography unless

otherwise stated.

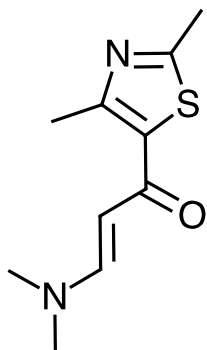
#### 4.10.2 Thiazole synthesis

##### 1-(2,4-Dimethyl-1,3-thiazol-5-yl)-1-ethanone (3)



3-Chloro-2,4-pentanedione (**2**) (3.58 g, 27 mmol, 3 mL) was weighed into 75 mL of dry ethanol in a 500 mL round bottom flask equipped with a stir bar and a reflux condenser. Thioacetamide (**1**) (2 g, 27 mmol) was added. The resulting mixture was refluxed under nitrogen gas for 3 hours and was allowed to cool. After the 3-hour period, the solution was poured into 100 mL of distilled water and was adjusted to a pH of 9 using saturated sodium carbonate. The organic product (**3**) was extracted with ether and dried with MgSO<sub>4</sub>. The solvent was removed via rotary evaporation. The residue was purified by chromatography on silica gel (1:1 hexane: ethyl acetate) to afford a light brown liquid (4.05 g, 98 % yield). <sup>1</sup>H NMR (500 MHz, CDCl<sub>3</sub>) δ 2.51 (s, 3H), 2.69 (s, 3H), 2.70 (s, 3H); <sup>13</sup>C NMR (125 MHz, CDCl<sub>3</sub>) δ 18.15, 19.51, 30.90, 131.39, 158.34, 168.55, 190.38. Mass spec. calc. for C<sub>7</sub>H<sub>9</sub>NOS: 155.040; found: 156.0 (100 %, M+H).

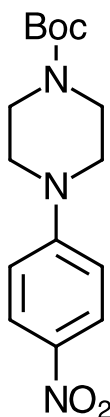
### 3-(Dimethylamino)-1-(2,4-dimethyl-1,3-thiazol-5-yl)-2-propen-1-one (4)



Compound (3) (6.5 g, 42 mmol) was weighed into 6.5 mL of N, N-dimethylformamide dimethyl acetal in a 500 mL round bottom flask equipped with a stir bar and a reflux condenser. The resulting mixture was refluxed under nitrogen gas for 21 hours at 120 °C then allowed to cool and the mixture was evaporated to dryness. The residue was recrystallized in equal amounts of diisopropyl ether and dichloromethane and purified by chromatography on silica gel (1:20 methanol: dichloromethane) to afford the product as a brown solid (6.8 g, 79 %).; mp 95-97 °C.; <sup>1</sup>H NMR (500 MHz, CDCl<sub>3</sub>) δ 7.64 (d, J = 12.05 Hz, 1H), 5.33 (d, J = 12.11 Hz 1H), 3.14 (d, 6H), 2.60 (s, 3H), 2.55 (s, 3H); <sup>13</sup>C NMR (125 MHz, CDCl<sub>3</sub>) δ 179.72, 165.48, 154.22, 153.37, 133.79, 94.26, 40.16, 19.33, 17.98.; Mass spec. calc. for C<sub>10</sub>H<sub>14</sub>N<sub>2</sub>OS: 210.083; found: 211.1 (100 %, M+H).

#### 4.10.3 Guanidine Synthesis

##### *Tert*-butyl-4-(*p*-nitrophenyl)-1-piperazinecarboxylate (7)

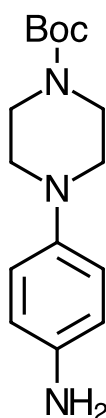


1-Fluoro-4-nitrobenzene (5) (2 g, 14.2 mmol, 1.5 mL), Boc-piperazine (6) (6.6 g, 35.6 mmol), and potassium carbonate (4.9 g, 35.6 mmol) were weighed into 40 mL of dimethylformamide (DMF) in a 500 mL round bottom flask equipped with a stir bar and a stirred at room temperature for 8 hours. The resulting mixture was diluted with water (100 mL). The organic product was extracted with dichloromethane and dried with MgSO<sub>4</sub>. The solvent was removed via rotary evaporation. The residue was purified by chromatography on silica gel (4:1 hexane:



ethyl acetate) to afford a bright yellow flaky solid (3 g, 69 %).; mp 145-147 °C; <sup>1</sup>H NMR (500 MHz, CDCl<sub>3</sub>) δ 8.14 (d, J = 8.0 Hz 2H), 6.83 (d, J = 8.25 Hz, 2H), 3.61 (s, 4H), 3.42 (s, 4H), 1.49 (s, 9H); <sup>13</sup>C NMR (125 MHz, CDCl<sub>3</sub>) δ 154.63, 154.55, 138.78, 125.98, 112.86, 80.39, 46.89, 43.11, 28.39; Mass spec. calc. for C<sub>15</sub>H<sub>21</sub>N<sub>3</sub>O<sub>4</sub>: 307.153; found: 308.2 (100 %, M+H).

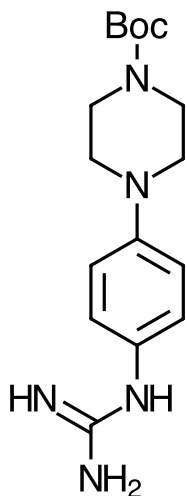
### ***Tert*-butyl-4-(*p*-aminophenyl)-1-piperazinecarboxylate (8)**



Compound (7) (1g, 3.3 mmol) was weighed into 20 mL of dry ethanol in a 100 mL round bottom flask equipped with a stir bar and a reflux condenser. Palladium on carbon (Pd/C) (35 mg, 6 mol %) was added. The resulting mixture was evacuated several times under vacuum and backfilled with hydrogen gas (H<sub>2</sub>). The mixture was stirred overnight under hydrogen gas. The mixture was filtered and washed with methanol. The solvent was removed via rotary evaporation. The residue was purified by chromatography on silica gel (3:2 hexane: ethyl acetate) to afford a purple solid (0.8 g, 89 %).; mp 103-105 °C; <sup>1</sup>H NMR (500 MHz, CDCl<sub>3</sub>) δ 6.81 (d, J = 8.3 Hz, 2H), 6.65 (d, J = 8.3 Hz 2H), 3.56 (s, 4H), 3.51 (s, 2H), 2.96 (s, 4H), 1.46 (s, 9H); <sup>13</sup>C NMR (125 MHz, CDCl<sub>3</sub>) δ 154.75, 144.4, 140.64, 119.1, 116.1, 79.9, 51.19, 51.14, 28.4; Mass spec. calc. for C<sub>15</sub>H<sub>23</sub>N<sub>3</sub>O<sub>2</sub>: 277.179; found: 278.2 (100 %, M+H).

## ***Tert*-butyl-4-(*p*-guanidinophenyl)-1-piperazinecarboxylate (**9**)**

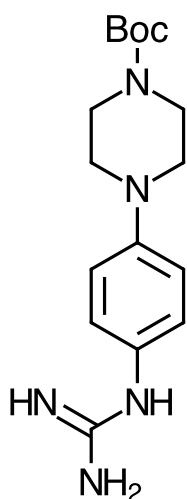
### **Condition 1**



To an ice-cold mixture of compound (**8**) (3.47g, 25 mmol) in 20 mL of ethanol was added nitric acid (0.9 mL of 70 % solution in water) dropwise with stirring. After the complete dropwise addition, cyanamide (2.5 mL) was added. The resulting mixture was heated at 100 °C for 18 hours under nitrogen gas. After cooling to room temperature, the mixture was poured into excess diethyl ether and aqueous sodium hydroxide was added until a basic pH was achieved. The ethereal layer was separated, and the aqueous phase was extracted with diethyl ether several times. The combined organic phases were washed with saturated sodium hydrogen carbonate (100 mL), brine (2X), water and dried on MgSO<sub>4</sub>, filtered, and evaporated to dryness. The residue was redissolved in isopropanol (50 mL) and decant off. The mixture re-evaporated to dryness. The residue was purified by chromatography on silica gel (9.5:0.5 dichloromethane: methanol) to afford a grey solid (0.4 g, 5 %).; mp 133-135 °C; <sup>1</sup>H NMR (500 MHz, CDCl<sub>3</sub>) δ 8.33 (s, 1H), 7.91 (s, 1H), 7.08 (d, J = 9.0 Hz, 2H), 7.03 (d, J = 9.0 Hz 2H), 4.71 (s, 2H), 3.49 (s, 4H), 3.02 (s, 4H), 1.36 (s, 9H); <sup>13</sup>C NMR (125 MHz, CDCl<sub>3</sub>) δ 154.79, 144.38, 143.39, 140.59, 119.4, 116.19, 79.84, 51.19, 51.18, 28.43; Mass spec. calc. for C<sub>16</sub>H<sub>25</sub>N<sub>5</sub>O<sub>2</sub>: 319.201; found: 320.2 (100 %, M+H).

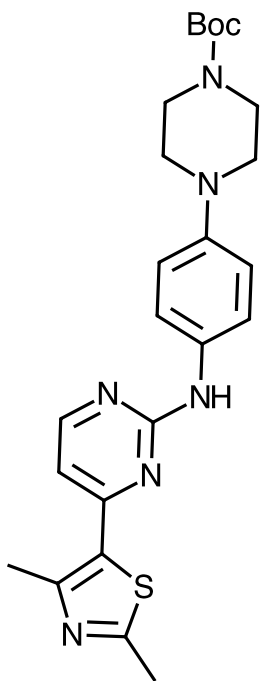
***Tert*-butyl-4-(*p*-guanidinophenyl)-1-piperazinecarboxylate (9)**

**Condition 2**



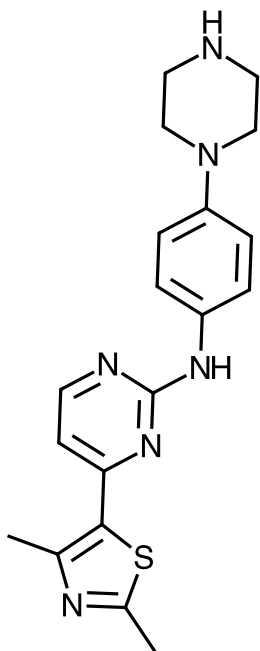
*Tert*-butyl-4-(*p*-aminophenyl)-1-piperazinecarboxylate (**8**) (4.5g, 16.2 mmol) in 100 mL of distilled water and dioxane (50/50), cyanamide (0.76 mL, 1.2 eqv.), and scandium triflate (0.79 g, 10mol %) were weighed into a 500 mL round bottom flask equipped with a stir bar and a reflux condenser. The mixture was heated to 100 °C for 12 hours. After cooling to room temperature, the resulting mixture was poured into excess ether and saturated aqueous sodium hydrogen carbonate (40 mL) was added until a basic pH was achieved. The aqueous layer was concentrated in vacuo, and the residue was purified by filtering through a silica gel pad and washed with methanol to afford a beige solid (3.62 g, 70 %); mp 133-135 °C; <sup>1</sup>H NMR (500 MHz, CDCl<sub>3</sub>) δ 8.33 (s, 1H), 7.91 (s, 1H), 7.08 (d, J = 9.0 Hz, 2H), 7.03 (d, J = 9.0 Hz 2H), 4.71 (s, 2H), 3.49 (s, 4H), 3.02 (s, 4H), 1.36 (s, 9H); <sup>13</sup>C NMR (125 MHz, CDCl<sub>3</sub>) δ 154.79, 144.38, 143.39, 140.59, 119.4, 116.19, 79.84, 51.19, 51.18, 28.43; Mass spec. calc. for C<sub>16</sub>H<sub>25</sub>N<sub>5</sub>O<sub>2</sub>: 319.201; found: 320.2 (100 %, M+H).

***Tert*-buty-4-(p-[4-(2,4-dimethyl-1,3-thiazol-5-yl)-2-pyrimidinylamino] phenyl)-1-piperazinecarboxylate (10)**



Compound (9) (0.5 g, 1.6 mmol), compound (4) (165 mg, 0.8 mmol), and sodium hydroxide (1 equivalence) were weighed into 10 mL of 2-methoxyethanol in a 250 mL round bottom flask equipped with a stir bar and a reflux condenser. The resulting mixture was heated at 125 °C for 22 hours under nitrogen gas. After cooling, the solvent was evaporated to dryness. The residue was purified by chromatography on silica gel (1:1 hexane: ethyl acetate) and recrystallized in ethanol to afford a brown solid (0.15 g, 39 %). ; mp 120-122 °C; <sup>1</sup>H NMR (500 MHz, CDCl<sub>3</sub>) δ 1.44 (s, 9H), 2.62 (s, 3H), 2.65 (s, 3H), 3.25 (s, 4H), 3.40 (s, 4H), 6.71 (s, 1H), 7.65 (s, 1H), 8.28 (d, J = 5.2 Hz, 2H), 8.46 (d, J = 5.2 Hz, 2H), 9.45 (s, 1H); Mass spec. calc. for C<sub>24</sub>H<sub>30</sub>N<sub>6</sub>O<sub>2</sub>S: 466.215; found: 467.1 (100 %, M+H).

**Deprotection of *tert*-buty-4-(*p*-[4-(2,4-dimethyl-1,3-thiazol-5-yl)-2-pyrimidinylamino]phenyl)-1-piperazinecarboxylate (**11**)**



Compound (**10**) (0.6 g) was dissolved in dichloromethane (10 mL), and trifluoroacetic acid (5mL) was weighed in a 250 mL round bottom flask equipped with a stir bar. The resulting mixture was stirred for 15 hours, and the solvent evaporated to dryness and recrystallized in ethanol to afford a brown solid (0.58 g, 97 %).; mp 113-115 °C; <sup>1</sup>H NMR (500 MHz, CDCl<sub>3</sub>) 8.39 (d, J = 8.3 Hz, 2H), 8.3 (d, J = 8.3 Hz, 2H), 7.54 (s, 1H), 7.47 (s, 1H), 7.03 (s, 1H), 3.49 (s, 4H), 2.71 (s, 4H), 2.71 (s, 3H), 2.67 (s, 3H), 1.27 (s, 1H); Mass spec. calc. for C<sub>19</sub>H<sub>22</sub>N<sub>6</sub>S: 366.16; found: 367.2 (100 %, M+H).

## 4.11 Conclusion and Future work

The synthesis of the intermediate target molecule was achieved. However, because of the low yield, further research would be required to make it economically (and/or medically) feasible. It can be concluded in this chapter that to get an optimal yield for the pyrimidine formation, one needs to avoid the use of a base which abstracts the acidic amine in the CYC 116 analogues produced. Because of the difficulties with the cold chemistry part of the project, once it was completed the project was ended and the radiolabelling steps were not carried out using the prosthetic group [ $^{18}\text{F}$ ]2-fluoroethyltosylate (FET) as well as the other acylated analogues. Going forward, this project will have to develop a more reliable and higher-yield synthesis to the common intermediate compound in order to be able to create a library of similarly structured compounds, which in turn will allow the goal of studying biological structure-function relationships with this proposed family of aurora kinase inhibitors.

## Chapter 5: Conclusion and Future work

As stated in the introduction, this is a wide-ranging thesis covering disparate areas of synthetic organic and metal-organic chemistry, unified by the general use of these projects in medicinal chemistry. As such, no single unified conclusion is possible; rather, the three projects advance knowledge in their respective areas of homogeneous catalysis (specifically, Suzuki-Miyaura cross-coupling), radioisotope separation, and radiolabeled pharmaceutical agents.

The Suzuki-Miyaura cross-coupling reaction is central to the design and synthesis of any number of new pharmaceutical molecules. The research presented in Chapter 2 looked at the electronic effects of different thiazole ligands and how they interacted with the metal to get the desired results. In Chapter 2, it was concluded that these catalysts (**2.3** and **2.4**) work very well with aryl bromides and aryl iodides, but they do not catalyze aryl chlorides.

The electronics have been tuned to favor either electron-withdrawing or electron-donating groups, the latter being unusual for these kinds of reactions. The reactivity of the prepared catalysts was tested using Suzuki-Miyaura cross-coupling reactions on various aryl halides with different boronic acids with an average yield of 80 % at 60 °C after 8 hours under mild conditions. In the future, the *o*- vs *m*- vs *p*-substitution with the same substituent will be performed to see how substitution at different positions affects the reactivity in the Suzuki coupling reactions and to see if these catalysts will be able to catalyze other palladium aided cross-coupling reactions such as Heck, Buchwald, Stille, Negishi or Kumada coupling reactions. In the future studies, it will be beneficial to

incorporate a broader range of substrates (other electron-donating and electron-withdrawing group).

In Chapter 3, a project studying the preparation and testing of solid support resin to allow high loading and selectivity of  $^{99}\text{Mo}/^{99\text{m}}\text{Tc}$  radioisotope generators using coordination chemistry was completed. It was concluded that the column loading efficiency increases upon the addition of an amine and there is a further increment in the loading efficiency with the addition of a positively charged epoxide. Grafting of the epoxide to the amines also increases the size of the resin beads because the number of positive charges on the resin increases. This subsequently improves binding onto the resin. Resins prepared had high loading and selectivity for molybdate and releasing pertechnetate. The resin prepared will allow for the current generator configuration to be used without change in operating procedures for the end user in the nuclear medicine departments at hospitals. Resins were modified to allow for better recovery of Tc without sacrificing molybdate loading. In the future, we are going to test the resin at the clinical stage to see if the data generated can complement current research in Canada into the production of  $^{99\text{m}}\text{Tc}$  production.

In Chapter 4, a project was initiated on the synthesis of a common intermediate that could be functionalized to create other analogues as well as being radiolabeled for F-18 compounds in the study of aurora kinase inhibitors. The synthesis of the common intermediate target molecule (CYC 116 analogues) was achieved. However, because of the low yield, further research would be required to make it economically (and/or medically) feasible. It can be concluded in this chapter that to get an optimal yield for the pyrimidine formation, one needs to avoid the use of a base which in essence abstract the acidic amine in the CYC 116 analogues produced. Because of the poor results in the cold chemistry



aspects of the project, the radiolabelling steps were not carried out using the prosthetic group [ $^{18}\text{F}$ ]2-fluoroethyltosylate (FET) nor with the other acylated analogues. Going forward, this project will have to develop a more reliable and higher-yield synthesis to the common intermediate compound in order to be able to create a library of similarly structured compounds, which in turn will allow the goal of studying biological structure-function relationships with this proposed family of aurora kinase inhibitors.

## Chapter 6: References

- (1) Chen, X.; Engle, K. E.; Wang, D.-H.; Yu, J.-Q. Pd(II)-Catalyzed C-H Activation/C-C Cross-Coupling Reactions: Versatility and Practicality. *Angew. Chem., Int. Ed.* **2009**, *48* (28), 5094–5115. <https://doi.org/10.1002/anie.200806273>.Pd(II)-Catalyzed.
- (2) Norio Miyaura, B.; Suzuki, A. Stereoselective Synthesis of Arylated (E)-Alkenes by the Reaction of Alk-1-Enylboranes with Aryl Halides in the Presence of Palladium Catalyst; *J. C. S. Chem. Comm.* **1979**, 590, 866-867.
- (3) Kodama, S.; Nakajima, I.; Kumada, M.; Suzuki, K. Nickel-Phosphine Complex-Catalyzed Grignard Coupling. *Tetrahedron*, **1982**, *38* (22), 3347–3354.
- (4) Tyrrell, E.; Brookes, P. The Synthesis and Applications of Heterocyclic Boronic Acids. *Synthesis*, **2004**, 4 469-483.
- (5) He, C.; Guo, S.; Huang, L.; Lei, A. Copper Catalyzed Arylation/C-C Bond Activation: An Approach toward  $\alpha$ -Aryl Ketones. *J. Am. Chem. Soc.* **2010**, *132* (24), 8273–8275. <https://doi.org/10.1021/ja1033777>.
- (6) Correa, A.; Mancheño, O. G.; Bolm, C. Iron-Catalysed Carbon-Heteroatom and Heteroatom-Heteroatom Bond Forming Processes. *Chem. Soc. Rev.* **2008**, *37* (6), 1108–1117. <https://doi.org/10.1039/b801794h>.
- (7) Kazemi, M.; Shiri, L.; Kohzadi, H. Recent Advances in Aryl Alkyl and Dialkyl Sulfide Synthesis. *Phosphorus, Sulfur Silicon Relat. Elem.* **2015**, *190* (7), 978–1003. <https://doi.org/10.1080/10426507.2014.974754>.
- (8) Vaska, L.; DiLuzio, J. W. Activation of Hydrogen by a Transition Metal Complex at Normal Conditions Leading to a Stable Molecular Dihydride. *J. Am. Chem. Soc.* **1962**, *84*, 679–680. <https://doi.org/10.1021/ja00863a040>.

- (9) Crabtree, R. H. *The Organometallic Chemistry of the Transition Metals*, 3rd ed.; Wiley inter-Science, **2001**.
- (10) Gillie, A.; Stille, J. K. Mechanisms of 1,1-Reductive Elimination from Palladium. *J. Am. Chem. Soc.* **1980**, *102* (15), 4933–4941. <https://doi.org/10.1021/ja00535a018>.
- (11) Luo, Q. L.; Tan, J. P.; Li, Z. F.; Nan, W. H.; Xiao, D. R. Suzuki-Miyaura Coupling of Aryl Iodides, Bromides, and Chlorides Catalyzed by Bis (Thiazole) Pincer Palladium Complexes. *J. Org. Chem.* **2012**, *77* (18), 8332–8337. <https://doi.org/10.1021/jo3011733>.
- (12) Korenaga, T.; Kosaki, T.; Fukumura, R.; Ema, T.; Sakai, T. Suzuki-Miyaura Coupling Reaction Using Pentafluorophenylboronic Acid. *Org. Lett.* **2005**, *7* (22), 4915–4917. <https://doi.org/10.1021/ol051866i>.
- (13) Miyaura, N.; Yamada, K.; Suzuki, A. A new stereospecific cross-coupling by the palladium-catalyzed reaction of 1-alkenylboranes with 1-alkenyl or 1-alkynyl halides; *Tetrahedron Lett.* **1979**, *36*, 3437–3440.
- (14) Lima, C. F. R. A. C.; Rodrigues, A. S. M. C.; Silva, V. L. M.; Silva, A. M. S.; Santos, L. M. N. B. F. Role of the Base and Control of Selectivity in the Suzuki-Miyaura Cross-Coupling Reaction. *ChemCatChem* **2014**, *6* (5), 1291–1302. <https://doi.org/10.1002/cctc.201301080>.
- (15) Khusnutdinova, J. R.; Milstein, D. Metal-Ligand-Cooperation. *Angew. Chem.* **2015**, *127* (42), 12406–12445. <https://doi.org/10.1002/ange.201503873>.
- (16) Bag, J.; Das, S.; Mukherjee, S.; Ghosh, P.; Pal, K. Competitive Electronic Effect of Ligand Substitution over the Role of Metal Ions (Ni and Co) on Unusual Amine-Imine Interconversion in Conjugated Amine-Ene-Imine Ligands. *New J. Chem.* **2023**, *47* (9), 4321–4336. <https://doi.org/10.1039/d2nj03355k>.

- (17) Barrios-Landeros, F.; Carrow, B. P.; Hartwig, J. F. Effect of Ligand Steric Properties and Halide Identity on the Mechanism for Oxidative Addition of Haloarenes to Trialkylphosphine Pd(0) Complexes. *J. Am. Chem. Soc.* **2009**, *131* (23), 8141–8154. <https://doi.org/10.1021/ja900798s>.
- (18) Chen, C.; Bellows, S. M.; Holland, P. L. Tuning Steric and Electronic Effects in Transition-Metal  $\beta$ -Diketiminato Complexes. *Dalton Trans.* **2015**, 16654–16670. <https://doi.org/10.1039/c5dt02215k>.
- (19) Van Leeuwen, P. W. N. M.; Kamer, P. C. J.; Reek, J. N. H.; Dierkes, P. Ligand Bite Angle Effects in Metal-Catalyzed C-C Bond Formation. *Chem. Rev.* **2000**, *100* (8), 2741–2769. <https://doi.org/10.1021/cr9902704>.
- (20) Abd-El-Aziz, A. S. *Biomedical Applications*; John Wiley, **2004**, 1-18.
- (21) Van Leeuwen, P. W. N. M.; Kamer, P. C. J.; Reek, J. N. H. The Bite Angle Makes the Catalyst, *Pure Appl. Chem.* **1999**, *71*, 1443-1452.
- (22) Pfaltz, A.; Drury III, W. J. Design of Chiral Ligands for Asymmetric Catalysis: From C<sub>2</sub>-Symmetric P,P- and N,N-Ligands to Sterically and Electronically Nonsymmetrical P,N-Ligands. *PNAS*, **2004**, *101* (16), 5723-5726. [www.pnas.org/cgi/doi/10.1073/pnas.0307152101](http://www.pnas.org/cgi/doi/10.1073/pnas.0307152101).
- (23) González, J. M.; Vidal, X.; Ortuño, M. A.; Mascareñas, J. L.; Gulías, M. Chiral Ligands Based on Binaphthyl Scaffolds for Pd-Catalyzed Enantioselective C-H Activation/Cycloaddition Reactions. *J. Am. Chem. Soc.* **2022**, *144* (47), 21437–21442. <https://doi.org/10.1021/jacs.2c09479>.

- (24) Noffke, A. L.; Habtemariam, A.; Pizarro, A. M.; Sadler, P. J. Designing Organometallic Compounds for Catalysis and Therapy. *Chem. Commun.* **2012**, 48 (43), 5219–5246. <https://doi.org/10.1039/c2cc30678f>.
- (25) Shen, Q.; Shekhar, S.; Stambuli, J. P.; Hartwig, J. F. Highly Reactive, General, and Long-Lived Catalysts for Coupling Heteroaryl and Aryl Chlorides with Primary Nitrogen Nucleophiles. *Angew. Chem. Int. Ed.* **2005**, 44 (9), 1371–1375. <https://doi.org/10.1002/anie.200462629>.
- (26) Usta, H.; Sheets, W. C.; Denti, M.; Generali, G.; Lu, S.; Yu, X.; Muccini, M.; Facchetti, A. Per Fluoroalkyl-Functionalized Thiazole – Thiophene Oligomers as N - Channel Semiconductors in Organic Field-Effects and Light- Emitting Transistors. *Chem. Mater.* **2014**, 26 (22), 6542–6556.
- (27) Fors, B. P.; Watson, D. A.; Biscoe, M. R.; Buchwald, S. L. A Highly Active Catalyst for Pd-Catalyzed Amination Reactions: Cross-Coupling Reactions Using Aryl Mesylates and the Highly Selective Monoarylation of Primary Amines Using Aryl Chlorides. *J. Am. Chem. Soc.* **2008**, 130 (41), 13552–13554. <https://doi.org/10.1021/ja8055358>.
- (28) Fodor, D.; Kégl, T.; Tukacs, J. M.; Horváth, A. K.; Mika, L. T. Homogeneous Pd-Catalyzed Heck Coupling in  $\gamma$ -Valerolactone as a Green Reaction Medium: A Catalytic, Kinetic, and Computational Study. *ACS Sustain. Chem. Eng.* **2020**, 8 (26), 9926–9936. <https://doi.org/10.1021/acssuschemeng.0c03523>.
- (29) Watson, D. A.; Su, M.; Teverovskiy, G.; Zhang, Y.; García-Fortanet, J.; Kinzel, T.; Buchwald, S. L. Formation of ArF from LPdAr(F): Catalytic Conversion of Aryl Triflates to Aryl Fluorides, *Science* **2009**, 325, 1661-1664.

- (30) Jos Terheijden, G. V. Syntheses and Structural Aspects of Rigid Aryl- Palladium (II) and -Platinum (II) Complexes. X-Ray Crystal Structure of o,o'-Bis[(Dimethylamino)Methyl]Phenyl- Platinum(II) Bromide. *J. Organomet. Chem.* **1986**, *315* (3), 401–417.
- (31) Watson, D. A.; Su, M.; Teverovskiy, G.; Zhang, Y.; Garcia-Fortanet, J.; Kinzel, T.; Buchwald, S. L. Formation of Arf from Lpdar(f): Catalytic Conversion of Aryl Triflates to Aryl Fluorides. *Science (1979)* **2009**, *325* (5948), 1661–1664.  
<https://doi.org/10.1126/science.1178239>.
- (32) Devendar, P.; Qu, R. Y.; Kang, W. M.; He, B.; Yang, G. F. Palladium-Catalyzed Cross-Coupling Reactions: A Powerful Tool for the Synthesis of Agrochemicals. *J. Agric. Food. Chem.* **2018**, *66*, 8914–8934. <https://doi.org/10.1021/acs.jafc.8b03792>.
- (33) Ning, F.; Wan, X.; Liu, X.; Yu, R.; Shui, J. Recent Advances in Phosphorus-Coordinated Transition Metal Single-Atom Catalysts for Oxygen Reduction Reaction. *ChemNanoMat.* **2020**, *6*, 1601–1610. <https://doi.org/10.1002/cnma.202000436>.
- (34) Wang, Y.; Wu, Q.; Zhang, B.; Tian, L.; Li, K.; Zhang, X. Recent Advances in Transition Metal Carbide Electrocatalysts for Oxygen Evolution Reaction. *Catalysts.* **2020**, *10*, 1–30. <https://doi.org/10.3390/catal10101164>.
- (35) Tole, T.; Jordaan, J.; Vosloo, H. Synthesis and Application of the Transition Metal Complexes of  $\alpha$ -Pyridinyl Alcohols,  $\alpha$ -Bipyridinyl Alcohols,  $\alpha$ ,  $\alpha'$ -Pyridinyl Diols and  $\alpha$ ,  $\alpha'$ -Bipyridinyl Diols in Homogeneous Catalysis. *Molecules.* **2018**, *23* (896), 1-60.  
<https://doi.org/10.3390/molecules23040896>.

- (36) Schubert, U.S.; Eschbaumer, C.; Andres, P.; Hofmeier, H.; Weidl, C. H.; Hertweck, E.; Dulkeith, E.; Morteani, A.; N.E. Hecker, J. F. *Synthetic Metals*. *Synth. Met.* **2001**, *121*, 11-.
- (37) Kaes, C.; Katz, A.; Hosseini, M. W. Bipyridine: The Most Widely Used Ligand. A Review of Molecules Comprising at Least Two 2,2'-Bipyridine Units. *Chem. Rev.* **2000**, *100* (10), 3553–3590. <https://doi.org/10.1021/cr990376z>.
- (38) Kaes, C.; Katz, A.; Hosseini, M. W. Bipyridine: The Most Widely Used Ligand. A Review of Molecules Comprising at Least Two 2,2'-Bipyridine Units. *Chem. Rev.* **2000**, *100* (10), 3553–3590. <https://doi.org/10.1021/cr990376z>.
- (39) Raganathan, K. G.; Schneider, H.-J. Nucleotide Complexes with Azoniacyclophanes Containing Phenyl-, Biphenyl-or Bipyridyl-Units, *J. Chem. Soc. Perkin. Trans.* **1996**, *2*, 2597-2600.
- (40) Beer, P. D.; Chen, Z.; Goulden, A. J.; Grieve, A.; Heseck, D.; Szemesa, F.; Wearb, T. Anion Recognition by Novel Ruthenium(II) Bipyridyl Calix[4]Arene Receptor Molecules, *J. Chem. Soc. Chem. Commun.*, **1994**. 1269-1271.
- (41) Constable, E. C.; Housecroft, C. E. More Hydra than Janus – Non-Classical Coordination Modes in Complexes of Oligopyridine Ligands. *Coord. Chem. Rev.* **2017**, *350*, 84–104. <https://doi.org/10.1016/j.ccr.2017.06.006>.
- (42) Chen, X. Y.; Yang, X.; Holliday, B. J. Photoluminescent Europium-Containing Inner Sphere Conducting Metallopolymer. *J. Am. Chem. Soc.* **2008**, *130* (5), 1546–1547. <https://doi.org/10.1021/ja077626a>.
- (43) Zaïm, A.; Nozary, H.; Guénée, L.; Besnard, C.; Lemonnier, J. F.; Petoud, S.; Piguet, C. N-Heterocyclic Tridentate Aromatic Ligands Bound to [Ln(Hexafluoroacetylacetonate)<sub>3</sub>]

- Units: Thermodynamic, Structural, and Luminescent Properties. *Chem. Eur. J.* **2012**, *18* (23), 7155–7168. <https://doi.org/10.1002/chem.201102827>.
- (44) Barbarella, G.; Melucci, M.; Sotgiu, G. The Versatile Thiophene: An Overview of Recent Research on Thiophene-Based Materials. *Adv. Mater.* **2005**, *17* (13), 1581–1593. <https://doi.org/10.1002/adma.200402020>.
- (45) Di, D.; In, R.; Chimiche, S.; Olivelli, P. Thiophene- Based Materials For Photovoltaic Applications. *Chimica organica*, **2012**. 1-269.
- (46) Ando, S.; Nishida, J. I.; Inoue, Y.; Tokito, S.; Yamashita, Y. Synthesis, Physical Properties, and Field-Effect Transistors of Novel Thiophene/Thiazolothiazole Co-Oligomers. *J. Mater. Chem.* **2004**, *14* (12), 1787–1790. <https://doi.org/10.1039/b403699a>.
- (47) Kagan, Jacques and Arora, S. K. The Synthesis of Alpha-Thiophene Oligomers by Oxidative Coupling of 2-Lithiothiophene. *Heterocycles* **1983**, *20* (10), 1937–1940.
- (48) Garnier, F.; Yassar, A.; Hajlaoui, R.; Horowitz, G.; Deloffre, F.; Servet, B.; Ries, S.; Alnot, P. Molecular Engineering of Organic Semiconductors: Design of Self-Assembly Properties in Conjugated Thiophene Oligomers. *J Am. Chem. Soc.* **1993**, *115* (19), 8716–8721. <https://doi.org/10.1021/ja00072a026>.
- (49) Chhabria, M. T.; Patel, S.; Modi, P.; Brahmshatriya, P. S. Thiazole a Review, Synthesis and Therapeutic. *Current Topics in Med. Chem.* **2015**, 2841-2862
- (50) Nayak, S.; Gaonkar, S. L. A Review on Recent Synthetic Strategies and Pharmacological Importance of 1,3-Thiazole Derivatives. *Mini-Rev. Med. Chem.* **2018**, *19* (3), 215–238. <https://doi.org/10.2174/1389557518666180816112151>.
- (51) Ganapathi, K.; Venkataraman, A. Chemistry of Thiazoles. *Proc. Indian Acad. Sci., A.*, **1945**, *22*, 362–378.



- (52) Mayer, R. Science of Synthesis: Houbenweyl Methods of Molecular Transformations. *Seances Acad. Sci.* **1966**, 12, 267.
- (53) Linker, G. J.; Van Duijnen, P. T.; Broer, R. Understanding Trends in Molecular Bond Angles. *J. Phys. Chem. A* **2020**, 124 (7), 1306–1311.  
<https://doi.org/10.1021/acs.jpca.9b10248>.
- (54) Huo, J.; Zeng, H. A Novel Triphenylamine Functionalized Bithiazole-Metal Complex with C60 for Photocatalytic Hydrogen Production under Visible Light Irradiation. *J. Mater. Chem. A Mater.* **2015**, 3 (12), 6258–6264. <https://doi.org/10.1039/c5ta00397k>.
- (55) Biosca, M.; Paptchikhine, A.; Pàmies, O.; Andersson, P. G.; Diéguez, M. Extending the Substrate Scope of Bicyclic P-Oxazoline/Thiazole Ligands for Ir-Catalyzed Hydrogenation of Unfunctionalized Olefins by Introducing a Biaryl Phosphoroamidite Group. *Chem. Eur. J.* **2015**, 21 (8), 3455–3464. <https://doi.org/10.1002/chem.201405361>.
- (56) Lee, J. H.; Curtis, M. D.; Kampf, J. W. Unusual Thermal Polymerization of 1, 4-Bis-5-(4, 4'-Dialkyl-2, 2'-Bithiazolyl)-1, 3-Butadiynes: Soluble Polymers from Diacetylenes. *Macromolecules* **2000**, 33 (6), 2136–2144. <https://doi.org/10.1021/ma9911290>.
- (57) Lin, W.; Sun, W.; Yang, J.; Shen, Z. Preparation and Magnetic Properties of Novel Supramolecular Complexes Containing Bithiazole Rings. *Mater. Chem. Phys.* **2008**, 112 (2), 617–623. <https://doi.org/10.1016/j.matchemphys.2008.05.099>.
- (58) Thore, S. N.; Gupta, S. v.; Baheti, K. G. Synthesis and Pharmacological Evaluation of 5-Methyl-2-Phenylthiazole-4-Substituted Heteroazoles as a Potential Anti-Inflammatory and Analgesic Agents. *J. Saudi Chem. Soc.* **2016**, 20, S46–S52.  
<https://doi.org/10.1016/j.jscs.2012.09.002>.

- (59) Micksch, M.; Tenne, M.; Strassner, T. Cyclometalated 2-Phenylimidazole Palladium Carbene Complexes in the Catalytic Suzuki-Miyaura Cross-Coupling Reaction. *Organometallics* **2014**, *33* (15), 3966–3976. <https://doi.org/10.1021/om5004336>.
- (60) Mawo, R. Y.; Johnson, D. M.; Wood, J. L.; Smoliakova, I. P. Synthesis and Structural Characterization of Enantiopure Exo and Endo Six-Membered Oxazoline-Derived Palladacycles. *J. Organomet. Chem.* **2008**, *693* (1), 33–45. <https://doi.org/10.1016/j.jorganchem.2007.10.011>.
- (61) Shannon, R. D. *Revised Effective Ionic Radii and Systematic Studies of Interatomic Distances in Halides and Chalcogenides*, *Acta Cryst.* **1976**, *32* 751-767.
- (62) Bondi, A. Van Der Waals Volumes and Radii. *J. Phys. Chem.* **1964**, *68*, 441–451.
- (63) Kosuru, S. R.; Lai, H. Y.; Yang, C. Y.; Senadi, G. C.; Lai, Y. C.; Chen, H. Y. Synthesis of a Palladium Complex Bearing 2-Phenylbenzothiazole and Its Application to Suzuki–Miyaura Coupling Reaction. *J. Chin. Chem. Soc.* **2019**, *66* (1), 110–113. <https://doi.org/10.1002/jccs.201800145>.
- (64) Janzen, D. E.; Bruening, M. A.; Sutton, C. A.; Sharma, A. R. Trithiacrown Palladium (II) Complexes with Cyclometallating Ligands: Isomer Effects, Intramolecular Palladium-Sulfur Interactions, and Reversible Pd(II/III) and Pd(III/IV) Oxidations. *J. Organomet. Chem.* **2015**, *777*, 31–41. <https://doi.org/10.1016/j.jorganchem.2014.11.023>.
- (65) John, E. B.; Alec, C. D.; Gray, H. B.; Green, J. C.; Nilay Hazari; Labinger, J. A.; Jay, R. W. Electronic Structures of Pd(II) Dimers. *Inorg. Chem.* **2010**, *49* (4), 1801–1810. <https://doi.org/10.1021/ic902189g>.
- (66) Powers, D. C.; Lee, E.; Ariafard, A.; Sanford, M. S.; Yates, B. F.; Canty, A. J.; Ritter, T. Connecting Binuclear Pd(III) and Mononuclear Pd(IV) Chemistry by Pd-Pd Bond

- Cleavage. *J. Am. Chem. Soc.* **2012**, *134* (29), 12002–12009.  
<https://doi.org/10.1021/ja3044401u>.
- (67) Chu, J. H.; Chen, C. C.; Wu, M. J. Palladium-Catalyzed Arylation and Alkylation of 3,5-Diphenylisoxazole with Boronic Acids via C-H Activation. *Organometallics* **2008**, *27* (20), 5173–5176. <https://doi.org/10.1021/om800606c>.
- (68) Cocco, F.; Zucca, A.; Stoccoro, S.; Serratrice, M.; Guerri, A.; Cinellu, M. Synthesis and Characterization of Palladium(II) and Platinum(II) Adducts and Cyclometalated Complexes of 6,6'-Dimethoxy-2,2'-Bipyridine: C(Sp<sup>3</sup>)–H and C(Sp<sup>2</sup>)–H Bond Activations. *Organometallics* **2014**, *33* (13), 3414–3424.  
<https://doi.org/10.1021/om5003057>.
- (69) Schneider, C.; Broda, E.; Snieckus, V. Directed Ortho -Metalation-Cross-Coupling Strategies. One-Pot Suzuki Reaction to Biaryl and Heterobiaryl Sulfonamides. *Org. Lett.* **2011**, *13* (14), 3588–3591. <https://doi.org/10.1021/ol201175g>.
- (70) Norio Miyaura, B.; Suzuki, A. Stereoselective Synthesis of Arylated ( E )-Alkenes by the Reaction of Alk-1-Enylboranes with Aryl Halides in the Presence of Palladium Catalyst, *J. C. S. Chem. Comm.* **1979**, 590, 866-867.
- (71) Staś, M.; Broda, M. A.; Siodłak, D. Thiazole–Amino Acids: Influence of Thiazole Ring on Conformational Properties of Amino Acid Residues. *Amino Acids* **2021**, *53* (5), 673–686. <https://doi.org/10.1007/s00726-021-02974-0>.
- (72) Fitton, P.; Rick, E. A. The Addition Of Aryl Halides To Tetrakis(Triphenylphosphine) Palladium(0). *J. Organomet. Chem.* **1971**, *28*, 287–291.

- (73) Alonso, D. A.; Nájera, C.; Pacheco, M. C. Highly Active Oxime-Derived Palladacycle Complexes for Suzuki-Miyaura and Ullmann-Type Coupling Reactions. *J. Org. Chem.* **2002**, *67* (16), 5588–5594. <https://doi.org/10.1021/jo025619t>.
- (74) Benhaddou, R.; Czernecki, S.; Ville, G.; Zegar, A. A Kinetic Investigation of Some Electronic Factors and Ligand Effects in the Heck Reaction with Allylic Alcohols. *Organometallics* **1988**, *7* (12), 2435–2439. <https://doi.org/10.1021/om00102a002>.
- (75) Sheldrick, G. M. Integrated Space-Group and Crystal Structure. *Acta Cryst. A* **2015**, *71*, 3–8.
- (76) Sheldrick, G. M. A Short History of SHELX. *Acta Cryst. A* **2008**, *64*, 112–122.
- (77) Sheldrick, G. M. Crystal Structure Refinement with SHELXL. *Acta Cryst. C* **2015**, *71*, 3–8.
- (78) Ruth, T. J. The Medical Isotope Crisis: How We Got Here and Where We Are Going. *J. Nucl. Med. Technol.* **2014**, *42* (4), 245–248. <https://doi.org/10.2967/jnmt.114.144642>.
- (79) Morrison, A. The Global Impact of <sup>99m</sup>Tc Shortages The Global Impact of Technetium-<sup>99m</sup>. *Environmental Scan*, **2010**, *11*, 1-9 .
- (80) Martini, P.; Boschi, A.; Cicoria, G.; Uccelli, L.; Pasquali, M.; Duatti, A.; Pupillo, G.; Marengo, M.; Loriggiola, M.; Esposito, J. A Solvent-Extraction Module for Cyclotron Production of High-Purity Technetium-<sup>99m</sup>. *Appl. Radiat. Isot.* **2016**, *118*, 302–307. <https://doi.org/10.1016/j.apradiso.2016.10.002>.
- (81) Dash, A.; Knapp, F. F.; Pillai, M. R. A. <sup>99</sup>Mo/<sup>99m</sup>Tc Separation: An Assessment of Technology Options. *Nucl. Med. Biol.* **2013**, *40*, 167–176. <https://doi.org/10.1016/j.nucmedbio.2012.10.005>.

- (82) Gagnon, K.; Bénard, F.; Kovacs, M.; Ruth, T. J.; Schaffer, P.; Wilson, J. S.; McQuarrie, S. A. Cyclotron Production of  $^{99m}\text{Tc}$ : Experimental Measurement of the  $^{100}\text{Mo}(p,x)^{99}\text{Mo}$ ,  $^{99m}\text{Tc}$  and  $^{99g}\text{Tc}$  Excitation Functions from 8 to 18 MeV. *Nucl. Med. Biol.* **2011**, *38* (6), 907–916. <https://doi.org/10.1016/j.nucmedbio.2011.02.010>.
- (83) Mang'era, K.; Ogbomo, K.; Zriba, R.; Fitzpatrick, J.; Brown, J.; Pellerin, E.; Barnard, J.; Saunders, C.; de Jong, M. Processing and Evaluation of Linear Accelerator-Produced  $^{99}\text{Mo}/^{99m}\text{Tc}$  in Canada. *J. Radioanal. Nucl. Chem.* **2015**, *305* (1), 79–85. <https://doi.org/10.1007/s10967-015-3997-5>.
- (84) Nawar, M. F.; Türler, A. New Strategies for a Sustainable  $^{99m}\text{Tc}$  Supply to Meet Increasing Medical Demands: Promising Solutions for Current Problems. *Front. Chem.* **2022**, *10*, 1–32. <https://doi.org/10.3389/fchem.2022.926258>.
- (85) Hasan, S.; Prelas, M. A. Molybdenum-99 Production Pathways and the Sorbents for  $^{99}\text{Mo}/^{99m}\text{Tc}$  Generator Systems Using  $(n, \gamma)^{99}\text{Mo}$ : A Review. *SN Appl. Sci.* **2020**, *2*(1782), 1–28. <https://doi.org/10.1007/s42452-020-03524-1>.
- (86) Nawar, M. F.; El-Daoushy, A. F.; Ashry, A.; Soliman, M. A.; Türler, A. Evaluating the Sorption Affinity of Low Specific Activity  $^{99}\text{Mo}$  on Different Metal Oxide Nanoparticles. *Inorganics (Basel)* **2022**, *10* (10). <https://doi.org/10.3390/inorganics10100154>.
- (87) Atia, A. A.; Donia, A. M.; Awed, H. A. Synthesis of Magnetic Chelating Resins Functionalized with Tetraethylenepentamine for Adsorption of Molybdate Anions from Aqueous Solutions. *J. Hazard Mater.* **2008**, *155* (1–2), 100–108. <https://doi.org/10.1016/j.jhazmat.2007.11.035>.

- (88) Nagai, Y.; Nakahara, Y.; Kawabata, M.; Hatsukawa, Y.; Hashimoto, K.; Saeki, H.; Motoishi, S.; Ohta, A.; Shiina, T.; Kawauchi, Y. Quality of  $^{99m}\text{TcO}_4^-$  from  $^{99}\text{Mo}$  Produced by  $^{100}\text{Mo}(n,2n)^{99}\text{Mo}$ . *J. Phys. Soc. Japan* **2017**, *86* (5).  
<https://doi.org/10.7566/JPSJ.86.053202>.
- (89) Stober, W.; Fink, A.; Ernst Bohn, D. Controlled Growth of Monodisperse Silica Spheres in the Micron Size Range. *J. Colloid Interface Sci.* **1968**, *26* 62-69.
- (90) Do, K. I.; And, K.; Kim, H. T. Formation of Silica Nanoparticles by Hydrolysis of TEOS Using a Mixed Semi-Batch/Batch Method. *J. Sol-Gel Sci. Technol.* **2002**, *25*, 183-189.
- (91) Matsoukas, T.; Gulari, E. Dynamics of Growth of Silica Particles from Ammonia-Catalyzed Hydrolysis of Tetra-Ethyl-Orthosilicate. *J. Colloid Interface Sci.* **1988**, *24* (1), 252-261.
- (92) Touzi, H.; Sakly, N.; Kalfat, R.; Sfihi, H.; Jaffrezic-Renault, N.; Rammah, M. B.; Zarrouk, H. Grafting of Anion Exchanging Groups on  $\text{SiO}_2/\text{Si}$  Structures for Anion Detection in Waters. *Sens. Actuators B Chem.* **2003**, *96* (1-2), 399-406.  
[https://doi.org/10.1016/S0925-4005\(03\)00578-1](https://doi.org/10.1016/S0925-4005(03)00578-1).
- (93) Kowalczyk, D.; Slomkowski, S.; Chehimi, M. M.; Delamar, M. Adsorption of Aminopropyltriethoxy Silane on Quartz: An XPS and Contact Angle Measurements Study. *J. Adhesion and Adhesives* **1996**, *16* (4), 227-232.
- (94) Atia, A. A.; Donia, A. M.; Awed, H. A. Synthesis of Magnetic Chelating Resins Functionalized with Tetraethylenepentamine for Adsorption of Molybdate Anions from Aqueous Solutions. *J. Hazard. Mater.* **2008**, *155* (1-2), 100-108.  
<https://doi.org/10.1016/j.jhazmat.2007.11.035>.

- (95) Serier, A.; Pascault, J. P.; My, L. T. Reactions in Aminosilane–Epoxy Prepolymer Systems I. Kinetics of Epoxy–Amine Reactions. *J. Polym. Sci. A Polym. Chem.* **1991**, *29* (2), 209–218. <https://doi.org/10.1002/pola.1991.080290208>.
- (96) Serier, A.; Pascault, J. P.; Lam, T. M. Reactions in Aminosilane-epoxy Prepolymer Systems. II. Reactions of Alkoxysilane Groups with or without the Presence of Water. *J. Polym. Sci. A Polym. Chem.* **1991**, *29* (8), 1125–1131. <https://doi.org/10.1002/pola.1991.080290806>.
- (97) Ou, Y.; Yang, F.; Chen, J. Interfacial Interaction and Mechanical Properties of Nylon 6-Potassium Titanate Composites Prepared by in-Situ Polymerization. *J. Appl. Polym. Sci.* **1997**, *64* (12), 2317–2322. [https://doi.org/10.1002/\(sici\)1097-4628\(19970620\)64:12<2317:aid-app7>3.0.co;2-o](https://doi.org/10.1002/(sici)1097-4628(19970620)64:12<2317:aid-app7>3.0.co;2-o).
- (98) Katayama, H.; Sen, S. Aurora Kinase Inhibitors as Anticancer Molecules. *Biochim Biophys Acta.* **2010**, *1799* (0), 829–839. <https://doi.org/10.1016/j.bbagr.2010.09.004>.
- (99) Maki, M.-H.; Wang, Y.-L. The Kinase Activity of Aurora B Is Required for Kinetochore-Microtubule Interactions during Mitosis. *Curr. Biol.* **2002**, *12*, 894-899.
- (100) Tang, A.; Gao, K.; Chu, L.; Zhang, R.; Yang, J.; Zheng, J. *Aurora Kinases: Novel Therapy Targets in Cancers*; 2017; Vol. 8. [www.impactjournals.com/oncotarget/](http://www.impactjournals.com/oncotarget/).
- (101) Willems, E.; Dedobbeleer, M.; Digregorio, M.; Lombard, A.; Lumapat, P. N.; Rogister, B. The Functional Diversity of Aurora Kinases: A Comprehensive Review. *Cell Div.* **2018**, *13* (7), 1-17. <https://doi.org/10.1186/s13008-018-0040-6>.
- (102) Navarro-Serer, B.; Childers, E. P.; Hermance, N. M.; Mercadante, D.; Manning, A. L. Aurora A Inhibition Limits Centrosome Clustering and Promotes Mitotic Catastrophe in

Cells with Supernumerary Centrosomes. *Oncotarget* **2019**, *10*, 1649-1659

[www.oncotarget.com](http://www.oncotarget.com).

- (103) Kimura, M.; Matsuda, Y.; Yoshioka, T.; Okano, Y. Cell Cycle-Dependent Expression and Centrosome Localization of a Third Human Aurora/Ipl1-Related Protein Kinase, AIK3. *J. Biol. Chem.* **1999**, *274* (11), 7334–7340. <https://doi.org/10.1074/jbc.274.11.7334>.
- (104) Rahimi, A. M.; Cai, M.; Hoyer-Fender, S. Heterogeneity of the NIH3T3 Fibroblast Cell Line. *Cells* **2022**, *11* (17) 1-19. <https://doi.org/10.3390/cells11172677>.
- (105) Kollareddy, M.; Dzubak, P.; Zheleva, D.; Hajduch, M.; Kollareddy, M.; Dzubak, P.; Zheleva, D.; Hajduch, M. Aurora Kinases: Structure, Functions And Their Association With Cancer, *Biomed, pap med.* **2008**, *152* (1), 27-33.
- (106) Quartuccio, S. M.; Schindler, K. Functions of Aurora Kinase C in Meiosis and Cancer. *Front. Cell Dev. Biol.* **2015**, *3*, 1-8. <https://doi.org/10.3389/fcell.2015.00050>.
- (107) Buschhorn, H. M. K.; Klein, R. R.; Chambers, S. M.; Hardy, M. C.; Green, S.; Bearss, D.; Nagle, R. B. Aurora-A over-expression in High-Grade PIN Lesions and Prostate Cancer. *Prostate* **2005**, *64* (4), 341–346. <https://doi.org/10.1002/pros.20247>.
- (108) Fancelli, D.; Berta, D.; Bindi, S.; Cameron, A.; Cappella, P.; Carpinelli, P.; Catana, C.; Forte, B.; Giordano, P.; Giorgini, M. L.; Mantegani, S.; Marsiglio, A.; Meroni, M.; Moll, J.; Pittalà, V.; Roletto, F.; Severino, D.; Soncini, C.; Storici, P.; Tonani, R.; Varasi, M.; Vulpetti, A.; Vianello, P. Potent and Selective Aurora Inhibitors Identified by the Expansion of a Novel Scaffold for Protein Kinase Inhibition. *J. Med. Chem.* **2005**, *48* (8), 3080–3084. <https://doi.org/10.1021/jm049076m>.



- (109) Ghose, A. K.; Herbertz, T.; Pippin, D. A.; Salvino, J. M.; Mallamo, J. P. Knowledge Based Prediction of Ligand Binding Modes and Rational Inhibitor Design for Kinase Drug Discovery. *J. Med. Chem.* **2008**, *48*, 5149–5171. <https://doi.org/10.1021/jm800475y>.
- (110) Urich, R.; Wishart, G.; Kiczun, M.; Richters, A.; Tidten-Luksch, N.; Rauh, D.; Sherborne, B.; Wyatt, P. G.; Brenk, R. De Novo Design of Protein Kinase Inhibitors by in Silico Identification of Hinge Region-Binding Fragments. *ACS Chem. Biol.* **2013**, *8* (5), 1044–1052. <https://doi.org/10.1021/cb300729y>.
- (111) Jiang, X.; Yu, J.; Zhou, Z.; Kongsted, J.; Song, Y.; Pannecouque, C.; De Clercq, E.; Kang, D.; Poongavanam, V.; Liu, X.; Zhan, P. Molecular Design Opportunities Presented by Solvent-Exposed Regions of Target Proteins. *Med. Res. Rev.* **2019**, *39*, 2194–2238. <https://doi.org/10.1002/med.21581>.
- (112) González-Loyola, A.; Fernández-Miranda, G.; Trakala, M.; Partida, D.; Samejima, K.; Ogawa, H.; Cañamero, M.; de Martino, A.; Martínez-Ramírez, Á.; de Cárcer, G.; Pérez de Castro, I.; Earnshaw, W. C.; Malumbres, M. Aurora B Overexpression Causes Aneuploidy and P21 Cip1 Repression during Tumor Development. *Mol. Cell. Biol.* **2015**, *35* (20), 3566–3578. <https://doi.org/10.1128/mcb.01286-14>.
- (113) Kaestner, P.; Stolz, A.; Bastians, H. Determinants for the Efficiency of Anticancer Drugs Targeting Either Aurora-A or Aurora-B Kinases in Human Colon Carcinoma Cells. *Mol. Cancer. Ther.* **2009**, *8* (7), 2046–2056. <https://doi.org/10.1158/1535-7163.MCT-09-0323>.
- (114) Girdler, F.; Gascoigne, K. E.; Evers, P. A.; Hartmuth, S.; Crafter, C.; Foote, K. M.; Keen, N. J.; Taylor, S. S. Validating Aurora B as an Anti-Cancer Drug Target. *J. Cell. Sci.* **2006**, *119* (17), 3664–3675. <https://doi.org/10.1242/jcs.03145>.

- (115) Lee, D. H.; Kim, C. G.; Lim, Y.; Shin, S. Y. Aurora Kinase a Inhibitor TCS7010 Demonstrates Pro-Apoptotic Effect through the Unfolded Protein Response Pathway in HCT116 Colon Cancer Cells. *Oncol. Lett.* **2017**, *14* (6), 6571–6577.  
<https://doi.org/10.3892/ol.2017.7023>.
- (116) Niu, H.; Manfredi, M.; Ecsedy, J. A. Scientific Rationale Supporting the Clinical Development Strategy for the Investigational Aurora A Kinase Inhibitor Alisertib in Cancer. *Front. Oncol.* **2015**, *5*, 1-9. <https://doi.org/10.3389/fonc.2015.00189>.
- (117) Durlacher, C. T.; Li, Z. L.; Chen, X. W.; He, Z. X.; Zhou, S. F. An Update on the Pharmacokinetics and Pharmacodynamics of Alisertib, a Selective Aurora Kinase A Inhibitor. *Clin. Exp. Pharmacol. Physiol.* **2016**, *43*, 585–601.  
<https://doi.org/10.1111/1440-1681.12571>.
- (118) Hauf, S.; Cole, R. W.; LaTerra, S.; Zimmer, C.; Schnapp, G.; Walter, R.; Heckel, A.; van Meel, J.; Rieder, C. L.; Peters, J. M. The Small Molecule Hesperadin Reveals a Role for Aurora B in Correcting Kinetochore-Microtubule Attachment and in Maintaining the Spindle Assembly Checkpoint. *J. Cell Biol.* **2003**, *161* (2), 281–294.  
<https://doi.org/10.1083/jcb.200208092>.
- (119) Bavetsias, V.; Linardopoulos, S. Aurora Kinase Inhibitors: Current Status and Outlook. *Front. Oncol.* **2015**, *5*, 1-10. <https://doi.org/10.3389/fonc.2015.00278>.
- (120) Dennis, M.; Davies, M.; Oliver, S.; D'Souza, R.; Pike, L.; Stockman, P. Phase i Study of the Aurora B Kinase Inhibitor Barasertib (AZD1152) to Assess the Pharmacokinetics, Metabolism and Excretion in Patients with Acute Myeloid Leukemia. *Cancer Chemother Pharmacol* **2012**, *70* (3), 461–469. <https://doi.org/10.1007/s00280-012-1939-2>.

- (121) Montalban-Bravo, G.; Garcia-Manero, G. Novel Drugs for Older Patients with Acute Myeloid Leukemia. *Leukemia*. **2015**, 29, 760–769. <https://doi.org/10.1038/leu.2014.244>.
- (122) Keen, N.; Taylor, S. Aurora-Kinase Inhibitors as Anticancer Agents. *Nat. Rev. Cancer*. **2004**, 4, 927–936. <https://doi.org/10.1038/nrc1502>.
- (123) Brust, P.; Van Den Hoff, J.; Steinbach, J. Development of <sup>18</sup>F-Labeled Radiotracers for Neuroreceptor Imaging with Positron Emission Tomography. *Neurosci. Bull.* **2014**, 30, 777–811. <https://doi.org/10.1007/s12264-014-1460-6>.
- (124) Vaquero, J. J.; Kinahan, P. Positron Emission Tomography: Current Challenges and Opportunities for Technological Advances in Clinical and Preclinical Imaging Systems. *Annu. Rev. Biomed. Eng.* **2015**, 17, 385–414. <https://doi.org/10.1146/annurev-bioeng-071114-040723>.
- (125) Jacobson, O.; Kiesewetter, D. O.; Chen, X. Fluorine-18 Radiochemistry, Labeling Strategies and Synthetic Routes. *Bioconjugate Chem. ACS* **2015**, 17, 1–18. <https://doi.org/10.1021/bc500475e>.
- (126) Almuhaideb, A.; Papathanasiou, N.; Bomanji, J. <sup>18</sup>F-FDG PET/CT Imaging in Oncology. *Annals of Saudi Medicine*. **2011**, 31, 3–13. <https://doi.org/10.4103/0256-4947.75771>.
- (127) Kurland, B. F.; Peterson, L. M.; Linden, H. M.; Mankoff, D. A. FDG PET and FES PET Predict PFS on Endocrine Therapy - Response. *Clinical Cancer Res.* **2018**, 24, 249–250. <https://doi.org/10.1158/1078-0432.CCR-17-2980>.
- (128) Raper, E. S. Complexes of Heterocyclic Thionates. Complexes of Monodentate and Chelating Ligands, **1996**, 153, 199-255.
- (129) Váry, M.; Perny, M.; Kusko, M.; Firicky, E. *Elektroenergetika*, **2011**, 4, 14-16.

- (130) Cukurovali, A.; Yilmaz, I.; Gur, S.; Kazaz, C. Synthesis, Antibacterial and Antifungal Activity of Some New Thiazolylhydrazone Derivatives Containing 3-Substituted Cyclobutane Ring. *Eur. J. Med. Chem.* **2006**, *41* (2), 201–207.  
<https://doi.org/10.1016/j.ejmech.2005.01.013>.
- (131) Karegoudar, P.; Karthikeyan, M. S.; Prasad, D. J.; Mahalinga, M.; Holla, B. S.; Kumari, N. S. Synthesis of Some Novel 2,4-Disubstituted Thiazoles as Possible Antimicrobial Agents. *Eur. J. Med. Chem.* **2008**, *43* (2), 261–267.  
<https://doi.org/10.1016/j.ejmech.2007.03.014>.
- (132) Wu, X.; Kassie, F.; Mersch-Sundermann, V. Induction of Apoptosis in Tumor Cells by Naturally Occurring Sulfur-Containing Compounds. *Mutat. Res. - Reviews in Mutation Research.* **2005**, *589*, 81–102. <https://doi.org/10.1016/j.mrrev.2004.11.001>.
- (133) Rashad, A. E.; Mahmoud, A. E.; Ali, M. M. Synthesis and Anticancer Effects of Some Novel Pyrazolo[3,4-d]Pyrimidine Derivatives by Generating Reactive Oxygen Species in Human Breast Adenocarcinoma Cells. *Eur. J. Med. Chem.* **2011**, *46* (4), 1019–1026.  
<https://doi.org/10.1016/j.ejmech.2011.01.013>.
- (134) Desai, N. C.; Harsora, J. P.; Monapara, J. D.; Khedkar, V. M. Synthesis, Antimicrobial Capability and Molecular Docking of Heterocyclic Scaffolds Clubbed by 2-Azetidinone, Thiazole and Quinoline Derivatives. *Polycycl. Aromat. Compd.* **2021**, *42* (7) 3924-3938.  
<https://doi.org/10.1080/10406638.2021.1877747>.
- (135) Jaishree, V.; Ramdas, N.; Sachin, J.; Ramesh, B. In Vitro Antioxidant Properties of New Thiazole Derivatives. *J. Saudi Chem. Soc.* **2012**, *16* (4), 371–376.  
<https://doi.org/10.1016/j.jscs.2011.02.007>.

- (136) Mohammadi-Farani, A.; Foroumadi, A.; Kashani, M. R.; Aliabadi, A. N-Phenyl-2-p-Tolylthiazole-4-Carboxamide Derivatives: Synthesis and Cytotoxicity Evaluation as Anticancer Agents, *Iran J. Medical Sci.* **2014**, *17* (7), 502-508.
- (137) Ahangar, N.; Ayati, A.; Alipour, E.; Pashapour, A.; Foroumadi, A.; Emami, S. 1-[(2-Arylthiazol-4-Yl)Methyl]Azoles as a New Class of Anticonvulsants: Design, Synthesis, in Vivo Screening, and in Silico Drug-like Properties. *Chem. Biol. Drug Des.* **2011**, *78* (5), 844–852. <https://doi.org/10.1111/j.1747-0285.2011.01211.x>.
- (138) Spielvogel, D. J.; Davis, W. M.; Buchwald, S. L. Preparation, Crystal Structure Analysis, and Catalytic Application of [(S)-BINAP]Ni(COD) and [(S)-BINAP]NiBr<sub>2</sub>. *Organometallics* **2002**, *21* (18), 3833–3836. <https://doi.org/10.1021/om020164j>.
- (139) Wang, S.; Midgley, C. A.; Scaërou, F.; Grabarek, J. B.; Griffiths, G.; Jackson, W.; Kontopidis, G.; McClue, S. J.; McInnes, C.; Meades, C.; Mezna, M.; Plater, A.; Stuart, I.; Thomas, M. P.; Wood, G.; Clarke, R. G.; Blake, D. G.; Zheleva, D. I.; Lane, D. P.; Jackson, R. C.; Glover, D. M.; Fischer, P. M. Discovery of N-Phenyl-4-(Thiazol-5-yl)Pyrimidin-2-Amine Aurora Kinase Inhibitors. *J. Med. Chem.* **2010**, *53* (11), 4367–4378. <https://doi.org/10.1021/jm901913s>.
- (140) Wang, S.; Meades, C.; Wood, G.; Osnowski, A.; Anderson, S.; Yuill, R.; Thomas, M.; Mezna, M.; Jackson, W.; Midgley, C.; Griffiths, G.; Fleming, I.; Green, S.; McNae, I.; Wu, S. Y.; McInnes, C.; Zheleva, D.; Walkinshaw, M. D.; Fischer, P. M. 2-Anilino-4-(Thiazol-5-Yl)Pyrimidine CDK Inhibitors: Synthesis, SAR Analysis, X-Ray Crystallography, and Biological Activity. *J. Med. Chem.* **2004**, *47* (7), 1662–1675. <https://doi.org/10.1021/jm0309957>.

- (141) Tsubokura, K.; Iwata, T.; Taichi, M.; Kurbangalieva, A.; Fukase, K.; Nakao, Y.; Tanaka, K. Direct Guanylation of Amino Groups by Cyanamide in Water: Catalytic Generation and Activation of Unsubstituted Carbodiimide by Scandium (III) Triflate. *Synlett* **2014**, 25 (9), 1302–1306. <https://doi.org/10.1055/s-0033-1341080>.
- (142) Vadagaonkar, K. S.; Kalmode, H. P.; Prakash, S.; Chaskar, A. C. Greener [3+3] Tandem Annulation-Oxidation Approach towards the Synthesis of Substituted Pyrimidines. *New J. Chem.* **2015**, 39 (5), 3639–3645. <https://doi.org/10.1039/c4nj02345e>.